

Department of Chemical Engineering
Technical University of Denmark

Graduate Schools
Yearbook
2004

Editors:
Kim Dam-Johansen
Martin Skov Skjøth-Rasmussen

Address: Department of Chemical Engineering
Søltofts Plads, Building 229
Technical University of Denmark
DK-2800 Kgs. Lyngby
Denmark

Telephone: +45 4525 2800
Fax: +45 4588 2258
e-mail: kt@kt.dtu.dk
Internet: <http://www.kt.dtu.dk>

Printed by: BookPartner, Nørhaven Digital
Copenhagen, Denmark
January 2005

ISSN: 1604-5521
ISBN: 87-91435-12-9

Contents

| | |
|--|---|
| PREFACE TO GRADUATE SCHOOLS YEARBOOK by Professor Kim Dam-Johansen | 1 |
|--|---|

Contributions

| | |
|--|----|
| Andersen, Michael <i>PM-IRRAS AS AN IN SITU METHOD FOR INVESTIGATIONS OF REACTIONS OF RELEVANCE FOR FUEL CELLS</i> | 3 |
| Andreasen, Anders <i>IMPROVED RESISTANCE TOWARDS OXYGEN CONTAMINATION OF MAGNESIUM: ALLOYING WITH AL AND CU</i> | 5 |
| d' Anterrosches, Loïc <i>GROUP CONTRIBUTION BASED PROCESS FLOWSHEET SYNTHESIS, DESIGN AND MODELLING</i> | 9 |
| Bech, Niels <i>IN-SITU FLASH PYROLYSIS OF STRAW</i> | 13 |
| Biran, Suzan <i>STABILITY OF ENZYMES IN GRANULAR ENZYME PRODUCTS FOR LAUNDRY DETERGENTS</i> | 15 |
| Chakraborty, Debasish <i>ONE STEP FLAME SYNTHESIS OF DIRECT METHANOL FUEL CELL CATALYST</i> | 19 |
| Christensen, Henrik <i>CONTINUES FLOW REACTORS AND PROCESS ANALYTICAL TECHNOLOGY IN PHARMACEUTICAL PRODUCTION</i> | 23 |
| Christensen, Steen <i>MULTILEVEL MODELING OF COMPLEX SYSTEMS</i> | 25 |
| Davidescu, Florin Paul <i>OPTIMIZING OPERATION OF CHEMICAL PLANTS USING MODEL PREDICTIVE CONTROL</i> | 27 |
| Egholm, Runi Ditlev <i>EMULSION DESIGN</i> | 29 |
| Folas, Geogios <i>MODELING OF COMPLEX MIXTURES CONTAINING HYDROGEN BONDING MOLECULES WITH THE CPA EOS</i> | 31 |
| Fosbøl, Philip Loldrup <i>CORROSION IN WET GAS PIPELINES</i> | 33 |
| Gabrielsen, Jostein <i>CO₂ CAPTURE FROM COAL FIRED POWER PLANTS</i> | 35 |
| Hansen, Morten Skov <i>INVESTIGATION OF SPONTANEOUS CELL CYCLE SYNCHRONIZATION IN SACCHAROMYCES CEREVISIAE</i> | 37 |
| Hansen, Natanya Majbritt Louie <i>DEVELOPMENT OF NEW SYNTHETIC MEMBRANES FOR USE IN GLUCOSE SENSORS</i> | 43 |
| Hansen, Thomas Steen <i>TESTING AND FABRICATION OF ALL POLYMER MICROPUMP</i> | 45 |
| Hindiyarti, Lusi <i>GAS PHASE SULFUR, CHLORINE, AND ALKALI METAL CHEMISTRY IN BIOMASS COMBUSTION</i> | 47 |
| Hindsgaul, Claus <i>DISINTEGRATION OF CHAR PARTICLES DURING THERMAL CONVERSION</i> | 51 |
| Hu, Guilin <i>SO₂ EMISSION FROM CEMENT PRODUCTION</i> | 55 |

| | |
|--|-----|
| Jiménez, Edgar Ramírez <i>DESIGN AND CONTROL INTEGRATION FROM A MODEL-BASED METHODOLOGY FOR REACTION-SEPARATION WITH RECYCLE SYSTEMS</i> | 61 |
| Johansen, Johnny <i>ONE-STEP PREPARATION OF ASYMMETRIC CERAMIC MEMBRANES BY CONTROLLED DEPOSITION OF FLAME-PRODUCED NANOPARTICLES</i> | 65 |
| Johansen, Kent <i>STATISTICAL METHODS FOR HISTORY MATCHING</i> | 71 |
| Jørgensen, Kåre <i>EFFECT OF FORMULATION INGREDIENTS ON DRYING KINETICS AND MORPHOLOGY OF PARTICLES FORMED DURING SPRAY DRYING</i> | 73 |
| Kristensen, Morten Rode <i>NUMERICAL SIMULATION OF IN-SITU COMBUSTION</i> | 79 |
| Larsen, Morten Boberg <i>COMBUSTION MECHANISMS USING WASTE AS A FUEL IN CEMENT PRODUCTION</i> | 81 |
| Larsen, Thomas Ricco Ølholm <i>TRIBOLOGICAL PROPERTIES OF POLYMER BASED COMPOSITES WHEN DRY-SLIDING AGAINST METAL COUNTERFACES</i> | 85 |
| Li, Hong Wen <i>INPUT MULTIPLICITY IN DISTILLATION</i> | 87 |
| Lin, Yi <i>NEW EQUATION OF STATE FOR ELECTROLYTES</i> | 91 |
| van Lith, Simone C. <i>RELEASE OF INORGANIC METAL SPECIES, SULFUR AND CHLORINE DURING COMBUSTION OF WOODY BIOMASS ON A GRATE</i> | 97 |
| Monsalvo, Matías A. <i>PHASE BEHAVIOUR AND VISCOSITY MODELLING OF REFRIGERANT-LUBRICANT MIXTURES</i> | 101 |
| Nielsen, Jens Kromann <i>RHEOLOGY, STRUCTURAL STUDIES AND SYNTHESIS</i> | 105 |
| Overgaard, Anne Kathrine Kattenhøj <i>COUPLING OF ACTIVE COMPONENTS TO SYNTHETIC POLYMERS</i> | 107 |
| Papaeconomou, Irene <i>INTEGRATION OF SYNTHESIS, DESIGN AND CONTROL OF BATCH PROCESSES FOR PRODUCT DESIGN</i> | 109 |
| Pedersen, Kim Vestergaard <i>APPLICATION OF FLY ASH IN CONCRETE</i> | 115 |
| Petersen, Trine Lütken <i>PEGYLATION OF ENZYMES: NOVEL IN-VITRO METHODS FOR THEIR STUDY AND SCALE-UP</i> | 117 |
| Rasmussen, Christian Lund <i>DIRECT PARTIAL OXIDATION OF NATURAL GAS TO LIQUID CHEMICALS</i> | 119 |
| Rasmussen, Jan Kamyno <i>DATADRIVEN AND MECHANISTIC MODEL BASED CONTROL AND OPTIMIZATION OF FED-BATCH FERMENTATIONS</i> | 121 |
| Sales-Cruz, Alfonso Mauricio <i>DEVELOPMENT OF A COMPUTER AIDED MODELING SYSTEM FOR BIO AND CHEMICAL PROCESS AND PRODUCT DESIGN</i> | 125 |
| Sloth, Jakob <i>FORMATION OF ENZYME GRANULES BY SPRAY DRYING</i> | 131 |
| Soni, Vipasha <i>MODELING AND DESIGN OF CHEMICALLY FORMULATED PRODUCTS</i> | 133 |

| | |
|---|-----|
| Suñé, Núria Muro <i>PREDICTION OF THE SOLUBILITY AND DIFFUSION PROPERTIES OF PESTICIDES IN POLYMERS</i> | 135 |
| Thaysen, Mads <i>SOFTWARE SENSORS FOR MONITORING INDUSTRIAL CULTIVATION PROCESSES</i> | 141 |
| Verdier, Sylvain <i>EXPERIMENTAL STUDY AND MODELLING OF ASPHALTENE PRECIPITATION CAUSED BY GAS INJECTION</i> | 145 |
| Villafáfila García, Ada <i>PREDICTION OF MINERAL SCALE FORMATION IN GEOTHERMAL AND OILFIELD OPERATIONS USING THE EXTENDED UNIQUAC MODEL</i> | 149 |
| Yebra, Diego Meseguer <i>EFFICIENT AND ENVIRONMENTALLY FRIENDLY ANTIFOULING PAINTS</i> | 155 |
| Zeuthen, Jacob <i>LABORATORY INVESTIGATION OF FORMATION OF AEROSOLS AND CHEMICAL REACTIONS IN FLUE GAS FROM BIOMASS- AND WASTE-COMBUSTION</i> | 161 |

Preface

The 2004 Chemical Engineering Graduate Schools Yearbook is the second yearbook published on behalf of our graduate students associated to the graduate schools of the department.

The yearbook is a successful medium in which, graduate students present the annual progress and status of their research projects, while newly matriculated graduate students present the background and aims that motivate their studies. Readers of the yearbooks may follow the progress of individual graduate students and studies during the entire enrollment period and read about the numerous high quality research activities at the department.

The present yearbook illustrates the broad spectrum of research activities performed by graduate students associated with the department. Our graduate students demonstrate first class and innovative research by mastering the use of chemistry and, chemical and biochemical engineering disciplines within major research fields such as: chemical kinetics and catalysis, process simulation and control, process integration and development, reaction engineering, thermodynamics and separation processes, oil and gas technology, combustion technology, polymers science, aerosols physics, mathematical modeling, and our newly established field of chemical, biochemical and pharmaceutical product design. The graduate students' individual works contribute significantly to the department's research activities, and is a factor that allows the department to continue to be among the leaders in its focused research areas.

It is with great pleasure that I present to you:

The Chemical Engineering Graduate Schools Yearbook 2004

Kim Dam-Johansen

Professor, Head of Department

**Michael Andersen**

Address: Høstvej 1B, 2800 Kgs. Lyngby
Phone: +45 4525 3136
Fax: +45 4593 2399
e-mail: manders@fysik.dtu.dk
www: www.icat.dtu.dk

Supervisor(s): Ib Chorkendorff
Søren Dahl, Haldor Topsøe A/S

Ph.D. Study
Started: September 2002
To be completed: September 2005

PM-IRRAS as an *in situ* Method for Investigations of Reactions Of Relevance for Fuel Cells

Abstract

In order to perform *in situ* measurements during heterogeneous reactions, such as water gas shift and methanol reforming on Pt(111) an existing Ultra High Vacuum (UHV) chamber has been rebuilt and expanded with a new High Pressure Cell (HPC), which allows us to perform Polarization Modulation Infrared Reflection Absorption Spectroscopy (PM-IRRAS). This system has been used to examine the isotopic exchange reaction of CO adsorbed on Pt(111) and CO adsorption on Pt(111) under elevated partial pressures of CO and H₂. The next reaction to be examined is the reforming of methanol on Pt(111).

Introduction

We employ PM-IRRAS as an *in situ* tool for measurements of reactions on model catalyst surfaces. This method is based upon the fact, that if a plane metal surface is illuminated by p- or s-polarized infrared light at near grazing incidence, around 82°, only p-polarized light can be absorbed by vibrational and rotational excitation of adsorbates, as the electrical component of s-polarized light will vanish due to destructive interference. In PM-IRRAS a fast modulation between s- and p-polarized light combined with electrical filtering and demodulation makes it possible to extract the reflectivities ($R_p - R_s$) and ($R_p + R_s$) of the sample. By taking the ratios between these, the absorption by adsorbates on the sample can be distinguished from gasphase absorption [1].

Specific Objectives

The idea behind this Ph.D. project is to investigate the poisoning mechanism in fuel cells such as the Polymer Electrolyte Membrane Fuel Cell (PEMFC) and the Direct Methanol Fuel Cell (DMFC). The key parameters are the nature of the poisoning adsorbates and the dynamics of the system. In this field results from *in situ* methods such as PM-IRRAS are needed, both from the viewpoint of understanding the fundamental mechanisms and for developing better and more resistant catalysts. To meet this lack of results an existing UHV chamber will be completely rebuilt and

fitted with a new HPC cell and a PM-IRRAS setup. Experiments will be done on platinum single crystals.

Experimental

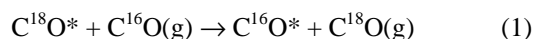
The apparatus used in this work consists of a UHV chamber and a High Pressure Cell (HPC), which can be separated from the main chamber by a high-pressure lock utilizing a Cu gasket. The UHV chamber works at a base pressure of 10⁻¹⁰ mbar and is equipped with the standard UHV methods X-ray Photoelectron Spectroscopy (XPS), Low Energy Ion Scattering Spectroscopy (LEISS), Low Energy Electron Diffraction (LEED), Electron Energy Loss Spectroscopy (EELS) and a Quadrupole Mass Spectrometer (QMS).

The Pt single crystal has the (111) orientation and is cleaned in 10⁻⁶ mbar O₂ at 773 K for 5 minutes followed by argon sputtering at 1273 K for 5 minutes and annealing at 1273 K for 2 minutes. When the crystal was heavily contaminated this procedure was repeated, until XPS and Low Energy Ion Scattering Spectroscopy LEISS showed no sign of impurities.

Isotopic Exchange of CO Adsorbed on Pt(111)

The adsorption of CO on Pt(111) in UHV and under elevated pressures of H₂ and CO has been studied, and the exchange reaction seen in equation 1 was examined [2]. First the Pt(111) sample was exposed to the sample to 6 L C¹⁸O, thereby achieving a coverage θ of 0.5. Then the sample was exposed to a pressure of

unlabeled CO and PM-IRRAS spectra were obtained during exposure.



* Denotes an adsorption site

Figure 1 shows a series of PM-IRRAS spectra obtained during exposure of the sample to $1.2 \cdot 10^{-6}$ mbar unlabeled CO.

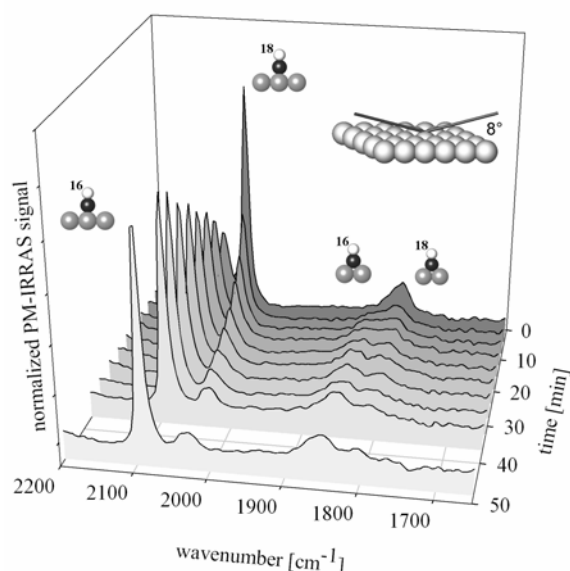


Figure 1 – PM-IRRAS spectra taken during exposure of a Pt(111) surface covered with C^{18}O and then exposed to $1.2 \cdot 10^{-6}$ mbar unlabeled CO

It is seen that both on-top and bridge site adsorbed CO is exchanged during the experiment. Quantification from these PM-IRRAS experiments is difficult, as dipole-dipole interaction leads to intensity borrowing effects. Therefore a series of experiments were conducted, wherein the precovered crystal was exposed to a fixed CO pressure for known periods of time.

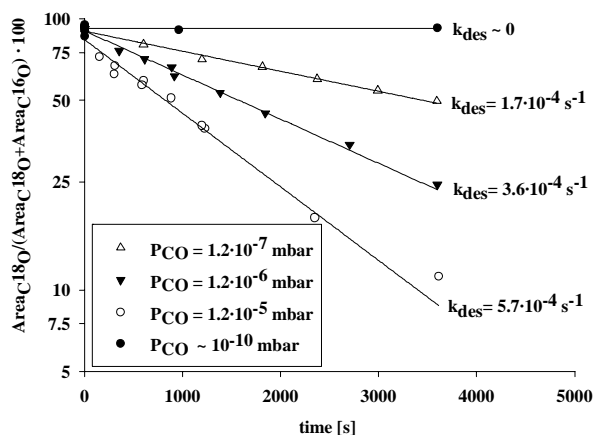


Figure 2 – CO areas measured by TPD after varying exposure times. The solid lines are obtained by fitting to the 1. Order desorption equation

Afterwards the coverages of C^{18}O and C^{16}O were measured with Temperature Programmed Desorption (TPD), the results can be seen in figure 2. By fitting to a first order desorption equation, the rate constants seen in figure 3 was calculated. In comparison with rate constants obtained from Pt nanoparticles on a carbon support [3], it was found seen that significantly lower CO partial pressures are needed to obtain similar rate constants for the Pt(111) surface. We speculate that this could be due to a continuous increase in CO coverage on Pt(111) with rising CO partial pressure, this pressure dependency has been confirmed with scanning tunneling microscopy[4]. On a Pt nanoparticle the CO coverage will be quantized, this could explain the higher CO pressures needed to obtain a significant exchange rate.

Methanol Reforming

Equation 1 shows the methanol reforming reaction:



Studies done on methanol synthesis on copper have shown that formate is the predominant surface species. PM-IRRAS studies could be very useful to identify the surface species and the reaction-limiting step in methanol reforming.

Results

The UHV chamber has been rebuilt and the PM-IRRAS equipment has been tested. The first system to be investigated was CO-Pt(111). Initial experiments on the methanol reforming process have been done.

Acknowledgements

We thank STVF for financing the rebuilding and purchasing of new equipment through the ‘‘Towards the Hydrogen Society’’ research programme.

References

1. T. Buffeteau, B. Desbat, J. M. Turlet, App. Spectrosc. 45 (3) (1991) 380-389.
2. M. Andersen, M. Johansson, I. Chorkendorff. In preparation.
3. J.C. Davies, R.M. Nielsen, L.B. Thomsen, I. Chorkendorff, Á. Logadóttir, Z. Lodziana, J.K. Nørskov, W.X.Li, B.Hammer, S.R. Longwitz, J. Schnadt, E.K. Vestergaard, R.T. Vang, F. Besenbacher, Fuel Cells, 4, (2004) 1-11.
4. S.R. Longwitz, J. Schnadt, E.K. Vestergaard, R.T. Vang, E. Lægsgaard, I. Stensgaard, H. Brune, F. Besenbacher, J.Phys.Chem.B, 108 (38) (2004) 14497-14502.



Anders Andreassen
Address: Materials research department, Risø National Laboratory, Frederiksborgvej 399, DK-4000 Roskilde, Denmark.
Phone: +45 4677 5776
Fax: +45 4677 5758
e-mail: anders.andreassen@risoe.dk
www: www.risoe.dk/afm/personal/andr/andr.htm

Supervisor(s): Ib Chorkendorff
Allan Schrøder Pedersen, Risø
Flemming Besenbacher, Aarhus University
Søren Dahl, Haldor Topsøe A/S

Ph.D. Study
Started: October 2002
To be completed: October 2005

Improved Resistance Towards Oxygen Contamination of Magnesium: Alloying with Al and Cu

Abstract

The main objective for this Ph.D. project is to explore new metals and alloys for hydrogen storage. In this study the effect of alloying with Al and Cu on the dehydrogenation kinetics of air exposed MgH_2 have been investigated. Compared to pure Mg we find a significant lowering of the apparent activation energy for dehydrogenation of both Mg-Al and Mg-Cu hydrides. This leads to the suggestion that the resistance towards oxygen contamination of Mg is improved by alloying with Al and Cu.

Introduction

The main topic of this Ph.D. project is to prepare and characterize new metals and alloys for hydrogen storage. Until now the focus have been on magnesium-based alloys.

Magnesium has a high theoretical hydrogen capacity of 7.6 wt. % H_2 . Thus fulfilling the DOE year 2010 target with respect to hydrogen density [1]. However, thermodynamics and kinetics dictate heating to above 300°C for hydrogen desorption. This has induced an extensive research in improving both kinetics and thermodynamic properties. In particular alloying with both transition and non-transition metals e.g. Al, Cu, Ni, Fe, Co, Mn [2,3] have been investigated. The price being reduced hydrogen capacity. Further, magnesium oxidizes readily when exposed to air [4]. Thereby creating a thin MgO surface layer retarding the transport of H-atoms [5-7] effectively limiting the kinetics.

In this yearbook a study on the effect of alloying Mg with Al and Cu on dehydrogenation kinetics of air-exposed samples is presented. Both pure Mg and Mg-Al and Mg-Cu alloys have been investigated with *in situ* time resolved X-ray powder diffraction (XRPD). From diffraction data phase fractions vs. time are derived i.e. kinetic information. By model fit apparent activation energies for dehydrogenation are extracted.

Experimental

The Mg-Cu and Mg-Al alloys subject to our investigations were prepared by arc melting stoichiometric amounts of magnesium and alloying element according to the composition $\text{Mg}_{17}\text{Al}_{12}$ and eutectic Mg/Mg₂Cu (approx. 85 atomic % Mg) in an Edmund Buhler Arc Melting system. The alloyed samples were melted repeatedly in an Argon atmosphere until the sample appeared homogeneous. Subsequently, the samples were ball milled for 10 min using WC balls. Magnesium powder was used as received from Sigma-Aldrich.

All samples were initially hydrogenated in a Sartorius high-pressure balancing unit described in detail elsewhere [8]. The samples were hydrogenated by applying a hydrogen pressure (99.9997 % purity from Air Liquide) of approx. 6-30 bar and a temperature in the range $350\text{-}400^\circ\text{C}$. The hydrogen uptake was determined by measuring the weight gain of the sample.

The X-ray instrument used for time resolved *in situ* XRPD was built around a Rigaku rotating anode (Cu K_α radiation, $\bar{\lambda} = 1.5418 \text{ \AA}$, 50 kV and 300 mA). The intensity of the diffracted beam was recorded with a curved position sensitive detector, INEL CPS 120, covering 120° in 2θ with a resolution of ca. 0.03° . The acquisition time per powder pattern was chosen to be in the range 45-150 s.

The *in situ* reactor cell have been described in detail by Clausen *et al.* [9]. The powder samples were loaded between plugs of quartz glass wool in a quartz capillary tube (0.7 mm O.D.) in order to fix the bed and allow a gas flow (Ar, 10 mL/min) through the sample during data acquisition. The samples were heated by a stream of hot nitrogen gas (20°C/min) to a constant temperature in the range 350-400 °C and the dehydrogenation was followed under isothermal conditions.

All samples were exposed to air at ambient conditions in between hydrogenation and XRPD experiment.

Results and discussion

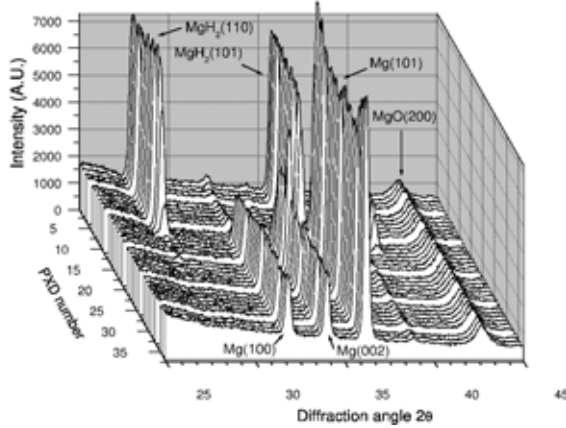


Figure 1 Time resolved *in-situ* powder X-ray diffraction of dehydrogenation of MgH_x ($x \approx 2$). A stack of 40 consecutive diffraction patterns measured at $T = 390^\circ\text{C}$ and with acquisition time $t = 182$ s.

Figure 1 shows *in situ* diffraction data for the dehydrogenation of pure MgH_2 . From the figure complete dehydrogenation is accomplished evident from the disappearance of the MgH_2 (110) and (101) reflections. Upon dehydrogenation Mg is formed evident from the appearance of Mg (110), (002) and (101) reflections. Further, the presence of a constant amount of MgO is noticed.

Figure 2 visualizes the dehydrogenation of MgH_2 -Al formed by hydrogenation (disproportionation) of the initial Mg-Al alloy. Simultaneous disappearance of both the MgH_2 and Al phase is observed. During dehydrogenation a Mg-Al alloy is reformed.

For the MgH_2/Mg_2Cu sample we observe no changes in the Mg_2Cu phase during dehydrogenation.

Normalized phase fractions, α , as a function of time for all three samples and all applied temperatures are determined by numerical integration using a natural spline interpolation/integration by Simpson's 1/3 rule algorithm in octave¹ of the (110) peak of MgH_2 using the following equation

$$\alpha_{MgH_2} = \frac{I_i - I_{\min}}{I_{\max} - I_{\min}}$$

I_i is the integrated intensity of the (110) peak in powder pattern number i and I_{\min} and I_{\max} is the minimum and maximum observed intensity of the (110)

peak, respectively. The background intensity is estimated by, I_{\min} , when the sample is assumed to be completely dehydrogenated.

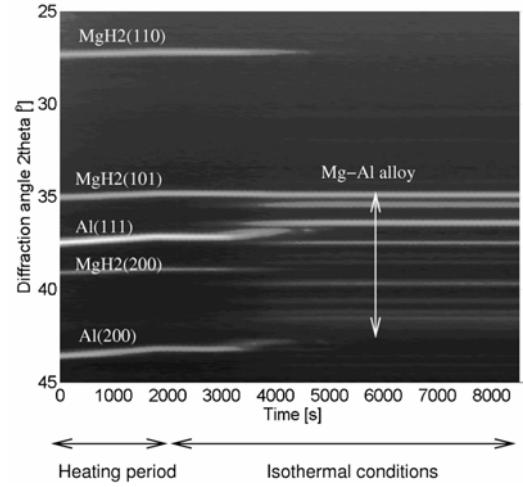


Figure 2 Time resolved *in situ* XRPD of the dehydrogenation of MgH_2 +Al. The graphic consists of 72 consecutive diffraction patterns stacked chronologically from left to right. Bright areas correspond to a high detector count rate (reflections), whereas dark areas correspond to low detector count rates (background). The isothermal reaction temperature is $T=400^\circ\text{C}$ and acquisition time is $t=150$ s.

Figure 3 shows phase fraction of MgH_2 in MgH_2/Mg_2Cu as a function of time calculated as outlines above for 4 different temperatures. A clear correlation between temperature and time of dehydrogenation is found resulting in faster dehydrogenation as the temperature is increased.

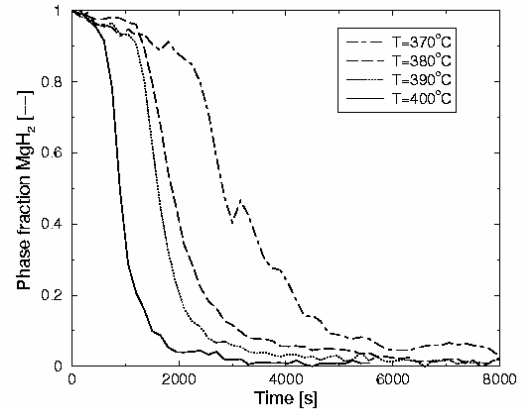


Figure 3 Phase fraction of MgH_2 as a function of time for dehydrogenation of Mg/Mg_2Cu . Phase fractions are derived from numerical integration of the MgH_2 (110) peak.

Rate constants for dehydrogenation are extracted by fitting a JMA type kinetic expression [10]

$$\alpha(t) = 1 - \exp(-(kt)^n)$$

to the calculated phase fractions as a function of time, where k is the rate constant assumed to be on Arrhenius form and n is the Avrami exponent often interpreted as the dimensionality of growth. By extracting rate constant as a function of temperature for all three samples an Arrhenius plot can be constructed (see figure 4). The apparent activation energy, E_A , of all three samples is found by linear regression. For pure Mg we find an apparent activation energy of 296 kJ/mol, for Mg-Al we

¹ GNU Octave is a high-level language, primarily intended for numerical computations. Available from <http://www.octave.org>

find $E_A = 160$ kJ/mol, and for Mg/Mg₂Cu $E_A = 137$ kJ/mol.

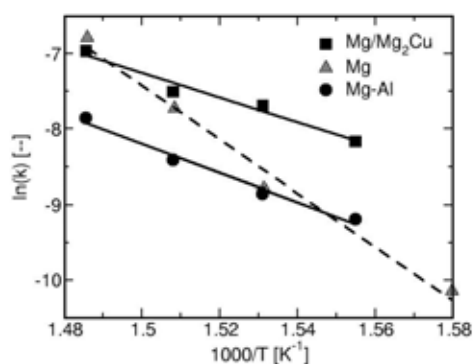


Figure 4 Arrhenius plot for dehydrogenation rate constants derived from a JMA fit for Mg, Mg/Mg₂Cu, and Mg-Al.

The Arrhenius analysis clearly shows a significant reduction in the dehydrogenation apparent activation energy upon alloying. Apparent activation energies for dehydrogenation of pure magnesium hydride are usually in the range 120-160 kJ/mol for *activated*² samples [11-13]. In figure 5 reported apparent activation energies for both activated and non-activated samples are compared. Alloyed samples are also included. There seems to be a trend of higher activation energies for the non-activated samples. This may be explained in terms of a MgO layer retarding the kinetics of the non-activated samples due to poor diffusion in MgO [5-7]. Interesting the air-exposed (non-activated) alloyed samples compare well with fully activated samples of pure Mg. The explanation probably relies on the fact that alloying with Cu and Al produces a compound less sensitive towards oxygen contamination; no crystalline MgO was found in the air-exposed samples by X-ray powder diffraction. Furthermore, it has also been suggested by Karty et al. [14] that the presence of Mg₂Cu provides an oxide free surface and favorable hydrogen diffusion paths. Effectively, the result of alloying with Al is the same as for Mg₂Cu, although the physical explanation is likely different, since the marginal stability of the Mg-Al (Andreasen *et al.* ref. 6 in publication list) alloys does not block oxide formation. Having both Al and Mg present in the surface layers, the formation of alumina, Al₂O₃, and MgAl₂O₄ spinel is possible [15]; both structures are substantially less dense than MgO and have good hydrogen diffusion channels.

² The term *activated* implies that the sample is hydrogenated/dehydrogenated for several cycles prior to kinetic measurements. The activation process covers different phenomena and includes penetration of the natural oxide layer on as-prepared samples (if previously exposed to air), followed by complete hydride formation, which leads to cracking of the particles, due to the expansion associated with the hydrogenation process combined with the brittle nature of most metal hydrides [3]. During the first hydrogenation/dehydrogenation cycles, the reaction rate increases due to the creation of fresh contamination-free surface and/or smaller particles (higher surface area and shorter diffusion paths) until a steady-state is reached.

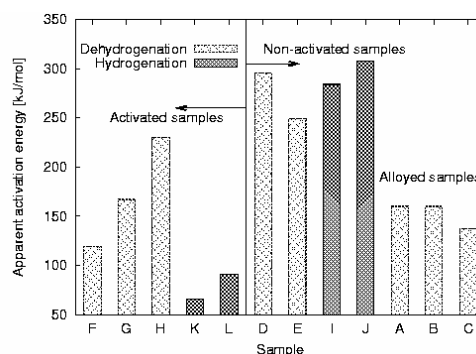


Figure 5 Apparent activation energies for Mg-based hydrides from literature review. See Andreasen *et al.* ref. 1. in publication list for detailed references.

Conclusions

Investigating the dehydrogenation kinetics of the hydrides of Mg, Mg-Al and Mg/Mg₂Cu by means of *in situ* time-resolved powder X-ray diffraction we find an apparent activation energy for dehydrogenation of air-exposed, non-activated MgH₂ of 296 kJ/mol.

Alloying with both Al and Cu leads to a significant lowering of the apparent activation energy of dehydrogenation to 160 kJ/mol and 137 kJ/mol, respectively, comparable to fully activated samples. We propose that this is, at least partially, due to the samples becoming more resistant towards oxygen contamination (MgO formation) upon alloying.

Acknowledgements

Financial support from the Center of Excellence “Towards the hydrogen based society”, through a research grant from The Danish Technical Research Council. The following people are greatly acknowledged for contributing to the experimental work presented in this article: Martin M. Nielsen, Jens W. Andreasen, and Nini Pryds (Risø), Robin Christensen, Alfons Molenbroek (Haldor Topsøe A/S), Torben R. Jensen, Ronni Burkarl, Bitten Møller, and Morten B. Sørensen (Aarhus University).

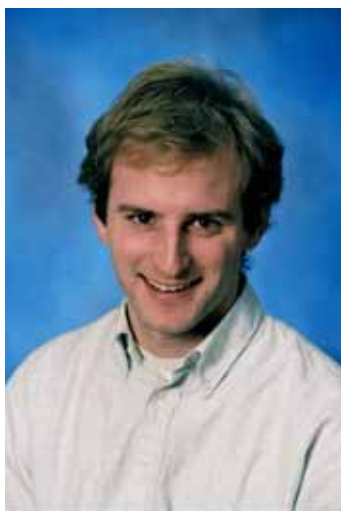
Reference

1. http://www.eere.energy.gov/hydrogenandfuelcells/mypp/pdfs/3.3_storage.pdf
2. <http://hydpark.ca.sandia.gov/>
3. L. Schlapbach, , Ed.; Hydrogen in Intermetallic Compounds II; volume **67** of *Topics in Applied Physics* Springer-Verlag: 1992.
4. V. Fournier, P. Marcus, I. Olejrod, *Surf. Interface Anal.* **34** (2002) 494-497.
5. R. Gonzalez, Y. Chen, K.L. Tang,, *Phys. Rev. B.* **26** (1982) 4637-4645.
6. T. Vegge, *Phys. Rev. B.* **70** (2004) 035412.
7. J. Töpler, H. Buchner, H. Säufferer, K. Knorr, W. Prandl, *J. Less-Common Met.* **88** (1982) 397--.
8. A. S. Pedersen, J. Kjøller, B. Larsen, and B. Vige-holm. *Int. J. Hydrogen Energy*, **8(3)** (1983) 205-211.

9. B. Clausen, G. Steffensen, B. Fabius, J. Villadsen, R. Feidenhans'l, *J. Catal.* **132** (1991) 524--.
10. C. H. Bamford, C. F. H. Tipper, Eds.; Reactions in the solid state; volume **22** of *Comprehensive chemical kinetics*, Elsevier, 1980.
11. J. Han, M. Pezat and J.-Y. Lee, *J. Less-Common Met.* **130** (1987) 395-402.
12. P. Tessier, E. Akiba, *J. Alloys Comp.* **302** (2000) 215-217.
13. J. F. Fernandez, C. R. Sanchez, *J. Alloys Comp.* **340** (2002) 189-198.
14. A. Karty, J. Grunzweig-Genossar, P. Rudman, *J. Appl. Phys.* **50** (1979) 7200--.
15. Y. L. Shoshin, R. S. Mudryy, E. L. Dreizin, *Combust. Flame* **128** (2002) 259-269
4. H. Lynggaard, A. Andreasen, C. Stegelmann, P. Stoltze, *Prog. Surf. Sci* **77** (2004), 71-137.
5. T.R. Jensen, A. Andreasen, T. Vegge, A.S. Pedersen, F. Besenbacher, A.M. Molenbroek. In: *Book of abstracts. International symposium on metal-hydrogen systems*, H. Figiel, P. Mietniowski, A. Paja (eds.), Crakow (2004).
6. A. Andreasen, J.W. Andreasen, R. Burkarl, B. Møller, M. Sørensen, M.M. Nielsen, A.M. Molenbroek, T.R. Jensen, In: *Book of abstracts. International symposium on metal-hydrogen systems*, H. Figiel, P. Mietniowski, A. Paja (eds.), Crakow (2004).
7. J.W. Andreasen, A. Andreasen, R. Christensen, A.M. Molenbroek, R. Feidenhans'l. In. *HASYLAB annual report 2003*. Part 1. (2004).

Publications

1. A. Andreasen, T. Vegge, A.S. Pedersen, *J. Phys. Chem. B.* (2004) Accepted.
2. A. Andreasen, J.W. Andreasen, R. Burkarl, B. Møller, M. Sørensen, M.M. Nielsen, A.M. Molenbroek, T.R. Jensen, *J. Alloys. Comps.* (2004) In review.
3. A. Andreasen, Risø-R-1484, (2004).
<http://www.risoe.dk/risub/AFM/ris-r-1484.htm>
8. A. Andreasen, In. *Graduate school yearbook 2003*, K. Dam-Johansen, M.S. Skjøth-Rasmussen (eds.), Depat. Chem. Eng., Technical University of Denmark (2004) 5-7.
9. A. Andreasen, H. Lynggaard, C. Stegelmann, P. Stoltze, *Surf. Sci.* **544** (2003) 5-23.



Loïc d'Anterroches

Address: CAPEC Building 227 Office 266
Phone: +45 4525 2911
Fax: +45 4593 2906
e-mail: loa@kt.dtu.dk
www: <http://www.capec.kt.dtu.dk>

Supervisor(s): Rafiqul Gani

Ph.D. Study

Started: September 2002
To be completed: August 2005

Group Contribution Based Process Flowsheet Synthesis, Design and Modelling

Abstract

The core idea is to apply the group contribution approach for property estimation to the synthesis, design and modelling of a flowsheet, with groups (or atoms, etc.) representing units, bonds representing streams, rules for molecule feasibility representing flowsheet feasibility and sum of group contributions representing the performance of the flowsheet.

Introduction

Modelling and simulation of a chemical process usually involve identifying the structure of the flowsheet representing the process, deriving model equations to represent each operation, and solving the resulting total model equations according to one of various available simulation strategies. The flowsheet synthesis problem determines the type of operations and their sequence needed to achieve the conversion of raw materials to some specified set of products. The flowsheet design problem determines the optimal values for the conditions of operation and other operation/equipment related variables for the synthesized flowsheet. The flowsheet modelling, synthesis and design problems are related since for generation and screening of alternatives, some form of flowsheet models are needed. Also, flowsheet models are needed for verification of the synthesis/design problem solution.

In contrast, a group-contribution (GC) based pure component property estimation of a molecule requires knowledge of the molecular structure and the groups needed to uniquely represent it. The needed property is estimated from a set of *a priori* regressed contributions for the groups representing the molecule. Having the groups and their contributions together with a set of rules to combine groups to represent a molecule, provides the possibility to “model” the molecule and/or a mixture of molecules. This also means that the reverse problem of property estimation, i.e., the design or synthesis of molecules having desired properties can be solved by generating chemically feasible molecular structures and testing for their properties. This reverse

problem is also known as computer aided molecular design (CAMD) (Achenie et al. 2002).

Let us now imagine that each group used to represent a fraction of a molecule could also be used to represent an operation in a process flowsheet. Just as in chemical property estimation, groups may have one or more free attachments, in process flowsheet “property” estimation, PGs may also have similar number of free attachments, for example, connecting streams. In this way, a set of PGs representing different types of operations may be created and the “properties” of a particular process flowsheet may be estimated by first identifying the PGs that will uniquely represent it and then by computing their contributions to the needed “property”.

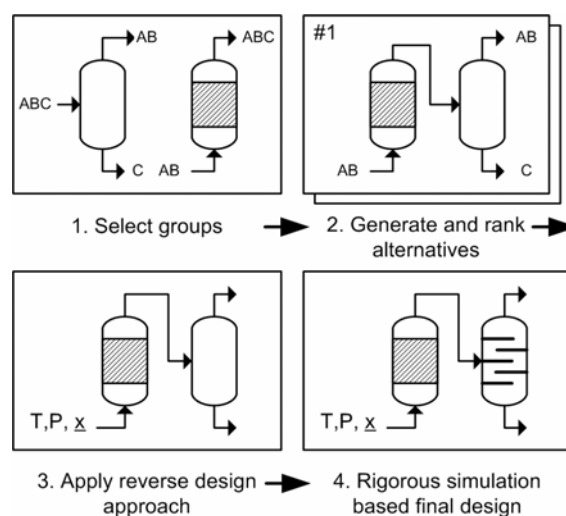


Figure 1. Overview of the framework

Consequently, chemical process synthesis/design problems can be solved through a CAMD-like approach as shown on the general overview of the method (see Figure 1.). It extends the PG-based method for distillation trains (Anterrosches and Gani 2004a) to include new cyclic azeotropic PGs, reactor PGs and mixer PGs within a generic computer aided flowsheet design (CAFD) approach.

Flowsheet Modelling and Design through Process-groups

To apply a group contribution method for flowsheet synthesis, design and modelling the following has been developed: rules for PG representation of flowsheets, a “property” model for separation process flowsheets and a reverse-model based method for flowsheet synthesis/design.

Definitions (Anterrosches and Gani 2004b)

Process-group (PG) - A PG is the representation of one or more unit operations. It has at least one inlet stream and one outlet stream as connections.

Structure or flowsheet structure - A structure or a flowsheet structure is defined as the ensemble of process-groups and the connections between the process-groups.

Flowsheet or process - A flowsheet or process provides details of the flowsheet structure and the corresponding flowsheet (design/operations) parameters such as stream composition, flowrate, pressure, temperature so that all the needed information for a process are available.

Flowsheet property - A flowsheet property is any property that provides a measure of the performance of the operations in the flowsheet and can be expressed as a function of the contributions of one or more unit-operations representing it.

Process-group representation of a flowsheet

Consider a simple process for the reaction of two components A and B to a third component C, which forms an azeotrope with B. The feed mixture is represented by inlet PGs (groups with one attachment), such as (iAB). The end-products (also groups with one attachment) are outlet PGs, such as (oC) (a pure product or purity $\geq 98\%$). An operation or a set of operations can be represented by a PG having at least one attachment that can be connected to an inlet PG and one attachment that can be connected to an outlet PG, such as (rAB/pABC) – a reactor PG, with A and B as reactants and A, B and C as products or (A/BC) – a separation PG, with A, B and C as inlet and pure A and a BC mixture as outlets. According to the combination rules of PGs (Anterrosches and Gani 2004a) and rules for

joining molecular CGs, an outlet of a PG can be connected to the inlet of another PG.

From the list of available PGs like (iAB), (oC), (rAB/pABC), (A/BC), etc., a feasible flowsheet structure can be created as shown in figure 2, where a reaction between A and B takes place forming a third component C, with C and B forming an azeotropic mixture. The products are separated first through a simple distillation column and then by a solvent based separation (represented by a cyclic azeotropic PG). The unused reactants are recycled back to the reactor. As in GC-based molecular property estimation (where the same groups may represent many molecules), the PGs are not component dependent, but component property dependent, thus the ability to use the same group with different components having similar properties.

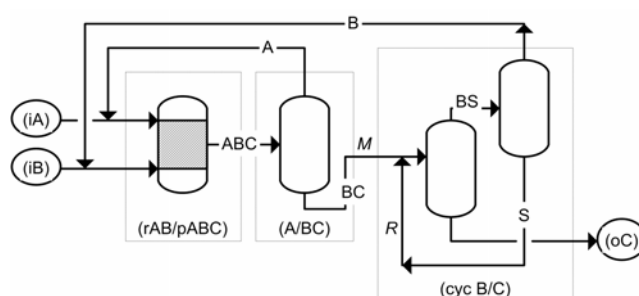


Figure 2. Simple process-group flowsheet representation

Reverse problem formulation

The driving force of component i with respect to component j , D_{ij} , in any operation involving reaction or separation can be modelled through modified driving force expression,

$$D_{ij} = \frac{x_i \beta_{ij}}{1 + x_i (\beta_{ij} - 1)} - x_i = y_i - x_i$$

where x_i and y_i are compositions of component i in two co-existing phases (for separation) or reactant and product (for reaction), respectively. β_{ij} is an adjustable parameter that may be a constant (for example, a constant relative volatility in the case of vapour-liquid separations) or a function of composition (in the case of an azeotropic mixture) or a function of reaction rates (in the case of a reacting system). A set of measured or predicted values of \underline{x} and \underline{y} provides the data needed to obtain the driving force model (Eq. 1). As Bek-Pedersen (2004) pointed out, as $D_{ij} \rightarrow 0$, no operation is possible while as $D_{ij} \rightarrow large$, operation becomes easy. Also, properties, $\underline{\theta}$, can be identified, which is inversely or directly proportional to D_{ij} . $\underline{\theta}$ is a vector of properties that are needed to maintain D_{ij} , for example, energy is needed to maintain a VLE system, solvent to break an azeotrope, or catalyst/reagent to promote a reaction.

A flowsheet property model

For operations involving two phases (vapour and liquid) the property needed to maintain D_{ij} of any separation is

heat added to the system. This flowsheet “property” has been modelled (Eq. 2) as the energy index E_x of a flowsheet.

$$E_x = \sum_{k=1}^{n=NG} Q_k = \sum_{k=1}^{n=NG} \left(\frac{1+p_k}{d_{ij}^k} \times a_k + A \right)$$

where E_x is the energy index of the flowsheet given in MkJ/hr, for a reference mass flowrate, Q_k is the total contribution of each PG, NG is the number of PGs, p_k the topology factor, $d_{ij}^k = D_{ijmax} = \overline{D}_i$ the maximum driving force of the k^{th} PG, a_k the contribution of the k^{th} PG and A a constant different for each type of PG.

$$p_k = \sum_{i=1}^{nt} \overline{D}_i$$

where nt is the number of tasks that should be performed before the task k in the ideal case and \overline{D}_i the driving force of task i . This topology factor, p_k , is a function of the attainable driving force, which is the D_{ij} actually used.

The contribution of the PG parameters, a_k , are normally regressed from experimental data. In the case of a cyclic azeotropic PG, a_k is a function of the internal recycle flow of the solvent. Every unit operation has a position in the flowsheet where it can “attain” the theoretical maximum driving force d_{ij}^k . At any other position, the unit operation will attain a lower driving force than the maximum. The reverse approach identifies d_{ij}^k and tries to find designs, if available, that matches (attain) this identified maximum.

Flowsheet structure evaluation

After the synthesis of feasible flowsheet structures through a CAMD like approach (Anterrosches and Gani 2004a), the property of the structures are easily calculated by application of models described by Eq. 2. The evaluation of the properties of the flowsheet structure is similar to the “test” step in CAMD. The property value is used in a qualitative sense to select the best or the set of best alternatives to a given process synthesis/design problem. At this stage of the design process, it is not necessary to perform mass and/or energy balance calculations with the PG-based method. In step 3 (see Fig. 1), from the PGs and their connections, it is possible to perform simple mass balance and/or energy balance calculations through a shortcut method (Anterrosches and Gani 2004b) in order to establish the set of primary design variables of the generated process flowsheet. This set of design variables represent the minimum number of variables through which a process flowsheet can be completely described (or in other words, all other secondary design variables can be calculated from these). The evaluation of a flowsheet property is performed in virtually no computer time as the calculations have the same level of complexity as the traditional GC methods for molecular property estimation. Therefore, it is possible

to screen a very large number of flowsheet alternatives very rapidly and with few calculations.

Results

The results presented here highlight the use of an extended set of models and process-groups. In particular, results related to the development and use of cyclic azeotropic PGs are presented.

Cyclic azeotropic PG creation

A new cyclic azeotropic PG has been derived from analysis of azeotropic mixtures to handle solvent based separations. The plots of D_{ij} as a function of solvent rate (see Fig 3), the solvent free d_{ij}^k between Acetone and Chloroform increases as a function of the amount of solvent used. Note that they also depend on the type of the solvent.

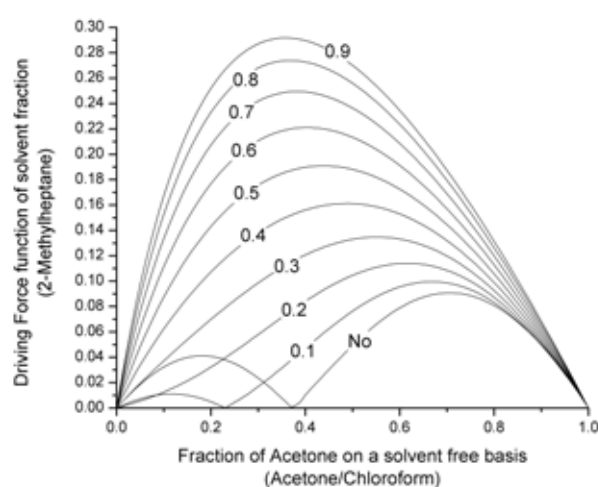


Figure 3. Solvent free driving force

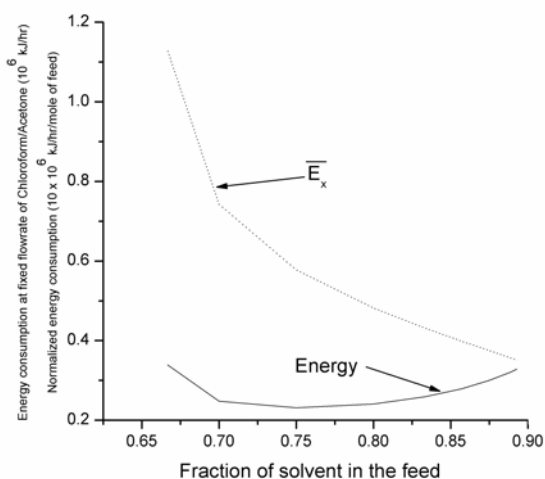


Figure 4. Energy and normalized energy function of solvent fraction

Considering the flowsheet of a solvent based separation (see cyc B/C) in Fig. 2), at a given total flowrate $M+R$, the energy index of the separation is inversely proportional to D_{ij} , which as Fig. 3 shows, is related to the amount (recycle R) and type of solvent (note that

different solvents may match the same D_{ij} curve). Thus the total contribution of the solvent based cyclic azeotropic PG, Q_k , can be expressed as:

$$Q_k = \frac{a_k(R)}{d_{ij}^k(R)}$$

Where $a_k(R)$ is the adjustable parameter a_k of the property model (Eq. 2) represented now as a function of recycle flow R , while, $d_{ij}^k(R)$ is the attainable D_{ij} represented as a function of R .

As in the development of any GC-based method for molecular property prediction, the parameters $a_k(R)$ and $d_{ij}^k(R)$ have been regressed through fitting experimental data. For the purposes of this work, a set of simulations with different recycle flowrate R has been performed to generate the pseudo experimental data.

Design/Simulation results

Consider the separation of Acetone/Chloroform into two pure products, which can be performed with a solvent based separation using a cyclic azeotropic (cyc B/C) PG. A target driving force of 0.33 is selected. Applying CAMD, a list of candidate solvents have been generated, from which, we find that the following two solvents, Benzene and 2-Methylheptane, match this target can be used. The target d_{ij}^k of 0.33 can be attained with a 2-Methylheptane fraction of 0.7 (we use 2-Methylheptane as it is environmentally more acceptable than benzene) with a reference mass flowrate for the recycle R of 2.33 kmole/hr. Through Eq. 4, the values of Q_k and R needed to match the target d_{ij}^k is obtained. Note that selection of solvent and R also fixes $a_k(R)$. The energy index $E_x = 0.138$ is now directly available. At this stage the reverse design approach (step 3, Fig. 1) is performed to obtain the flowrate, temperature, pressure and composition of all the streams using the generated design specifications of the 2 columns in the (cyc B/C) PG. Bek-Pedersen and Gani (2004) provides the needed reverse algorithm. The primary design variables for each column are, reflux, number of stages, feed stage location and top product purity. Using these results as an initial estimate, the final (optimal) design based on rigorous simulation is easily obtained. Figure 4 shows the calculated plots of energy consumption for acetone-chloroform separation as a function of solvent fraction in the feed calculated by rigorous simulation. The results confirm the primary design and that \bar{E}_x decreases with an increase of d_{ij}^k . The choice of 0.7 for solvent fraction matches quite closely to the rigorous simulation based optimum solution. The regressed tables of all PGs together with the detailed results from this example and other examples involving reactor PGs can be obtained from the authors.

Conclusion

The paper has presented a CAMD-like concept of PG contributions for process flowsheet property estimation, synthesis and design. This concept has been transformed

into a computer aided tool through the development of a set of PGs representing various types of operations typically found in chemical processes. Properties that may be used as a measure of performance of a process have been identified and modeled as a function of PGs. This has resulted in a CAMD-like approach for CAFD. Current and future work is preparing a set of industrial case studies applying the methodology.

References

1. L. Achenie, R. Gani, V. Venkatasubramanian, 2002, Computer Aided Molecular Design - Theory & Practice, Elsevier Science B.V., Computer Aided Chemical Engineering 12
2. L. d'Anterrosches, R. Gani, 2004, Group Contribution Based Process Flowsheet Synthesis, Design and Modelling, Computer Aided Process Engineering, 18 379-384
3. L. d'Anterrosches, R. Gani, 2004, Group contribution based process flowsheet synthesis, design and modelling, Fluid Phase Equilibria, Elsevier, Amsterdam.
4. E. Bek-Pedersen, R. Gani, 2004, Design and synthesis of distillation systems using a driving force based approach, Chemical Engineering and Processing, 43, 251-262

**Niels Bech**

Address: Bygning 229, DK-2800 Lyngby
Phone: +45 4525 2851
Fax: +45 4588 2258
e-mail: nsb@kt.dtu.dk
www: www.chec.kt.dtu.dk

Supervisor(s): Kim Dam-Johansen
Peter A. Jensen

Ph.D. Study

Started: September 2004
To be completed: August 2007

In-Situ Flash Pyrolysis of Straw

Abstract

Energy derived from straw remains a largely untapped energy resource offering a significant potential in the cereal-growing parts of the world. The main barrier for introducing straw to the energy market competitively is its higher cost relative to fossil fuels. The thermochemical process Flash Pyrolysis is capable of converting straw to an attractive liquid fuel. This project focuses on developing an ablative flash pyrolysis process specifically targeted for the production of heavy fuel substitute Bio-oil from straw.

Introduction

Bioenergy in the form of straw represents a significant energy source on a world-wide scale but is today largely unutilized. According to FAO [1], the aggregate world production of cereals including barley, mixed grains, oats, rye sorghum, triticale and wheat amounted to 814 million tons in 2003 of which wheat constituted close to 70%. Geographically, the most significant wheat production areas were Western Europe (17%), North America (16%), India (12%) and the former USSR (12%). Assuming a straw/grain ratio equivalent to the Danish average for 1994-1996 of 40% [2] and straw availability for energy to be 50%, these areas potentially have a virtually untapped energy reserve equivalent to 117 mill. tons (approx. 650 mill. barrels) of heavy fuel originating from wheat. For 2003, this amount of energy corresponded to 24 days of OPEC crude oil production (27 mill. barrels/day) [3] or a market value close to \$30 bill. For the net energy importing areas (i.e. North America, Western Europe and India), utilization of straw for energy production is thus a CO₂ neutral prospect to gain more independence from the historically less stable oil exporting regions.

Unfortunately, straw does not possess the attractive properties that crude-oil products do such as a relatively high volumetric energy content, good transportability, standardized specifications and simplicity in use. The result is that utilization of straw is only practiced under primitive conditions where it is readily available or where massive public subsidies or regulation warrant it. Apart from the unresolved problems in handling combustion of raw straw, the expense associated with

logistics (e.g. baling, storage and transport) is the single largest barrier for utilizing straw efficiently in competition with fossil fuels under free market conditions. Access to an uninterrupted supply of fuel is also of importance to energy consumers and accordingly, expenses arising from long-distance transport of straw-derived energy need to be insignificant compared to the value of the fuel itself in order to market the product successfully.

Specific Objectives

As suggested above, successfully unleashing energy production from straw commercially depends on optimizing collection and distribution systems and improving properties affecting costs associated with its combustion. Generally, liquid energy products are attractive in these areas and consumers are willing to pay a higher price for them relative to solid (e.g. straw) and gaseous (e.g. natural gas) fuels as they are less appealing due to the complications of utilization and transportation, respectively. Converting straw to liquid nearby its place of origin therefore appears advantageous, provided the costs for doing so are not prohibitive.

Flash pyrolysis is a thermochemical process which under conditions of medium temperature and short residence time converts organic materials to char, tar and gas. Tar, a homogeneous mixture of organics and water commonly referred to as Bio-oil, is a highly compressed energy carrier and may be used in the existing combustors and distribution systems for fossil heavy fuel, while gas can be utilized for process heat.

Table 1

Reported flash pyrolysis yields of main fractions in weight percent of feed on moisture free basis under specified process conditions. Results have been normalized, if needed, to obtain full mass balance closure. To obtain tar yield, add yields of organics and water. FB (fluid bed); AP (ablative plate); Mill (ablative pyrolysis mill); VRT (vapor residence time); MSW (municipal solid waste); PS (particle size); * water of reaction estimated (not reported in source).

| <i>Reactor</i> | <i>Organics</i> % | <i>Gas</i> % | <i>Char</i> % | <i>Water</i> % | <i>Temp.</i> °C | <i>VRT</i> <i>ms</i> | <i>Feedstock</i> | <i>Reactor</i> <i>Scale</i> | <i>PS</i> <i>µm</i> | <i>Source</i> |
|----------------|----------------------|-----------------|------------------|-------------------|--------------------|-------------------------|--------------------|--------------------------------|------------------------|---------------|
| FB ash | 40 | 30 | 20 | 10 | 500 | n.a. | MSW | Full size | <1200 | [4] |
| FB Sand | 60 | 17 | 18 | 5 | 520 | 540 | Wheat straw | Pilot | <595 | [5] |
| FB sand | 69 | 5 | 14 | 12 | 500 | 600 | Poplar | Pilot | <595 | [6] |
| Mill | 47 | 23 | 6 | 14* | 600 | 90,000 | Pine | Bench | 595-841 | [7] |
| FB sand | 45 | 15 | 29 | 11* | 473 | 8,100 | Fir | Batch lab | 300-425 | [8] |
| AP | 59 | 5 | 26 | 10 | 600 | 1,710 | Pine | Bench | <6250 | [9] |
| Cone | 54 | 32 | 14 | 12* | 600 | 330 | Pine | Bench | 200 | [10] |
| FB sand | 51 | 16 | 18 | 15 | 515 | 500 | Wheat chaff | Pilot | <1000 | [11] |
| FB sand | 66 | 11 | 12 | 11 | 504 | 500 | Poplar | Pilot | <1000 | [11] |
| FB sand | 45 | 18 | 29 | 8 | 550 | 500 | Wheat straw | Pilot | <250 | [11] |
| FB sand | 39 | 21 | 30 | 10* | 450 | 3,000 | Wheat straw | Bench | <1000 | [11] |
| FB sand | 65 | 10 | 13 | 12* | 430 | n.a. | Hardwood | Bench | <1000 | [11] |

For straw, the yields of Bio-oil, char and gas are approximately 50, 30 and 20% on dry weight basis (see Table 1). Straw is a relatively inexpensive material provided baling and transportation are not needed. This implies that capital cost is of higher importance for in situ conversion and the development of a high capacity compact reactor system is a cardinal point. Accordingly, the main objective of the project is to identify a suitable reactor system and optimize its performance.

Modelling and Experimental Work

Fluid bed and ablative reactors are the two principal technologies available for flash pyrolysis. In the former, biomaterial is introduced into a bed of hot fluidized inert material, usually sand. Although a well-known technology, fluid beds do have several disadvantages including the requirement for a large flow of inert gas for heat transport and fluidization, a relatively poor capacity/volume ratio and the need for small particle size feed. Therefore, the project focuses on developing and optimizing a novel ablative process for straw flash pyrolysis.

A model for flash pyrolysis of straw is being developed and validated by lab experiments. Based on the model, a reactor system will be developed and tested in pilot scale. Finally, produced Bio-oil is tested as replacement for heavy fuel in a burner test rig and a business plan for commercialization of the process developed.

Acknowledgements

The project is partly funded by DTU as part of the Innovation PhD Program and by the Nordic Graduate School in Biofuels Science and Technology.

References

1. FAOSTAT data, last accessed December 2004.
2. Handbook for Farm Management (Håndbog til driftsplanlægning), Landbrugsforlaget, Aarhus, 2003.
3. OPEC Annual Statistical Bulletin 2003, Organization of the Petroleum Exporting Countries, Vienna, 2004.
4. Chang, P.W., Preston, G.T. The Occidental Flash Pyrolysis Process. In: Sofer, S.S., Zaborsky, O.R. (eds.) Biomass Conversion Processes for Energy and Fuel, Plenum Press, New York, 1981, 173-185.
5. Scott, D.S., Piskorz, J. Can. J. Chem. Eng., 62, 1984, 404-412.
6. Liden, A.G., Berruti, F., Scott, D.S. Chem. Eng. Comm., 65, 1988, 207-221.
7. Reed, T.B. Principles and Operation of a Novel "Pyrolysis Mill". In: Thermochemical Conversion Program Annual Meeting, Solar Energy Research Institute, Golden, CO, 1988, 248-258.
8. Samolada, M.C., Vasalos, I.A. Fuel, 70, 1991, 883-889.
9. Peacocke, G.V.C., Bridgwater, A.V. Biomass and Bioenergy, 7, 1994, 147-154.
10. Wagenaar, B.M., Prins, W., van Swaaij, W.P.M. Chem. Eng. Sci., 49, 1994, 5109-5126.
11. Scott, D.S., Majerski, P., Piskorz, J., Radlein, D. A. J. Anal. Appl. Pyrolysis, 51, 1999, 23-37.



Suzan Biran

Address: Department of Chemical Engineering
Søltofts Plads, Building 229
Technical University of Denmark
DK-2800 Kgs. Lyngby

Phone: +45 4525 2920
Fax: +45 4588 2258
e-mail: sb@kt.dtu.dk
www: www.chec.kt.dtu.dk

Supervisor(s): Anker Jensen
Søren Kiil
Poul Bach, Novozymes A/S
Ole Simonsen, Novozymes A/S

Ph.D. Study
Started: September 2003
To be completed: August 2006

Stability of Enzymes in Granular Enzyme Products for Laundry Detergents

Abstract

Enzymes are important constituents in laundry detergents due to their contribution to a more effective and milder washing process (lower energy and water consumption, less wear of fabric). Storage stability of detergent enzymes is a significant quality parameter considered in the development of a new product. The complexity of the detergent matrix implies the presence of a complicated mechanism involved in the inactivation. It is believed that a combination of factors such as humidity, released H_2O_2 , autolysis of enzymes, high local pH in the granule, oxygen, defects in granulate structure and other detergent components plays a role in the activity loss. The aim of this project is to investigate the factors responsible for the inactivation of enzymes and propose new formulations and protective components for improved stability.

Introduction

Enzymes are used today in a wide range of industrial processes and in consumer products. The largest application of industrial enzymes is in detergents. The detergent industry absorbs about 45% of enzyme sales in western Europe and more than 25% of the total worldwide enzyme production [1]. After being produced by submerged microbial fermentation, enzymes are recovered and sold as either powder or liquid products for industrial use. In powdered laundry detergents, they are granulated and covered with a protective coating to prevent dust allergies and increase the stability of enzymes.

The main enzyme activity in biological laundry detergents is protease, which acts on organic stains such as grass, blood, egg and human sweat. However, it has become more common in recent years to include a "cocktail" of enzyme activities including lipases and amylases. Lipases are effective on stains resulting from fatty products such as oils and fats, while amylases help remove starchy food deposits. More recently, color enhancing and "anti-bobbling" washing powders have been developed which contain cellulases. The mode of action of such cellulases is to remove detached cellulose

fibrils, which cause a progressive dulling of the color as dirt is trapped on the rough surface of the fabric.

Laundry detergents typically consist of a mixture of separate granular materials including surfactants, builders, bleaching agents and enzymes. The surfactants are the main cleaning agent, while the builders provide alkalinity and ionic strength to the wash liquor. Bleaching agents are added to provide a white shine and remove stains on the fabric. A modern bleaching agent is Sodium Percarbonate (SPC), which decomposes in water and releases hydrogen peroxide, being the actual bleaching chemical. In addition to these, powdered laundry detergents contain soil anti-deposition polymers, anti-corrosion agents, perfumes etc.

Enzymes are fragile biomolecules. They can lose their activity in environments, like detergents, where harsh chemicals are present. In practice the enzymes lose a significant part of their activity over a time period of several weeks. To overcome this problem, manufacturers prefer to add more enzyme granules in their products to have satisfactory wash performance. However, this results in an increase in the production cost of the laundry detergent. Partly to obtain a better

stability during storage, the enzyme containing particles are typically coated by layers of salts, polymers and/or waxes. This reduces the rate of diffusion of aggressive species into the particles where reaction with the enzymes may cause deactivation. Furthermore, the particles are often formulated with anti-oxidants, such as thiosulfates, to minimize deactivation reactions. For the enzymes in laundry detergents, the deactivation is mainly related to the release of hydrogen peroxide from the bleaching chemicals in a moisture-containing atmosphere. Moreover, humidity, autolysis of enzymes, high local pH in granule, oxygen, defects in granulate structure and other detergent components are some of the factors affecting the granulate stability during storage.

The present understanding of inactivation mechanism of detergent enzymes during storage [2] involves diffusion of water vapor through bleaching particles, where SPC is “activated” and hydrogen peroxide is released. The subsequent diffusion of hydrogen peroxide vapor in the enzyme granule results in oxidation of methionine and tyrosine residues in the enzyme. The sulfur in methionine, found in the active site of Savinase (protease), can be oxidized to sulfoxide and further to sulfone by hydrogen peroxide. The fact that enzyme activity is reduced significantly even in non-bleach containing detergents implies that other mechanism(s) are also involved in deactivation of granulates.

Specific Objectives

The objective of this project is to understand the inactivation mechanism of detergent enzymes during storage. It is also aimed to investigate the effect of different detergent ingredients on the granulate stability. According to the new findings, the previously proposed mechanism can be confirmed or modified. In light of the results, new stability-enhancing components or coatings will be proposed and tested for their efficiency in reducing enzyme deactivation in powdered detergents.

Experimental Setup

The set up provides controlled conditions of H_2O_2 (g) concentration, humidity, temperature and oxygen concentration, to which enzymes are exposed.

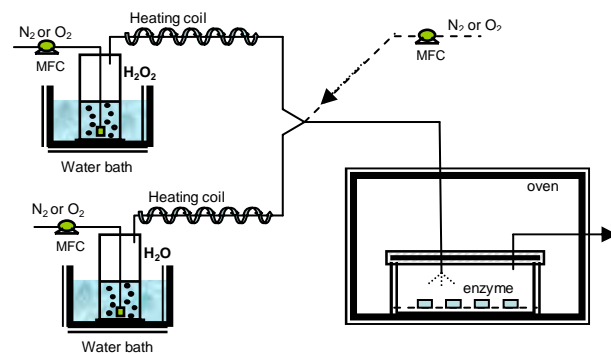


Figure 1: Sketch of the enzyme exposure setup

Results and Discussion

The initial experiments involved finding a method for generation and measurement of hydrogen peroxide vapor. A gas stream was bubbled through two impingers connected in series [3]. The first impinger containing hydrogen peroxide solution of known concentration was used for generation of hydrogen peroxide vapor and the second one filled with distilled water to absorb the released H_2O_2 . Samples taken from the second impinger were analysed for hydrogen peroxide concentration by measuring the oxidation of Leuco-crystal violet under catalysis of horseradish peroxidase [4]. Figure 2 shows the good agreement between experimental results and the literature data.

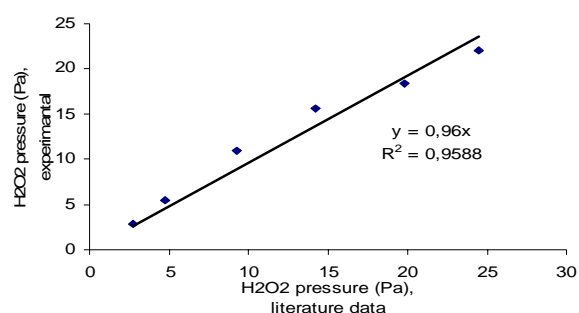


Figure 2: Comparison of experimental results and literature data

The inactivation kinetics of the freeze-dried Savinase (major detergent enzyme) was investigated as a function of H_2O_2 (g) concentration, relative humidity, temperature and presence of oxygen. Figure 3 shows a typical trend in the activity loss of the enzyme.

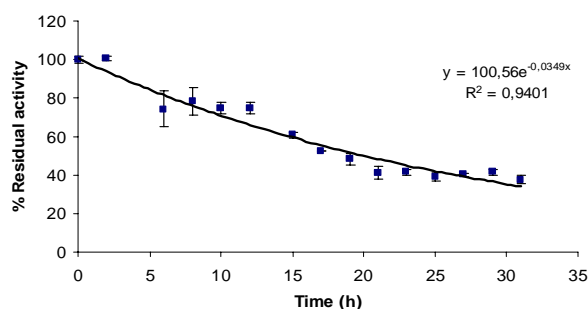


Figure 3: Inactivation curve of freeze-dried Savinase at 35°C, $P_{H_2O_2}=9.8$ Pa and 70% RH

The current results imply that a combination of humidity and hydrogen peroxide vapor is responsible for the decrease in the enzyme activity.

To reveal the mechanism of inactivation, it was focused on the autolytic activity and oxidation of the enzyme. Proteolysis was studied by sodium dodecyl sulfate poly acrylamide gel electrophoresis (SDS-PAGE) and by measuring the total protein content of the samples. Two methods were employed for this purpose:

Lowry [5] and Bradford [6]. The fact that the Bradford method can not detect peptides with molecular weight below 5kDa provides a tool for measuring the extent of proteolysis by following the increase in Lowry and decrease in Bradford protein.

Figure 4 illustrates a gel of SDS-PAGE. Savinase subjected to 70% RH, 10 and 20Pa hydrogen peroxide vapor was analysed for autolytic activity. The main band at 26.7 kDa represents Savinase. The low molecular protein bands are considered as impurities in the original protein sample, since they are present in the 0h-samples. A proteolytic activity was not detected by this method, since the formation of new low molecular weight peptides and/or the decrease in the main Savinase band were not clearly seen.

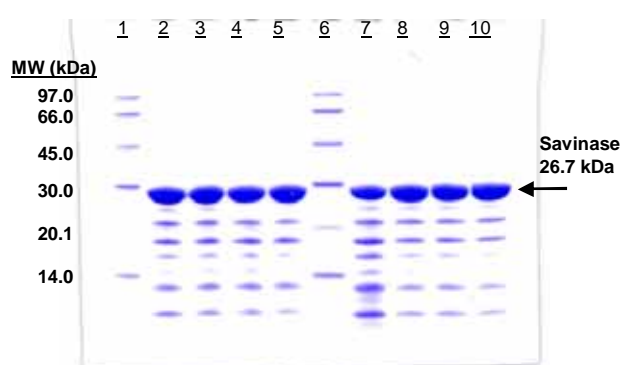


Figure 4: SDS-PAGE gel of freeze dried Savinase exposed to 70% RH and a) 10 Pa H₂O₂ lines: 2 -0h, 3-20h, 4 -43h, 5 -70h; b) 20 Pa H₂O₂ (g) lines: 7-0h, 8 -21h, 9 -42h, 10 -64h. Lanes: 1 & 5 - Low molecular weight standards.

Further investigation of proteolytic activity was done by measuring the total protein content of the samples. Figure 5 and 6 show the variation of Lowry and Bradford protein with increasing exposure time of the enzymes, respectively. For both methods there is no significant increase or decrease in the measured protein content. Consequently, both qualitative and quantitative investigations revealed that proteolysis does not occur during the exposure of Savinase to the tested conditions.

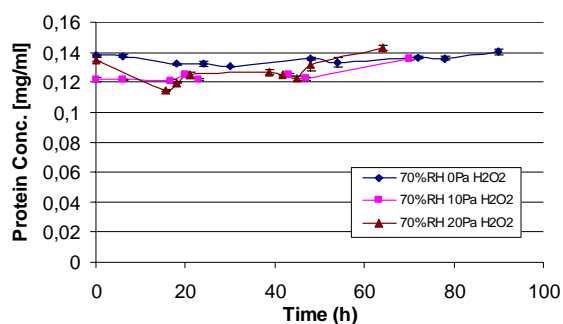


Figure 5: Lowry protein content

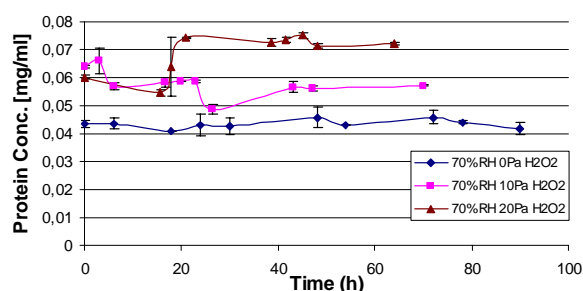


Figure 6: Bradford protein content

The oxidative effect of hydrogen peroxide on Savinase was investigated by analyzing the exposed samples by HPLC-MS in Single Ion Monitoring (SIM) mode. The preliminary results indicate that the native form of the enzyme decreases and oxidative forms increase (Figure 7). However, the total ion signal substantially was reduced implying a loss of protein in the HPLC column or a disability of the selected SIM mode. To see the full picture, it was decided to focus on the whole ion scan.

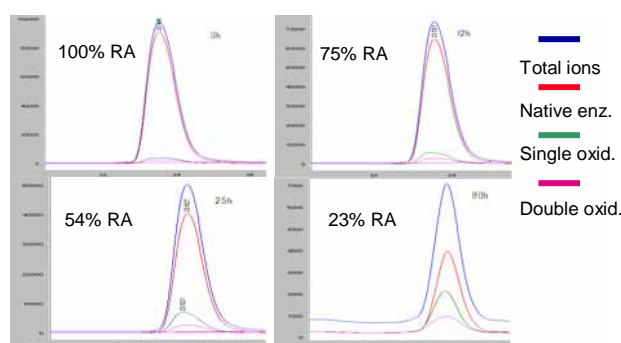


Figure 7: MS – SIM mode results of Savinase showing the native, single and double oxidized forms of the enzyme exposed to hydrogen peroxide for 0, 12, 25 and 80h. The % residual activity (RA) is indicated on the graphs.

The present understanding of Savinase inactivation implies that oxidation of the Methionine at position 222, which is close to the active site of the enzyme, is responsible for the loss of activity [7]. The presence of 2 more Methionine residues in the enzyme structure makes it difficult to directly correlate the activity decrease to the oxidation of the enzyme. Peptide mapping of protein digest will be further investigated for the location of the oxidized residue(s).

Assuming that single and double oxidized forms of the enzyme are inactive, the decrease of % residual activity was compared with the decrease in the relative area of the native enzyme. From figure 8 it is clearly seen that while the activity is exponentially reduced the native form decreases linearly. This implies that beside oxidation other mechanism(s) are involved.

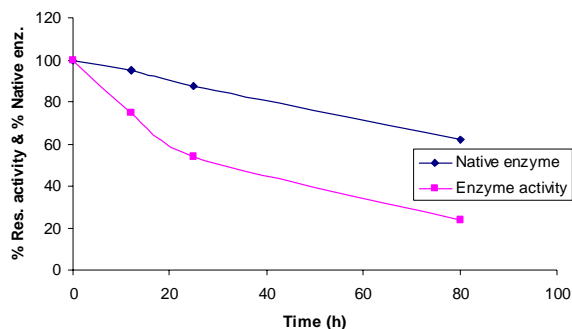


Figure 8: Comparison of activity loss with the decrease in the native form of Savinase

Conclusions and Future Work

An accurate method for the generation and measurement of low concentrations of hydrogen peroxide vapor was established. The experimental setup provides controlled conditions for the exposure of freeze-dried enzymes to different concentrations of hydrogen peroxide vapor, relative humidity and oxygen. The effect of these factors is being studied for the determination of the inactivation kinetics of Savinase and the calculation of inactivation coefficients. The present results indicate that a complex mechanism is involved in the enzyme inactivation. Agglomeration and 3D structural changes will be studied by Native-PAGE. The decomposition rate of hydrogen peroxide vapor over detergent ingredients, coating layer chemicals and antioxidants will be measured. New enzyme formulations will be tested for improved enzyme stability.

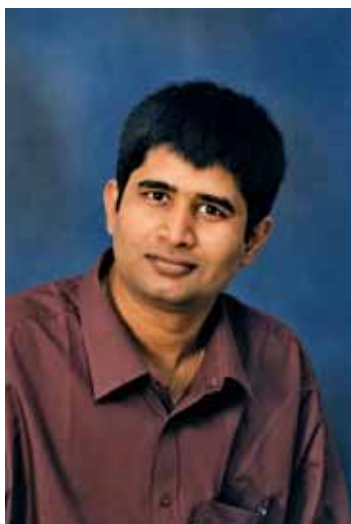
Acknowledgements

I would like to thank to Svend Kasgaard (Novozymes A/S) for his help in the MS study of the oxidized Savinase and to Novozymes Bioprocess Academy for supporting this project.

References

1. G. Broze (Edr.), Handbook of Detergents, Part A: Properties, Surfactant Science Series Vol. 82, Marcel Dekker, Inc. New York, 1999, p.639.
2. Simonsen, O. and Langemo, H., 2001, Mechanism of Deactivation of Enzymes and Sodium Percarbonate (SPC) in HDP, 40th International Detergency Conference Proceedings, 228-231.
3. Meyer, J., Krast, U., 1999, Workplace monitoring of gas phase hydrogen peroxide by means of fluorescence spectroscopy, Analytica Chimica Acta, Vol. 401, 191-196.
4. Mottola, H.A., Simpson, B.E., Gorin, G., 1970, Absorptiometric determination of hydrogen peroxide in submicrogram amounts with leuco crystal violet and peroxidase as catalyst, Analytical Chemistry, Vol. 42, No. 3, 410-411.

5. Lowry, O.H., Rosebrough, N.J., Farr, R.J., Randall, R.J., 1951, Protein measurement with the Folin phenol reagent, Analytical Biochemistry, 193, 265-275.
6. Bradford, M.M., 1976, A Rapid and Sensitive Method for the Quantitation of Microgram Quantities of Protein Utilizing the Principle of Protein-Dye Binding, Analytical Biochemistry, 72, 248-254.
7. DePaz, R.A., Dale, D.A., Barnett, C.C., Carpenter, J.F., Gaertner, A.L., Randolph, T.W., 2002, Effects of drying methods and additives on the structure, function, and storage stability of subtilisin: role of protein conformation and molecular mobility, Enzyme and Microbial Technology, 31, 765-774.



Debasish Chakraborty
Address: ICAT, Dept. of Chemical Engineering
Building 312
Technical University of Denmark
Phone: +45 4525 3125
Fax: +45 4593 2399
e-mail: dc@kt.dtu.dk
www: www.icat.dtu.dk
Supervisor(s): Tue Johannessen
Hans Livbjerg
Ib Chorkendorff

Ph.D. Study
Started: April 2003
To be completed: March 2006

One Step Flame Synthesis of Direct Methanol Fuel Cell Catalyst

Abstract

Flame synthesis is studied as a one-step preparation method of anode for direct methanol fuel cells (DMFC) by combustion of Ru-acetylacetonate and Pt-acetylacetonate in a quenched-cooled flame reactor. In contrary to the conventional supported PtRu/C catalyst, this method produced unsupported PtRu deposits on carbon gas diffusion layers (GDL). It has been observed that the anode prepared in this method shows higher performance than the anode prepared from supported PtRu/C catalysts available commercially.

Introduction

Direct methanol fuel cell (DMFC) has the potential to replace the combustion engine in vehicular applications. The device uses a liquid fuel, which means that the existing fuel supply, storage, and delivery systems could be used possibly with a few minor modifications. Also methanol can be produced from natural gas, coal or biomass. Compared to the hydrogen fuel cell, which is also in consideration as a future energy conversion device, direct methanol fuel cell has the advantages of ease of fuel supply and storage (1). DMFC can be operated at lower temperature than the internal combustion engine (ICE) and this will certainly reduce the polluting nitrogen oxides produced by ICE. DMFC offers another unique advantage for city driving; its efficiency increases as the load on the fuel cell decreases, which is exactly the opposite of the heat engines.

However, it has not yet been possible to develop DMFC of acceptable cost, which can give performance comparable to that of its main competitor, i.e. heat engines. The cost of DMFC depends mainly on the electrolyte membrane and the Pt based catalysts, that has the highest activity for methanol oxidation (2). The cost of the membrane can be reduced by the growth of the market, but the only way to lower the cost of the catalyst is to reduce the amount of Pt used without sacrificing the performance(3). Therefore, it is necessary to improve the catalyst performance.

In DMFC carbon supported Pt-Ru catalyst is used. Substantial enhancements in activity were found for platinum modified with a second metal like ruthenium. One hypothesis for this enhancement of activity is that the second component such as Ru acts as a redox co-catalyst with the methanol adsorbing and dehydrogenating on the Pt whilst the poisoning residue was chemically oxidized on the co-catalyst. The other explanation is that the second component acts as an agent which weakens the adsorption of residues on Pt via a ligand effect and/ or promoting the electrosorption of water at lower potentials and thus accelerating the removal of residues (1). Whichever is the mechanism, it might be concluded that for improved performance, it is necessary to have a well-mixed Pt-Ru bimetallic alloy as catalyst. The general ways of making catalyst are co-impregnation, sequential impregnation, co-precipitation, absorbing alloy colloids or surface organometallic chemistry techniques. However, it could be difficult to achieve the desired close proximity of the active components by the conventional methods as the active components might deposit on different sites on the support. Moreover, all of these processes need several stages for making active catalyst. Flame pyrolysis can be a viable alternative to replace the wet processes with a one step continuous process.

Flame pyrolysis has been successfully used to produce catalysts (4). In flame pyrolysis, precursors are rapidly evaporated as they are exposed to high flame temperatures resulting in vapours that react forming intermediate and product molecules and clusters that

quickly grow to nano-sized particles by coagulations and/or surface reaction (5). The precursors and the products have very high chances to mix intimately before the particles are formed. This intimate mixing can result in higher degree of alloying and greater proximity of active elements of the catalysts.

The work presented here describes results of our effort to develop a one step synthesis method of unsupported DMFC anode catalyst in terms of the physical and chemical characterization of the catalysts and comparing their methanol oxidation activity with a commercial PtRu/C catalyst.

Experimental

The flame synthesis setup is shown in Figure 1.

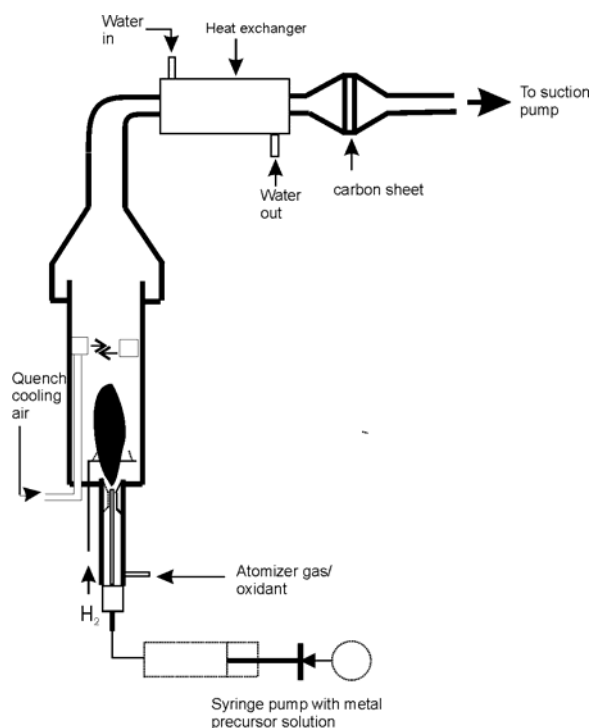


Figure 1: Outline of the flame synthesis equipment

The precursors, ruthenium (III) acetylacetonate ($\text{Ru}(\text{acac})_3$, Sigma-Aldrich) and platinum (II) acetylacetonate ($\text{Pt}(\text{acac})_2$, Aldrich Chem.Co), were dissolved in solvent containing isooctane and tetrahydrofuran at a volume ratio of 4 to 1. The solution was pumped through a nozzle to spray the precursor solution to the flame. The dispersion and combustion gas was introduced through a slit surrounding the nozzle. Supporting hydrogen flames were also created by introducing hydrogen horizontally of the main flame. The product particles were collected on the carbon-based fuel cell gas diffusion layer (GDL) by passing the flame outlet aerosols through it.

Based on collaboration with IRD Fuel A/S, a test fuel cell was built (Figure 2). The graphite bipolar plates had machined flow structures with serpentine flow pattern, capable of accommodating electrodes of maximum 3.14 cm^2 .

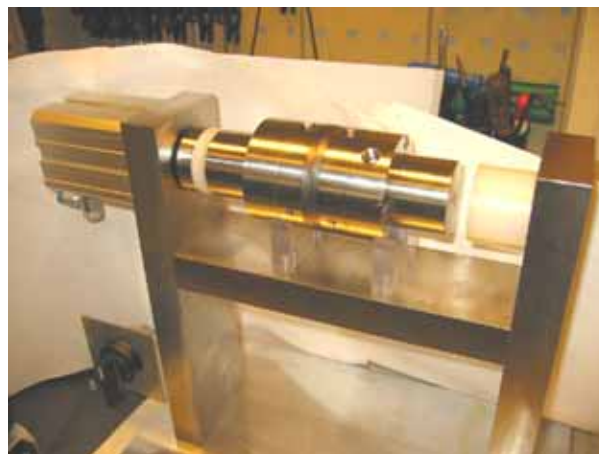


Figure 2: Photograph of the test fuel cell

The system is equipped with two humidifiers for humidifying the inlets to anode and cathode. The inlet to the anode and cathode sections of the fuel cell travelled along serpentine channels and picked up water coming from the humidifiers separated from the flow by Nafion membranes.

The activity of the catalysts were tested in the cell with $1.0 \text{ M CH}_3\text{OH}$ at the anode and H_2 at the cathode side. For comparison, 10 % PtRu/C catalyst from E-TEK was also tested for the reaction.

Results and Discussion

SEM image of a metal deposited carbon sheet showed the structures of the support (Figure 3). The deposit grows on the fibres of the GDL and consists of agglomerates of smaller primary particles sticking together. The fluffy nature of the deposits makes them porous and penetrable the reactants and products.

Figure 4(a) and 4(b) are the TEM images depicting the morphology of the particles deposited on a TEM grid from the top of the flame. Figure 4(a) shows the particle size ranges from $\sim 2 \text{ nm}$ to $\sim 5 \text{ nm}$. Figure 4(b) is a close-up picture of one particle. It shows a spherical morphology with lighter region near the periphery and darker inside region. This might be due to the segregation of lighter elements (i.e. Ru or RuO)

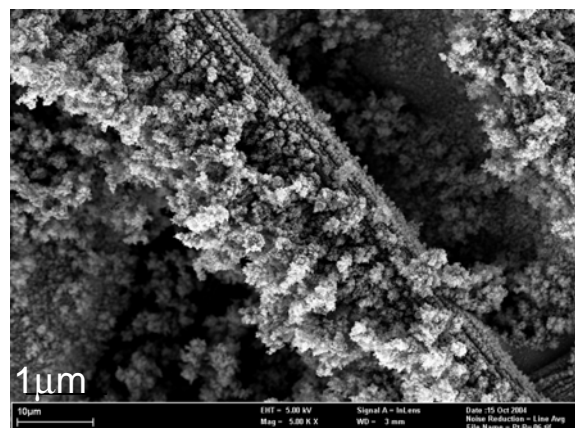


Figure 3. SEM image of the film of PtRu particles on carbon sheet

to the outer surface of the sphere. In that case the inner surface will be mostly Pt or Pt compounds.

Table 1. Binding energies of different species from curve fitted spectra

| | Pt/C | PtRu(3:1)/C | PtRu(1:1)/C |
|---------------------------|----------|-------------|-------------|
| 1 st component | 71.5ev | 71.66 ev | 71.78 ev |
| 2 nd component | 72.48 ev | 73.1 ev | 73.2 ev |
| 3 rd component | 74.9 ev | 74.55 ev | 74.65 ev |

Table 2. Relative intensities of different species from curve fitted spectra

| | Pt/C | PtRu(3:1)/C | PtRu(1:1)/C |
|---------------------------|-------|-------------|-------------|
| 1 st component | 45.8% | 44.6% | 36.3% |
| 2 nd component | 50% | 52% | 60% |
| 3 rd component | 4.2% | 3.4% | 3.7% |

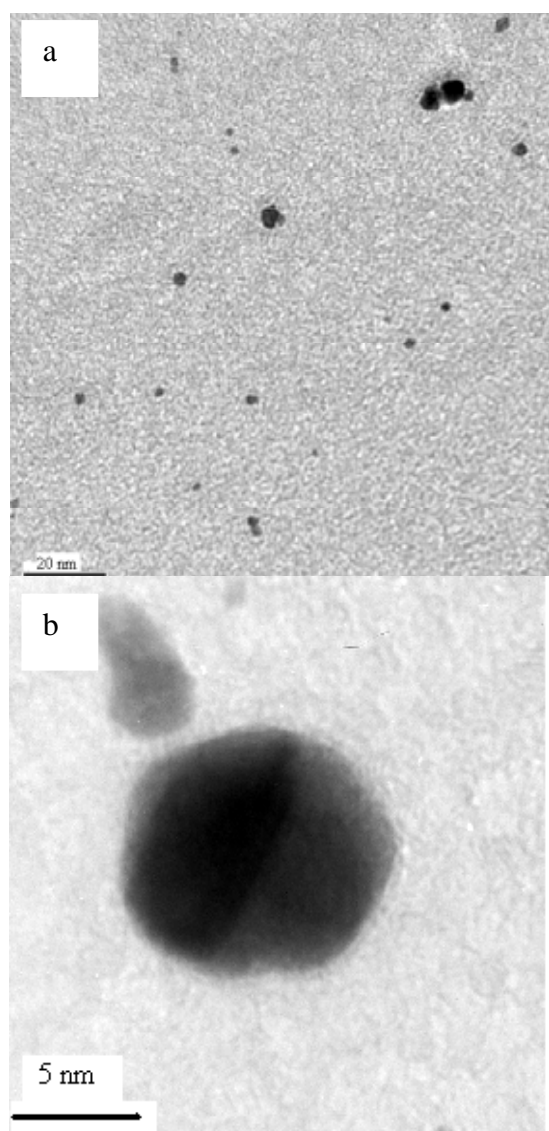


Figure 4: TEM micrographs of particles (a), and a single particle (b), produced by the flame.

Figure 5 shows the X-ray diffraction patterns of the flame synthesized Pt/C and PtRu/C catalysts. In both cases, the five characteristic peaks of the face-centred

cubic (f.c.c.) crystalline structure of Pt, namely the (111), (200), (220), (311) and (222) are seen. Peaks around 43° and 55° are associated with reflections from graphite (101) and (222) planes. Unfortunately, no information about RuO₂ could be obtained from xrd because the most intense peak (for plane (110)) occurs at 28.27° and is obscured by the most intense graphite peak. Peaks associated to h.c.p. Ru were not observed. To characterise the electronic states of the deposits, X-ray photoelectron spectroscopy was carried out on several samples. The spectra showed the presence of Pt and Ru in the deposits. Furthermore, in

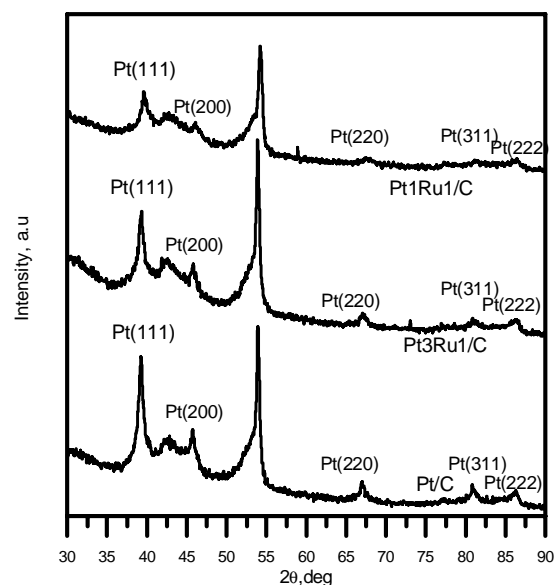


Figure 5. X-ray diffraction pattern of Pt/C; Pt3Ru1/C; and Pt1Ru1/C, where the number after the metal is the respective atomic fraction.

order to understand the electronic states of Pt in the catalyst, the Pt 4f region has been investigated in detail (Figure 5). The spectra could be deconvoluted into three components. Considering the fact that higher oxidation states of Pt will have higher binding energies, the three peaks could be attributed to Pt⁰, Pt²⁺, and Pt⁴⁺. The binding energies and area ratios of different components are shown in Table 1 and Table 2.

The anode polarization curve (Figure 6) clearly shows that the unsupported flame synthesized Pt1Ru1/C catalyst performs better than the supported PtRu/C (10 % Pt,E-TEK). Even though the onset potential are almost same (~210 mV) for both the catalysts, as the current density becomes higher, the overpotential for methanol oxidation becomes lower for flame synthesized Pt1Ru1 compared to that for Pt1Ru1/C from E-TEK.

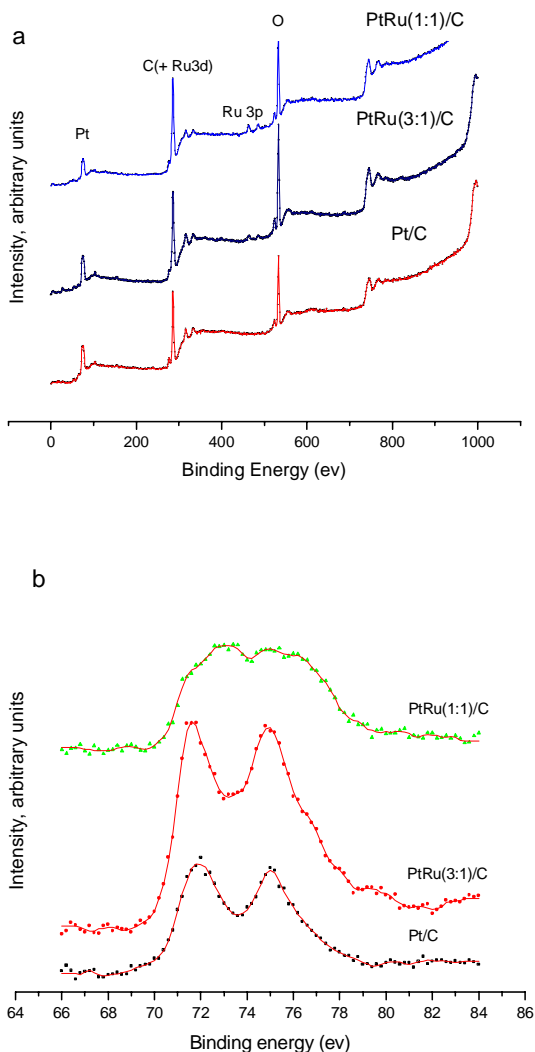


Figure 5: X-ray photoelectron spectra of different catalysts showing all possible peaks (a), and Pt 4f peaks (b).

Conclusion

We have presented the results of a one-step method for synthesis of unsupported PtRu anode catalyst for DMFC. The characterization of the catalysts made at the preliminary stage showed that nano-particles were produced and also high degree of alloy formation was observed. The catalyst performed better than the commercially available PtRu/C (E-TEK) catalyst for the electrochemical oxidation of methanol. We think that the preliminary results are promising and further research could result in an effective one step method for DMFC catalyst preparation.

Acknowledgement

We would like to thank Dr. Jon C. Davies (European Commission, DG JRC, The Netherlands) for the SEM image. We are also thankful to IRD Fuel Cells A/S for providing the carbon support and the

design for the test fuel cell unit. The author wish to thank the Technical University of Denmark for supporting the project with a Ph.D. scholarship. The project is also partially supported by PSO-project 5357.

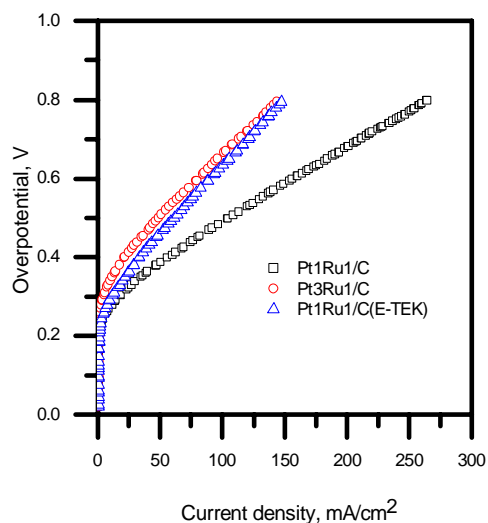


Figure 6: Anode polarization curve for methanol oxidation at 90°C.

References

1. McNicol, B. D.; Rand, D. A. J.; Williams, K. R. J. *J. of Power Sources* 83, 15-31. 1999.
2. Carrette, L.; Friedrich, K. A.; Stimming, U. *CHEMPHYSICHEM* 1, 162-193. 2000.
3. Cha, S. Y.; Lee, W. M. J. *Electrochem. Soc.* 146[11], 4055-4060. 146.
4. Johannessen, T.; Koutsopoulos, S. *J.Catal.* 205[2], 404-408. 2002.
5. Pratsinis, S. E. *Prog. Energy Combust. Sci.* 24, 197-219. 1998.



Henrik Christensen

Address: CHEC, Dept. of Chemical Engineering
Building 229, Office 052
Phone: +45 4525 2890
Fax: +45 4588 2258
e-mail: hc@kt.dtu.dk
www: www.chec.kt.dtu.dk
www.lundbeck.com
Supervisor(s): Søren Kiil
Kim Dam-Johansen
Ole Nielsen, H. Lundbeck A/S
Michael Bech Sommer, H. Lundbeck A/S
Ph.D. Study
Started: September 2004
To be completed: September 2007

Continuous Flow Reactors and Process Analytical Technology in Pharmaceutical Production

Abstract

The design of an efficient reactor system for a chemical reaction requires knowledge on the kinetic data related to the reaction. Kinetics makes it possible to simulate how the reaction is affected by different reaction conditions. This is a discipline, which has not yet been widely used in the pharmaceutical industry. However, due to environmental, economical and quality considerations an increasing interest in this field has appeared. This gives the opportunity for investigating the possibilities for the implementation of new reactor configurations and analysis techniques, which provides a more detailed understanding of the chemical process.

Introduction

The production of Active Pharmaceutical Ingredients (API) is a special area compared to other chemical productions. Typically, the amounts of products produced are rather small, but on the other side the trade prices on the products are high [1]. This has resulted in little focus on process development and optimization from an engineering point of view.

Reactions traditionally take place in batch reactors. These reactors can be used for a range of reactions and in terms of documentation it is convenient to trace errors back to the source. From a scale up point of view batch reactors give rise to a number of challenges: Loss of selectivity and formation of hot spots due to slow mixing and problems with exothermic reactions due to a high volume to surface ratio [2]. This has the consequence that a reaction, which performs satisfying in gram-scale, may fail when it is performed in kg-scale. Until now the typical way of solving these upscale problems has been to change the critical steps in the synthesis rather than finding a convenient solution by changing from batch reactors to other reactor configurations. This has the drawback that it is time consuming to develop a new synthesis route and it may result in additional synthesis steps or use of excess of chemicals, which all-together means that the turnover may decrease.

However, a number of changes in the pharmaceutical market have made it relevant to investigate the possibility of optimizing or changing some of the existing production methods. The competition has increased, due to generic production and more attention on the environmental impact is paid.

An aspect, which until now has also prevented the pharmaceutical industry in process development and implementation of new techniques, is the commitments to the US Food and Drug Administration (FDA). The FDA is responsible for the guidelines that ensure the quality of the pharmaceuticals [3].

Until August 2003 the accepted way of ensuring a product with a given quality was to describe the production method in every detail and finally receive an approval from FDA. From that stage no changes on the approved method are allowed without preapproval from the FDA. This means that even if the production method is inefficient, it is not possible to optimize the process without using precious time on new approvals.

The FDA has now realized that the lack of optimization has resulted in excessive manufacturing costs. Therefore the FDA has encouraged the pharmaceutical industry to implement new technologies. The new technologies shall ensure a more effective, safe, and affordable production of pharmaceuticals and by that help the consumer to get the pharmaceuticals; they need to improve their health.

These requirements may be met by the implementation of Process Analytical Technology (PAT) [4]. The aim of this technique is to provide a more complete understanding of the chemical process. Through the use of modern analysis equipment real time concentration profiles can be recorded for a chemical process. Based on these profiles operating conditions may be changed during the process and the final quality may be improved [5].

To investigate these new possibilities for the manufacturing of pharmaceuticals the Department of Chemical Engineering at the Technical University of Denmark and the pharmaceutical company H. Lundbeck A/S has agreed on a partnership with the main title: "Active Pharmaceutical Ingredients".

Specific Objective

The main objective of this project is to investigate the opportunity for implementation of new reactor configurations in pharmaceutical production, which allow continuous operation.

The reactor design will be based on a kinetic study of a relevant type of reaction in terms of pharmaceutical production. The kinetic study is desired in order to produce a kinetic model, which is able to predict the reaction rate under different conditions.

Effort will also be devoted to investigate the possibilities for monitoring the reaction with online techniques.

Chemical Reaction

Mono-substituted aryl piperazines are of great importance in the pharmaceutical production, and they can be produced by the Buchwald-Hartwig amination reaction. Therefore the chemical reaction in figure 1 has been chosen for a case study.

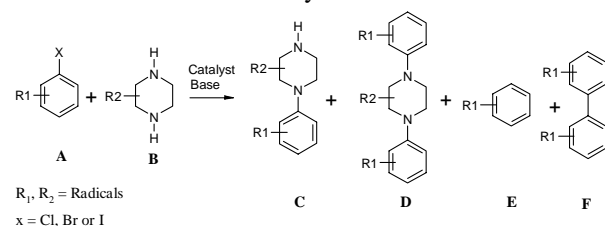


Figure 1: Formation of aryl piperazine by Buchwald-Hartwig amination reaction. R1 and R2 may be bonded to any carbon atom in the respective molecule.

The Buchwald-Hartwig amination reaction is the coupling between an aryl halogen (A) and a primary or a secondary amine (B) in the presence of a homogeneous palladium catalyst and a base. The products are: Mono-substituted aryl piperazine (C), bi-substituted aryl piperazine (D), reduced aryl halogen (E) and homo-coupled aryl halogen (F). However, it is only C, which is desired. D, E and F are unwanted side products.

So far the reaction has been carried out in batch reactors, and the two following strategies have been

used in order to avoid formation of D. One strategy has been to introduce a protection group, which protects one of the two nitrogen atoms in B [6]. Another strategy has been to change the ratio between A and B [7].

However, from an economic point of view, it will be favorable if the reaction can be carried out without the introduction of protection groups and with equivalent amounts of A and B, or even better with an excess of A.

The Buchwald-Hartwig amination reaction will form the base for the kinetic study, which will be build on the chemical reaction mechanisms described in the literature [8 and 9]. In parallel with the kinetic study the opportunity of online concentration measurements will be evaluated.

Acknowledgements

This project is performed in close collaboration with H. Lundbeck A/S. H. Lundbeck A/S provides the laboratory facilities and their expertise on organic synthesis.

References

1. K.F. Jensen, Chemical Engineering Science, 2001, 56, 293-303.
2. N.G. Anderson, Organic Process Research & Development 2001, 5, 621. Contents
3. <http://www.fda.gov/opacom/morechoices/mission.html>
4. <http://www.fda.gov/cder/ops/pat.htm>
5. <http://www.ptemag.com/pharmtecheurope/article/articleDetail.jsp?id=129539&pageID=1>
6. Hepperle, M.; Eckert, J.; Gala, D.; Shen, L.; Evans, A.; Goodman, A., Tetrahedron Letters, 2002, 43, 3359-363.
7. Zhao, S.; Miller, A.; Berger, J.; Flippin, L., Tetrahedron Letters, 1996, 37, 4463-4466.
8. Urgaonkar, S.; Xu, J.; Verkade, J., Journal of Organic Chemistry, 2003, 68, 8416-8423.
9. Wagaw, S.; Rennels, R.A.; Buchwald, S.L., Journal of American Chemical Society, 1997, 119, 8451-8458.

**Steen Christensen**

Address: CAPEC, Dept. of Chemical Engineering
Building 227, Office 224
Technical University of Denmark

Phone: +45 4525 2912
Fax: +45 4593 2906
e-mail: sch@kt.dtu.dk
www: www.capec.dtu.dk

Supervisor(s): Jens Abildskov

Ph.D. Study

Started: August 2004
To be completed: July 2007

Multilevel Modeling of Complex Systems

Abstract

A large part of all chemical systems can only be fully understood based on physical and chemical property data. Property data can not be calculated in a fully rigorous fashion. Normally semi-quantitative property prediction models (SQPP) have been used but they all have weaknesses and limitations concerning size and complexity of the molecules. In a highly competitive climate, chemical engineers are forced to rely increasingly on predicted data. The purpose of this project is to develop a methodology for extracting maximum information from available experimental results. The project will combine SQPP models with molecular modelling to give qualified prediction of pure and mixture behaviour of novel compound groups to minimize extensive experimental data generation.

Introduction

The motivation for this project is the need for precise control of product properties and the development of a microscopic and mesoscopic understanding that allows creation and design of new product solutions to meet specific marketplace demands. Traditionally, process systems engineering (PSE) is concerned with the computer-aided design of products and processes, and the operation and control of these processes throughout their lifecycle. The overwhelming majority of all chemical systems can only be fully understood based on accurate physical and chemical property data. Such property data can not be calculated in a fully rigorous fashion, so chemical engineers have for decades developed numerous semi-quantitative property prediction models. Great emphasis has been on models of residual properties of pure components and mixtures and excess property models for liquid mixtures. As the materials of interest to the modern chemical industry become ever more complex, PSE relies on increasingly sophisticated molecular modelling (MM) techniques for the characterization of their properties and behaviour. The use of advanced equations of state within mathematical process models is now well established, as is the use of molecular modelling for the derivation of parameters used in these equations, e.g. by generation of "pseudo-experimental" data points to complement real experimental data that

are available. During the past fifteen years, theoretical and algorithmic advances along with the revolution in computing technology have made it possible for design questions of practical importance to be addressed by MM. The advances offered by these methods will continue to make inroads in the chemical and related industries in the coming decade. The project is based on providing the physical property data necessary in five industrial cases.

Industrial Case Studies

The scenario varies between the different cases and thereby the information and selection of properties of which knowledge is desired. The five cases are:

1. Mono-, di- and triglycerides
2. Polyglycerols
3. Pyrazines
4. Furaneol
5. γ - and δ -lactones

In general properties (pure component and mixture) relevant for synthesis and purification are desired. The glyceride case involves non-equilibrium phenomena. The crystals which precipitate are unstable and a solid exothermic transformation which often occurs upon storage changes the product properties significantly.

Methodology

A general approach for handling a compound group of interest includes four steps:

1. Search literature sources for all relevant physical property data (liquid densities, vapor pressure data, PVT data, phase diagram data, mixture equilibrium data vapour-liquid-equilibrium (VLE), liquid-liquid-equilibrium (LLE), solid-liquid-equilibrium (SLE), activity coefficients at infinite dilution, excess volumes etc.).
2. Test existing property prediction methods (if available) both for pure compounds and mixtures.
3. Obtain relevant properties from molecular modelling. For developing molecular models use known data to establish suitable potentials.
4. Combine results of molecular modelling with semi quantitative equations to do the full simulations/designs.

How to enable design engineers to accomplish steps 3-4 within established CAPE frameworks is unclear at this point.

γ - and δ -lactones

γ - and δ -lactones (Figure 1) are internal esters of hydroxy acids. The small lactones are good solvents for industrial cleaning products like paint strippers and deinking and adhesive removers. They also have application as a chemical intermediate in agrichemicals, pharmaceuticals and dyes. The lactones are also known as fragrances naturally occurring in fruits like apricots and peaches. The lactones are purified by distillation. In order to model the fractionation of these compounds it is necessary to have access to physical

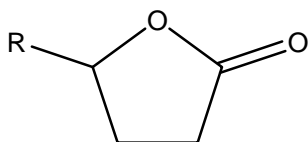


Figure 1: Basic structure of γ -alkyl- γ -lactone

properties and as these are not commonly known from the literature, prediction is an attractive way to circumvent this problem. The lactones are often formed by lactonization of the corresponding hydroxy acid esters (methyl esters). The hydroxy acids are even more scarcely described in the literature. So the main problem to describe is the ring closure reaction of the hydroxy acids and the equilibrium associated with this process. Analytically it is a problem to determine the purity of the lactones as varying amounts of water may shift the equilibrium towards the open form, i.e. the hydroxy acid. This can partly explain the limited publications of experimental results.

In Figure 2 the heat of formation is plotted for a set of lactones against the length of the alkane side chain R (see Figure 1). 3 experimental values are known [1-2]. Three group contribution methods (GCM) [3-5] were

used to predict the heat of formation Marrero/Gani (M&G), Constantinou/Gani (C&G) and Joback/Reid (J&R). Finally the semi empirical quantum mechanics method MOPAC [6] was used to calculate the heat of formation.

Except for J&R all the predictive models gives acceptable results. The best predictions are obtained with MOPAC.

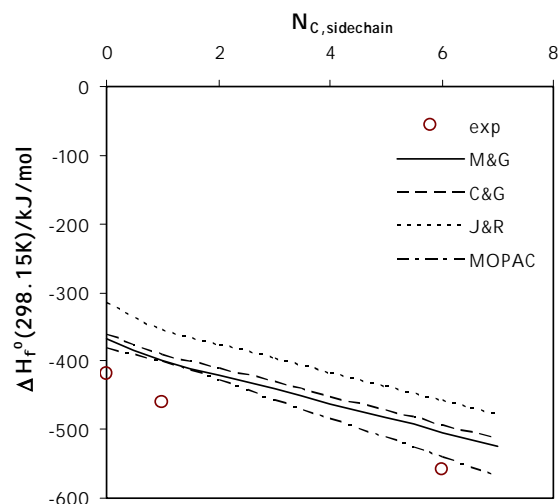


Figure 2: Heat of formation for γ -lactones as function of the length of alkane side chain R

The evaluation of the prediction of heat of formation by the GCM's and the MOPAC package for the lactones are eased by the available experimental data. The real challenge of the methodology lies in compound groups like the hydroxy acids where experimentation is difficult and the access to experimental results is limited. In such cases one must rely on predictive models and then make decisions based on comparisons of the predicted properties by the different models.

The future challenges of the project are to expand the work to mixture properties and also working with the other industrial case studies.

References

1. K.B. Wiberg, R.F. Waldron, *J. Am. Chem. Soc.* 113 (1991) 7697-7705.
2. M.L.P. Leitao, H. Pilcher, Y. Meng-Yan, J.M. Brown, A.D. Conn, *J. Chem. Thermodyn.* 22 (1990) 885-891.
3. J. Marrero, R. Gani, *Fluid Phase Equilib.* 183-184 (2001) 183-208.
4. L. Constantinou, R. Gani, *AIChE J.* 40 (10) (1994) 1697-1710.
5. K.G. Joback, R.C. Reid, *Chem. Eng. Comm.* 57 (1987) 233.
6. T. Clark, *A Handbook of Computational Chemistry*. Wiley, 1985.

**Florin Paul Davidescu**

Address: CAPEC, Dept of Chemical Engineering
Building 227, Office 250
Phone: +45 4525 2801
Fax: +45 4593 2906
e-mail: fpd@kt.dtu.dk
www: www.capec.kt.dtu.dk

Supervisor(s): Sten Bay Jørgensen

Ph.D. Study

Started: February 2004

To be completed: February 2007

Optimizing Operation of Chemical Plants Using Model Predictive Control

Abstract

The project purpose is to develop methods for analysis of controllability and constructive application of optimizing control techniques for complex processes such as mass/heat integrated processes. In particular the study will focus on the heat integrated distillation pilot plant at CAPEC, Department of Chemical Engineering where the practical implementation of the advanced optimizing control techniques, as model predictive control will be accomplished.

Introduction

To remain competitive on the market, any chemical plant has to be designed and operated optimally [1]. The latter requirement implies the ability to respond fast to changes in demand including raw material quality and with minimum raw material and energy consumption. In the chemical/process industry process integration is increasingly implemented in order to improve material and energy efficiency. The case of energy integration means that the heat removed in one part of a process is recovered and reused in other parts of the process. Energy integration in this case means coupling several physical processes either within the same piece of equipment or between units that perform different physical/chemical tasks. Referring to the case of the same piece of equipment the case of reactive distillation can be mentioned, in which reaction and separation are conducted simultaneously. Another example is periodically operated reactors, which are effectively both reactors and heat or mass exchangers. A third example that is relevant for this project is energy-integrated distillation. In any of these examples, and especially in the case of the energy integrated distillation the integration means an important increase in the complexity of the process and in the possible nonlinear behaviour of the process. This increased complexity can potentially lead to difficulties for the plant operability and control. Still, in order to take advantage of the full economic potential of such integrated processes, methods for analysing their operability should be developed and methods for constructive application of advance control techniques

have to be developed. In this project methods for analysis of controllability and constructive application of advanced control will be developed and investigated. Application of these methods will be illustrated on the existing heat integrated distillation pilot plant at CAPEC, Department of Chemical Engineering.

Specific Objectives

The first objective is to provide a procedure for development of a decentralized control structure for a complex real plant which is capable of handling specific types of process nonlinearities such as fold and hopf points [2].

The second objective is to provide an analysis procedure for investigating to what extent such a decentralized control structure can become self-optimizing [3] or form the basis for an optimizing control layer.

The third objective is to define and analyze an optimizing control problem using model predictive control (MPC) based upon the developed decentralized control structure.

The fourth goal is to show the complex behaviour and demonstrate optimal operation on the heat integrated distillation pilot plant. Finally the time varying operations of start up and shut down will be optimized using MPC.

Status

In order to design a decentralized control structure capable of handling the specific nonlinearities of a complex system will be analysed based on the nonlinear dynamic model for the specific plant. A simplified

model for the heat integrated distillation plant has been modified and analysed. This model is currently under experimental evaluation on the plant using a decentralised control structure designed to handle the expected fold bifurcation near optimal operation.

Experimentally will both continuous plant operation and the time varying cases of start-up and shutdown, which are most relevant for batch operation be investigated.

Conclusions

An important process control problem for complex process like energy and mass integrated plants is defined and under investigation. The focus is the nonlinear behavior with fold or hopf points within the operation window and the question how optimal operation can be based on a decentralized control structure, which handles these specific nonlinearities

References

1. Boris M. Russel and others. Computers and Chemical engineering, 26 (2002) 213-225.
2. Hongwen Li, Rafiqul Gani, Sten Bay Jørgensen: Ind. Eng. Chem. Res., 42, (2003) 4620-4627.
3. Sigurd Skogestad, Journal of process control, 10, (2000) 487-507.
4. J. M. Maciejowski, Predictive Control with Constraints, Pearson Education Limited, U.K., 2002



Runi Ditlev Egholm
Address: KT, DPC Building 423,
Room 220
Phone: +45 4525 6825
Fax: +45 4588 2161
e-mail: rde@kt.dtu.dk
www: www.student.dtu.dk/~s973640/

Supervisor(s): Peter Szabo

Ph.D Study

Started: July 2004

To be completed: June 2007

Emulsion Design

Abstract

Emulsions display complicated flow behaviour due to the interaction between the rheological properties and the microstructural morphology. The coupling between rheology and morphology can be studied by solving the governing flow equations using numerical methods that can handle two phase flows. One promising approach is the Volume of Fluid (VOF) method which is efficient for flows involving large surface deformations. In order to investigate how the microstructure of emulsions is influenced by the flow field we are currently working on implementing the VOF method together with a Finite Element Method.

Introduction

Emulsions consist of two immiscible phases, one phase being dispersed as droplets in the other continuous phase. Depending on its thermodynamic properties an emulsion can either be stable (colloidal) or unstable (non-colloidal). In order to keep non-colloidal emulsions in their emulsified state it is necessary to add mechanical energy to the mixture by creating some type of strong flow field to keep the drops from coalescing and thereby forming two immiscible continuous phases. The size distribution and geometry of the dispersed droplets is highly dependent on the type and strength of flow present in the emulsion. In a simple flow field like simple shear the drops will elongate in the direction of the flow. However, at some critical shear rate the drops will break up into a number of smaller drops.

Some of the earliest experimental investigations of the drop deformation in shear flows was carried out by Taylor in the 1930's [1-2]. Taylor compared his measurements to predictions obtained by solving the governing flow equations (Navier-Stokes) analytically. He found good agreement at low to medium deformation. However, the analytical solutions were based on the small deformation assumption and could therefore not predict the drop behavior at large deformations. During the 60's and 70's the advances

in computing power lead to a large research effort in numerics which made it possible to solve flow problems with complicated geometry and even with multiple phases and free surfaces. In connection with multiphase and free surface problems the Marker and Cell (MAC) method [3] and Volume of Fluid (VOF) [4] were developed. These methods, unlike Lagrangian methods, can be used to describe the development of surfaces with time without distorting the calculational mesh. Because the mesh is undistorted these methods can be used for solving large deformation problems and even phase separation (e.g. drop breakup) without having to remesh. These methods are therefore well suited for solving the flow and drop deformation in emulsions and especially the VOF method has been used extensively in recent years for simulating emulsion flow, e.g. ref. [5,6].

Specific Objectives

One of the main goals of this research project is to improve or find new constitutive relations for emulsion flows, e.g. relations between shear strength and drop size distribution. In order to carry out such investigations we have started implementing a finite element Navier-Stokes solver together with the VOF method. The idea is to be able to simulate the drop deforma-

tion and drop breakup in simple flow fields. We also want to be able to carry out simulations when several drops are close together in order to get as close to real emulsion behaviour as possible. Finally, we want to be able to carry out simulations where surfactants are present on the interface between the drop and continuous phase because surfactants are often present as stabilizing agents in real emulsions. From simulations we seek information that can help us set up constitutive relations governing emulsion behaviour.

Theory

In this section a short introduction to the theory behind the VOF method will be given. When solving problems with movable surfaces one procedure is to advect the nodes on the surface in time. However, one major problem with this method is that large deformations result in large mesh distortions which usually lead to instability problems. The VOF method is based on a so called color function. The calculational domain is split up into a number of small cells and in each cell the color function has a value that corresponds to the volume fraction of one phase relative to the other phase. Thus the color function (F) is given by:

$$F = \begin{cases} 1, & \text{Fluid 1} \\ 0, & \text{Fluid 2} \end{cases}$$

For cells through which an interface runs the value of F is between 0 and 1. The evolution of the interface as a function of time is carried out by advecting the two phases using the color function:

$$\frac{\partial F}{\partial t} + \nabla \cdot (F\mathbf{u}) = 0$$

where \mathbf{u} is the velocity vector. In connection with the VOF method it is necessary to reconnect the interface after each time step. Several reconnection procedures have been proposed in the literature, e.g. [5,6]. One of the most widespread methods is the piecewise linear reconnection algorithm (PLIC) originally introduced by DeBar [4]. In this method the interface is estimated from plane segments (or line segments in 2D) running through each interface cell. In each cell the normal vector to the plane segment is estimated from the gradient of the color function. The segment divides the cell in two distinct volumes one belonging to the drop phase and the other belonging to the continuous phase. The position of the plane is chosen in such a way that the volume fraction of the drop phase corresponds to the value of the color function in the cell. The flow field is obtained by solving the incompressible Navier-Stokes equation:

$$\frac{\partial \mathbf{u}}{\partial t} + \mathbf{u} \cdot \nabla \mathbf{u} = \nu \nabla^2 \mathbf{u} - \nabla p + \mathbf{f} \quad (1)$$

with the incompressibility condition:

$$\nabla \cdot \mathbf{u} = 0 \quad (2)$$

In Eq. (1), p is the pressure, ν is the kinematic viscosity and \mathbf{f} is the body force term which for the droplet interface contains the interfacial tension. The interfacial tension can be included using either the continuous surface force formulation (CSF) [7] or the continuous surface stress formulation (CSS) [8].

Conclusion

The morphology of the drops in emulsions is highly dependent on the stresses from a flow field. In order to gain insight into the mechanism governing the microscopic morphology numerical methods developed for multiphase and free surface flows have proved to be useful [5-8]. One of the most popular methods is the Volume of Fluid (VOF) method which can be used to simulate the deformation and also drop breakup without having to implement any remeshing procedures. Our plan is to implement the VOF method in conjunction with a finite element model wherein interfacial tension is included. Furthermore, the influence of surfactants on the interfacial tension should be taken into account because surfactants are usually added to emulsions as stabilizing agents. From simulated data we want to investigate if constitutive relations between flow parameters and drop morphology can be obtained.

Acknowledgements

The author is supported by the Danish Technical Research Council (grant no. 26-03-0282).

References

1. G. I. Taylor, Proc. Roy. Soc. A 138 (1932) 41-48.
2. G. I. Taylor, Proc. Roy. Soc. A 146 (1934) 501-523.
3. F. H. Harlow, J. E. Welch, The Physics of Fluids 8 (1965) 2182-2189.
4. R. B. DeBar, Fundamentals of the KRAKEN code, Internal report, Lawrence Livermore Laboratory, 1974.
5. Y. Renardy, M. Renardy, Journal of Computational Physics 183 (2002) 400-421.
6. D. Gueyffier, J. Li, A. Nadim, R. Scardiovelli, S. Zaleski, Journal of Computational Physics 152 (1999) 423-456.
7. J. U. Brackbill, D. B. Kothe, C. Zemach, Journal of Computational Physics 100 (1992) 335-354.
8. B. Lauffaurie, C. Nardone, R. Scardiovelli, S. Zaleski, G. Zanetti, Journal of Computational Physics 113 (1994) 134-147.



Georgios Folas

Address: IVC-SEP Dept. of Chemical Engineering
Building 229
Technical University of Denmark

Phone: +45 4525 2869
Fax: +45 4588 2258
e-mail: gf@kt.dtu.dk
www: www.ivc-sep.dtu.dk

Supervisor(s): Georgios M. Kontogeorgis
Michael L. Michelsen
Erling H. Stenby

Ph.D. Study
Started: November 2003
To be completed: October 2006

Modeling of Complex Mixtures Containing Hydrogen Bonding Molecules with the CPA EoS

Abstract

The cubic-plus-association (CPA) equation of state has been applied to different types of equilibria (vapor – liquid, liquid – liquid and solid – liquid) of industrially important binary mixtures of alcohol/glycol – water and alcohol – hydrocarbon systems. Very satisfactory vapor – liquid and liquid – liquid correlation of alcohol– water systems is achieved with a common interaction parameter over an extended temperature and pressure range. The CPA equation of state combined with a chemical reaction model provides excellent results of the freezing behavior of selected alcohol/glycol aqueous systems, including the formation of the characteristic solid complex phase.

The CPA equation of state predicts satisfactorily vapor – liquid and solid – liquid equilibria of alcohol – hydrocarbon systems, while adequate vapor – liquid/liquid – liquid/solid – liquid equilibria results can be achieved with a common interaction parameter. Moreover, satisfactory prediction was achieved for the multiphase equilibria of water – alcohol – hydrocarbon systems based solely on binary interaction parameters.

Introduction

The Cubic-Plus-Association (CPA) Equation of State (EoS) is a thermodynamic model which combines the well known Soave-Redlich-Kwong (SRK) EoS for describing the physical interactions with the Wertheim's first order perturbation theory, which can be applied to different types of hydrogen bonding compounds. The fact that the CPA model explicitly takes into account the interactions encountered in mixtures of associating compounds makes it applicable to multicomponent, multiphase equilibria for systems containing associating components. Mixtures of associating components, and in particular mixtures of water and alcohols or glycols with hydrocarbons, are of great interest to the oil and gas industry. Accurate description of such systems is a challenging problem of high technological importance for several petrochemical processes.

CPA is recently extended to the SLE of alcohol–hydrocarbon, alcohol/glycol–water systems including the modeling of the characteristic solid-complex phase which occurs at intermediate concentrations of MEG/methanol and to the multiphase equilibria of alcohol-water-alkane systems.

Results

Figure 1 presents VLE/LLE/SLE correlation results of the binary system of methanol-cyclohexane using a common interaction parameter $k_{12}= 0.04$, while figure 2 demonstrates the ability of the model to satisfactorily calculate the VLE of ethanol-water system with a common interaction parameter $k_{12}= -0.11$ over an extended temperature and pressure range.

Figure 3 presents SLE of MEG-water system included the solid-complex phase. CPA with a single interaction parameter $k_{12}= -0.115$ provides a correlation of both freezing curves over a temperature range of more than 50K. The characteristic solid-complex phase which is formed at intermediate concentrations of MEG mole fraction is modeled using a simple chemical reaction model.

Conclusions

Work in the project so far has demonstrated that the CPA equation of state is able to handle many systems of interest to the oil and gas processing industry. These systems contain a wide-ranging array of different fluid types, including highly associating fluids such as acetic acid, over a range of temperatures and pressures and

including phase equilibrium between vapour, liquid and solid phases depending on the conditions of interest.

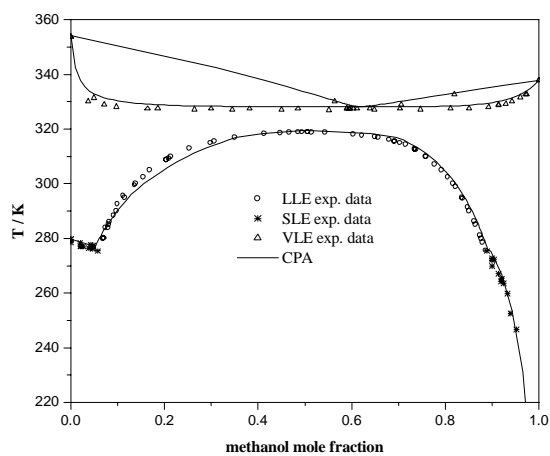


Figure 1. VLE, LLE and SLE in the system methanol-cyclohexane using a single binary interaction parameter over the whole range.

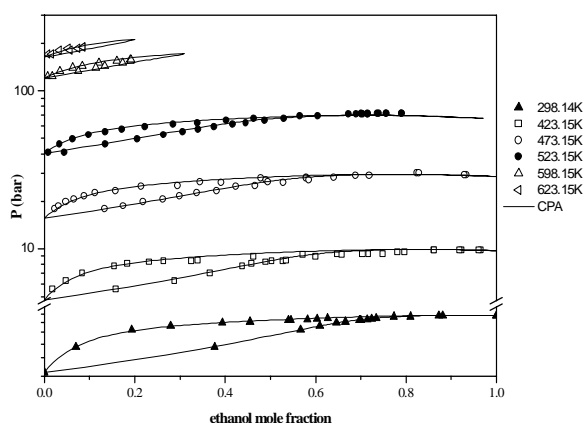


Figure 2. VLE in the system ethanol – water.

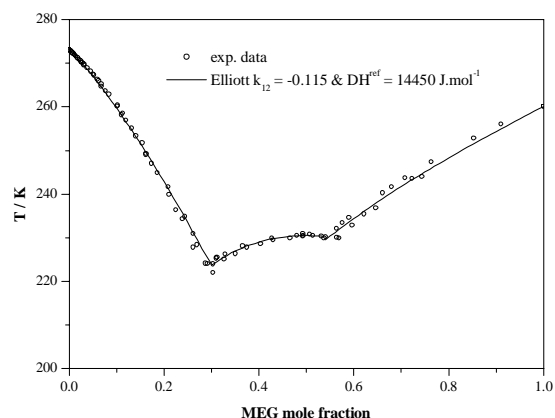


Figure 3. SLE in the system monoethyleneglycol (MEG)-water, including the hydrate region. The two branches of the SLE are captured by the model. The hydrate phase that forms in the range 0.3 to 0.6 mole fraction MEG is modeled using a simple chemical reaction model.

Acknowledgements

The author gratefully acknowledges Statoil for the financial support of this work.

List of Publications

1. Georgios K. Folas, Samer O. Derawi, Michael L. Michelsen, Erling H. Stenby and Georgios M. Kontogeorgis, Recent applications of the cubic-plus-association (CPA) equation of state to industrially important systems. (**Fluid Phase Equilibria**, *in press*)
2. G.K. Folas, J. Gabrielsen, M.L. Michelsen, E.H. Stenby, G.M. Kontogeorgis, Application of the Cubic-Plus-Association (CPA) Equation of State to Cross-Associating Systems (submitted for publication)



Philip Loldrup Fosbøl
Address: IVC-SEP, Dept. of Chemical Engineering
Building 229, office 218 (to be changed)
Technical University of Denmark
Phone: +45 4525 2868
Fax: +45 4588 2258
e-mail: plf@kt.dtu.dk
www: www.ivc-sep.kt.dtu.dk/staff/PLF/
Supervisor(s): Kaj Thomsen
Erling H. Stenby
Kim Rasmussen, Mærsk Oil and Gas A/S
Ph.D. Study
Started: February 2004
To be completed: January 2007

Corrosion in Wet Gas Pipelines

Abstract

Wet gas is natural gas containing small amounts of CO_2 and is saturated in water. During transportation in pipelines, water condenses at the cold pipe wall and CO_2 is dissolved in water. The electrolytic environment is prone to corrode the lower peripheral part of the pipeline. Various corrosion products are produced, some protecting against corrosion, depending on the chemical environment. An equilibrium model of the corrosion products will be build using the extended UNIQUAC model. The model will be expanded to include diffusion and reaction at the surface of the pipe-wall to get an understanding of the mechanism behind CO_2 corrosion.

Introduction

Corrosion is a general problem, it propels most of the maintenance and repair costs of the industry in general. The oil and petroleum industry observes wide corrosion problems both at rigs and sub-sea. Some areas are obviously critical but others are vital for the company. Key areas are economy, environment and health. Consider the alarming impact a breakdown could have on the environment, the lives of employees but also to the production and economy of the company. Unfortunately the companies most often deal with the problems as they arise, instead of focusing on potential problems to prevent them from occurring.

The literature has dealt with this problem since before the start of oil production. Through the recent years some significant advances has been made on a real description of the CO_2 corrosion mechanism, [1-3].

The aim of this study is to extend the present understanding of CO_2 corrosion by using the extended UNIQUAC model to describe the activity of the electrolytic aqueous phase and modeling the equilibria and tendency for protective corrosion products to form.

Specific objectives

CO_2 corrosion is the main part of this study. The first phase of this study has been concentrated on making an extended literature study on existing knowledge of CO_2 corrosion. The study has, besides other things, shown that scale formation of corrosion

products is one of the important factors in determining corrosion. $\text{FeCO}_3(\text{s})$ scale and solubility are some of the key factors. The forth coming objects will be to regress the parameters of the chemical system of CO_2 corrosion for the extended UNIQUAC model. Following it will be derived which chemical factors control the dissolution of $\text{FeCO}_3(\text{s})$ at equilibrium. The further goals will be to link the model into an extended model which takes care of diffusion of $\text{CO}_2(\text{aq})$ to the steel surface, diffusion through the porous corrosion product layer and finally surface reaction at the steel. The reaction at the surface forms the protective corrosion product. The mechanism of corrosion is shown in figure 1.

Results and discussion

The model of CO_2 corrosion

Figure 1 shows the important layers next to pipe wall. The bulk phase contains the aqueous phase of electrolyte and dissolved $\text{CO}_2(\text{aq})$. The corrosive $\text{CO}_2(\text{aq})$ will find its way from the bulk phase to the surface by first transportation through a turbulent layer, second diffusion through a thin liquid film, third diffusion through a porous corrosion product layer and finally reaction at the surface, producing more corrosion product or dissolving corrosion product. The activities of species will be described by the extended UNIQUAC model.

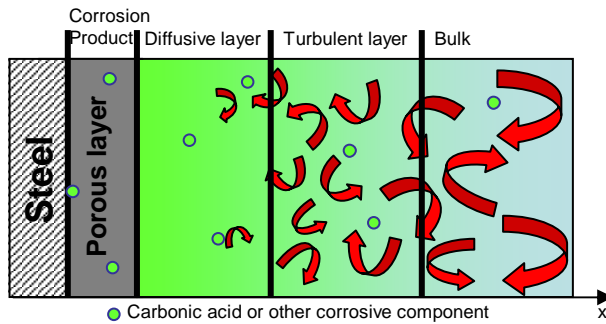


Figure 1: The figure shows the bulk phase containing corrosive species. They diffuse to the steel through a porous corrosion product layer, where they are reduced to corrosion products.

The real Perspective

This project is of great economic importance for the oil industry. Corrosion in wet gas pipelines is widespread in the North Sea. Wet gas is moved from wells to platforms through 16" (40.6cm) pipelines, at long distances. A profile at the bottom of the sea is plotted in figure 2.

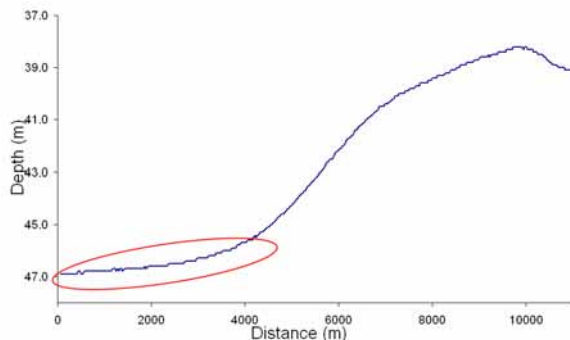


Figure 2: Profile of pipeline at the bottom of the sea. The pipeline is dug a few meters below the sea bed.

There is a level difference from the inlet to the outlet of approximately 10 meters which causes problems with respect to general liquid holdup and local accumulation. Due to the small slope of the pipe, high corrosion is seen in the first part of the pipeline just after the inlet, encircled in figure 2. The higher corrosion in the inlet could also be linked to the higher temperature which can be seen in table 1:

| Pipe | T(°C) | P(barg) | L(m ³ /day) |
|--------|-------|--------------|------------------------|
| Inlet | 45 | Approx. 65 | 2.3 |
| Outlet | 23 | Inlet P-5bar | 6.5 |

The table shows how temperature, pressure and liquid phase flow varies from the inlet to the outlet. The temperature does not fall significantly in the pipeline. It means that liquid holdup is the controlling factor of corrosion. The column L in table 1 is the liquid phase. L is build up between the inlet and the outlet. This is due to the wet gas is saturated with water which at the bottom of the sea, condenses on the colder pipe-wall. A small liquid phase of Glycol and pH-stabilizer is injected at the pipe-inlet, to prevent hydrate plugs along the pipeline. The pH-stabilizer is NaOH which is used

for controlling the chemical environment to prevent corrosion.

The amount of water in the inlet gas phase is very small, contributing with 0,1bar of the total pressure. Still it is one of the most significant factors controlling CO₂ corrosion. CO₂(g) is injected with a partial pressure of approximately 1bar and the CO₂(g) flow is much higher than liquid flow, up to volumetrically 130 times greater than the liquid flow. This way the gas phase acts as a storage of CO₂(g) to be dissolved in the liquid phase. Figure 3 shows an ideal calculation of the electrolytic chemical environment mentioned above.

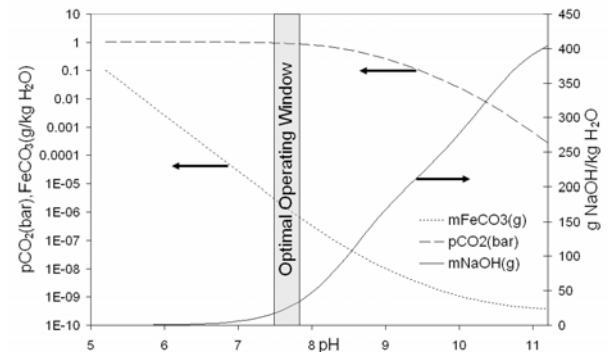


Figure 3: Ideal calculation of chemical environment in the pipes

When no pH-stabilization (NaOH) is added, the pH is 5 and a high solubility of FeCO₃(s) is seen. When small amounts of NaOH is added the pH increases fast and at an addition of approximately 25g NaOH/kg H₂O the pH is 7,5. The key, as mentioned before, is the solubility of FeCO₃(s) which decreases in the pH interval 5 to 7,5 from 0.1g/kgH₂O to 10⁻⁶g/kgH₂O. It is central to notice that above pH=8 significant amounts of CO₂(g) is dissolved in the liquid phase, neutralizing the NaOH and not effectively using it for pH-stabilization. The operating window, shown in figure 3 tells the engineer the correct amount of NaOH to inject with this amount of CO₂(g) flow to prevent iron dissolution and to keep the use of NaOH down to an economical level but also to prevent dissolution of CO₂(g) in the liquid phase.

Conclusion:

Corrosion can be avoided by planning and being alert at the production site. It is important always to have an understanding of the chemicals. This project will expand the understanding of CO₂ corrosion.

Acknowledgement:

I would like to thank Kaj Thomsen for his support in my studies and to Kim Rasmussen, Mærsk, for providing the production data.

References

- Nordsveen M, Nestic S, Nyborg R, et al., Corrosion 59 (5): 443-456, 2003
- Nestic S, Nordsveen M, Nyborg R, et al., Corrosion 59 (6): 489-497, 2003
- Nestic S, Lee KLJ, Corrosion 59 (7): 616-628, 2003



Jostein Gabrielsen

Address: IVC-SEP Dept. of Chemical Engineering
Building 229
Technical University of Denmark
Phone: +45 4525 2869
Fax: +45 4588 2258
e-mail: jog@kt.dtu.dk
www: www.ivc-sep.dtu.dk

Supervisor(s): Georgios M. Kontogeorgis
Michael L. Michelsen
Erling H. Stenby

Ph.D. Study
Started: November 2003
To be completed: October 2006

CO₂ Capture from Coal Fired Power Plants

Abstract

Partial pressures of carbon dioxide (CO₂) over aqueous solutions of monoethanolamine (MEA) have been correlated using a simple approach where only one chemical equilibrium reaction is taken into account, and assuming ideal gas and ideal liquid properties. The approach combines the Henry's law constant and the chemical reaction equilibrium constant for the formation of carbamate for primary alkanolamines, resulting in an explicit expression for calculating the partial pressure of CO₂ over an aqueous MEA solution. Accurate values for the partial pressure of CO₂ are obtained for a limited loading-, temperature-, and pressure range which is useful in modelling CO₂ capture from coal fired power plants.

Introduction

Approximately one third of all CO₂ emissions from human activity come from generating electricity. Therefore CO₂ capture and storage from fossil fuel power plants presents an opportunity to achieve large reductions in greenhouse gas emissions without having to change the energy supply infrastructure and without having to make large changes to the basic process of producing electricity.

CO₂ capture from process streams is an established concept which has achieved industrial practice. There are different process schemes for integrating CO₂ capture with combustion available including pre-, post-, and oxyfuel-combustion. The focus of our work is on post-combustion capture which means that CO₂ is removed from the flue gas; therefore the combustion process is not directly affected. However, energy for the CO₂ removal is taken from the power process, thus lowering the net efficiency of the power production.

There are several techniques for CO₂ capture from process gas streams, of which chemical absorption using alkanolamines in a packed absorption tower is the most commonly used. The technology is currently widely used, though for applications of a scale much smaller than power plant flue gas cleaning. A bottleneck in the process of capturing CO₂ from flue gases with aqueous alkanolamines is the large amount of energy needed to regenerate the absorption liquid which in turn decreases

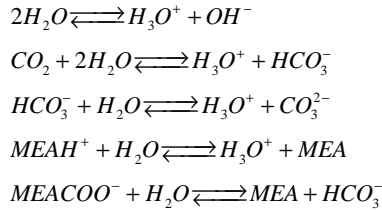
the efficiency of the power plant dramatically. Efficiency reduction for coal fired power plants lies in the range of 7 to 12 %, depending on the alkanolamine and the packing of the absorption tower, which gives a relative decrease in efficiency in the range from 15 to 22 % (Lyngfelt et al.) [1]. The largest contribution to the efficiency decrease originates in the energy needed in the desorption of CO₂.

The focus of our work is to contribute to the modeling and simulation of both the absorption and desorption of CO₂ in aqueous alkanolamines in order to develop reliable tools for the design and optimization of the process. The system is very complex due to the fact that it contains weak electrolytes. Among the key parameters in the design process are the thermodynamics associated with the phase equilibria of systems containing CO₂-water-alkanolamines, the kinetics of the chemical reactions involved and the mass transfer in the system.

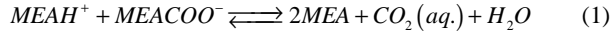
A simple thermodynamic model for MEA

To be able to develop more efficient processes for the separation of acid gases from flue gases, thermodynamic modeling of the vapor-liquid phase equilibrium is the first step. Most thermodynamic models used to represent the vapor-liquid equilibria of CO₂ in an aqueous solution of alkanolamines are very complex and require a large amount of adjustable

parameters. This is due to the fact that the alkanolamines are weak electrolytes and chemical reactions between alkanolamine and CO₂ occur in the liquid phase. Another problem concerning the representation of the vapor-liquid equilibria is that the experimental data existing are not always plentiful and reliable. There is a large scattering particularly at low partial pressures and loadings. In this work a very simple model has been developed for representing the VLE of aqueous alkanolamine solutions. The chemical equilibrium taking place in the liquid phase when CO₂ is absorbed in an aqueous solution of MEA (monoethanolamine) can be written with the following equilibrium equations:



The reaction of CO₂ with aqueous MEA can, given that the loading (moles of dissolved CO₂/moles of alkanolamine) is in the region between 0.02 and 0.48, be approximated by a single chemical equilibrium reaction Astarita [2].



Equation (1) neglects the presence of bicarbonate (HCO₃⁻), hydroxide (OH⁻), and carbonate (CO₃²⁻) ions since the concentration of these ions will be very small in the region of loading which of interest to describe in CO₂ capture from power plants fired with fossil fuels. Given the following definitions:

$$\theta = \text{loading} = \frac{\text{mole } CO_2}{\text{mole amine}}$$

$$a_0 = \text{initial concentration of amine} = \frac{\text{amine}}{\text{amine} + H_2O}$$

K_{CO_2} = combined Henry's law and equilibrium constant for partial pressure of CO₂ over the solution

X_{CO_2} = molefraction of chemically bound CO₂ in the solution

T = temperature (Kelvin)

the concentration of the species involved in the chemical reaction can be written in the following manner:

$$[MEA] = (1 - 2\theta)a_0$$

$$[MEAH^+] = [MEACOO^-] = \theta a_0$$

$$[CO_3^{2-}] \cong [HCO_3^-] \cong 0$$

The expression for the partial pressure of CO₂ can now be written as shown in equation (2).

$$p_{CO_2} = K_{CO_2} X_{CO_2} \frac{a_0 \theta}{(a_0 (1 - 2\theta))^2} \quad (2)$$

Where the combined equilibrium – and Henry's law constant is given by equation (3):

$$\ln K_{CO_2} = A + \frac{B}{T} + Ca_0 \theta \quad (3)$$

A, B and C are all parameters that have to be regressed from experimental data. Some calculations are shown in figure 1.

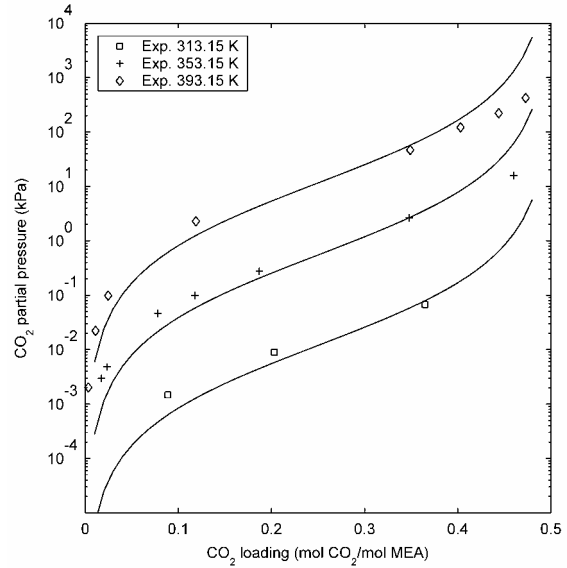


Figure 1 Comparison of model correlation results (solid lines) with experimental data for CO₂ equilibrium partial pressures over an aqueous 30 wt % MEA solution.

Acknowledgements

The author gratefully acknowledges Nordic Energy Research for the financial support of this work.

References

1. Lyngfelt, A., & Leckner, B. Technologies for CO₂ separation, Second Nordic Minisynposium on Carbon Dioxide Capture and Storage. Göteborg, 2001
2. Astarita G., Mass transfer with chemical reactions, Elsevier Publishing Company, Amsterdam/London/New York, 1967

List of Publications

1. J. Gabrielsen, M.L. Michelsen, E.H. Stenby, G.M. Kontogeorgis, A Model for Estimating CO₂ Solubility in Aqueous Alkanolamines (submitted for publication)
2. G.K. Folas, J. Gabrielsen, M.L. Michelsen, E.H. Stenby, G.M. Kontogeorgis, Application of the Cubic-Plus-Association (CPA) Equation of State to Cross-Associating Systems (submitted for publication)

**Morten Skov Hansen**

Address: DTU Building 229
Phone: +45 4525 2804
Fax: +45 4588 2258
e-mail: msh@kt.dtu.dk
www: www.capec.kt.dtu.dk

Supervisor(s): Sten Bay Jørgensen
John Villadsen

Ph.D. Study
Started: February 2001
To be completed: August 2004

Investigation of Spontaneous Cell Cycle Synchronization of *Saccharomyces Cerevisiae*

Abstract

In experimental yeast cultivations, yeast itself is able to invoke sustained oscillations. Understanding of the mechanisms causing cell cycle synchronization may also reveal information about the internal regulatory mechanisms which are active near the critical dilution rate. Experimentally observed oscillation periods exhibit a large variation at a fixed dilution rate. Often the oscillation period is lower than the steady state doubling time for the cultivation but oscillation periods longer than the doubling time are also found in my experiments. The aim of the proposed population balance model is to provide a plausible understanding for the fact that oscillation periods can be longer than the doubling time of the population.

Introduction

An interesting characteristic seen in laboratory scale *Saccharomyces cerevisiae* cultivations, is the ability of yeast itself to invoke spontaneous oscillations in continuous aerobic, glucose limited conditions. Several different modes of oscillations have been found. 1) Glycolytic oscillations with oscillation period in the range of seconds, 2) Oscillations of the population in the range of ~50 minutes which are independent of the dilution rate, 3) Cell cycle synchronization where the period of oscillation depends on the dilution rate. In the following the focus will be on the third kind of oscillations.

At non-oscillatory cultivation conditions, *S. cerevisiae*, shows two different growth regimes; at low dilution rates the growth is purely oxidative, and the main products are biomass and CO₂; at high dilution rates the growth is changed to oxido-reductive, and also ethanol is formed. The dilution rate, where ethanol appears, is called the critical dilution rate (D_{crit}). Since the maximal productivity of biomass (D_x) is reached near D_{crit} , it is of significant interest to perform cultivations as close to the critical dilution rate as possible. The point of incipient ethanol formation is also termed the respiratory bottleneck [1].

The interest in the cell cycle synchronization is motivated by the fact that these oscillations show ethanol formation at dilution rates significantly below the critical dilution rate. This observation indicates that

the ethanol formation at the critical dilution rate in non synchronous cultures may not be solely explained by a limited respiratory capacity, and an understanding of the mechanisms that cause cell cycle synchronization may also reveal understanding concerning the regulatory mechanisms that are active near the critical dilution rate. Such insight may be essential for maximizing productivity of continuous cultivations.

Background

To explain the mechanism for the spontaneous synchronization of the cell cycle, some kind of "communication" between the cells has to take place. Thus, there must be some "signalling" metabolite(-s) which make the communication possible. During synchronized cell growth the oscillations can be observed in many variables, such as CO₂, O₂, dissolved oxygen, ethanol, acetate etc. and also in internal metabolites, such as amino acids, NADH, protein and the carbohydrate storage compounds glycogen, trehalose, [2,3].

In laboratory bioreactors, oscillations in yeast cultivations are often seen, and they can be difficult to avoid as only small disturbances in the cultivation conditions can possibly invoke the synchronization. This normal behaviour was also expected with the strain CEN.PK113-7D but numerous experiments failed to give spontaneous self sustained oscillations. Thus a method to induce oscillations seemed necessary.

The progression through the cell cycle is divided into four different phases (Figure 1); the first phase is a growth phase called G_1 . Here the cell size is increased and storage compounds are accumulated in the preparation for the cell division/budding. Once the cell has reached a critical size, it progress past a START point and enters the S-phase characterized by replication of the DNA and emergence of a bud, the beginning of a new daughter cell. When the cell has progressed past the START point it will not stop the division before it is back in the G_1 -phase again.

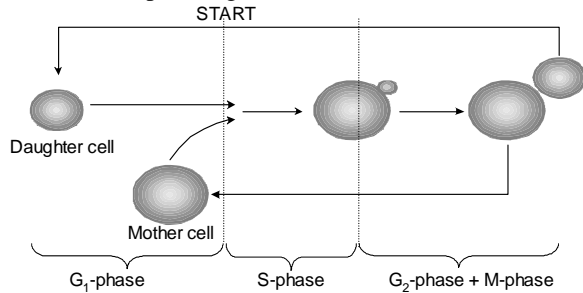


Figure 1 Schematic overview of the cell cycle. Once the cell is past the G_1 -phase it will not stop before it reaches the G_1 -phase again.

After proper DNA replication a new growth phase called G_2 is entered; here preparation for the final segregation of the newly copied DNA into the newly formed daughter cell takes place. The actual segregation and physical division is performed in the final M-phase. The newly formed mother and daughter cells are born into the G_1 -phase and everything starts over again. Because the cells will not progress past START before reaching a proper size a deprivation of substrate would make cells already past START finish the cell cycle and end up in G_1 -phase, while cells already in the G_1 -phase will not start a new cell cycle. This observation provides the foundation for the method to provoke cell synchronization. This method developed and was tested in two experiments.

Experimental observations

Since cells will not progress past the START point unless certain growth conditions are present it was investigated how a stop in substrate feed influenced the number of budding cells (Figure 2). From the figure it is seen that the stop triggers budding as well as an increase in the number of dividing cells during the first 20 minutes after the stop. After another 50 minutes the number of budding cells starts decreasing. To investigate if stop in feed flow can be used as inducer of cell synchronization a procedure using three successive stops in the feed flow where each stop lasted for 30 minutes was tested. The procedure was tested on two parallel experiments. The results are shown in Figure 3. An obvious question when inspecting the oscillations is if these oscillations simply are a synchronization effect, or if the average cell behaviour is different when growing under cyclic conditions. The average CO_2 concentration of the two experiments during the oscillations in Figure 3 was compared and it was found

that the difference is only 0.2%. In a period of 25 hours prior to the forcing of the oscillations, the difference between the CO_2 signals was calculated to be 0.4%. I.e. the net CO_2 production does not change during oscillations.

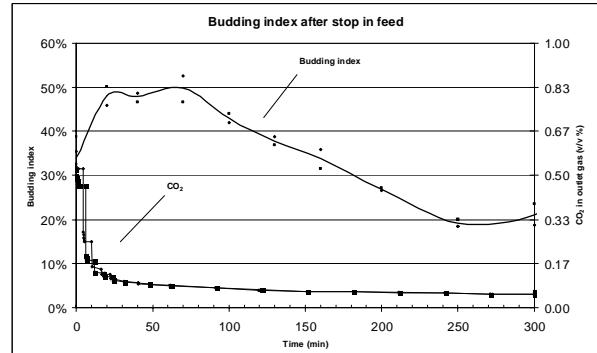


Figure 2 Development in the number of budding cells after stop of feed flow.

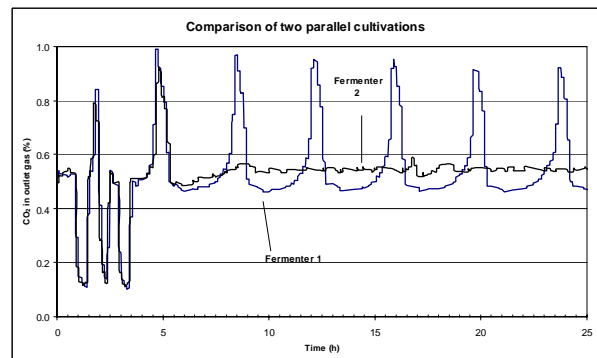


Figure 3 Example of oscillations induction in a continuous cultivation with the yeast strain *S. cerevisiae* CEN.PK113-7D. Two cultivations were run in parallel resulting in an oscillating and non oscillating culture. The average CO_2 concentration in the outlet gas was equal for the two fermentations.

If the whole population grows in synchrony, the asymmetric division of the yeast cell is expected to result in an oscillation period which is equal to or below the doubling time of the population ($T_{doubling} = \ln(2)/D$). If this is the case washout of the cells is avoided. However the oscillation period is in my experiments often seen to be much longer than the doubling time. To describe this observation a model was constructed.

Oscillations in a mixed population of synchronous and asynchronous cells

The search for mechanisms responsible for sustained oscillations in *S. cerevisiae* has been intensely pursued by several investigators. This search has revealed several general conditions which have to be fulfilled for sustained oscillations to appear [4-8]. Generally speaking the models proposed explain many of the phenomena encountered in oscillating cultivations, but in the case where the experimental

oscillation period, T_{osc} , exceeds the doubling time ($\ln(2)/D$), the previous models do not predict the experimental results any more. In my work very long oscillation periods were observed, and also in literature oscillation periods longer than the doubling time are reported (Figure 4).

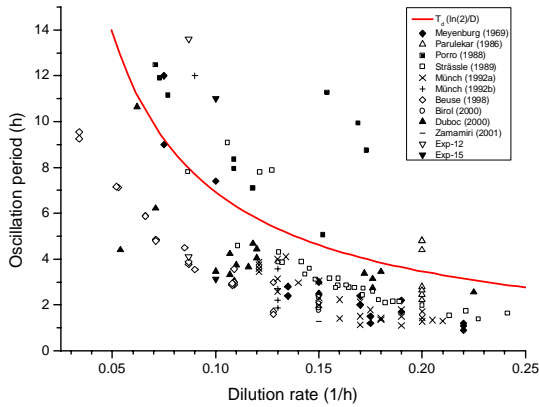


Figure 4 Oscillation periods for *S. cerevisiae* as a function of dilution rate collected from different sources. The solid line is the doubling time ($\ln(2)/D$) for a given dilution rate [7-16].

In order to develop a population balance model one must assume a certain population structure. This requires a hypothesis for the cell cycle of *S. cerevisiae* and for how the lengths of mother and daughter phases interact. In Figure 1 a very simple model of the cell cycle is shown, but in other cases the genealogical age will change the time a mother or daughter cell use in a specific phase and thus render this picture more complicated. The proposed models in this paper, describe the oscillatory behaviour of yeast cultivations, by dividing the population into categories such as daughter cells and mother cells. In some cases these classes are further subdivided to improve the description of the population.

The main purpose of my model is to describe the population structure of a cultivation when the oscillation period is longer than or equal to the doubling time. The model should of course also be able to explain oscillations with a duration shorter than the doubling time (which even the one population model can). The experimental results used to investigate oscillations are often derived from cell counting and budding index as used here - rather than on cell mass. On this basis the model is based on cell *number* concentrations.

This modelling work uses the concept that part of the population is growing asynchronously wherein cells always divide, while another part of the population is showing synchronous growth with a discrete division point. With this model structure oscillation periods longer than the doubling time will result in a washout of the synchronous population. To avoid this, an extra coupling between the two populations has to be

included. The cells in the asynchronous population can be recruited by the synchronous subpopulation. This recruitment is described by a first order reaction step with the rate $\gamma N_a(t)$ (N_a is the cell number and γ the rate constant). In Figure 5 the model concept is illustrated¹. It differs substantially from conventional models used to describe oscillations in yeast cultivations.

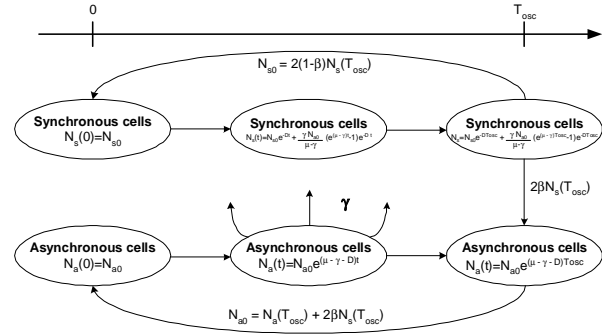


Figure 5 Illustration of the model concept. At the time of division cells are transferred from the synchronous population to the asynchronous sub-population, and cells in N_s will again start growing at T_{osc} , but in a new generation, which again will start from time zero. Cells are continuously transferred from the asynchronous- to the synchronous sub-population during the whole interval $]0, T_{osc}[$.

In the present model it is assumed that the recruitment of cells from the asynchronous population occurs continuously over time, but the justification for the introduction of the parameter γ is based on the observations in laboratory cultivations where ethanol and acetate are formed at the entrance to the division process [2,9].

In reality γ may not be a constant. It could be that the rate of transfer of cells from N_a to N_s depends on the environment which must vary when the culture is partly synchronized. Thus at the peak of ethanol or acetate secretion γ could for example be greater. In [17] it was found that the higher the level of storage carbohydrates were, the higher amount of cells did start dividing when subject to substrate changes. This means that in a more detailed model than used here $\gamma = F(\text{ethanol, acetate, storage carbohydrates})$.

Transfer of cells to the asynchronous culture at T_{osc} could be amplified by a poor regulation of the cycling time. Also the synchronous culture may accumulate internal metabolites (glycogen and trehalose) that increase the fraction of cells transferred to the asynchronous culture, β . Here however the parameters γ and β are kept constant for the sake of simplicity.

The model is used on two examples; the first example is based on the data from Experiment 12, where the fermentation conditions are given in Table 1. This example is used at conditions where the oscillation

¹ The entire model will be given in my thesis work.

period is close to the doubling time of the population, where most other models fail to describe the behaviour.

Table 1 Cultivation conditions for example 1, data from Experiment-12.

| Parameter | Value |
|---------------|-------|
| D (1/h) | 0.10 |
| T_{osc} (h) | 6.84 |
| BI_{min} | 0.20 |
| BI_{max} | 0.43 |

In the second example the results from [8] is used, where a oscillating continuous culture is grown at a dilution rate of 0.071 h⁻¹, the complete cultivation conditions are given in Table 2. The data are chosen to verify the model for an oscillation period well below the average doubling time. The cultivation data in Table 2 is passed into the model for different values of B_a ².

Table 2 Cultivation conditions for example 2, data from [8].

| Parameter | Value |
|---------------|-------|
| D (1/h) | 0.071 |
| T_{osc} (h) | 6.22 |
| BI_{min} | 0.07 |
| BI_{max} | 0.543 |

As we do not have the relation between the budding index and the growth rate for the asynchronous population (B_a), we use this as a free parameter in the model.

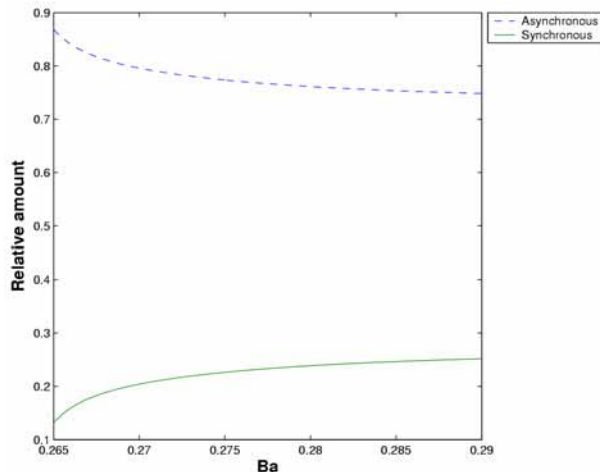


Figure 6 Plot of the relative amount of asynchronous (hatched line) and synchronous (full line) cells as function of the budding index of the asynchronous population (example 1).

It is interesting to see that the budding index of the asynchronous culture only gives solutions in the range

² Budding index of an asynchronous growing culture (dependent on the dilution rate).

0.316-0.375, which means that the growth rate of the asynchronous culture has to be relatively high. In a completely asynchronous growing culture at the same cultivation conditions with the same strain, the budding index was measured to be in the range 30-35%, which seems plausible in this context.

From the model the relative size of the synchronous population can be calculated for the two examples, and the results are shown in Figure 6 and Figure 7. It is easily seen that the first example with a relative small distance between the maximum and minimum budding index and at the same time a rather long oscillation period (Figure 6) has a relative smaller amount of synchronous cells in the population. During the given conditions the models predicts that there can be no more than 39% of the cells in the population which are growing synchronously.

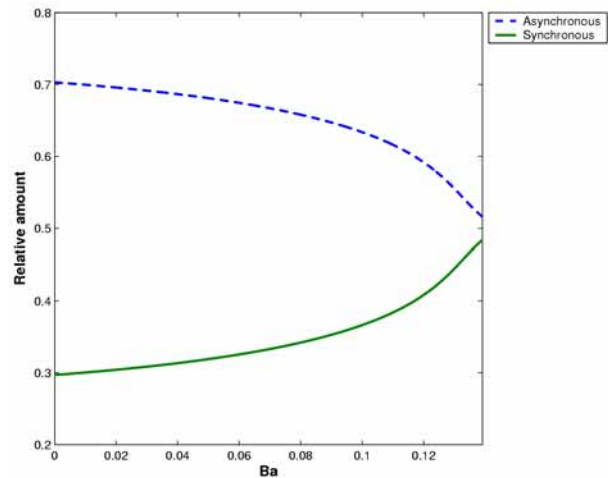


Figure 7 Plot of the relative amount of asynchronous (hatched line) and synchronous (full line) cells as function of the budding index of the asynchronous population in example 2.

Conclusion

In order to investigate the oscillatory behaviour methods have been investigated to ensure oscillations in all experiments. From the oscillations obtained large variation in the oscillation period is observed. A model has been developed, which is able to predict oscillation periods longer than the doubling time of the population. The degree of synchronization can be determined from measurements in the budding index and oscillation period, for a given dilution rate. A very simple way of getting an idea of the actual state of the oscillations.

The two examples on which the model is evaluated indicate that the longer oscillation periods may be interpreted as a small fraction of cells which growing synchronously while the asynchronous population is rather large and helps avoiding washout. The synchronous population which is responsible for the oscillations is maintained by the asynchronous population by recruitment from the synchronous population. This mechanism requires communication

between the cells, which is hypothesised to originate from the formed ethanol and acetate at the entrance to the S-phase, however this mechanism is not included into this model, which only is concerned about the cell number concentrations of the two subpopulations.

References:

1. Sonnleitner, B. & Käppli, O. Growth of *Saccharomyces cerevisiae* Is Controlled by Its Limited Respiratory Capacity: Formulation and Verification of a Hypothesis. *Biotechnol. Bioeng.* **28**, 927-937 (1986).
2. Duboc, P., Marison, I. & von Stockar, U. Physiology of *Saccharomyces cerevisiae* during cell cycle oscillations. *Journal of Biotechnology* **51**, 57-72 (1996).
3. Hans, M.A., Heinzle, E. & Wittmann, C. Free Intracellular Amino Acid Pools During Autonomous Oscillations in *Saccharomyces cerevisiae*. *Biotechnol. Bioeng.* **82**, 143-151 (2003).
4. Strässle, C., Sonnleitner, B. & Fiechter, A. A predictive model for the spontaneous synchronization of *Saccharomyces cerevisiae* grown in continuous culture. I. Concept. *Journal of Biotechnology* **7**, 299-318 (1988).
5. Bellgardt, K.-H. Analysis of synchronous growth of baker's yeast. Part I: Development of a theoretical model for sustained oscillations. *Journal of Biotechnology* **35**, 19-33 (1994).
6. Bellgardt, K.-H. Analysis of synchronous growth of baker's yeast. Part II: Comparison of model prediction and experimental data. *Journal of Biotechnology* **35**, 35-49 (1994).
7. Beuse, M., Bartling, R., Kopmann, A., Diekmann, H. & Thoma, M. Effect of the dilution rate on the mode of oscillation in continuous cultures of *Saccharomyces cerevisiae*. *Journal of Biotechnology* **61**, 15-31 (1998).
8. Duboc, P. & von Stockar, U. Modeling of oscillating cultivations of *Saccharomyces cerevisiae*: Identification of population structure and expansion kinetics based on on-line measurements. *Chemical Engineering Science* **55**, 149-160 (2000).
9. Meyenburg, K.v. Katabolit-Repression und der Sprossungszyklus von *Saccharomyces cerevisiae*. 1969. ETH Zürich. Ref Type: Thesis/Dissertation
10. Parulekar, S.J., Semones, G.B., Rolf, M.J., Lievense, J.C. & Lim, H.C. Induction and Elimination of Oscillations in Continuous Cultures of *Saccharomyces cerevisiae*. *Biotechnol. Bioeng.* **28**, 700-710 (1986).
11. Porro, D., Martegani, E., Ranzi, M.B. & Alberghina, L. Oscillations in Continuous Cultures of Budding Yeast: A Segregated Parameter Analysis. *Biotechnol. Bioeng.* **32**, 411-417 (1988).
12. Strässle, C., Sonnleitner, B. & Fiechter, A. A predictive model for the spontaneous synchronization of *Saccharomyces cerevisiae* grown in continuous culture. II. Experimental verification. *Journal of Biotechnology* **9**, 191-208 (1989).
13. Münch, T. Zellzyklusdynamik von *Saccharomyces cerevisiae* in Bioprozessen. 1992. Eidgenössischen Technischen Hochschule Zürich. Ref Type: Thesis/Dissertation
14. Münch, T., Sonnleitner, B. & Fiechter, A. New insights into the synchronization mechanism with forced synchronous cultures of *Saccharomyces cerevisiae*. *Journal of Biotechnology* **24**, 299-314 (1992).
15. Birol, G., Zamamiri Abdel-Quader, M. & Hjørtsø, M.A. Frequency analysis of autonomously oscillating yeast cultures. *Process Biochemistry* **35**, 1085-1091 (2000).
16. Zamamiri Abdel-Quader, M., Birol, G. & Hjørtsø, M. Multiple Stable States and Hysteresis in Continuous, Oscillating Cultures of Budding Yeast. *Biotechnol. Bioeng.* **75**, 305-312 (2001).

17. Guillou, V., Plourde-Owobi, L., Parrou, J.L., Goma, G. & Francois, J. Role of reserve carbohydrates in the growth dynamics of *Saccharomyces cerevisiae*. *FEMS Yeast Research* **4**, 773-787 (2004).

**Natanya Majbritt Louie Hansen**

Address: Building 423, room 206
Phone: +45 4525 6819
Fax: +45 4588 2161
e-mail: nha@polymers.dk
www: www.polymer.dk

Supervisor(s): Søren Hvilsted
Michael Gerstenberg, Novo Nordisk A/S

Ph.D. Study
Started: January 2004
To be completed: December 2006

Development of New Synthetic Membranes for Use in Glucose Sensors

Abstract

Membranes are a crucial part of glucose sensors for in-vivo use and the demands on the material properties are numerous. These requirements can be met by careful selection of chemical characteristics of two polymers joined into block copolymers. In the current project, synthesis of amphiphilic copolymers are proposed utilizing atom transfer radical polymerization (ATRP); a controlled radical polymerization method. Preliminary studies have shown that polymers with narrow polydispersity indexes can be obtained by this method.

Introduction

It is expected that Diabetes Mellitus will reach epidemic dimensions in the next decades. Type 2 diabetes, which often is related to insulin deficiency in the body, is rapidly growing among the world population as the Western way of life is adapted. Especially among the Asian population a disproportional large number of new type 2 diabetes have been observed as the life style has changed. From being considered as an 'old age disease', the age is rapidly declining for the onset of type 2 diabetes. Furthermore, only approximately half of all people with diabetes have been diagnosed. Poorly administered diabetes treatment can lead to difficult late complications such as cardiovascular diseases, kidney damage, and blindness. Thus, there exists a large and resource demanding task to treat people with diabetes. However, studies have shown that late complications can be reduced significantly by tight control of the glucose level in the body. For the immediate insulin demanding type 1 diabetes, glucose monitoring is an important part in maintaining a normal way of life. The right mix of insulin types can be found and low sugar levels (hypoglycemia), which can lead to unconsciousness and loss of life, can be avoided [1].

Membranes are integrated in many different types of glucose sensors. In the traditional glucose biosensors for in-vivo use, membranes have several functions such as [2]:

- Reduction of the glucose concentration with regard to the oxygen concentration.

- Ensuring biocompatibility.
- Encapsulation of non biocompatible materials in the sensor (such as enzymes).
- Reduction of signal from interfering substances (such as C-vitamin and pain killers).

Biosensors intended for in-vivo use are subject to the harsh conditions resulting from the immune response and are therefore demanding from a materials choice perspective. To reduce the response, segments incorporating e.g. polyurethane have been utilized in block copolymer design, however, there still exists a growing need for developing copolymers which can form layers with predetermined bulk and surface properties.

Objective

Numerous patents and articles have been published on the materials suited for membranes. Block copolymers have been an often sought route, since they can be tailored to have the desired multifunctionality. In the current project amphiphilic copolymers i.e. copolymers containing both a hydrophilic and a hydrophobic functionality are sought.

It is important that the copolymer can be made into thin films in order for key parameters such as the permeability of glucose and other penetrants to be measured.

Synthesis method

A strategy for the synthesis of the copolymers is atom transfer radical polymerization (ATRP), a technique of controlled/"living" radical polymerization

developed by Matyjaszewski [3]. The method involves the use of a metal catalyst (Mt), a multidentate ligand (L) and a halogenated initiator, which all interact with the active polymer chain (see Fig. 1). There exists equilibrium between an activated ($R\cdot$) and a dormant ($R-X$) polymer species with the deactivation reaction being kinetically favoured. Ideally, this eliminates the possibility of two activated polymer chain ends encountering to give termination, while in practice termination does occur.

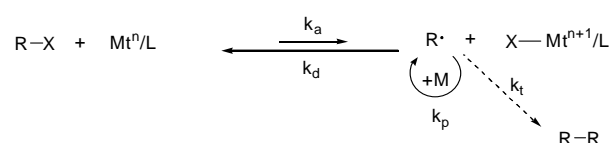


Figure 1. Mechanism of ATRP. Mt=metal catalyst, R=polymer chain, X=halogen, M=monomer, L=ligand. k_a , k_d , k_p and k_t are the rates of activation, deactivation, propagation and termination, respectively

Using the ATRP method polymer products with well-defined structures and narrow molecular weight distributions can be obtained and the potential polymer structures are numerous. The product of an ATRP reaction is a potential initiator for yet another reaction, as it still has the halogen moiety in the growing chain end. This allows reactivation of the chain end and makes ATRP especially suited for synthesizing tailored block copolymers.

Results

A number of preliminary syntheses have been run with methyl methacrylate (MMA) to test the polymerization method with the used setup. The polymerizations have been carried out in xylene using Cu(I)Br as catalyst and varying the ligand. Three different ligands used in the literature [4] have been studied: 1,1,4,7,7-pentamethyldiethylene triamine (PMDETA), 1,1,4,7,10,10 hexamethyltriethylene tetramine (HMTETA) and 2,2'-bipyridine (Bipy). The results of these syntheses have been satisfactory with low polydispersity index (PDI) and number average molecular weights (M_n) close to the target of 20,000 g/mol (table 1).

Table 1 Results of preliminary ATRP of MMA

| Sample | Ligand | PDI ^a | M_n^a (g/mol) | Yield (%) |
|--------|--------|------------------|--------------------|--------------|
| 1 | PMDETA | 1.07 | 15,400 | 38 |
| 2 | HMTETA | 1.21 | 22,500 | 89 |
| 3 | Bipy | 1.20 | 22,600 | 40 |

^aDetermined by size exclusion chromatography

Future work

Using the experience from the preliminary testing the polymerization of the amphiphilic block copolymers will be undertaken.

The future work will include characterisation of the synthesised block copolymers with regard to structure including nuclear magnetic resonance spectroscopy (¹H-NMR) and infrared spectroscopy (IR) in addition to size exclusion chromatography (SEC). Once fabricated in thin films, the relation between bulk structure and chemical and physical properties (such as the permeability and tensile strength) will be evaluated in addition to the surface ordering and chemistry.

Acknowledgements

I would like to thank Novo Nordisk A/S for supporting this project.

References

1. For a more detailed description of Diabetes, see e.g. www.diabetes.org.
2. D. M. Fraser, "Biosensors in the Body: Continuous *in vivo* Monitoring", John Wiley & Sons, 1997, Chapter 1.
3. J.-S. Wang, K. Matyjaszewski, *J. Am. Chem. Soc.*, 117 (1995) 5614 – 5615
4. J. Xia, K. Matyjaszewski, *Macromolecules* 30 (1997) 7697 - 7700



Thomas Steen Hansen

Address: Building 423 room 220
 Phone: +45 4525 6825
 Fax: +45 4588 2161
 e-mail: tsh@polymers.dk
 www: www.polymer.dk

Supervisor(s): Ole Hassager

Ph.D. Study

Started: October 2004
 To be completed: September 2007

Testing and Fabrication of All Polymer Micropump

Abstract

The main objective of the project is to examine and test microfluidic pumps produced with polymers. Currently the main field of research is the AC electroosmotic micropump, which has the advantage of a simple structure, no movable parts and low requirements to the applied potential. The AC electroosmotic micropump is a relative new discovery and initial research implies numerical simulations of the system in order to optimise the geometry and generate an understanding of the phenomenon producing the pumping effect.

Introduction

The ability to control chemical processes on the micrometer scale has many interesting perspectives and is a field in fast expansion. One of the main issues when dealing with microsystems is the pumping of fluid. Several techniques have been used for this purpose and one of the most interesting is the electroosmotic pump. A special case of this pump is the asymmetric AC electroosmotic pump (ACEO) first suggested by Ajdari¹. The pump consists of an array of asymmetric electrodes in a channel with an AC potential between the electrodes. This is presented in figure 1. The advantages of the pump are the simple construction, no moveable parts and require a low potential (1-5 V). The

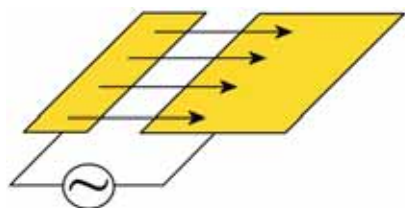


Fig. 1 The principle of an ACEO pump. The asymmetric shape of the electrodes creates an asymmetric electric field, which induces a non-zero horizontal force to the ions in the fluid. The friction between the ions and the fluid creates a pumping effect from the small to the large electrode.

ACEO pump has been described both experimentally²⁻⁷ and theoretically^{1,2,8,9}, but no numerical simulations of the system have been performed. As a mean to optimise

the geometry numerical simulations of the ECEO pump were therefore performed.

Theory

The three governing equations when simulating the ACEO pump are Poisson's equation (1), the mass transfer equation (2) and the incompressible Navier-Stokes equation (3).

The electric regime is described by Poisson's equation, and simplifying the system to a monovalent salt yields equation (1) where ϕ is the potential, ρ is the

$$\nabla \phi = -\frac{\rho}{\epsilon} = -\frac{F \cdot (c^+ - c^-)}{\epsilon} \quad (1)$$

space charge density and ϵ is the dielectric constant of the fluid, F is Faradays constant, c^+ and c^- are the concentration of the positive and negative ions.

The flux of the charged ions is found by using the

$$\frac{\partial c_i}{\partial t} + \mathbf{v} \cdot \nabla c_i = D_i \cdot \nabla^2 c_i + z_i \cdot u_i \cdot \nabla (c_i \cdot \nabla \phi) \quad (2)$$

mass transfer equation¹⁰ (2), where D is the diffusion coefficient, \mathbf{v} is the flowfield with the components v_x and v_y , z is the charge of the ion and u is mobility.

The fluid mechanical part of the system is determined by the incompressible Navier-Stokes equation (3a) and (3b), where ρ_{dens} is the density of the fluid, μ is the viscosity and p is the pressure. The last term in eq. (3a) is the force caused by the moving ions.

$$\rho_{dens} \left(\frac{\partial \mathbf{v}}{\partial t} + \mathbf{v} \nabla \mathbf{v} \right) = -\nabla p + \eta \cdot \nabla^2 c_i + \sum z_i \cdot F \cdot c_i \cdot \nabla \phi \quad (3a)$$

$$\nabla \cdot \mathbf{v} = 0 \quad (3b)$$

Using equation (1), (2), and (3) it has been possible to perform numerical simulations of ACEO pump and optimise the geometry to its maximum performance.

Results and Discussion

The numerical simulations revealed that especially the height of the channel is important for the pumping properties. The propulsion of the fluid occurs at the walls near the surface of the electrodes and in contrary to normal systems the pump is most efficient at low diameters. The maximum pressure the pump is capable of delivering is approximately inversely proportional to the squared height of the channel. Another interesting perspective revealed by the numerical simulations was the pumps ability to pump in both directions. The

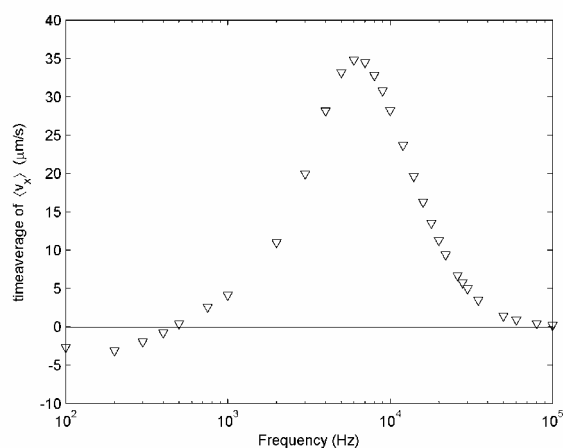


Fig. 2 A simulated frequency sweep of the micropump. The pump is capable of pumping in the reverse direction at low frequencies. .

pumping direction can be reversed by lowering the frequency of the AC potential, which enhances the positive prospects of the ACEO pump. The result of a simulation series is presented in figure 2.

The numerical simulations were followed up with experimental work and a pump was produced using classical lithographic methods for microsystems. A picture of a pump is presented in figure 3. The electrodes are gold layers on glass. The produced pump has been tested and showed a pumping effect and the expected ability to pump in both directions. One of the problems with the current design and fabrication method is that the electrode array is damaged at high potentials (above 2-3 V). This problem could be solved by choosing another material than gold for the electrodes, because gold does not have good adhesive properties with glass. Recent research has shown that the conductive polymer poly-3,4-ethylenedioxythiophene (PEDT) (figure 4) can be produced with a relatively simple method and have conductivity¹³ up to 1000 S/cm. PEDT

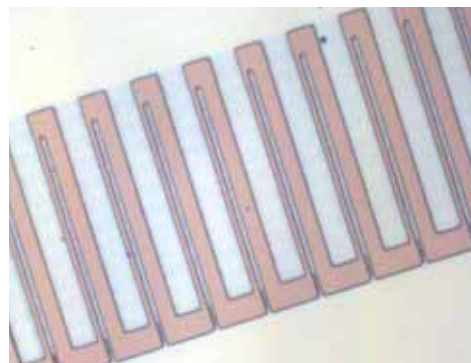


Fig. 3 A picture of the micropump seen from above. The pump consists of gold (bright) on glass (dark). The small electrodes have a size of 4 μm and the large electrodes have a size of 20 μm .

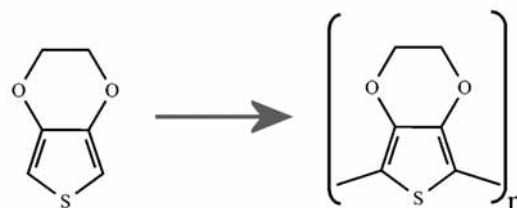


Fig. 4 The polymerization of 3,4-ethylenedioxythiophene yields the .

has the advantage of stability in aqueous solutions and micro patterning abilities.

The future work concerns the development of methods for handling and fabrication of the polymer micropump and studies of PEDT's properties in the microfluidic environment.

References

- 1 A. Ajdari, *Physical Review E*, 2000, **61**, 45;
- 2 A. B. D. Brown, C. G. Smith and A. R. Rennie, *Physical Review E*, 2000, **63**, 16305
- 3 N.G. Green, A. Ramos, A. González, H. Morgan, A. Castellanos, *Physical Review E*, 2000, **61**, 4011
- 4 N.G. Green, A. Ramos, A. González, H. Morgan, A. Castellanos, *Physical Review E*, 2002, **66**, 26305
- 5 M. Mpholo, C. G. Smith and A. B. D. Brown, *Sensors and actuators B*, 2003, **93**, 262
- 6 V. Studer, A. Pépin, T. Chen, A. Ajdari, *The Analyst*, 2004, **129**, 944;
- 7 S. Debesset, C.J Hayden, C. Dalton, J.C.T Eijkel, A. Manz, *Lab on a Chip*, 2004, **4**, 396;
- 8 N.G. Green, A. Ramos, A. González, H. Morgan, A. Castellanos, *Physical Review E*, 2000, **61**, 4019
- 9 N. A. Mortensen, L. Belmon, L. H. Olesen. And H. Bruus, *Not published yet*;
- 10 E. Yeager, J.O. Bockris. B. E. Conway and S. Sarangapani, *Comprehensive treatise of electrochemistry* 6, 1983, 1st ed., Plenum Press;
- 11 E. Gileadi, *Electrode kinetics*, 1993, 1st ed., VCH;
- 12 R. Byron, W. E. Stewart and E. N. Lightfoot, *Transport phenomena*, 2001, 2nd ed., Wiley;
- 13 B. Winther-Jensen and K. West, *Macromolecules* 2004, **37**, 4538-4543;



Lusi Hindiyarti

Address: Building 229, room 130
Phone: +45 4525 2922
Fax: +45 4588 2258
e-mail: lh@kt.dtu.dk
www: www.chec.kt.dtu.dk

Supervisor(s): Peter Glarborg
Hans Livbjerg
Flemming Frandsen

Ph.D. Study
Started: September 2003
To be completed: August 2006

Gas Phase Sulfur, Chlorine, and Alkali Metal Chemistry in Biomass Combustion

Abstract

The high-temperature sulfur/chlorine/potassium chemistry has important implications for sulfur/chlorine emissions (SO_2 , HCl), aerosol formation (KCl , K_2SO_4) and deposits formation in combustion. The S/Cl/K chemistry in combustion involves both gas phase and condensed phase reactions. An attempt to improve the gas phase chemistry model with addition of aerosol formation to the model is still on going work. The model will be validated using experimental results. A better understanding of the gas phase chemistry and successful modeling of these components may facilitate development of more efficient methods to minimize emission and operation problems in biomass or waste combustion also in boiler design.

Introduction

Combustion and gasification of renewable fuels (biomass, waste) involves a number of chemical reactions, which are important for emissions, aerosol formation and deposition/corrosion. The high-temperature sulfur/chlorine/potassium chemistry has important implications for sulfur/chlorine emissions (SO_2 , HCl), aerosol formation (KCl , K_2SO_4) [1,2] and deposits formation in combustion [3].

Significant efforts in the past have focused on chlorine and sulfur chemistry, but little is known about alkali metal chemistry or the interaction between S, Cl and K. The S/Cl/K chemistry in combustion involves both gas phase and condensed phase reactions [4]. Despite the practical importance of Cl/S/K-interactions, few attempts have been made to understand the detailed kinetics of the system. Current modeling is largely limited to chemical equilibrium calculations. Such calculations do not account for kinetic limitations, which are known to be important for conversion of HCl to Cl_2 or SO_2 via SO_3 to H_2SO_4 . Conversion of KCl to formation of K_2SO_4 , a critical step in aerosol formation, is presumably also kinetically limited but little is known.

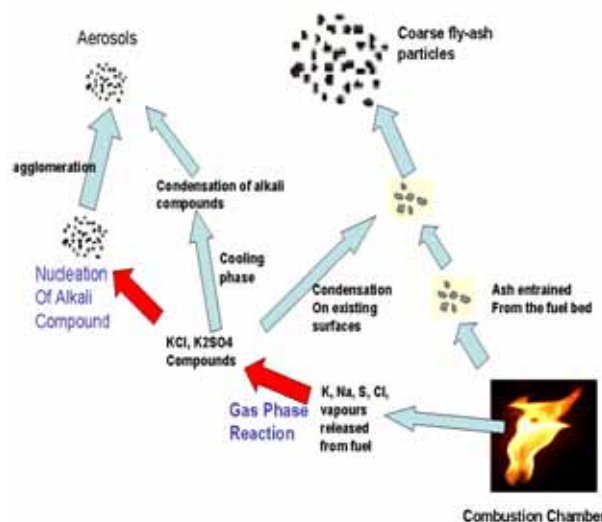


Figure 1: Illustration of the release and fate of K, Na, Cl, and S in biomass combustion (modified from [5])

A better understanding of the gas phase chemistry of these components may facilitate development of more efficient methods to minimize emission and operation problems in biomass or waste combustion systems.

Objective

The objective of this project is to improve the fundamental knowledge of the gas phase chemistry which is important for emissions, aerosol or deposit

formation in combustion of biomass and waste. The aim is to improve the available detailed chemical kinetic model for conversion of chlorine, sulfur and alkali-containing species and their interaction. Such a chemical description can be implemented in reactor models and used to simulate effect of fuel and process parameters on emissions and operation.

Modeling

Gas Phase Chemistry

Presently, existing kinetic models; provide a fairly good description of hydrocarbon oxidation and nitrogen chemistry in high temperature processes. Also a significant knowledge about sulfur and chlorine chemistry is available. In the latest research, a detailed mechanism for alkali metal chemistry and S/Cl/K/Na interactions has been proposed [6]. Using the proposed mechanisms mentioned above as starting mechanisms, the model is expected to be extended and improved by conducting several experiments related to the system. The experimental and modeling work will be a step-by-step attempt to extend our knowledge of this chemistry. The experimental results are interpreted in terms of a detailed reaction mechanism, using the CHEMKIN software package.

Aerosol Formation

In biomass combustion as described in the figure 1 above, the gas phase chemistry of alkali metal, sulfur and chlorine is also accompanied by aerosol formation. In order to be able to model the system closely to the reality, the attempt to couple the gas phase chemistry and aerosol formation is being made.

Formation of aerosols is initiated by a nucleation process, which is a first order phase transition problem, where there is discontinuous change between two phases. There are several models for nucleation theory, but classical nucleation theory incorporated with a curvature dependent surface tension earlier used by Christensen et. al [7] is being used here. An attempt to include aerosol formation model by homogeneous nucleation to the CHEMKIN code is still on going work

Experimental work

The experiments are taking place in a laboratory flow reactor under well-controlled reaction conditions. A reactor set-up equipped with a 3 heating zones oven (figure 2) is used to simulate the system. The separate heating zones are useful to maintain a constant temperature in the KCl feeding tube, and a certain setting temperature in the reaction zones (we can change the temperature of the reactions zone in a range from 800 – 1100 °C, and maintain the feeding system of KCl to be in constant temperature, around 800 °C). The feeding of KCl is done using packed alumina pellets impregnated with KCl and placed in tube in a certain position to ensure a constant temperature. Thereby, a nitrogen stream can be saturated with a certain amount

of KCl. There are two flows for the inlet gases to the reactor. First is the primary flow, nitrogen, as mentioned above, and the other gases is fed into the secondary flow in order to avoid the reaction to occur before the reaction zones.

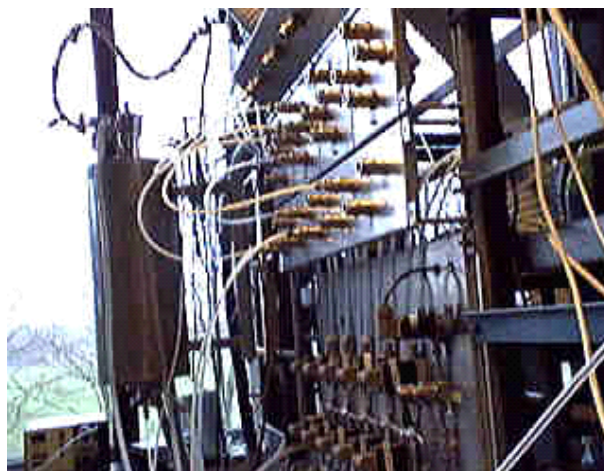


Figure 2: Laboratory flow reactor setup equipped with a 3 heating zone oven for conducting gas phase experiments. The reactor consists of a main alumina tube and an upper inner alumina tube for KCl feeding.

Three different types of experiments were planned in order to study the gas phase chemistry. The first experiment was conducted in order to investigate the amount of potassium release and possibility of it to deposit on the wall. The experiments are done using the set-up equipped with a filter to catch aerosols formed.

For the second type of experiment the influence of potassium chloride on the oxidation of CO is investigated. Potassium in the gas phase will influence the oxidation reaction of CO, $\text{CO} + 0.5\text{O}_2 \rightarrow \text{CO}_2$ by interaction with the radical pool.

Since analysis methods for alkali metal in the gas phase are hardly available, we use an indirect method by applying another gas phase system, which the mechanism has been well known. And CO oxidation as mentioned above is selected to be used.

In the third type of experiment K/Cl/S interactions will be investigated by introducing SO₂ to the system.

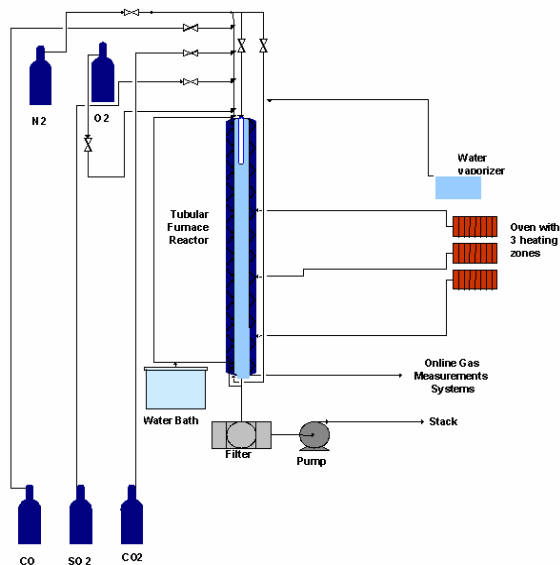


Figure 3: Sketch of complete experimental set-up, some modifications is being made when necessary in order to run different type of experiments.

Result and Discussion

Modeling

Using starting reaction mechanism and thermodynamic properties proposed by Glarborg and Marshall [6], preliminary gas phase modeling is conducted. The results (figure 4) indicate that formation of Potassium Sulfate in the gas phase will increase by increasing the temperature. To model the real combustion system, we need to include an aerosol formation model to the current gas phase chemistry model. An attempt to include a nucleation model to the system to model the aerosol formation is still on going work.

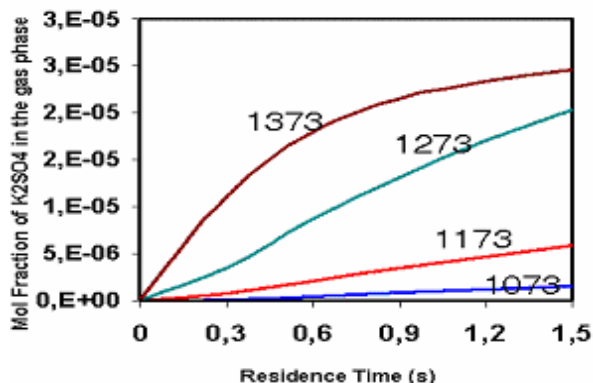


Figure 4: Mol Fraction of K_2SO_4 formed in the gas phase with inlet composition (in moles) KCl: 0.22; SO_2 : 0.04; O_2 : 7.06; H_2O :32.94; and N_2 : 159.40; in different temperature (K) and residence time.

Calculations including a simple condensation model [6] to the system show a significant difference in the formation of K_2SO_4 in the gas phase, as can be seen in figure 5.

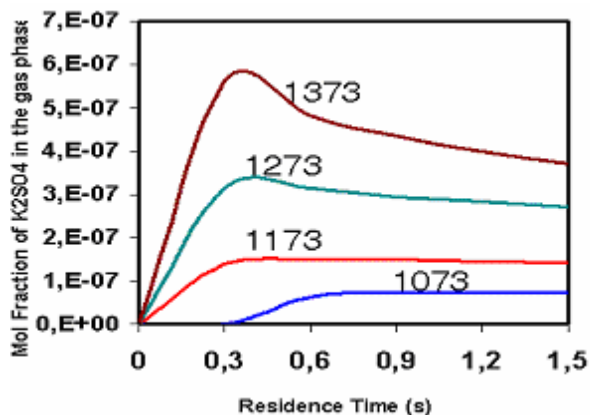


Figure 5: K_2SO_4 formation in the gas phase by inclusion of condensation model with inlet composition (in moles) KCl: 0.22; SO_2 : 0.04; O_2 : 7.06; H_2O :32.94; and N_2 : 159.40; in different temperature (K) and residence time.

Thus we can see that inclusion of aerosol formation to the model will be a significant influence. Aerosol formation by homogeneous nucleation using classical theory modified with curvature dependent surface tension [7] was simulated which gives us result as can be seen in figure 6. It shows that by increasing the saturation ratio of K_2SO_4 in the system, the nucleation of aerosols particle will increase.

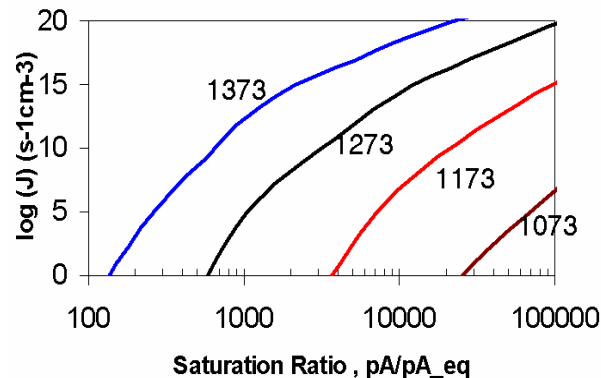


Figure 6: Aerosol formation by homogeneous nucleation in different temperature (K) and saturation ratio, using equation earlier proposed by Christensen et. al. [7]

Experimental work

Mass balance experiments in order to investigate the possibility of KCl sitting/sticking on the reactor (alumina tube) wall were being done. The result is still uncertain since it is quite difficult to conduct the mass balance measurements. If a small amount of KCl does deposit on the wall of alumina tube after being released to the gas phase, we might need to include this consideration to our model.

Since it is difficult to analyze the gas phase of alkali metal, we conduct some experiments in order to study

indirectly the KCl chemistry analysis in the gas phase. Several runs of CO oxidation with interaction of KCl in the gas phase have been conducted, and the preliminary results show that the presence of KCl will inhibit the CO oxidation. Some results can be seen in figure 7 and 8.

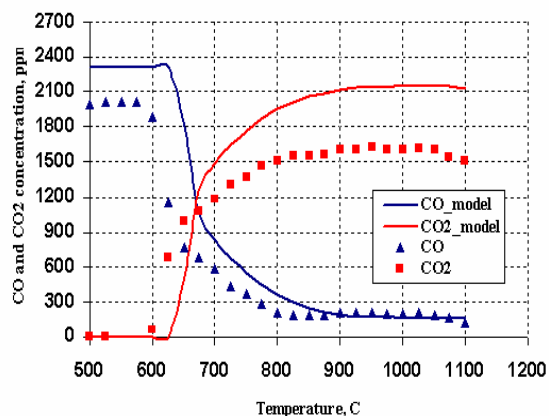


Figure 7: The molar fractions of CO and CO₂ outlet from the reactor from CO oxidation experiment without KCl addition, inlet composition CO: 2200 ppm; H₂O: 0.05; N₂: 0.9; and O₂ from gas impurity; the solid lines are model's result and the dots are experimental result.

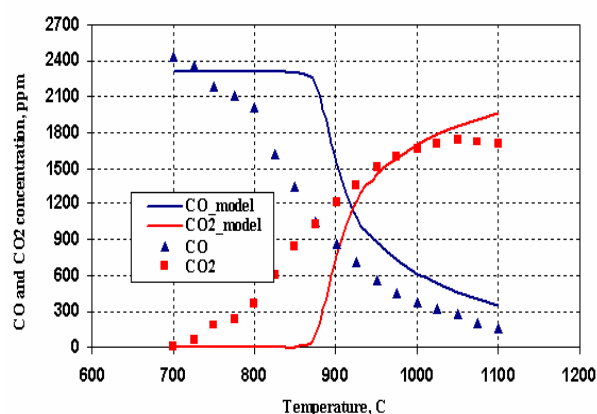


Figure 8: The molar fractions of CO and CO₂ outlet from the reactor from CO oxidation experiment with 300 ppm KCl addition, inlet composition CO: 2200 ppm; H₂O: 0.05; N₂: 0.9; KCl : 300 ppm and O₂ from gas impurity; the solid lines are model's result and the dots are experimental result.

Both the result of the model and the experiment show that CO oxidation will initiate at a quite low temperature around 600 °C. Addition of KCl inhibits the CO oxidation and shift the initiation temperature to higher values. We can say that the finding of the experimental work agree quite well with the model proposed but it seems that in the model the influence of potassium to the system is more pronounced than the findings from the experimental work.

By doing sensitivity analysis and adjusting the rate constants of some of the reactions, we expect that we will improve the model.

Some more reliable experimental work and a thorough analysis need to be done in order to improve the model.

Conclusion

Successful modeling validated with experimental data will be useful to simulate the gas phase chemistry in the combustion system so that it may facilitate the development of more efficient methods to minimize emission and operation problems in biomass or waste combustion also in boiler design.

Future work

Several experiments to simulate the real combustion system condition will be done in the near future, and attempt to include aerosol formation in the gas phase mechanisms in CHEMKIN code is also still on going work. CFD will also be used to model the system in the reactor.

Acknowledgements

Financial support for this project by PSO-Elkraft is gratefully acknowledged. Also acknowledgement is for the technicians in the CHEC group for invaluable helps in the setting up of experimental work.

References

1. K.A. Christensen, H. Livbjerg, *Aerosols science and Technology*, (2000) 33, 470-489.
2. L.B. Nielsen, H. Livbjerg, *J. Aerosol Sci.* (1996), 27(I), S367-S368.
3. H.P. Michelsen, O.H. Larsen, F.J. Frandsen, K.D. Johansen, *Fuel Process. Technol.* (1998), 54, 95-108.
4. K. Iisa, Y. Lu, *Energy & Fuels* (1999), 13, 1184-1190.
5. I. Obernberger, T. Brunner and M. Joller, *Characterization and Formation of Aerosols and Fly ashes from Biomass Combustion*, Report EU Project 'Aerosols from Biomass Combustion', 2001.
6. P. Glarborg, P. Marshall, submitted paper for publication, 'Mechanism and Modeling of Gaseous Alkali Sulfate Formation', *Combust. Flame*, In Press 2004.
7. K.A. Christensen, PhD Thesis, Aerosol Laboratory, Chemical Engineering, DTU



Claus Hindsgaul

Address: CHEC, Dept. of Chemical Engineering,
Building 227, Office 114

Phone: +45 4525 2831

e-mail: chi@kt.dtu.dk

www: www.chec.kt.dtu.dk

Supervisors: Anker Degn Jensen
Bjørn Qvale, MEK-DTU
Ulrik Henriksen, MEK-DTU

Ph.D. Study

Started: February 2003

To be completed: February 2006

Disintegration of Char Particles during Thermal Conversion

Abstract

The disintegration of char during thermal conversion such as combustion and gasification can be an important factor in the conversion process as the particle size distribution changes and internal surfaces are exposed. In this project the strength and diffusive properties of wood char during combustion will be investigated in order to gain knowledge on the disintegration processes and aid detailed modelling of particle conversion and reactors.

Introduction

The increased utilisation of biomass as fuel for energy production has led to the need for detailed understanding of the behaviour of biomass during thermal conversion. In fixed bed co-current gasification and combustion, the gas permeability of the reaction zone depend heavily on the particle geometry, in particular the particle size distribution. If the char particles break into smaller particles these may cause undesired increases in pressure drop through the particle bed as well as dead zones and channelling, resulting in decreases in efficiency and stability of the reactor. Fluid bed reactors are sensitive to the particle size distribution in order to control fluidisation and the amount of particles escaping the reactor unconverted.

The strength properties and disintegration behaviour of biomass char is a topic, where knowledge is yet very sparse. Wood is known to retain much of its physical structure during charring, and char is thus a highly anisotropic material. Detailed knowledge of the microstructure and physical properties of wood are available, but it has only to a very limited extend been utilised to evaluate the properties of wood char in the combustion science. For example, the limited data available on diffusion and heat transfer in char generally assume complete isotropy. This is unfortunate since the mechanical strength of a material is sensitive to inhomogeneities in the material, which can be caused by anisotropic gas and heat transfer.

The goal of this project is to investigate the strength development and breakage behaviour of wood char during conversion. Experimental determination of

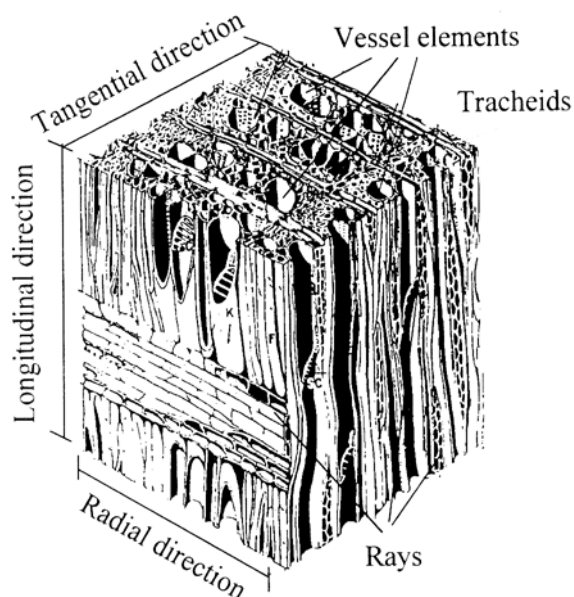


Figure 1: Microstructure of hardwood [1]

anisotropic diffusion properties and mechanical strength of wood char from different species will be made, and the results will be evaluated taking into account the wood char microstructure. By way of mathematical modelling, the processes and parameters determining char breakage will be investigated.

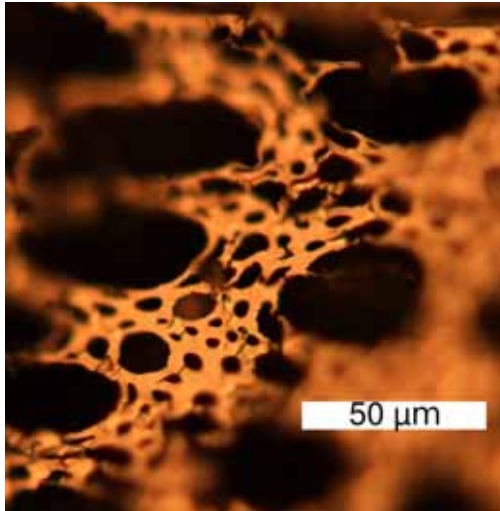


Figure 2: Beech wood char. The structure is almost identical to that of the virgin wood, with wood cells and large vessel pores. (Optical micrograph)

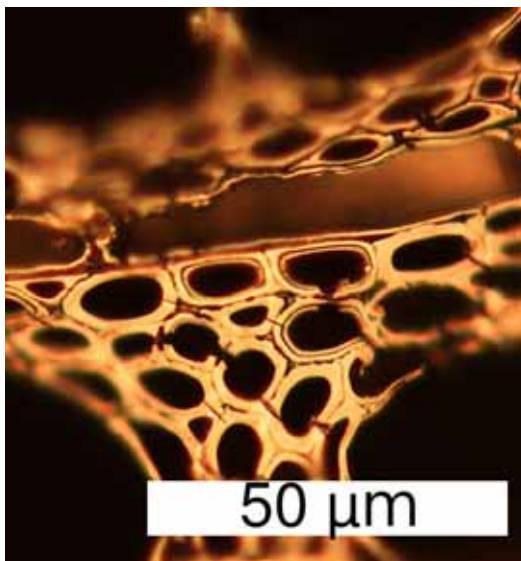


Figure 3: Beech wood, which has been pyrolysed and converted 40-50%. The middle lamella between the wood cells seems to have been converted first. (Optical micrograph)

Char microstructure

The microstructure of the wood is retained very well in the wood char – despite the severe mass loss (75%) and shrinkage occurring during the conversion from wood to char (pyrolysis). A sketch of hardwood microstructure is shown in Figure 1. Like wood is an orthotropic material i.e. it has different strength properties in three major orthogonal directions: (1) along the stem (*longitudinal*), (2) along the annual rings (*radial*) and (3) *tangential*.

Light microscopy is used to investigate the structural

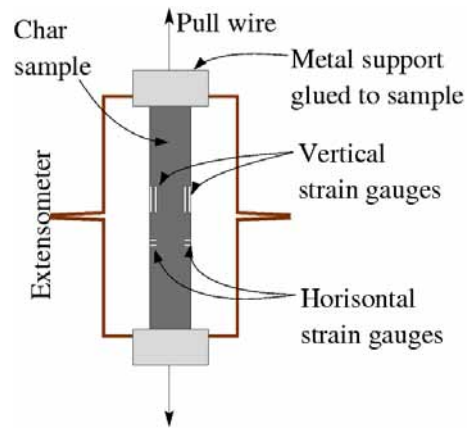


Figure 4: Sketch of tensile strength test setup.

changes in the converted wood char. High resolution optical microscopy of cold char samples are shown in Figures 2 and 3. Figure 2 shows a micrograph of a wood char surface orthogonal to the longitudinal direction. The original wood cell walls and larger vessel lumen structures are easily recognisable. Figure 3 shows a micrograph of a similar surface of wood char, which has been converted 40-50% by CO₂ gasification at 700°C. Here the *middle lamella* (the lignin rich glue between the wood cells) appears to have vanished.

The appearance of continuously converting char samples are studied in a stereoscope equipped with a small high temperature oven (heating stage microscopy). During these experiments the oven is purged with 100% CO₂. Fast motion recordings of the char conversion shows the structural shrinkage and breakdown of the char samples, although the lower resolution of the stereoscope does not reveal details within the wood cells as those seen in Figures 2 and 3. Using this method it has been observed that bulk shrinkage did not occur before a certain amount of time/conversion followed by steady bulk shrinkage.

Strength testing

The strength properties of the char depend on the microstructure development outlined above. It will be measured by uniaxial tensile tests in the three major directions at different degrees of conversion.

Figure 4 shows a sketch of the tensile strength test setup used during the first test. The char sample was a 80 mm long pyrolysed beech stick. The curvature and oval cross section of the sample caused by the pyrolysis was eliminated by removing some of its surface material using fine sandpaper. Then metal supports with wire connectors were fixed to the sample ends using Araldit® glue. In order to be able to measure the strain in the sample, four strain gauges were glued onto the sample surface as indicated in Figure 4: Vertical and horizontal strain gauges at both the left and right side near the centre of the sample. Two vertical extensometers were attached to the metal supports in

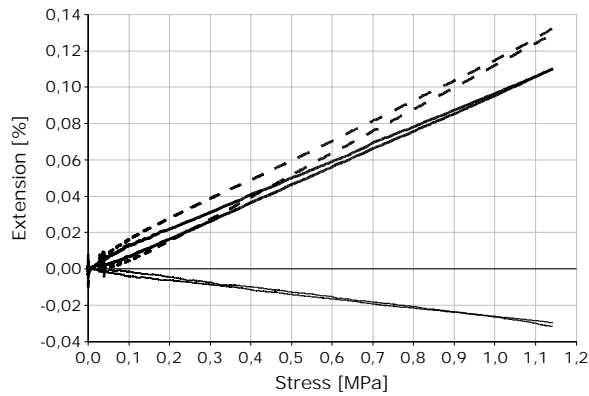


Figure 5: Results of uniaxial tensile test. Dashed: Extensometers, Thick solid: longitudinal strain gauges, Thin solid: vertical strain gauges.

order to verify the measurements of the corresponding vertical strain gauges. The actual test was conducted at BYG on DTU on their 100 kN tension machine equipped with a force measurement cell to record the actual tensile force applied to the wires. Increasing tension was slowly applied until breakage.

Figure 5 shows the results of the initial tensile test. The results from the measurement pairs are very consistent. The strain differences between right and left at low stresses can be explained by some initial bending, and evens out at higher stresses. The vertical strains as measured by the strain gauges and the extensometers are qualitatively very similar, but the extensometer strains are approx. 20% higher. This difference is larger than expected, and has not yet been explained. The slope of the vertical strains in Figure 5 is the longitudinal stiffness (*longitudinal Youngs modulus*, $E_l = \epsilon_l / \sigma_l$, where ϵ_l and σ_l are the longitudinal strain and stress) of the char. E_l was found to be approximately 1 GPa. Assuming plane isotropy, the longitudinal Poissons ratio, μ_l , can be found as the ratio of the tangential strain to the vertical strain ($\mu_l = \epsilon_t / \epsilon_l$), approximately 0.28. Failure occurred at a stress of $\sigma_l = 1.15$ MPa near one of the metal supports. Since only one specimen has yet been tested, it may or may not have been caused by a local weakness. Thus the true longitudinal tensile strength may turn out to be higher than 1.15 MPa, when more samples have been tested.

Diffusion measurements

A Wicke Kallenbach cell, where diffusion through a plane sample can be studied, has been built at The Department of Chemical Engineering. Figure 6 shows a diagram of a Wicke Kallenbach cell. The sample is placed between two isobaric chambers (where each of the gases are injected) and sealed so that any gas exchange between the chambers has to pass through the sample. Two pure gases are blown onto the sample surface in each chamber. “Gas A” in “chamber A” and “Gas B” in “chamber B”. The gas flow from chamber A will contain small amounts of gas B due to the gas transfer from chamber B through the sample. By

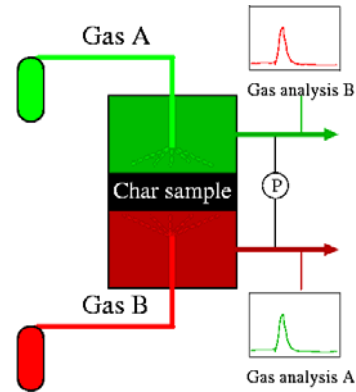


Figure 6: Schematic diagram of a Wicke Kallenbach diffusion cell

analysing this concentration, the amount of gas B passing through the sample can be quantified. The same procedure is applied simultaneously to quantify the transfer of gas A through the sample. It is essential that there is a very low pressure difference between the sample surfaces in order to avoid forced convection through the sample. Grahams law can be used to verify this, when the gas transfer of both gases are quantified simultaneously as described above. Grahams law predicts that for ordinary and Knudsen diffusion (that is, with negligible forced flow and surface diffusion), the ratio of the opposing flow rates of the gases equals the square root of the ratio of their molar masses.

In the present Wicke Kallenbach setup (Figure 7), three pure gases will be used: CO, CO₂ and NO. These gases were chosen because of their relevance in gasification and combustion processes, and the availability of gas analysers for these gases. The char sample is cylindrical (thickness ~10 mm, diameter



Figure 7: Picture Wicke Kallenbach cell setup at CHEC

~10 mm) and the sides are sealed with silicon paste. The chambers and sample are kept inside a ventilated transparent plastic box for safety. In order to minimise the pressure difference between the chambers, the (vertical) exit pipes from the chambers have large diameters and are merged downstream the gas analysis sample points. They form the inverse U-shape in the top of Figure 7). The pressure difference between the chambers is surveyed both by a micromanometer and by Grahams law; Grahams law is known to fail when surface diffusion is significant, which may be the case with adsorbable gases or materials with very small micropores (<5 nm)[2].

The uniaxial permeability can be measured in the Wicke Kallenbach setup by using a single gas, applying a pressure difference between the chambers and measuring the gas flow.

Investigation of samples with different orientations will give information on the orthotropic diffusion and permeability properties of the char samples. The development of diffusion properties during conversion will be investigated by observing samples subjected to different degrees of gasification conversion.

Modelling

A mathematical model will be developed to model the local processes inside a single wood char particle during thermal gasification. The model will focus on parameters and processes relevant to the microstructure development and physical strength of the particle.

Conclusion

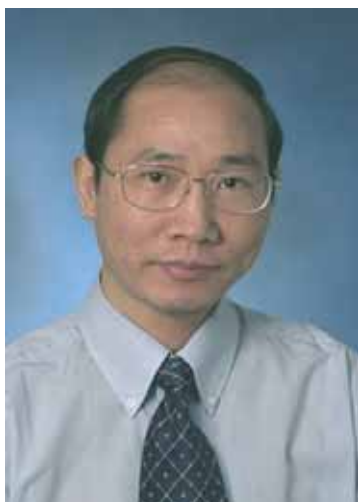
Several methods are being developed and will be applied in order to gain knowledge on char disintegration during thermal conversion.

References

1. J. F. Siau, Transport Processes in Wood, Springer-Verlag, 1984
2. Omata, H. and Brown, L.F., Using the dusty gas diffusion equation in catalyst pores smaller than 50 Å radius, AIChE Journal, vol. 18, no. 5, pp. 967-75, 1972

Acknowledgements

This project is kindly funded by the energy research programme (EFP) of the Danish Energy Agency. It is a cooperative effort between the CHEC group at the Department of Chemical Engineering and the Biomass Gasification Group at the Department of Mechanical Engineering at DTU.



Guilin Hu

Address: Building 229, Søltofts Plads, DTU
 Phone: +45 4525 2829
 Fax: +45 4588 2258
 e-mail: gh@kt.dtu.dk
 www: www.chec.kt.dtu.dk

Supervisor(s): Kim Dam-Johansen
 Stig Wedel

Ph.D. Study
 Started: February 2004.
 To be completed: January 2007

SO₂ Emission from Cement Production

Abstract

The emission of SO₂ from cement production is mainly caused by the oxidation of the pyrite contained in the raw materials in the cyclone preheater in the “dry process”. The emission level of SO₂ from the process is determined by the oxidation reaction of the pyrite and the direct sulfation reaction of limestone particles in the cyclone preheater. The oxidation of the pyrite contained in the raw materials in a cyclone preheater-like environment is shown strongly influenced by temperature, oxygen concentration, particle size and flow condition, and may proceed in two different ways depending on reaction conditions. The pyrite will most likely be oxidized directly to form iron oxides and sulfates at lower temperature and higher oxygen concentration, but will most likely be transformed through a two-step process, i.e. first thermal decomposition and then successive oxidation. The direct sulfation reaction of limestone in a cyclone preheater-like environment involves complicated gas-solid reaction mechanism, and was shown to have varying apparent reaction orders with respect to SO₂ under different reaction conditions. This phenomenon may be explained by a three-step surface reaction mechanism based on crystal point defect theory and solid state activity at the solid surface.

Introduction

Today, the so called “dry process” is the dominating process technology used for cement production due to its superior energy efficiency. In this process, raw materials are first milled to the required particle size and mixed to form raw meal (homogenised mixture of raw material powders). Raw meal is then heated up in a cyclone preheater through direct heat exchange with the hot flue gas from the rotary kiln and/or the calciner. After preheating, raw meal passes first through the calciner, where limestone in the raw meal is calcined. The calcined raw meal goes then into the rotary kiln, where the raw meal is burned at high temperature to form cement clinker. The formed clinker is then cooled down and milled to produce final cement products. Figure 1 illustrates an in-line dry kiln system with a preheater consisting of 5 cyclones (the upper 4 cyclones are used for preheating).

In each stage, the raw meal particles are suspended in the up-going hot flue gas in the riser in cocurrent flow, and heated up. The solid phase is then separated in the cyclone and enters the stage underneath. The flow in the preheater is cocurrent in each cyclone, but count current in general. Raw meal is typically heated up from app. 350K to app. 1073K before it enters the calciner. The

flue gas is typically cooled down from app. 1173K to app. 573K.

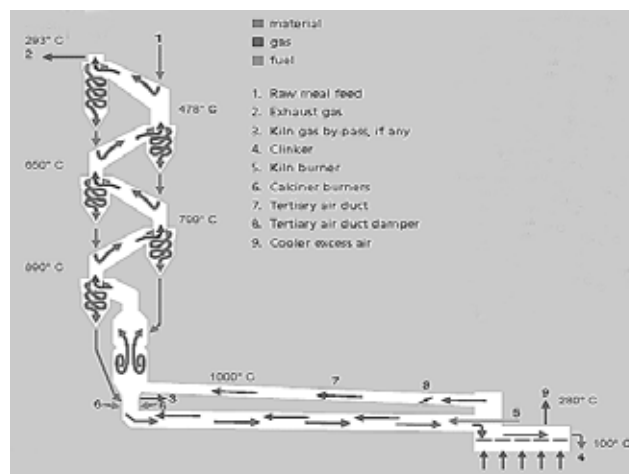


Figure 1 Illustration of a 5 stage cyclone preheater.

Cement production uses different limestone, clay and shale as raw materials. These raw materials are all natural minerals, and contain often a few percent of pyrite (FeS₂).

During the preheating process in the cyclone preheater the sulfur contained in the pyrite is oxidized to SO₂ by the hot and oxidative flue gas from the rotary kiln and/or the calciner. Part of the formed SO₂ is absorbed by the limestone particles in the raw meal. The rest is released into atmosphere with flue gas, and is the main source of SO₂ emission from cement production. The emission level of SO₂ from different plants can vary from a few hundred ppm to several thousand ppm depending on the raw materials used. It is desired that this emission is reduced as much as possible in the benefit of better environment.

Specific Objectives

In this project, the oxidation of the pyrite contained in the raw materials and the sulfation reaction between limestone and SO₂ will be studied in laboratory scale reactors under the conditions similar to those in a cyclone preheater with the purpose of getting better understanding on the mechanisms and kinetics which are necessary for effective abatement of SO₂ emission from cement production. Based on the experimental results mathematical models will be established for process simulation.

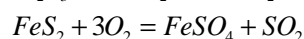
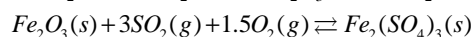
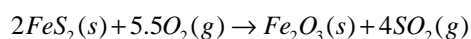
Formation of SO₂

The formation of SO₂ in cyclone preheater is mainly from the oxidation of the pyrite contained in the raw materials.

Pyrite (FeS₂) is a naturally occurring material that can be found in concentrated form in nature and also as impurity in coal and many other minerals. The wide occurrence of pyrite in different minerals and coals makes it today one of the main sources of SO₂ emission from different industrial activities, such as metallurgical industry, power production and cement production. In oxygen containing atmosphere, the sulfur contained in pyrite is oxidized to form SO₂ gas. The iron in pyrite is oxidized to form iron oxides (hematite Fe₂O₃ and magnetite Fe₃O₄) as the main solid products and iron sulfates (ferrous sulfate FeSO₄ and ferric sulfate Fe₂(SO₄)₃) as the minor solid products.

The transformation of pyrite in oxygen containing atmosphere is a complicated process, and will proceed by different mechanisms under different conditions. Parameters such as temperature, particle size, flow condition and property of the surrounding atmosphere can all together affect the transformation process.

In the past decades, lots of scientific research works have been performed in order to clarify the mechanisms and kinetics of pyrite transformation under different conditions. These investigations [1-12] showed that the transformation of pyrite in oxygen containing atmosphere will happen by two different ways depending on actual conditions such as temperature, oxygen concentration, flow condition, particle size, etc. At lower temperature (< ca. 500-550°C) and higher oxygen concentration, pyrite will more likely be oxidized directly according following overall reactions:



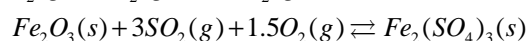
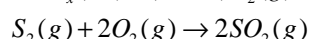
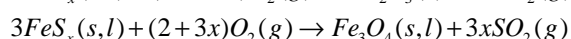
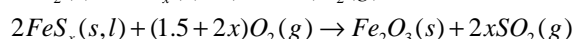
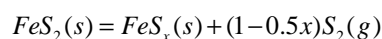
The direct oxidation process follows an unreacted core model for unchanging particle. This can be well illustrated by following SEM (Scanning Electron Microscopy) picture [1]:



Figure 2 SEM picture of a partially oxidized pyrite particle [1].

The direct oxidation of pyrite was reported to be controlled by inward diffusion of oxygen due to the formation of ferric/ferrous sulfate [9]. Iron sulfates have much larger molar volume than pyrite and ferric/ferrous oxide. The formation of ferric/ferrous sulfates will create a pore blocking effect, which in turn will cause diffusion difficulty.

At higher temperature (>500-600°C) or lower oxygen concentration, pyrite will more likely undergo first thermal decomposition to form porous pyrrhotite (FeS_x, 2>x≥1). The formed pyrrhotite is then oxidized successively. The whole process can be represented by following overall reactions:



The happening of this process can be well illustrated by the following SEM picture [3], which shows a partially reacted pyrite particle with an unreacted pyrite core, porous pyrrhotite layer formed by thermal decomposition and a rim of hematite (oxidation product of pyrite/pyrrhotite) at the particle surface.

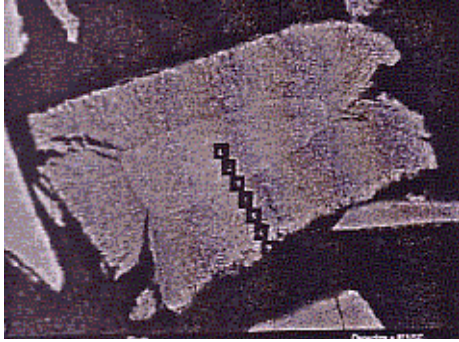


Figure 3 SEM picture that shows a partly decomposed pyrite particle in an oxygen containing atmosphere [3].

Recent investigation [3] showed that in cyclone preheater-like environment, the oxidation of pyrite contained in shale is strongly influenced by temperature, oxygen concentration and flow condition, and proceeds relatively fast at temperature around 673-823K, which is typical temperature area in the first two stage cyclones of the cyclone preheater. There is still no clear evidence that can show by which process the oxidation of pyrite contained in shale will proceed in a cyclone preheater-like environment.

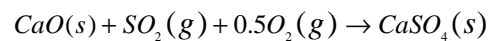
In this project the oxidation of pyrite contained in shale in cyclone preheater-like environment will be investigated further in order to get better understanding of the mechanism.

Absorption of SO₂ on limestone

Limestone (CaCO₃) is one of the most important and basic ingredients for Portland cement production. Limestone is fortunately also a sorbent of SO₂, and is widely used in different desulphurisation processes.

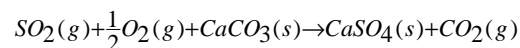
The absorption of SO₂ on limestone can happen in two different ways.

Under the conditions (higher temperature and lower CO₂ partial pressure) where calcination of limestone can take place, limestone will first undergo calcination before it reacts with SO₂ due to the much faster reaction rate of calcination than sulfation reaction. The sulfation of limestone under such conditions is also called “indirect sulfation”, and can be represented by following overall reactions:



Under conditions (lower temperature and higher CO₂ partial pressure) where calcination of limestone does not happen, limestone will react directly with SO₂.

The direct sulfation reaction of limestone can be represented by following overall reaction:



The absorption of SO₂ in the preheater happens mainly by this direct sulfation reaction. In the preheater, the relatively low temperature (up to around 1073K) and the high CO₂ content (around 30 vol.%) prevent the calcination of the limestone particles.

Preliminary investigation in a fixed-bed reactor [13] has shown that the direct sulfation reaction in a cyclone preheater-like environment is significantly influenced by the temperature, gas composition (SO₂, O₂, CO₂ and water vapour) and limestone particle properties. It was found that the mechanism of direct sulfation reaction is much more complicated than the above overall reaction. It was for example observed that the apparent reaction order with respect to SO₂ at 823K varies with the concentration of SO₂ in the gas phase as illustrated in figure 4.

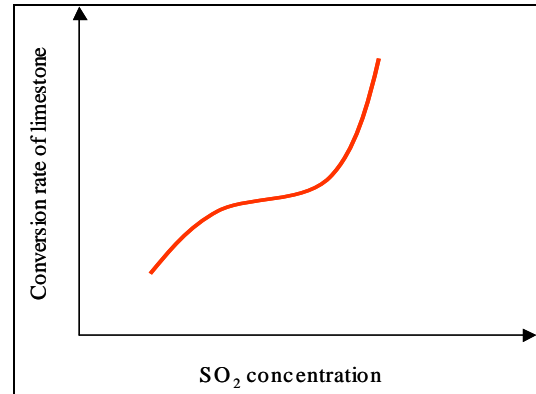


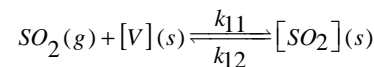
Figure 4 Illustration of the change of limestone conversion rate with SO₂ concentration in a cyclone preheater-like environment.

The sulfation reaction showed a near zero order behavior at mediate SO₂ concentrations, but higher order at both higher and lower SO₂ concentrations.

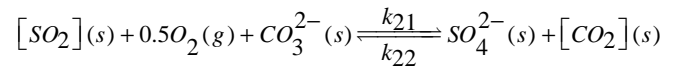
Simple application of mass action law in this case is not sufficient to explain this phenomenon.

To explain the observed phenomenon, following three-step surface reaction mechanism based on crystal point defect theory and solid state activity at the surface is suggested for this reaction:

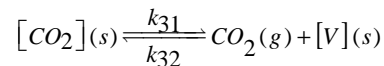
Step 1, chemisorption of SO₂ on the active sites on the solid surface:



Step 2, surface oxidation of the adsorbed SO₂:



Step 3, desorption of CO₂:



Here [V] represents vacancies of anions at the solid surface. Vacancies are point defects in crystalline materials, normally called Schottky defects, a kind of disorder in crystalline materials [14]. The existence of Schottky defects is an intrinsic property of crystalline materials. The thermodynamic basis for the existence of disorder is the increase of entropy caused by disorder. The point defects are not still standing, but moving randomly. The amount of vacancies increases exponentially with temperature according to following equation:

$$N_v = NB \exp(-\Delta H / (2RT))$$

The vacancies can also be caused by aliovalent impurities in the crystal. These defects are called extrinsic defects. The existence of other cations of lower valence will for example create more anion vacancies due to the requirement of electrical neutrality.

In this suggested mechanism, the vacancies caused by missing anions at the solid surface are supposed to be the active sites. Figure 5 illustrates the suggested sulfation process:

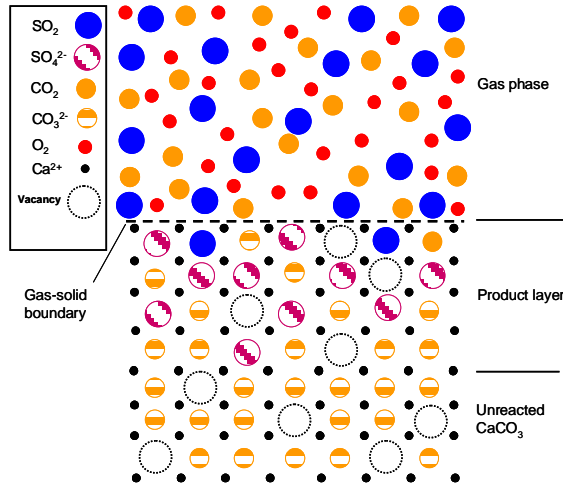


Figure 5 Illustration of the suggested gas-solid reaction mechanism.

As shown in figure 5, the reaction happens at the surface of the solid. In the first step SO_2 occupies the vacancy at the surface, and forms a kind of intermediate. In the second step, this intermediate is oxidized to form SO_4^{2-} coupled with the transformation of CO_3^{2-} to CO_2 . In the third step, CO_2 is desorbed from the occupied vacancy. In the product layer, SO_4^{2-} diffuses toward the main phase of CaCO_3 , while CO_3^{2-} diffuses toward the surface of the solid. The migration of these anions happens through the vacancies [14]. The solid state activities of anions CO_3^{2-} (a_1) and SO_4^{2-} (a_2) at the surface are important parameters for the reaction, and will have significant influence on the rate of the sulfation reaction. For pure solid, the activity is normally assumed to be 1. But in the case of sulfation, the product layer cannot be assumed to be a pure substance. The crystal lattice of the product layer will

contain in high or low degree other anions (SO_4^{2-} in CO_3^{2-} or CO_3^{2-} in SO_4^{2-}) in order that the reaction can proceed. The solid state activities of these two kind of anions depend on the rate of the reaction, the ionic diffusion rate of these two kind of anions and the stage of the sulfation. In the case of fast reaction rate and slow ionic diffusion, the surface will be dominated by SO_4^{2-} . This will mean that the activity will be high for SO_4^{2-} , but low for CO_3^{2-} . The proceeding of the reaction depends on the activity of CO_3^{2-} . Lower CO_3^{2-} activity will slow down the reaction. There will be established a kind of balance under different reaction conditions. This process is in certain degree comparable to gas-liquid reaction except that:

- There is no convection in the solid phase;
- The ionic diffusion in solid state is much slower compared to in a liquid;
- The reaction takes place only at the solid surface.

The sulfation process will be controlled by different steps under different conditions and different sulfation stages. By assuming that the reaction rate equals to the reaction rate of the controlling step and the other two steps are assumed in equilibrium state, the following rate expressions can be obtained:

When step 1 is the controlling step:

$$r_{s,1} = k_{11} \left(C_{\text{SO}_2} - \frac{\beta C_{\text{CO}_2}}{K_1 K_2 K_3 C_{\text{O}_2}^{1/2}} \right) \frac{1}{\left(1 + \frac{\beta C_{\text{CO}_2}}{K_2 K_3 C_{\text{O}_2}^{1/2}} + \frac{C_{\text{CO}_2}}{K_3} \right)}$$

When step 2 is the controlling step:

$$r_{s,2} = k_{21} a_1 \left(C_{\text{SO}_2} C_{\text{O}_2}^{1/2} - \frac{\beta C_{\text{CO}_2}}{K_1 K_2 K_3} \right) \frac{1}{\left(\frac{1}{K_1} + C_{\text{SO}_2} + \frac{C_{\text{CO}_2}}{K_1 K_3} \right)}$$

When step 3 is the controlling step:

$$r_{s,3} = k_{31} \left(C_{\text{O}_2}^{1/2} C_{\text{SO}_2} - \frac{\beta C_{\text{CO}_2}}{K_1 K_2 K_3} \right) \frac{1}{\left(\frac{\beta}{K_1 K_2} + \frac{\beta C_{\text{SO}_2}}{K_2} + C_{\text{O}_2}^{1/2} C_{\text{SO}_2} \right)}$$

The use of solid state activity at the surface in these rate expressions makes a bridge between chemical reaction and the influence from ionic diffusion, and reflects directly the actual process happened at the solid surface. The observed phenomena in this investigation can be explained well by the surface oxidation reaction, i.e. step 2 in the suggested mechanism. In the rate expression for step 2, a_1 acts like a counterbalance. The observed special behavior of the reaction order with respect to SO_2 can be explained by the variation of solid state activities of carbonate and sulfate ions at the surface under different reaction conditions. (More details about this can be read in reference [13]).

In order to simulate the flow conditions in an industrial cyclone preheater, a pilot scale cyclone preheater

consisting of 2 stage cyclones (as illustrated in figure 6) will be built.

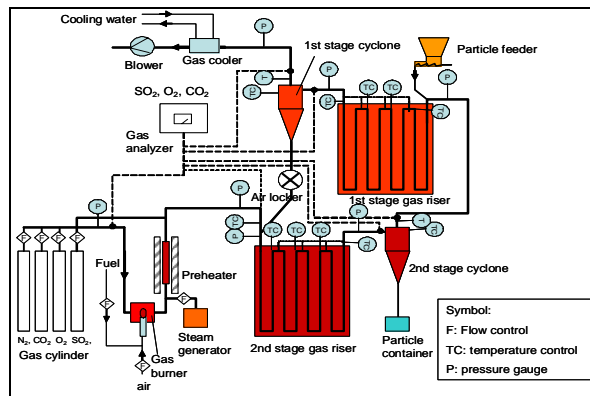


Figure 6 Illustration of the design of a pilot scale cyclone preheater consisting of two stage cyclones.

The first two stage cyclones are the most critical part concerning the SO₂ emission from the system due to the fact that the conditions in these two stage cyclones are favourable for SO₂ formation, but not for the sulfation of limestone. With this pilot cyclone preheater the oxidation of the pyrite and the sulfation reaction can be investigated under flow conditions close to those in a industrial cyclone preheater.

Based on the experimental results from the fixed-bed reactor and the pilot scale cyclone preheater mathematical models will be developed for the simulation of the formation of SO₂ and the successive absorption of SO₂ on limestone particles in the preheater.

Conclusion

The emission of SO₂ from cement production is mainly caused by the oxidation of the pyrite contained in the raw materials. The emission level from the process is determined by the oxidation reaction of the pyrite and the direct sulfation reaction of limestone particles in the cyclone preheater. The formation and absorption of SO₂ in the cyclone preheater involve complicated mechanisms. A good knowledge of these mechanisms is necessary for the effective abatement of SO₂ emission from cement production.

The oxidation of pyrite contained in the raw materials is strongly influenced by temperature, oxygen concentration, particle size and flow conditions, and may proceed by two different ways depending on the reaction conditions. The pyrite will most likely be oxidized directly to form iron oxides and sulfates at lower temperature and higher oxygen concentration. At higher temperature or lower oxygen concentration, the pyrite will most likely be transformed through a two step process, i.e. first thermal decomposition and then successive oxidation.

Preliminary investigation showed that the absorption of SO₂ on limestone in a cyclone preheater-like environment involves complicated gas-solid reaction mechanism. One of the observed phenomena in this investigation is the varying apparent reaction order with

respect to SO₂ under different reaction conditions, which is not able to be explained by a simple use of mass action law. The observed phenomenon may be explained by a three-step surface reaction mechanism based on crystal point defect theory and solid state activity at the surface.

Nomenclatures

a: solid state activity;

B: constant.

C: concentration, mol/m³;

ΔH : enthalpy of formation, J/mol vacancy;

*K*₁: equilibrium constant m³/mol;

*K*₂: equilibrium constant, (m³/mol)^{0.5};

*K*₃: equilibrium constant, mol/m³;

*k*₁₁: reaction rate constant, m/s;

*k*₁₂: reaction rate constant, mol/(m²s);

*k*₂₁: reaction rate constant, (mol/(s²m))^{0.5};

*k*₂₂: reaction rate constant, mol/(m²s);

*k*₃₁: reaction rate constant, mol/(m²s);

*k*₃₂: reaction rate constant, m/s;

*N*_v: number of vacancy;

N: total number of lattice site;

R: gas constant;

*r*_s: surface reaction rate, mol/(m²s);

T: temperature, K;

β : ration between the solid state activities of sulfate ion and carbonate ion at the solid surface.

Acknowledgements

This work was carried out as a part of the Combustion and Harmful Emission Control (CHEC) research program at the Department of Chemical Engineering, Technical University of Denmark, and financially supported by FL Smidth A/S.

References

- Dunn, J. G. and De, G. C. and O'Connor, B. H.; Thermochemica Acta, 145 (1989) 115-130.
- Dunn J. G. and De, G. C.; Thermochemica Acta, 155 (1989) 135-149.
- Hansen, Jens-Peter.; Ph. D. thesis in the Department of Chemical Engineering, Technical University of Denmark, August 2003.
- Huffman, Gerald P.; Huggins, Frank E.; and Levasseur, Armand A.; Fuel, 68 (1989) 485-490.
- Jorgensen, F. R. A. and Moyle, F. J.; Journal of Thermal Analysis, 25 (1982) 473-485.
- McLennan, A. R.; Bryant, G. W.; Stanmore, B. R. and Wall, T. F.; Energy and Fuel, 14 (2000) 150-159.
- Prasad, A.; Singru, R. M. and Biswas, A. K., Phys. Stat. Sol. (a) 87 (1985) 267-271.
- Schoenlaub, Robert A.; Journal of the American Ceramic Society, 52(1) (1969) 40-43.
- Schorr, J. R. and Everhart, J. O.; Journal of the American Ceramic Society, 52(7) (1969) 351-354.
- Schwab, George-Maria and Philinis, John; J. Am. Chem. Soc., 69(11) (1947) 2588-2596.
- Srinivasachar, S.; Helble, J. J. and Boni, A. A.; Prog. Energy Combust. Sci., 16 (1990) 281-292.

12. ten Brink, Harry M.; Eenkhoorn, Simon and Hamburg, Gerrit; Fuel, 75(8) (1996) 945-951.
13. Vuthaluru, H. B.; Eenkhoorn, S.; Hamburg, G. and Heere, P. G. T.; Fuel Processing Technology, 56 (1998) 21-31.
14. Hu, Guilin; Dam-Johansen, Kim; Wedel, Stig; Hansen, Jens-Peter; "Preliminary laboratory investigation of SO₂ - absorption on limestone in cement plant cyclone-preheater-like environments", Conference paper to 7th World Congress of Chemical Engineering which will be held July, 2005, Glasgow, Scotland.
15. West, Anthony R. Basic Solid State Chemistry, John Wiley & Sons, Ltd., 1999.

**Edgar Ramírez Jiménez**

Address: CAPEC, Dept. of chemical engineering
Building 227, Office 224
Technical University of Denmark
Phone: +45 4525 2912
Fax: +45 4593 2906
e-mail: erj@kt.dtu.dk
www: www.capec.kt.dtu.dk

Supervisor(s): Rafiqul Gani

Ph.D. Study

Started: September 2002
To be completed: August 2005

Design and Control Integration from a Model-Based Methodology for Reaction-Separation with Recycle Systems

Abstract

This contribution presents the latest results of a systematic model-based methodology for the design and analysis of processes with a Reaction-Separation with Recycle (RSR) structure. The methodology subdivides the problem into three main stages, where the first two stages identify a common set of design and process (control) related variables and their role in design and operation of the process using simple but appropriate models for the specific analysis tasks. Based on this analysis, the methodology determines the design-operation targets, the design-process variables that can attain these targets and the operational ranges for a stable operation. The main features of this model-based methodology is presented and illustrated through a case study involving the Tennessee-Eastman (Challenge) Problem.

Introduction

Integrated process and control (structure) design aims to satisfy simultaneously, the increasing demands for the development of environmentally benign, economically profitable yet technically operable processes. In order to achieve this, the recycle of mass and energy within the process, which introduces new challenges to modelling, design and control of the process, need to be considered ([1], [2]). Also, [3] and [4] highlighted the roles of models in the simulation, design and control of chemical processes and suggested a more intelligent use of models in an advice role to solve process engineering problems related to synthesis, design and control. Through a systematic model-based parametric sensitivity analysis of the RSR structure of the processes, some of the complex interactions in the non-linear behaviour of the process can be understood. The objective of the parametric sensitivity analysis is to identify a common set of design and process (control) variables that affect the decisions related to the design as well as control (structure) of the process, the desired values for these variables and their upper and/or lower bounds. Since these variables affect the design and control related decisions, their effect can therefore be evaluated through the behaviour of the process measured in terms of a set of performance criteria.

Therefore, integration of aspects of design and control of a chemical process with an RSR structure can be achieved in the early stages of the design process if the model-based analysis is performed simultaneously with the conceptual design calculations.

The objectives of this contribution is to present some of the new features of the model-based methodology developed earlier by [5] and highlight its application through the well-known Tennessee Eastman Challenge Problem (TE).

Methodology Overview

The model-based methodology comprises of three successive stages where special purpose models are used for parametric sensitivity analyses in the first two stages and validation in the third stage. Since integration of design of the process and its control structure involves simultaneously solving these two problems in the early stages of the design process, it is necessary to use appropriate models representing specific features (operation, behaviour) of the process and the variables which may affect them. Figure 1 highlights the roles of a class of design and process (control) variables typically found in processes with an RSR structure are listed (on the left hand side of Fig. 1). In *Stage 1*, some of the design variables are combined together into

coupled parameters or dimensionless numbers (such as Da , the Damköhler number). The models in *Stage 1* are therefore based on these coupled variables and the objective is to find the values of these variables where the process has the optimal behaviour. Therefore, for different values of the design variables (listed in Fig. 1), the model equations are solved to obtain values of the process variables (listed in Fig. 1), which are then used to estimate the variables that determine the process behaviour (performance). This helps to decide target values for the coupled variables for the design variables (corresponding to the desired process performance), the operational limits (in terms of the process variables) and desired (target) of the process behaviour. All these variables, affect the design of the process as well as the design of the control structure.

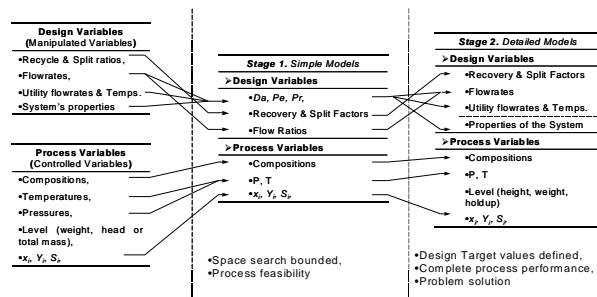


Figure 1. The roles of design and process variables in *Stages 1* and *2*.

In *Stage 2*, the coupled parameters or dimensionless numbers are decoupled, generating therefore, a new model, which obviously, is more complex than the model in *Stage 1*. The objective here is to find the design variables (listed under *Stage 2* of Fig. 1) that can match the process behaviour (defined by the process variables) and the target values of the *Stage 1* design variables. If the *Stage 1* design targets cannot be matched, new targets are set until a match is found. As highlighted in Fig. 1, the results from the model-analysis determine the operational feasibility of the process as well as the search space for the design-process variables. In *Stage 2*, the overall design targets are set and the values for a minimum set of design and process variables that matches this target is found. This means that all the design-control structure related decisions needed to make in the early stages of the design process has been made. The process can be described in terms of the performance it will give, the values of the design variables that can achieve it and values of the process variables that will be attained by the process. From a control structure point of view, these process variables will need to be controlled by manipulating the identified design variables. Also, these calculated values correspond to the set points for the manipulated and controlled variables. The models in *Stages 1* and *2* are quite simple as they only include the features of the process that need to be studied. In *Stage 3*, a rigorous model of the process is used to validate the design decisions and if necessary, to improve the design. The results from *Stages 1* and *2* are used as

initial estimates, therefore, the robustness and efficiency of the rigorous model-based solver is improved. Typically, steady state as well as dynamic simulation models can be used at this stage, while in *Stages 1* and *2*; mainly steady state models are used.

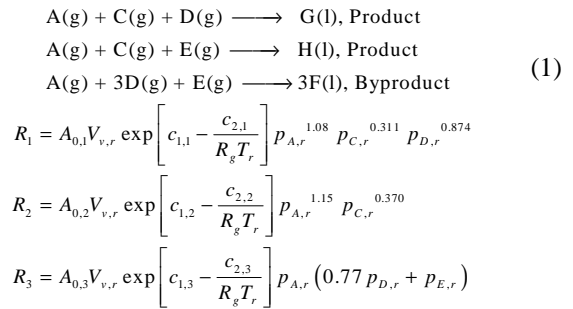
Study Case

The TE Problem ([6]) has been selected in order to highlight some of the features of the model-based methodology for integrated design and control structure.

Process Description

The TE process produces two products (G & H) from four reactants (A, C, D, E), while B and F are an inert and a byproduct, respectively. The process has five major unit operations: a reactor, a product condenser, a vapour-liquid separator, a recycle compressor and a product stripper (a typical RSR structure). The gaseous reactants are fed to the reactor reacting to form liquid products. The reactor product stream passes through a cooler for condensing the products and from there to the vapour-liquid separator. Non-condensed components are recycled through a compressor back to the reactor feed. Condensed components move to a product-stripping column to remove the remaining reactants by stripping with the feed stream of C. Product G and H exit the stripper base and are separated in a downstream refining section which is not included in the TE problem. The inert and byproduct are purged from the separator.

The reactions, which are all irreversible and exothermic, are modelled by the following kinetic rate expressions,



One of the main characteristics of the TE problem, also studied by others (for example, [7] and [8]), is the highly non-linearity and open-loop unstable behaviour of the process, due mainly to the reactions occurring in the system.

Stage 1: Use of models with coupled (design) parameters

A model that includes the reaction kinetic expressions for the reactor but the separation operations are modelled for specified separations (fixed separation factors) has been developed according to the method outlined by [5]. The important behaviour to model is the effect of the recycle flow on the reactor operation, since it is the chief source of non-linear behaviour and assuming that the separation problem can be designed to

match the separation factors used. The derived *Stage 1* model has the following assumptions:

1. A constant pressure is assumed in the reaction zone, so $p_{i,r} = y_{i,r} P_{T,r}$
2. Reaction 1 is taken as a reference due to its highest sensitivity to temperature
3. The feed flow rate of component A is considered as the reference flow rate
4. No recovery of products or byproducts is considered

The steady state mass and energy balances for all the unit operations are represented in their compact form by,

$$\mathbf{0} = \mathbf{f}\{\mathbf{x}, \mathbf{d}, \mathbf{p}\} \quad (2)$$

where,

$$\mathbf{x} = [y_i, T_6, T_7, T_{cw,out}]^T, \quad i = A, \dots, H \quad (3)$$

$$\mathbf{d} = [Da, \delta_c, \alpha_i, \sigma]^T, \quad i = A, \dots, E \quad (4)$$

$$\mathbf{p} = [A_{0,k}, c_{1,k}, c_{2,k}, \Delta H_{f,k}^0, \dots]^T, \quad k = 1, 2, 3 \quad (5)$$

In the above equations, vector \mathbf{x} represents the unknown process (state) variables; vector \mathbf{d} represents the design variables, such as the Damköhler number (Da), heat elimination capacity variable (δ_c), the recovery (α_i) and purge factors (σ); vector \mathbf{p} represents the reaction parameters such as the heats of formation and kinetic constant. The Da number, which represents the relation between the rate of reaction and flow rate of the feed stream, is defined here as,

$$Da = \frac{A_{0,1} \exp(c_{1,1} - \gamma_1) P_T^{2.265} V_R}{F_{A,1}} \quad (6)$$

Step 1.1 Model-based Analysis

The model represented by Eqs. 2-5 represent a set of non-linear algebraic equations in terms of vector \mathbf{x} , requiring the specification of the fixed parameters vector \mathbf{p} and the adjustable design variables vector \mathbf{d} . Figure 2 shows the results for the G/H selectivity or mass ratio (S_{GH}) and reactor heat duty (Q_r) for different values of recovery factors α_C with respect to Da . It can be noted that the recycle of reactants back to the reactor has a positive effect on its performance, evaluated through S_{GH} . However, as α_C increases, the heat content in the reactor also increases, due to the production of component G with is the most exothermic of the reactions taking place. Therefore, as the amount of reactants in the reactor increases, the heat in the reactor increases until the desired operation can no longer take place.

Another measure of the process performance is the conversion of component A, x_A , which may be considered as a limiting reactant as it is present in all the reactions. Figure 3 shows the behaviour of x_A vs. Da for different values of α_A . Since high recoveries are usually

preferred, a low Da number operation can achieve higher conversions, although this may imply high sensitivity to disturbances and short operating ranges. It is well known that in processes with RSR structures, at low Da , the process usually has the snow-ball effect on the recycle flow due to disturbances in the feed flow rate ([5]).

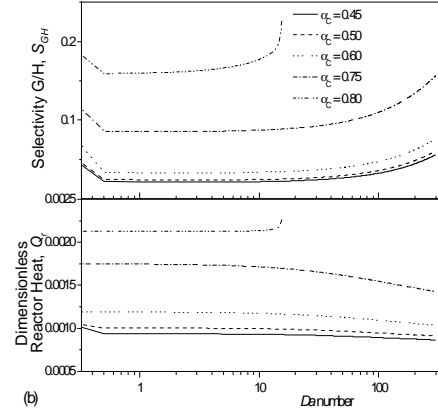


Figure 2. S_{GH} and Q_r vs. Da for different α_C .

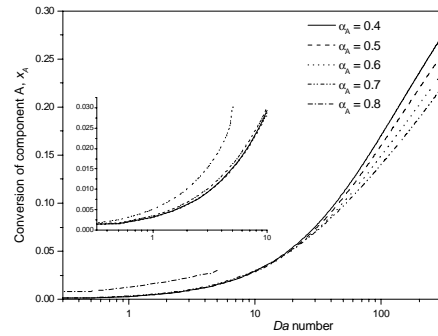


Figure 3. x_A vs. Da for different α_A .

From the above analysis, the target values for the design variables (Da and α_A) can be selected. This will give, in turn, the desired performance. Also, the model solutions at the selected design variables provide the corresponding process variable values. Selecting upper and lower bounds on the design variables, define therefore, the operational window, which is chosen so as to avoid high sensitivity (such as snow-ball effect) and/or unstable behaviour. Note that choices of the design variables for the above process variables, also determine the optimal value for the recycle flow and its effect on the process. The objective here is to make these decisions without the need or use of rigorous model based simulation, since at this early stage of the design, enough data or information is usually not known to perform such calculations.

Stage 2: Use of models with decoupled design variables

The results from *Stage 1* are used as targets that will now be matched with design variables typically encountered in process design and/or control. For example, Eq. 6 is now used to replace Da in the model

and the process performance and design targets are matched with the adjustable variables from Eq. 6 (the feed flow rate F_{A1}). Also, all assumptions considered in *Stage 1* are now removed. That is, the separation process is modelled to match the separation factor used in *Stage 1* (this will now give, for example, the temperature and pressure where a single stage vapour-liquid separation will take place). The model used in this work is that proposed [9] where energy balances for the reactor, the product separator, the stripper and the mixing zone have been added to the models given by [6].

Step 2.1. Model-based Analysis

The developed model can be used for steady state as well as dynamic simulations and contains 30 ordinary differential equations and 160 algebraic equations. The model has 11 manipulated (design) variables and fixed process parameters. The objective has been to first match the steady state design obtained in *Stage 1* and then to study the dynamic behaviour in open-loop and in closed-loop (by incorporating a control scheme using the set of identified manipulated and control variables from *Stage 1*). While the steady state design can be matched, the process shows highly non-linear process behaviour and the open loop instability, which without any control action reaches shutdown limits within approximately 60 minutes from the start of operation. Detailed simulation results, the model equations and its analysis for *Stages 1* and *2* can be obtained from the authors.

Conclusions

The results obtained from the systematic model-based parametric sensitivity analysis has been useful not only to identify operational constraints and/or limiting conditions, but also to identify set of manipulative and control variables that may be useful for control structure design. The analysis also provides the set-point values for the control variables matching the desired target performance of the process. The final step of validation through control schemes is currently being developed. For the TE problem, as far as validation of the design is concerned, *Stage 3* is not necessary since the *Stage 2* simulations validate the reported design. Current work is also developing a collection of case studies with their corresponding models and model analysis results.

Acknowledgements- It is gratefully acknowledged the financial support from The National Council for Science and Technology of México (CONACYT) to this Ph.D. project.

References

1. W.L. Luyben, *Ind. Eng. Chem. Res.*, 33, (1994) 299-305.
2. J. Morud, S. Skogestad, *J. Proc. Cont.*, 6 (2/3) (1996) 145-165.
3. R. Gani, J.P. O'Connell, *Comps. Chem. Eng.*, 25 (2001) 3-14.

4. B.M. Russel, J. P. Henriksen, S.B. Jørgensen, R. Gani, *Comps. and Chem. Eng.*, 26 (2002) 213-225.
5. E. Ramírez, R. Gani, 2004, in: A. Barbosa-Povoa, H. Matos (Eds.), *CACE-18*, Elsevier, The Netherlands, 2004, p. 469-474.
6. J.J. Downs, E.F. Vogel, *Comps. Chem. Eng.*, 17 (3) (1993) 245-255.
7. T.J., McAvoy, N. Ye, *Comps. Chem. Eng.*, 18 (1994) 383-413.
8. N.L. Ricker, *Comp. Chem. Eng.*, 19 (9) (1995) 949-959.
9. T. Jockenhövel, L.T. Biegler, A. Wächter, *Comps. Chem. Eng.*, 27 (2003) 1513-1531.

List of Publications

1. E. Ramírez R. Gani, Analysis of Design and Operation of Processes with Reaction-Separation Systems, ECCE-4 Conference, Granada, Spain, 20-25 September, (2003),
2. E. Ramírez, R. Gani, Model-based Analysis of Reaction-Separation Systems with Recycle, AIChE Annual Meeting, San Francisco, Ca., USA, 16-21 November, (2003),
3. E. Ramírez, R. Gani, A Methodology for the Analysis and Design of Reaction-Separation-Recycle systems, XXV Reunión Anual de la AMIDIQ, Pto. Vallarta, México, 4-7 May, (2004),
4. E. Ramírez, R. Gani, A Systematic Approach for the Design and Analysis of Reaction-Separation Systems with Recycle, ESCAPE-14 Conference, Lisbon, Portugal, 16-19 May, (2004),
5. E. Ramírez, R. Gani, A Methodology for the Analysis and Design for Reaction-Separation Systems with Recycle, FOCAPD 2004 Conference, Princeton, New Jersey, 11-16 July, (2004).
6. E. Ramírez, R. Gani, About the Study of Reaction Separation with Recycle Systems through a Systematic Approach, CHISA Conference, Prague, Czech Rep., 22-26 August, (2004).
7. E. Ramírez, R. Gani, On the Design of Reaction-Separation with Recycle Systems, AIChE Annual meeting, Austin, TX, USA, 2-7 November, (2004).



Johnny Johansen

Address: Building 227, room 122
Phone: +45 4525 2963
Fax: +45 4593 2399
e-mail: joj@kt.dtu.dk
www: www.icat.dtu.dk

Supervisor(s): Tue Johannessen
Hans Livbjerg

Ph.D. Study

Started: February 2003
To be completed: January 2006

One-step Preparation of Asymmetric Ceramic Membranes by Controlled Deposition of Flame-Produced Nanoparticles

Abstract

Asymmetric ceramic membranes are formed using a porous substrate tube (or surface) as a filter for flame produced, airborne nanoparticles (Andersen et al., 2002). The general principle behind flame synthesis of materials is the decomposition and/or oxidation of evaporated metal-precursors in a flame thereby forming stable metal-oxide monomers followed by nucleation, aggregation and - to some extent - coalescence of aggregated nano-particles. The product gas from a flame aerosol process is drawn through a macro-porous substrate by a vacuum pump thereby creating what in principle is a thin filter cake on the surface of the substrate.

The top-layer can be deposited directly on a coarse pore structure (>5 micrometer). Particles do not penetrate deep into the support structure due to the "lack" of fluid forces on the particles. This is an advantage compared with the preparation using a colloid suspension where several deposition steps are necessary in order to avoid penetration of the suspension due to the capillary forces.

We demonstrate a reduction in pore size from several micrometers of the macro-porous support to single digit nanometer mean pore size of the deposited micro-porous top-layer, i.e. a reduction of three orders of magnitude in pore size in one deposition step.

Introduction

Ceramic membranes are highly porous and are in general characterized by their high permeability but low selectivity. The use of highly porous ceramic membranes is favorable in high temperature applications where polymeric membranes can not be used. Inorganic membranes in general have higher chemical, thermal and mechanical stability than polymeric membranes. These properties make the use of ceramic membranes very attractive, even within areas where polymeric membranes are dominating today. This is mainly due to the higher resistance to mechanical and chemical degradation, which can result in a significant increase in membrane lifetime [1]

Porous membranes play an increasingly more important role in chemical reactor design, since chemical membrane reactors offer new and exciting possibilities for reactor design. Many heterogeneous catalytic reactions are endothermic, reversible and limited by chemical equilibrium and the conversion to the desired product may be favored at high temperature. In such cases, the use of inorganic membranes as both separator and reactor in a single unit operation may shift

the equilibrium conversion if one of the products can be made to diffuse through the membrane at a rate much greater than the other products or reactants.

As will be shown in the present study, membrane top-layers prepared by deposition of flame-produced nanoparticles may result in a reduction of the pore size of the substrate by three orders of magnitude in a one-step-process. This can be done within the time-scale of an hour. This is in sharp contrast to the wet preparation techniques that needs several times of precipitation, filtration, drying and calcinations steps before nano-scale membranes can be produced.

Specific Objectives

The scope of this Ph.D. project is to develop porous membranes with pores in the nano (and sub-nano) meter range, synthesized by flame synthesis. These membranes can then be coated with a catalyst layer to enhance the formation of the desired reaction product.

Flame Synthesis

Membranes consisting of one or more metal oxides can be synthesized by flame pyrolysis [2,3]. The general

principle behind flame pyrolysis is the decomposition and oxidation of evaporated organo-metallic precursors in a flame, thereby forming metal oxide monomers. The precursors (presently $\text{Al}(\text{acac})_3$ and $\text{Mg}(\text{acac})_2$; acac=acetyl acetonete) are sublimated into a stream of N_2 in a saturator unit as shown in figure 1. The precursor stream is then mixed with air and a fuel, which can be methane or hydrogen depending on the desired flame temperature.

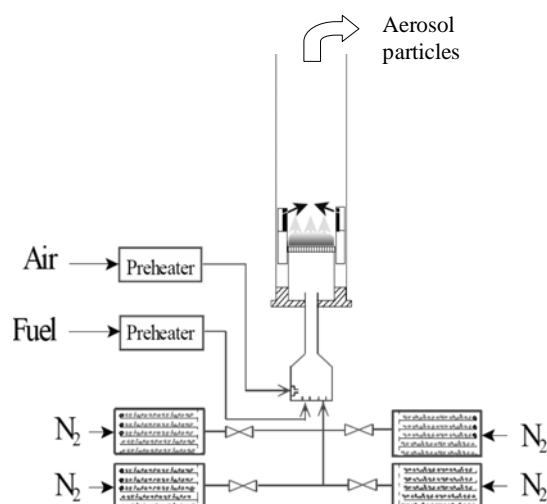


Figure 1: Schematic drawing of the flame synthesis setup.

In the flame the organic part of the precursor will decompose and combust, resulting in a metal oxide monomer, i.e. a molecule. Because of the extreme super-saturation created in the flame due to the low vapor pressure of metal oxides, the monomers will nucleate homogeneously and agglomerate to form aggregates of large ensembles of monomers. At high temperature, these aggregates will then sinter together to form single particles. If the flame temperature and the residence time are sufficiently high, the formed oxide particles will be spherical due to the fast coalescence at the high temperatures in the flame. This is desirable when synthesizing membranes, since the closest packing, and thereby the smallest pores, is achieved when the particles are spherical.

The primary product from the flame pyrolysis is an aerosol of metal oxide particles in the nano-size range. The aerosol gas from the flame can be utilized for several different purposes, depending on synthesis parameters and on the precursors fed to the flame. With the present technology it is possible to make supported catalysts composite metal oxides, catalytically active surfaces and porous ceramic membranes [2,3]. When producing catalysts the specific surface area normally has to be high in order to get very active catalysts. In flame synthesis, the high specific surface area can be achieved by quench cooling the aerosol gas with cold air after a short residence time in the flame zone [4]. The precursor will be transformed to metal oxide particles, but the residence time at the very high temperatures in the flame will be reduced, so that the

extensive sintering can be avoided. This results in the formation of agglomerates that will only sinter very little, due to the rapid reduction in temperature. Mixed metal oxides can be synthesized by leading two precursors to the flame simultaneously, e.g. Al and Mg precursors, which will lead to the formation of the AlMg_2O_4 spinel structure.

Membrane Formation

Membrane layers can be formed by using a porous substrate tube (or surface) as a nano-particle filter. The aerosol gas from the flame is led past a porous substrate, where a part of the gas is sucked through the substrate, thereby creating a thin filter cake on the surface of the substrate [3]. This is illustrated in figure 2, where the porous substrate is a tube on which the deposition takes place on the inside, while suction is applied on the outer side of the tube.

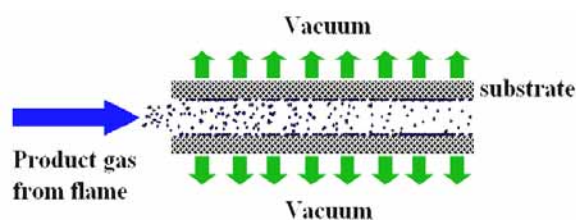


Figure 2: The aerosol phase from the flame is led through a porous substrate tube by applying vacuum on the outer side of the support tube and the particles form a layer on the inner side of the substrate.

The top-layer can be deposited directly on a coarse pore structure, which is in contrast to the use of wet colloidal suspensions, which require several deposition steps – each with a smaller particle size. In the flame aerosol process, the Brownian motion of the aerosol particles is fast compared to the fluid velocity through the substrate and the particles will not penetrate very deeply into the substrate. Particle deposition will initially take place inside the substrate pores, but because of the fast Brownian diffusion and the deposition of particles will rapidly decrease the pore diameter at the pore mouth, and hence lead to pore mouth blocking. After pore mouth blocking a top-layer will start to form. The top-layer deposition rate can be as low as 5-10 nm/min, which facilitates the production of very thin membranes needed for high fluxes [5]. A membrane consisting only of the substrate with the separating membrane layer located only in the upper part of the substrate pore mouths would be an interesting product, but because the pore mouth blocking happens within minutes or less. At the moment it has not been possible to produce such a product. Furthermore, there are several unresolved issues regarding stability of such a membrane.

The pore diameter of the deposited top-layer depends on the size of the aerosol particles, which can be controlled by changing the feed rate of metal

precursor to the flame. Since the feed rate can be changed continuously - by changing the temperature of the sublimation unit or the flow of gas through the unit - also the particle size and thereby the pore diameter can be changed continuously, which greatly facilitates the one-step synthesis of a top-layer, where the pore diameter is decreased to less than 10 nm from a substrate pore size of several microns. Figure 3 shows the saturation temperature of the sublimation unit in such an experiment and the corresponding precursor concentration in the flame during deposition of an alumina top-layer. The precursor concentration is an exponential function of the temperature and since the particle diameter depends on the precursor concentration to the third power, a small decrease in saturator temperature leads to a dramatic reduction of the particle size.

The deposition is carried out in a deposition cell that is heated to 300°C in order to obtain a thermally accommodated membrane layer, which is more stable towards phase transformations during subsequent heating. There is, however, a problem when depositing alumina top-layers, since alumina nano-particles below roughly 10nm in size only are of the γ - or δ -phase, which is a meta-stable phase, i.e. not thermodynamically stable. The alumina membranes, furthermore, have poor chemical stability [1], but the synthesis method is easily transferred to other metal oxides, so in this context alumina serves as a model system. Other oxides such as MgO and MgAl₂O₄ have also been applied in the membrane formation process.

The pressure drop across the membrane is very uniform and the membrane will be without cracks, because any non-uniformity in the pressure drop will be leveled out by a temporary increase in the local deposition rate.

Characterization

For characterization of the porous α -Al₂O₃ substrate a permeation method is used, where hydrogen, helium and nitrogen are used as permeate gases. The model proposed by [3] for the gas permeation in porous ceramic membranes has been used for the evaluation of the structural parameters of the substrate, equation 1:

$$F = \frac{Q P_0 l}{A \Delta P} = \frac{d_p}{3} \sqrt{\frac{8 R T}{\pi M}} \frac{\varepsilon}{\tau} + \frac{d_p}{32 \mu} \frac{\varepsilon}{\tau} \bar{P} \quad (1)$$

Here, F is the permeance, Q is the volumetric flow rate measured at atmospheric pressure P_0 , l is tube thickness, \bar{A} is the logarithmic mean area of the membrane, ΔP is the pressure drop across the substrate, M is the molecular weight of the permeation gas, and \bar{P} is the mean gas pressure in the substrate. From permeation data, the average pore diameter, d_p and the structure parameter ε/τ can be estimated for the substrate.

After deposition, the top-layer and the substrate are again characterized by permeability measurements. The measured permeation flow will be influenced both by the resistance in the top-layer and the resistance in the substrate. The permeability data for the membrane top-layer are therefore extracted using a resistance-in-series model [3], where the permeation data for the substrate is subtracted from the data from dual-layer system. The data from the three permeation gases (He, H₂, and N₂) are normalized with their molecular weights and the viscosities of the gasses according to:

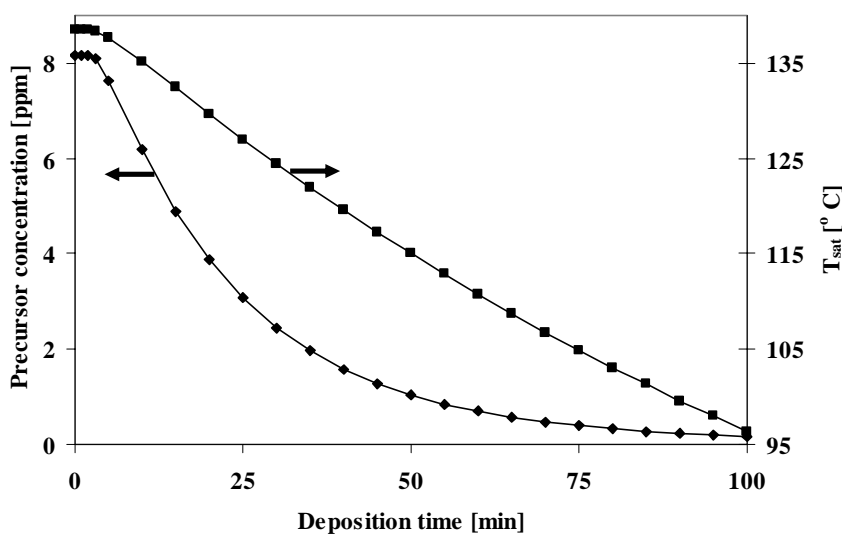


Figure 3: Saturation temperature of the sublimation unit and the corresponding precursor concentration in the flame during deposition. The drop in saturator temperature give a high drop in precursor concentration results in an even more significant reduction in particle size from the flame unit.

$$Y = F_i \sqrt{M_i} \text{ or } Y = F_i \sqrt{M_i} / \delta \text{ and } X = \frac{\bar{P} \sqrt{M_i}}{\mu_i}$$

Normalized permeation data for a substrate and the deposited alumina top-layer can be seen in figure 4. There is a strong linear dependence of the normalized permeation, Y , on the normalized pressure, X , for the substrate. For the top-layer, the pressure dependence is almost negligible, i.e. the slope is close to zero, which indicates that the dominant transport mechanism through the top-layer is Knudsen diffusion.

Membrane properties

The membranes have been synthesized using a macro-porous α -aluminum substrate tube, and the top-layers have primarily been made of Al_2O_3 , MgO , and MgAl_2O_4 spinel. The lowest pore diameters, estimated to be as low as 2 nm, have been achieved by the dynamic deposition method. When depositing dynamically, the particle size from the flame exhaust is continuously decreased from an average particle size around 40 nm towards particles close to or smaller than one nanometer in size. Consequently, the membrane layer is “closed” with smaller and smaller particles and we have obtained membrane layers where Knudsen separation has been achieved in the time scale of an hour starting off with a macro porous support.

Currently, membrane layers consisting of MgO and MgAl_2O_4 spinel exhibits the best thermal stability, whereas alumina membranes made of ultra-fine particles have very poor thermal stability. Those alumina structures are also very sensitive to humid conditions. The poor stability of alumina is – as already mentioned – probably caused by the fact that the crystal phase formed by flame synthesis of alumina nanoparticles is not the most stable α -alumina phase. As a consequence the alumina top-layer is degraded when it is exposed to high temperatures or water. Magnesia and MgAl_2O_4 spinel do not exhibit the same problem with phase transitions, and hence are more stable top-layers.

Figure 5 shows a SEM picture of a membrane cross section. The top-layer membrane is MgO on top of an $\alpha\text{-Al}_2\text{O}_3$ substrate. The MgO layer has been produced using $\text{Mg}(\text{acac})_2$ as the precursor. The formed top-layer has good thermal stability and the adhesion to the substrate is very good. In addition, the small inserts show the sharp interface between the top-layer and the substrate, which is remarkable keeping the difference of three orders of magnitude in pore size in mind. The top view shows the very homogeneous surface once a well-defined top-layer is formed after closing the pore mouths of the substrate.

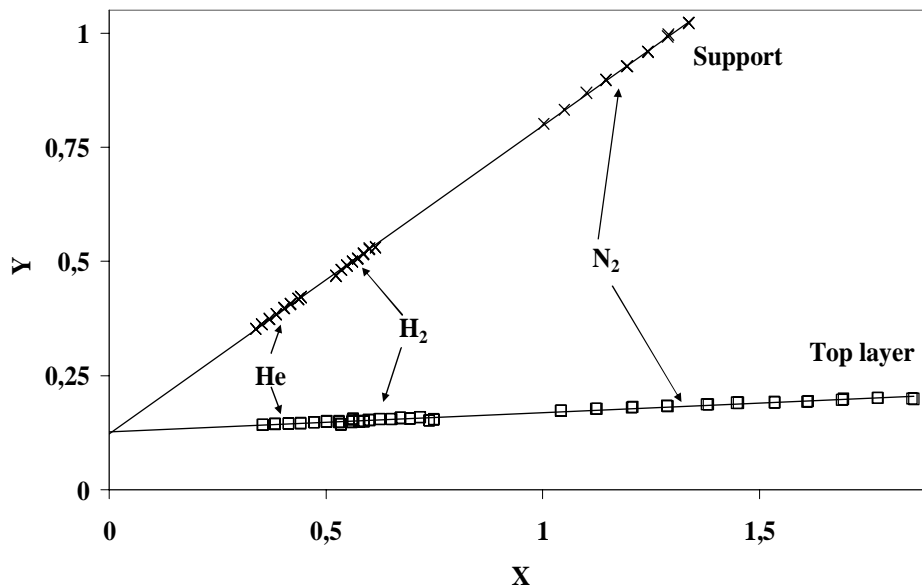


Figure 4: Dependence of $Y = F_i \sqrt{M_i}$ or $Y = F_i \sqrt{M_i} / \delta$ on the $X = \frac{\bar{P} \sqrt{M_i}}{\mu_i}$ for all gasses

H_2 , He and N_2 together in the support and top layer after 20 minutes of alumina deposition. $T_{\text{SAT}} = 138^\circ\text{C}$

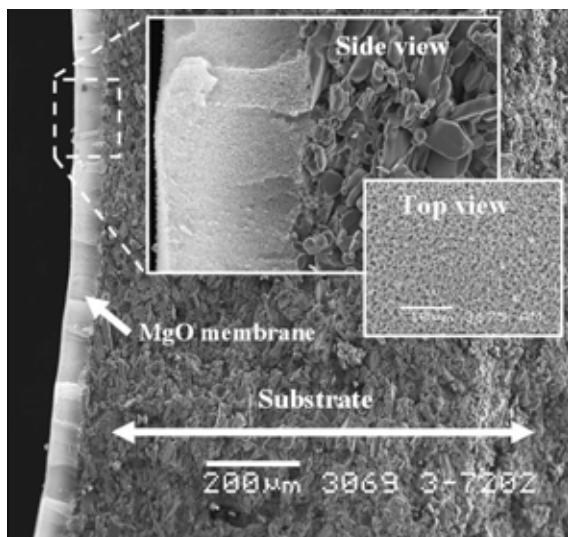


Figure 5: SEM picture of a membrane cross section. The membrane consist of a MgO top-layer and an Al_2O_3 substrate. The small inserts shows the insignificant penetration of the top-layer in to the support and also – from the top – a very homogeneous surface compared with the very rough alumina support.

Summary

The experiments have shown that it is possible to produce membranes with estimated pore sizes down to 2 nm by controlled deposition of flame synthesized nano particles. The MgO top-layer deposited on the macro porous substrate has good thermal stability and very good adhesion to the support.

The synthesized membranes are analyzed using a two-layer membrane permeation model. The model assumes a mixed Poiseuille flow and Knudsen flow in the substrate and pure Knudsen flow in the top-layer. The model connects the measured transport properties of the membranes to the membrane structure. The data used for the analysis are obtained from BET measurements, density measurements, and by permeability measurements with hydrogen, nitrogen, and helium as permeate gases. The data is then combined to give an estimate of the pore size.

Outlook

It has already been mentioned that one can produce both composite metal oxides and supported catalysts by flame pyrolysis, simply by feeding suited precursors to the flame. Examples of synthesized composite oxides are: MgAl_2O_4 [6] and ZnAl_2O_4 spinel [7]. Examples of produced catalysts are: Pt/TiO_2 , Au/TiO_2 and $\text{Cu/ZnO/Al}_2\text{O}_3$. As a part of an ongoing research project, active catalyst material has been successfully deposited on various surface materials [8]. Since both membranes and catalysts can be prepared by flame synthesis, the potential for making catalytic membrane reactors seem inherent.

Acknowledgements

The α -alumina support tube used in this study were supplied by Haldor Topsøe A/S, Lyngby, Denmark.

References

1. A. J. Burgraaf & L. Cot, *Fundamentals of Inorganic Membrane Science and Technology*, Elsevier Science, Amsterdam, 1996.
2. Andersen et. al, *J. Nanoparticle Res.*, 4(5), (2002), 405.
3. M. Mosleh, *Preparation of Micro Porous Ceramic Membranes by Flame Generated Aerosol Nano-Particles*, PhD thesis, Department of Chemical Engineering, Technical University of Denmark, 2004
4. Hansen et. al, *AIChE J.*, 47, 2000, 2413
5. Johannessen et. al, *ChERD*, 82(11), 2004, 1444-1452
6. J.R. Jensen, *Flame synthesis of composite oxides for catalytic applications*, PhD thesis, Department of Chemical Engineering, Technical University of Denmark, 2001
7. Jensen et. al, *J. Nanoparticle Res.*, 2, 363, 2000
8. Thybo et. al, *J. Catal.*, 223 (2), 271, 200



Kent Johansen
Address: IVC-SEP Department of
Chemical Engineering
Building 229, room 244
Phone: +45 4525 2876
Fax: +45 4588 2258
e-mail: keji@kt.dtu.dk
www: www.ivc-sep.kt.dtu.dk

Supervisors: Alexander A. Shapiro
Erling H. Stenby

Ph.D Study
Started: September 2004
To be completed: July 2007

Statistical Methods for History Matching

Abstract

A precise description of the physical properties of an oil reservoir can facilitate the operation of the oil field. Traditionally, the parameters determining the nature of the reservoir are determined by laboratory measurements and by history matching of the initial production data. In history matching logged production data is fitted using a full reservoir simulation. This process is very time consuming even when the simulations are carried out on powerful computers. Therefore, an alternative method to perform the history matching or parts of this is desired. This project deals with the application of statistical methods to carry out history matching and reservoir characterization.

Introduction

History matching is an important part of the characterization of an oil or gas reservoir. It is a process where production data from the initial stage of reservoir development is used to determine reservoir parameters and to predict the production in advance. The particular parameters measured at the production site are the injection rate, the oil production rate, the water cut, the gas-oil ratio, the bottom-hole pressures and others, as functions of time. History matching involves determination of permeability, porosity, relative permeabilities etc. Traditionally, full scale simulations on computers are carried out until the simulated production history matches the production history from the actual field sufficiently well. The method suffers from the fact that full scale simulations are computationally hard and time consuming. Also, the method demands an element of human intervention whenever parameters are adjusted which again makes the task of history matching a slow process. It is the aim of this project to develop a method which can facilitate the history matching of oil reservoirs.

Specific Objectives

The specific objectives of the project are the development of a viable method which can facilitate the process of history matching. The methods should honor the recorded production history from the field as well as honoring possible geological knowledge from e.g. test drillings or seismic surveys.

Results and Discussion

Geostatistics is concerned with the description of *spatially varying* properties in geology and petroleum engineering. In general, geostatistics provides a statistically reliable means of estimating geologic properties of an oil reservoir from a limited number of samples. A frequently used method to carry out a spatial interpolation is the so-called *kriging*-technique which uses a linear estimator of the form [1]:

$$\hat{z}_0 = w_0 + \sum_{i=1}^N w_i z_i = w_0 + \mathbf{w}^T \mathbf{z} \quad (1)$$

Here, each measurement is weighted with weights determined from the so-called kriging equations.

$$Cw = \text{Cov}\{Z_0, \mathbf{Z}\} \Leftrightarrow \begin{bmatrix} C_{11} & \dots & C_{1N} \\ \vdots & \ddots & \vdots \\ C_{N1} & \dots & C_{NN} \end{bmatrix} \begin{bmatrix} w_1 \\ \vdots \\ w_N \end{bmatrix} = \begin{bmatrix} C_{01} \\ \vdots \\ C_{0N} \end{bmatrix} \quad (2)$$

where C_{ij} is the covariance between the sampled points and where C_{0i} is the covariance between the sampled data and the estimated point. These quantities can be obtained from experimental or estimated semivariograms.

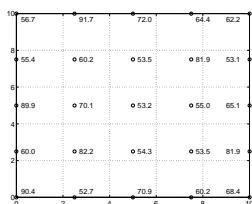


Figure 1: Sampled permeabilities.

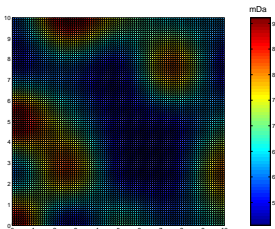


Figure 2: Kriged permeability field.

History Matching with Neural Networks

From simulations in a reservoir simulator a basis for the model building is obtained. The simulation results are used to develop statistical methods which efficiently correlate production data with the correct physical parameters of the reservoir. In the initial investigations a simplified oil reservoir is the basis for simulation. Possible methods for correlation may be

- Neural networks
- Regression techniques, i.e. statistical methods
- Time series

Neural networks have already been applied to the problem of correlating the simulated production history with some physical parameters. The networks have been trained to estimate 3 physical properties of a reservoir. A lot of work needs to be conducted but results indicate that neural networks are suitable to carry out an automated history matching.

Table 1: Estimation errors from neural networks.

| Network | Estimation error |
|------------------|------------------|
| 1 (Porosity) | -0.4% |
| 2 (Permeability) | 4.7% |
| 3 (Geometry) | 3.0% |

Work with neural networks has suggested that the processing and manipulation of the raw simulation

data is a central point before a proper performance can be realized. Furthermore, **Integration of physical knowledge** is essential when neural networks are constructed.

Conclusion

Neural networks can be used to automated history matching but adequate training data must be present. Preprocessing and manipulation of the raw data is also an essential task to be met along with the integration of physical knowledge.

Future work

Combination of the geostatistics with the history matching is an obvious extension of the work. A method which incorporates geologic measurements with the production history will not only be geologically reliable but also honor the production history. Such a model can be expected to possess better predictive capabilities compared to models which do not honor both the production history and the geology. Therefore, work should be invested in development of a method where production history can be conditioned on the geostatistical model.

The problem of conditioning production history as well as geological measurements on the model is addressed in [2] where a history matching method which preserves the geological properties is developed. [3] use a streamline based method to compute sensitivities of the the water cut with respect to the permeability field. In a gradient based optimization these sensitivities are used to match the simulated production with the recorded history.

Acknowledgements

The project is part of the Molecular Products and Product Technology (MP₂T) in the graduate school in chemical engineering. The industrial cooperator is Dansk Olie og Naturgas.

References

- [1] Isobel Clark. *Practical Geostatistics*. Applied Science Publishers LTD, 1984.
- [2] F. Roggero and L. Y. Hu. Gradual deformation of continuous geostatistical models for history matching. *Society of Petroleum Engineers*, (49004), 1998.
- [3] Hao Cheng, Arun Kharghoria, Zhong He, and Akhil Datta-Gupta. Fast history matching of finite-difference models using streamline-derived sensitivities. *Society of Petroleum Engineers*, (89447), 2004.



Kåre Jørgensen

Address: Building 229, room 114
Phone: +45 4525 2831
Fax: +45 4588 2258
e-mail: kj@kt.dtu.dk
www: www.chec.kt.dtu.dk

Supervisor(s): Anker Degn Jensen
Kim Dam-Johansen
Poul Bach, Novozymes A/S

Ph.D. Study
Started: February 2002
To be completed: August 2005

Effect of Formulation Ingredients on Drying Kinetics and Morphology of Particles Formed During Spray Drying

Abstract

In this work drying kinetics and morphology development of slurry droplets are investigated through drying of ~250-355 μm droplets in a Droplet Dryer. The droplets experience free fall in an electrically heated drying tower ($T_{\text{drying air}} = 25\text{-}225\text{ }^{\circ}\text{C}$) where the water content of the droplets is determined by sampling through sampling ports in the tower walls. Morphology is determined by capturing the droplets in paraffin oil or by investigating the dry particles under light and scanning electron microscopy. Experimental results for droplet drying rate (possibly combined with effect of morphology) will be compared to mathematical models, and suggestions for increasing the drying rate while retaining a solid, spherical, high-density particle with good friability will be given.

Introduction

Spray drying processes are used throughout numerous industries for the production of easy-to-handle, easily transportable, storage stable particulate solid products. Products produced by spray drying include: Pharmaceuticals, foods, chemicals, cosmetics, detergents, ceramics, dyes, and fertilizers [1].

Spray drying is characterised by being a unique way of producing a particulate solid product from a solution, slurry or paste in a single operation.

Studies into spray drying processes have traditionally focused on [2]:

1. Atomisation studies, where droplet size distributions, feed characteristics, atomiser design, pressure/rotational speed and throughput are investigated.
2. Studies of gas flow patterns and droplet/particle residence times.
3. Single droplet drying studies, which give information about the development of particle morphology and drying rate.
4. Mathematical models to correlate experimental data to simulate whole dryer performance by predicting droplet drying rates and drying behaviour.

The increased application of spray drying to produce high value-added products e.g. for the pharmaceutical, cosmetics or food industries, where the cost of the spray drying stage is less important than for bulk foods such

as milk powder, has greatly increased the focus on a detailed understanding of the droplet drying process.

With the introduction of computational fluid dynamics (CFD) to simulate gas and particulate motion in a spray dryer the interest in droplet/particle drying rate and its effect on particle morphology has increased further. The drying rate as well as the quality of the spray dried product, e.g. with respect to friability (i.e. mechanical strength), flowability, bulk and particle density, particle size distribution (PSD), low moisture content to ensure good storage stability of active ingredients (e.g. API's, enzymes, flavours, aromas, etc.), is greatly dependent on the particle morphology [3,4].

The drying rate and the morphology of spray dried droplets/particles depend on both slurry (i.e. formulation) and process conditions. For the most common case where hot air is used to dry off solvent water, the parameters include:

- Formulation:
 - Solid content.
 - Size and size distribution of primary particles in the slurry.
 - Polymeric material with high molecular weight.
 - Inorganic salts which may lower the vapour pressure.
 - Initial droplet temperature.
 - Viscosity.

- Process conditions:
 - Temperature of drying air.
 - Relative humidity of drying air.
 - Air/liquid flow rate.
 - Droplet size.
 - Injection velocities of droplets.

The only way to increase the knowledge about droplet drying and morphology development is to perform experiments and attempt to model the drying rate and morphology in dependence of the parameters just listed.

Specific Objectives

The primary objective of this PhD project is to increase the knowledge about the effect of formulation ingredients on the drying kinetics and morphology development in slurry droplets formed by atomisation.

Through experimental work on a newly constructed Droplet Dryer (see description in section “Experimental setup” and Fig. 2) data will be generated, which give information about drying kinetics and morphological development for droplets produced from slurry formulations. A model will be set up to predict the drying kinetics and possibly also the morphology development.

Experimental setup

Droplet generation

In this PhD project a new approach to slurry droplet generation has been taken. A so-called JetCutter[®] is used and the droplet generation principle – sketched in Fig. 1 – is briefly as follows (for further details please refer to [5] and [6]):

The slurry is passed through a nozzle of size $\varnothing 100\text{--}300\ \mu\text{m}$ using compressed nitrogen. A liquid jet is formed, which exits the nozzle at 5-20 m/s, thus giving a slurry mass flow rate of 0.1-0.5 g/s. A fast-rotating cutting wheel with 24-240 wires of diameter $\varnothing 100\ \mu\text{m}$ cuts through the liquid jet to produce cylindrical droplets, which quickly become spherical due to the surface tension.

The width of the droplet size distribution produced by the JetCutter[®] depends on the viscosity of the slurry, since a too low viscosity ($< \sim 10\ \text{mPa}\cdot\text{s}$) will result in the production of satellite droplets, a less well-defined PSD, and increase the risk of droplet collision in the air.

Droplet drying

Once the droplets are generated they experience free fall into a 6 meter tall ($\varnothing 200\ \text{mm}$) electrically heated drying tower (see Fig. 2), where drying air of temperature 25-250 °C is fed cocurrently with the droplets at a velocity of 0.1-1 m/s. Through ports in the drying tower droplet sampling for drying rate and morphology can be performed. The dried particles are collected in the bucket at the bottom of the tower, where the exhaust air is led to the building ventilation system.

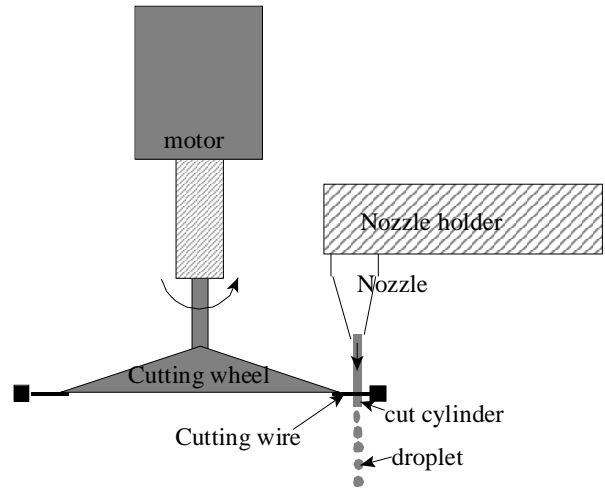


Figure 1: Sketch of the droplet generation principle in the JetCutter[®].

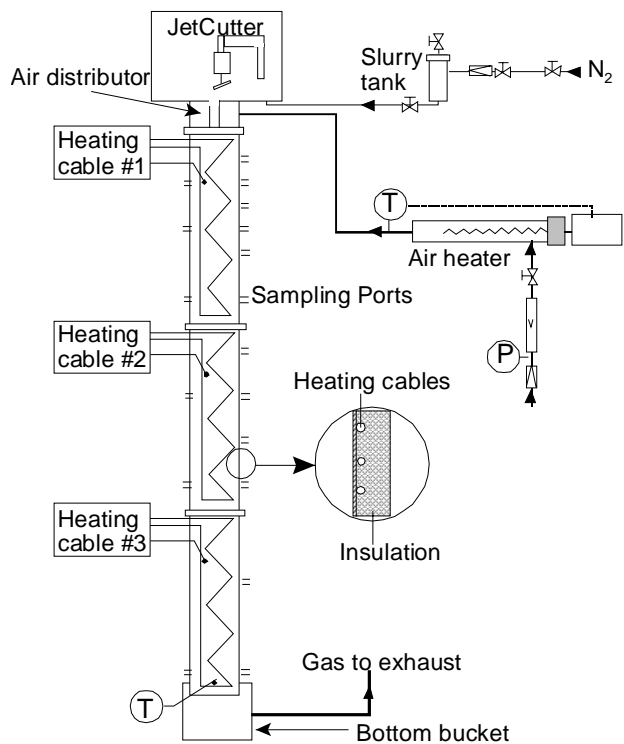


Figure 2: Drawing of Droplet Dryer experimental setup.

Droplet sampling

The sampling device has a diameter of 50 mm and is constructed from stainless steel and equipped with a thin aluminium foil cup ($\varnothing 39\ \text{mm}$), which contain a thin layer of paraffin oil. The sampling device can be inserted into the drying tower to collect droplets/particles at different locations both axially and radially through the sampling ports. When the droplets are sampled in the paraffin oil the water evaporation is significantly reduced during the sampling period. The sampling period lasts 3-60 seconds depending on where in the tower the sampling is performed and on the water content of the droplets.

After sampling the cups are weighed in order to determine the mass of droplets sampled. The water

content of the droplets/particles is determined by Karl Fischer titration.

Particles are also sampled for morphology investigation through the sampling ports and from the dried particles in the bottom bucket. Later, these particles can be evaluated for friability, e.g. by exposing them to controlled impact and/or shearing conditions. The mechanical evaluation of the particle friability may be performed as described in the work of Jørgensen [7], who investigated different types of enzyme granules.

Primary particles

Slurries are produced from different types of primary particles – as listed in Table 1:

Table 1: Size and span for primary particles to be investigated.

| | TiO ₂ (Kronos 2044) | Al ₂ O ₃ (ALCAN MA2LS) | Al ₂ O ₃ (ALCOA CT3000SG) | Corn starch | Wheat starch | Rice starch |
|---------------------|--------------------------------------|--|---|----------------|-----------------|----------------|
| d ₅₀ -µm | 0.37 | 10.1 | 0.3 | 13.5 | 19.8 | 5.2 |
| span | 0.8 | 1.3 | n.a. | 1.1 | 1.0 | 1.5 |

Size measurements have been performed using laser diffraction.

Modelling

A model for the slurry droplet drying taken from Abuaf and Staub [8] is set up and solved. The model assumes the slurry droplet to dry in two phases. The **first phase** is usually termed the constant rate period (CRP) and starts with a rapid approach of the droplet temperature to the wet-bulb temperature. The droplet temperature is assumed to be uniform throughout the droplet. After the initial heat up the droplet surface is still saturated with liquid water and the drying rate (in kg/m²/s) is constant and is determined by the resistance to heat and mass transfer in the gas film at the saturated droplet surface. The droplet dries and shrinks (as sketched in Figure 3A) as if it was a pure water droplet with the equations for mass and energy given in Eq. 1 and Eq. 2:

$$\frac{dm_l}{dt} = -\frac{k_m M_w 4\pi}{\frac{1}{2}(T_p + T_\infty) R} R_p^2 (P_{vi} - P_{v\infty}) \quad (1)$$

$$(m_s C_{ps} + m_l C_{pl}) \frac{dT_p}{dt} = h 4\pi R_p^2 (T_\infty - T_p) + \lambda_w \frac{dm_l}{dt} \quad (2)$$

where m_l [kg] is the mass of liquid in the droplet; k_m [m/s] is the convective mass transfer coefficient for water vapour at the droplet surface to the bulk drying air; R_p [m] is the droplet radius; P_{vi} and $P_{v\infty}$ [Pa] are the water vapour pressure at the droplet surface (index i for interface) and in the drying air bulk phase, respectively. T_p and T_∞ [K] are the droplet and drying air bulk temperatures, respectively; M_w [kg/mol] is the molecular mass of water, and R [J/mol/K] is the universal gas constant. In Eq. 2 m_s [kg] is the mass of solids within the droplet (assumed constant); C_{ps} and C_{pl} [J/kg/K] are the heat capacities of the solid material and the liquid (water), respectively; h [W/m²/K] is the convective heat transfer coefficient, and λ_w [J/kg] is the

latent heat of vaporisation of water at the droplet temperature.

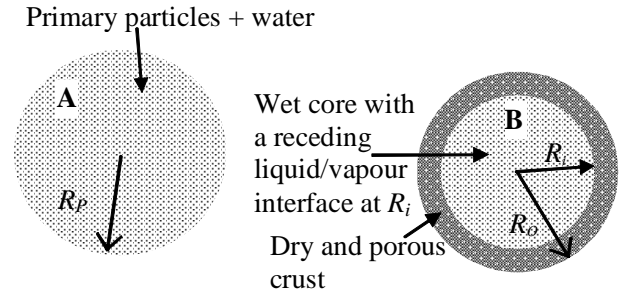


Figure 3: Model of drying of a slurry droplet during A - the first phase of drying (CRP), and B - second phase of drying.

As the drying progresses, water evaporates and the droplet shrinks, the primary particles in the droplet will eventually start to touch each other. When this happens the CRP is considered over, and the droplet/particle shape is now given.

During the **second phase** of drying, sketched in Fig. 3B, the primary particles can compact no further, and a dry crust is formed while a liquid-vapour interface recedes towards the centre of the particle. Heat is conducted through the dry crust to the interface from the particle surface, and water is evaporated and diffuses back towards the particle surface. The diffusion of water vapour becomes slower as the crust thickens thereby decreasing the evaporation rate and thus giving the alternative name for the second phase of drying, namely the *falling rate period*.

The mass balance for the second phase of drying can be described briefly by Eq. 3 with the introduction of a mass transfer resistance in the crust given by a Maxwell-Stefan type diffusion, which accounts for a flux of water vapour, which is unidirectional [8]:

$$\frac{dm_l}{dt} = \frac{M_w D_v P_T \ln \frac{P_T - P_{vi}}{P_T - P_{vo}}}{RT_{ave} \left(\frac{1}{R_o} - \frac{1}{R_i} \right)} \quad (3)$$

where D_v [m²/s] is the diffusion coefficient of water vapour in drying air; P_T [Pa] is total pressure of water vapour and air (=10⁵ Pa) in the drying air; T_{ave} [K] is the average temperature of the crust. α [-] is the void fraction of the dry crust, and the exponent n is a parameter giving the relationship between the porosity and tortuosity of the crust and assumed to be equal to 1 [8] (equivalent to straight pores in the crust). P_{vi} and P_{vo} [Pa] are the partial pressure of the vapour at the inner and outer surfaces of the dry spherical crust, respectively (see Fig. 3B). P_{vi} is assumed to be the saturation pressure of vapour at the wet core temperature. R_o [m] is the radius of the dry spherical crust, i.e. the particle diameter, while R_i [m] is the diameter of the shrinking wet core.

The mass transfer from the outer surface of the droplet/particle is given by Eq. 4, which is similar to the one presented in Eq. 1:

$$\frac{dm_l}{dt} = -\frac{k_m M_w 4\pi}{\frac{1}{2}(T_o + T_\infty)R} R_o^2 (P_{vo} - P_{v\infty}) \quad (4)$$

where T_o [K] is the temperature at the outer surface of the particle.

The heat to the wet particle core is transferred first by convection from the ambient air and then by conduction through the dry crust. Thus assuming quasi-steady state conditions the temperature of the outer and inner surface of the crust can be calculated following the energy equation in Eq. 5:

$$(m_{sdi} C_{ps} + m_l(t) C_{pl}) \frac{dT_i}{dt} = \frac{T_\infty - T_i}{\frac{1}{h4\pi R_o^2} + \frac{R_o - R_i}{k_{ps} 4\pi R_o R_i}} + \lambda_w \frac{dm_l}{dt} \quad (5)$$

here m_{sdi} [kg] is the amount of solid material inside the receding wet core; T_i [K] is the temperature at the liquid-vapour interface and therefore also of the entire wet core; R_o and R_i are the outer and inner crust radii of the particle as indicated by Fig. 3B; h [W/m²/K] is the heat transfer coefficient from the ambient air to the outer surface of the dry crust, while k_{ps} [W/m/K] is the thermal conductivity of the dry porous crust between R_o and R_i .

After setting up and solving the ordinary differential equations for mass, droplet shrinking, and energy, the droplet/particle mass, diameter, temperature, and crust thickness can be tracked as a function of time given the ambient temperature, relative humidity, and initial droplet diameter.

Results and discussion

This section will present and discuss the experimental and modelling results obtained from droplet drying experiments on slurries containing TiO₂ primary particles of size $d_{50} = 0.37 \mu\text{m}$.

Drying conditions

So far experiments have been performed under similar drying conditions as indicated in Table 2. Three slurry formulations have been investigated, containing 29.3, 39.2, and 48.9 wt.% TiO₂, respectively.

Table 2: Summary of drying conditions for the experimental results.

| | |
|---------------------------------------|-----------------------|
| Drying air temperature | 250 °C |
| Cocurrent air flow velocity in tower | 0.1 m/s |
| Droplet size produced (main fraction) | 250-355 μm |

Morphology

Figures 4a-d show SEM pictures of the produced particles. It can be seen that they are all non-spherical and contain holes or indentations.

A cut-through particle revealing the internal structure can be seen in Fig. 4d. The indentation is clearly not as deep in Fig. 4d as in the case of the 29.3 wt.% slurry in Fig. 4a, and the internal structure in the remainder of the particle in Fig. 4d appear quite homogeneous.

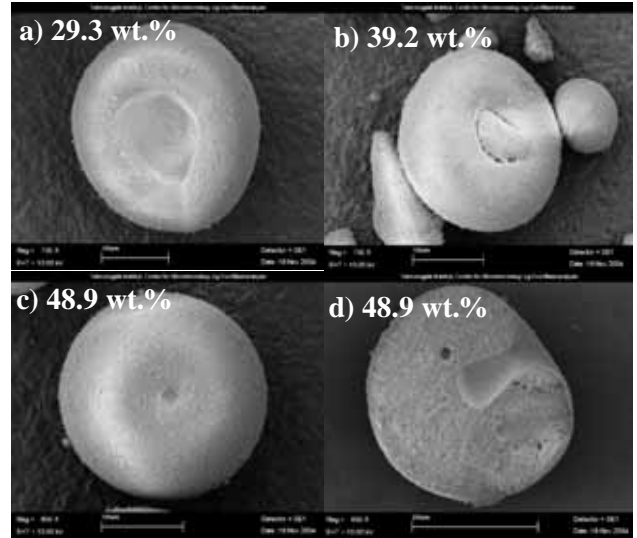


Figure 4: All particles are TiO₂ slurry droplets dried in a 250 °C dry air atmosphere. a) 29.3 wt.% TiO₂ (0012-028). b) 39.2 wt.% TiO₂ (0047-029). c) 48.9 wt.% TiO₂ (0045-026). d) A cut through a particle produced from a 48.9 wt.% TiO₂ slurry revealing the internal structure and the indentation.

The morphology of the particle presented in Fig. 4d is most likely the result of an implosion, as is suggested by the shape and curvature of the indentation walls.

As can be seen in Fig. 4a-c the indentations seem to be greater for particles produced from slurries with smaller initial solid fractions. This was also observed by Liang *et al.* [9] when spray drying a slurry of SiO₂ primary particles. This indicates that the small primary particles do not allow for a liquid water transport to the particle surface, which is fast enough to keep the surface wetted and thereby keep up with the evaporation [9]. When the crust starts to form, the outer diameter of the droplet/particle is locked, while the primary particles in the interior remain separated by liquid [10].

Primary particles are deposited on the inside of the crust at a constant high packing density as the water is drawn to the liquid/vapour evaporation interface. This theory is supported by the SEM picture in Fig. 4d, which does not indicate any gradient in primary particle packing through the dried particle. The water and primary particle transport leads to the formation of a partial vacuum in the droplet/particle centre and a pressure difference between the void and the ambient air arises. This will lead to a collapse/implosion of the particle if the crust is not strong enough to withstand the pressure difference, thus creating the indentation.

Drying kinetics

Figure 5 shows the water content in the droplets sampled. There are some scattering in the results from the water determination procedure, but it is clearly possible to distinguish between the water content of the individual experiments until a distance of approx. 3500 mm from the tower top is reached. Hereafter the water

content is so low (< 5 wt.%) that the uncertainties in the water determination method dominate.

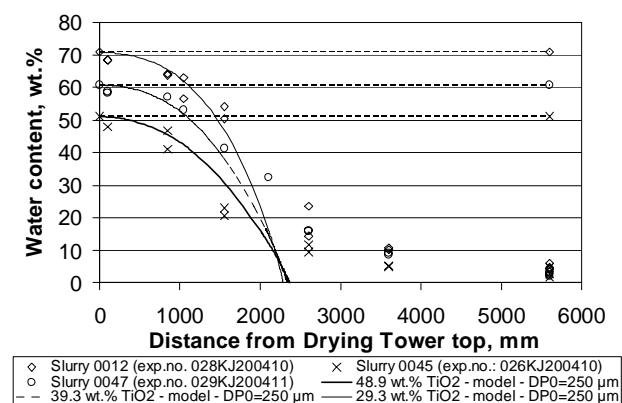


Figure 5: Drying rate – water content in the droplets sampled as a function of the distance from the drying tower top. Initial droplet diameter in model is 250 μm .

By applying an initial droplet diameter of 250 μm in the droplet drying model acceptable agreement between model and experimental results can be obtained down to approx. 1500 mm from the top of the tower. After approx. 2000 mm the model predicts the droplet to dry still faster and faster. However, this is not seen in the experiments, where the drying rate decreases as indicated by the levelling off of the drying curve in Fig. 5.

The lower drying rate observed experimentally, compared to the model, may possibly be explained by the early crust formation in the experiments. This enhances the resistance to heat and mass transfer and also the water content in the wet core is greater than in the model which prolongs the drying time. This may explain why the model fails to capture the decreasing drying rate.

Results from slurry droplet drying experiments performed by Büttiker [11] also reveal a tendency to a decrease in drying rate once the crust has formed. Furthermore, the decreasing drying rate after crust formation is supported by numerous results from droplet drying experiments by e.g. Nesic and Vodnik [12] – drying of colloidal silica, Ali *et al.* [13] – organic pigment, and Cheong *et al.* [14] – sodium sulphate decahydrate.

Conclusions and future work

A novel Droplet Dryer experimental setup is used to investigate the drying kinetics and morphology of ~250-355 μm slurry droplets with initial solid fractions of 30, 40, and 50 wt.% TiO₂ at an ambient drying air temperature of 250 °C.

The morphology of the dried particles is investigated using Scanning Electron Microscopy. The SEM pictures show that all the particles produced have an indentation. The size and shape of the indentation supports the theory that the particles implode as a result of a pressure relief between a sub-atmospheric pressure in a void formed in the particle centre and the ambient pressure.

The void is formed during the 2nd phase of drying when primary particles suspended in the particle core are deposited and pack at a higher density at the inside of the receding liquid/vapour interface. A larger indentation is observed for particles produced from a slurry of lower initial solid fraction.

Experiments are conducted to determine the drying kinetics of the droplets while they experience free fall down the length of the drying tower. The experimental results are compared to a model developed by Abuaf and Staub [8] and fairly good agreement is seen the first approx. 1500 mm from the tower top. The model does not take into account the early formation of a crust while the water content of the wet core is still close to the initial water content of the droplet. This may possibly explain why the model fails to capture the decreasing drying rate observed in the experimental results after approx. 2000 mm from the drying tower top.

This is an on-going work, where future experiments among other things will include changes in the

- drying air temperature,
- slurry formulation composition e.g. with respect to solid content and size of primary particles.

Further modelling considerations will be done to simulate the drying kinetics observed during the experiments. The PhD project of Jakob Sloth will continue the work described here and furthermore cover the areas of thermal enzyme deactivation and investigation of more complex formulations.

Acknowledgements

This project is performed in collaboration with Novozymes A/S, who also financially supports the project. Furthermore, this project is financially supported by the Novozymes Bioprocess Academy.

The CHEC Research Centre is financially supported by the Technical University of Denmark, Elsam A/S, Energi E2 A/S, Eltra, Elkraft System, the Danish Technical Research Council, the Danish Research Programme, Nordic Energy Research, EU, and industrial partners.

References

1. K. Masters, Spray drying handbook, 4th edition, George Godwin, London, 1985, pp. 76, 185, 481.
2. D.E. Walton, The morphology of spray-dried particles – A qualitative view, Dry. Technol. 18 (2000) 1943-1986.
3. C.J. King, Control of food-quality factors in spray drying, pp. 69-76 in Proceedings of fourth international drying symposium, Kyoto, Japan, 09-12 July, 1984, edited by R. Toei and A.S. Mujumdar.
4. T.M. El-Sayed, D.A. Wallack, C.J. King, Changes in particle morphology during drying of drops of carbohydrate solutions and food liquids. 1. Effects of composition and drying conditions, Ind. Eng. Chem. Res. 29 (1990) 2346-2354.

5. U. Prüße, B. Fox, M. Kirchhoff, F. Bruske, J. Breford, K.-D. Vorlop, The jet cutting method as a new immobilization technique, *Biotech. Techniques* 12 (1998) 105-108.
6. K.-D. Vorlop, J. Breford, Production of solid particles from a liquid medium, German Patent DE 4424998, 1994.
7. K. Jørgensen, Design of a Shear and Impact Resistant Enzyme Granule, MSc Thesis, Department of Chemical Engineering, Technical University of Denmark, 2002.
8. N. Abuaf, F.W. Staub, Drying of liquid-solid slurry droplets, pp. 277-284 in *Drying '86 volume 1, Proceedings of the fifth international symposium on drying*, editor: Mujumdar, A.S., Springer-Verlag, Berlin, F.R. Germany, 1986.
9. H. Liang, K. Shinohara, H. Minoshima, K. Matsushima, Analysis of constant rate period of spray drying of slurry, *Chem. Eng. Sci.* 56 (2001) 2205-2213.
10. W.J. Walker Jr., J.S. Reed, S.K. Verma, Influence of slurry parameters on the characteristics of spray-dried granules, *J. Am. Ceram. Soc.* 82 (1999) 1711-1719.
11. R. Büttiker, *Erzeugung von gleich grossen Tropfen mit suspendiertem und geloestem Feststoff und deren Trocknung im freien Fall*, PhD thesis, Swiss Federal Institute of Technology Zurich, Switzerland, 1978, pp.76-103.
12. S. Nestic, J. Vodnik, Kinetics of droplet evaporation, *Chem. Eng. Sci.* 46 (1991) 527-537.
13. H.H. Ali, C.J. Mumford, G.V. Jeffreys, G.S. Bains, A study of evaporation from, and drying of, single droplets. In: A.S. Mujumdar, M. Roques, eds., *Drying '89, Proceedings from 6th International Drying Symposium*, Versailles, France, September 1988, 378-385.
14. H.W. Cheong, G.V. Jeffreys, C.J. Mumford, A receding interface model for the drying of slurry droplets, *A.I.Ch.E. J.* 32 (1986) 1334-1346.

Dept. of Chem. Eng., Technical University of Denmark, 2004.

5. K. Jørgensen, A.D. Jensen, P. Bach, K. Dam-Johansen, Effect of formulation ingredients on drying kinetics and morphology of particles formed during spray drying, *article submitted to 7th World Congress of Chemical Engineering, 10-14 July 2005, Glasgow, Scotland.*

List of Publications

1. K. Jørgensen, P. Bach, A.D. Jensen, Design of impact resistant enzyme granules, Oral presentation (O-13-004) at 1st European Symposium on Product Engineering, part of 4th European Congress of Chemical Engineering, Granada, Spain, 21-25 September 2003.
2. A.D. Jensen, K. Jørgensen, P. Bach, Test af mekanisk stabilitet af enzymgranulater til vaskepulvere, *Dansk Kemi* 10 (2003) 18-21.
3. K. Jørgensen, P. Bach, A.D. Jensen, Impact and attrition shear breakage of enzyme granules and placebo particles – application to particle design and formulation, *Powder Technol.* 149 (2004) 157-167.
4. K. Jørgensen, Droplet Dryer: An experimental setup to investigate the drying kinetics of droplets under spray drying conditions. Design, construction and commissioning, CHEC Report no. R0403,



Morten Rode Kristensen
Address: Building 229, Room 244
Phone: +45 4525 2876
Fax: +45 4588 2258
e-mail: mrk@kt.dtu.dk
www: www.ivc-sep.kt.dtu.dk

Supervisors: Per G. Thomsen
Michael L. Michelsen
Erling H. Stenby

Ph.D. Study
Started: August 2004
To be completed: August 2007

Numerical Simulation of In-Situ Combustion

Abstract

In-situ combustion is the process of injecting oxygen (or air) into oil reservoirs to oxidize the heaviest components of the crude oil and enhance recovery through the heat and pressure produced. Although technically and economically attractive, in-situ combustion has not yet achieved widespread commercial use mainly due to a limited mechanistic understanding of the process and the lack of numerical simulators to predict field performance. Thus, the motivation for addressing in-situ combustion is the current (i) lack of process understanding, (ii) lack of mechanistically accurate simulation models and (iii) lack of efficient numerical methods to resolve the multiscale phenomena in in-situ combustion processes.

Introduction

The world continues to rely substantially on petroleum fossil fuels as a primary energy source. While the number of new discoveries of petroleum reservoirs decreases, the need to produce the known reservoirs more effectively increases. The in-situ combustion recovery process, in which oxygen is injected into the reservoir, has great potential in aiding to meet this requirement.

Process Description

In-situ combustion is the most complex of the enhanced oil recovery processes as it combines mechanisms of many of the other recovery processes [1]. The oil in the reservoir is ignited near the injection well (in forward combustion) either spontaneously after oxygen injection or by external means. The displacement is governed by several different mechanisms:

- The temperature increase caused by combustion increases the mobility of the oil.
- Vaporization of connate water forms a steam zone acting as a steam drive.
- Vaporization of a portion of the crude oil may form a miscible displacement.

- High-temperature combustion products may form an in-situ CO_2 flood.

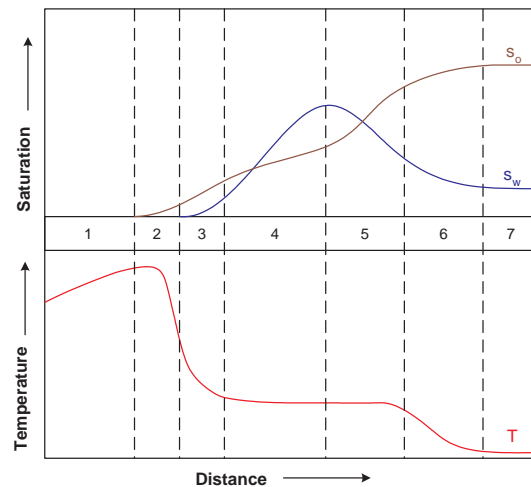


Figure 1: Characteristic regions of an in-situ combustion process. Qualitative temperature and oil and water saturation profiles are shown.

As seen from Figure 1 a number of characteristic regions can be identified in an in-situ combustion process:

- 1: Burned zone.** The burned zone contains injected oxygen (or air) and possibly a residue of burned fuel. Due to heat losses, the temperature increases downstream until the location of the combustion zone is reached.
- 2: Combustion zone.** Injected oxygen and fuel react generating heat and combustion gases.
- 3: Vaporization zone.** Light components of the hydrocarbons are vaporized and transported downstream.
- 4: Steam zone.** In-situ generated steam condenses.
- 5: Hot water bank.** Condensation of the steam results in a hot water bank.
- 6: Oil bank.** Oil bank is displaced by the hot water bank.
- 7: Initial zone.** The zone still unaffected by the in-situ combustion process.

Mathematical Formulation

The governing equations for in-situ combustion can be derived from the conservation of mass, momentum and energy. For the flow of a component i in n_p phases the continuity equation is written as:

$$\frac{\partial}{\partial t} \left[\phi \sum_{j=1}^{n_p} \omega_{ij} \rho_j s_j \right] = q_i - \nabla \cdot \left[\sum_{j=1}^{n_p} \omega_{ij} \rho_j \mathbf{u}_j \right] \quad (1)$$

in which ϕ is the porosity, s_j the phase saturation, ρ_j the phase density and ω_{ij} the mass fraction of component i in phase j . q_i represents sources and sinks. The phase velocity is given by Darcy's Law:

$$\mathbf{u}_j = -\frac{\mathbf{k}k_{rj}}{\mu_j} \cdot (\nabla P_j - \rho_j g \nabla D) \quad (2)$$

in which P_j is the phase pressure, D the depth, μ_j the phase viscosity and k_{rj} the relative permeability of phase j . When considering a thermal recovery process, the energy conservation equation must be included. When neglecting kinetic energy, potential energy and viscous dissipation, the energy equation may be written as:

$$\begin{aligned} \frac{\partial}{\partial t} \left[(1 - \phi) \rho_r C_r T + \phi \sum_{j=1}^{n_p} h_j \rho_j s_j \right] = \\ \nabla \cdot [\mathbf{k}_r \nabla T] - \nabla \cdot \left[\sum_{j=1}^{n_p} h_j \rho_j \mathbf{u}_j \right] + \sum_{i=1}^{n_r} \Delta H_i r_i \end{aligned} \quad (3)$$

in which h_j is the enthalpy of phase j , r_i is the kinetic expression for the i th chemical reaction with corresponding reaction enthalpy ΔH_i and, finally, ρ_r , C_r

and \mathbf{k}_r are the density, specific heat and conductivity of the reservoir rock, respectively.

Modelling the complex physics of in-situ combustion is indeed nontrivial. Some of the major modelling challenges include (i) modelling of both high and low temperature combustion reactions, (ii) coupling between chemical kinetics and phase equilibria and (iii) accounting for heat losses to the rock formation.

From a numerical point of view, in-situ combustion simulation poses many interesting challenges. The presence of slow and fast phenomena in in-situ combustion leads to a stiff set of equations requiring special solution techniques. Also, resolving the sharp temperature changes around the combustion front requires a fine mesh. In other regions with more gradual temperature changes a coarse mesh will suffice. Thus, adaptive mesh refinement should be used keeping a fine mesh resolution in the combustion zone. Finally, excessive computation times call for parallelization of the code.

Conclusion

The purpose of this Ph.D. project is to improve the current state of in-situ combustion models as well as to develop efficient numerical methods for simulation.

References

- [1] Larry W. Lake. *Enhanced Oil Recovery*. Prentice Hall, Upper Saddle River, New Jersey, 1989.

List of Publications

- [1] Morten Rode Kristensen, John Bagterp Jørgensen, Per G. Thomsen, and Sten Bay Jørgensen. An ESDIRK method with sensitivity analysis capabilities. *Computers and Chemical Engineering*, 28(12):2695–2707, 2004.
- [2] Morten Rode Kristensen, John Bagterp Jørgensen, Per G. Thomsen, and Sten Bay Jørgensen. Efficient sensitivity computation for nonlinear model predictive control. In Frank Allgöwer, editor, *NOLCOS 2004*, pages 723–729, September 1-3, 2004. 6th IFAC-Symposium on Nonlinear Control Systems.
- [3] Morten Rode Kristensen, John Bagterp Jørgensen, Per G. Thomsen, Michael L. Michelsen, and Sten Bay Jørgensen. Sensitivity analysis in index-1 differential-algebraic equations by ESDIRK methods. Submitted to IFAC World Congress, Prague, Czech Republic, July 4-8, 2005.



Morten Boberg Larsen

Address: Institut for Kemiteknik
Bygning 229
DK-2800 Kgs. Lyngby

Phone: +45 4525 2829
Fax: +45 4588 2258
e-mail: mbl@kt.dtu.dk
www: www.chec.kt.dtu.dk

Supervisor(s): Kim Dam-Johansen
Lars Skaarup Jensen, F.L. Smidth A/S
Peter Glarborg
Flemming Frandsen

Ph.D. Study
Started: October 2003
To be completed: September 2006

Combustion Mechanisms Using Waste as a Fuel in Cement Production

Abstract

The aim of this PhD-project is to investigate combustion mechanisms of waste when used as a fuel in the cement production. In particular the study is focused on combustion mechanisms of lumpy fuels when fired in the Hotdisc-unit developed by F.L. Smidth. The study is composed of four main components: Literature study, mathematical modeling, pilot scale/laboratory scale experiments and full scale measurements on industrial scale. A combination of the four elements should contribute to further development of the Hotdisc unit and to create further knowledge regarding the combustion mechanisms of lumpy fuels.

Introduction

The production of cement clinker is a very energy intensive process that traditionally has been depended on coal, oil and other resources of fossil fuel. The use of waste as a fuel in kiln-systems for cement production is an economically and environmentally feasible way to get rid of waste and replace non-renewable fossil fuel.

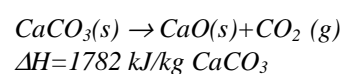
In the recent years, the use of waste in cement production has increased. Approximately 12% of the total fuel-usage in the production of cement is covered by use of waste in the EU. In Germany this figure has increased from 4% in 1987 to 30% in 2001. At some cement-plants more than 90% of the fuel-usage comes from waste. The different kind of waste employed at this moment in kiln-systems for cement production, are used tires, municipal waste, plastics and biomass [1]. In the future, it is expected, that the ability to use waste as fuel in the cement-industry will become even more important.

The advantages of using waste in the cement production are:

- The residual ash formed during combustion is incorporated into cement. This is classified as reuse by EU, whereas ash formed in traditional waste incineration plants is classified as disposal [2].

- The price of the fuel (waste) is cheaper than conventional fossil fuels and sometimes the price is negative, i.e. the cement manufacturer is paid to receive the fuel.
- The utilization of waste in the cement industry creates further research in the areas of environmentally and economically utilization of waste.

The Hotdisc-technology, which is developed at F.L. Smidth A/S, is used for combustion of lumpy wastes in the cement-industry. Figure 1 shows a schematic drawing of the Hotdisc-unit, which consists of a rotating plate in a combustion chamber, at which the combustion of the waste takes place. The waste is admitted to rotating disc together with preheated atmospheric air (Tertiary air, 850-900°C) followed by subsequent ignition and combustion releasing the energy for calcination of the limestone, which is a major component in the cement manufacturing process:



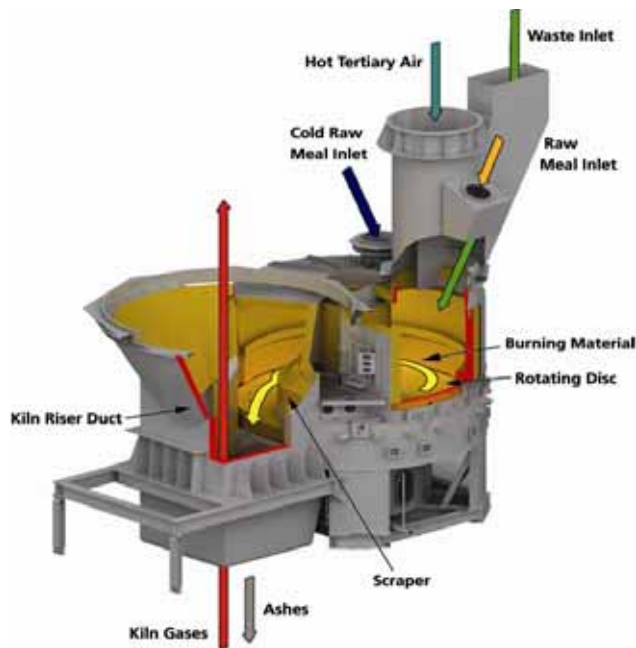


Figure 1 – Schematic drawing of the Hotdisc

This endothermic reaction is the most energy consuming process in cement kilns, which uses approximately 65% of the fired energy input [3]. Different elements in the waste, as Fe, Al and Si, are implemented into the cement in their oxidized forms (Fe_2O_3 , Al_2O_3 , SiO_2). Waste and ashes, which is not burned completely at the Hotdisc enters the conventional system for calcination.

At the end of the disc the remaining solids are transported to the conventional part of the kiln system. An important feature of processing waste in a cement kiln is the high residence time at high temperature, which ensures a complete conversion of polluting organic species. This issue has been of major concern in conventional waste incineration.

Specific Objectives

The aim of the ongoing industrial Ph-D study is to create knowledge to further develop the Hotdisc process and other applications for use of waste in cement production. The knowledge should be based on scientific methods. In particular the project is focused on the combustion mechanisms of waste, which include a detailed scientific description of the different stages in the combustion of the solid fuel and furthermore a scientific approach should be applied in order to understand the formation of inorganic pollutants, i.e. NO_x . The four main components of the PhD study are as follows:

- Literature study
- Mathematical modeling
- Pilot scale / laboratory scale experiments
- Full scale measurements

Furthermore, a successful project should contribute to the earning of F.L. Smidth A/S in the future and to help to ensure the position of F.L. Smidth as one of the leading companies in the world supplying solutions to the cement industry.

Furthermore it is expected, that the share of cement factories utilizing waste will increase in the future due to tighter legislation, which also demands that a good knowledge in the field of waste utilization is present in F.L. Smidth.

A successful project should also contribute with positive benefits for the society in general. In Denmark a successfully project should contribute to a high level of knowledge within the field of waste utilization, which eventually could lead to the formation of new firms and jobs. Globally, the utilization of waste in the cement industry replaces fossil fuel and creates increased research in the field of waste utilization induced by the free market mechanisms.

Results

The first step in the combustion for a lumpy piece of fuel is pyrolysis (or devolatilization), where the fuel releases its volatile components (e.g. gasses and tars). If oxygen is present in sufficient amounts, the volatiles may burn in a flame front above the pyrolysing fuel. Pyrolysis has been widely studied in connection with pulverized coal combustion of small particles, where the chemical kinetics is the rate controlling step. However, a significant difference exists for large particles, because also mass, heat transfer and effect of secondary reactions must be included to interpret the pyrolysis of thick particles. A series of experiments are performed in order to elucidate the fundamental aspects of flaming pyrolysis.

Thick pieces (5-20mm) of tread rubber for trucks were cut into desired shapes and placed into a specially designed holder, where the sample was insulated on all sides except the upper side, as shown in figure 2.

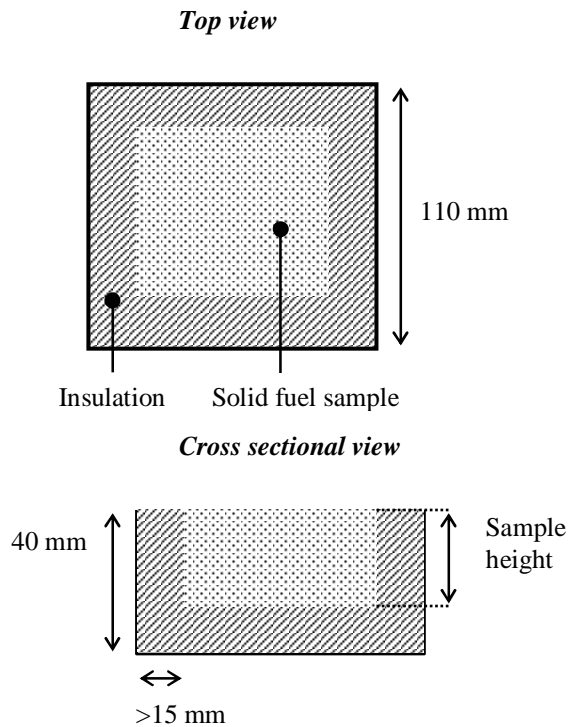


Figure 2 – Schematic drawing of holder used for flaming pyrolysis experiments

The holder containing the insulated solid fuel sample is placed in a hot chamber with a specified temperature and oxygen concentration. The sample is observed and the time when the flame extinguishes is referred to as the time of flaming pyrolysis, i.e. the time when the release-rate of volatile gasses is not sufficient to maintain a flame or no more volatiles are present in the solid fuel.

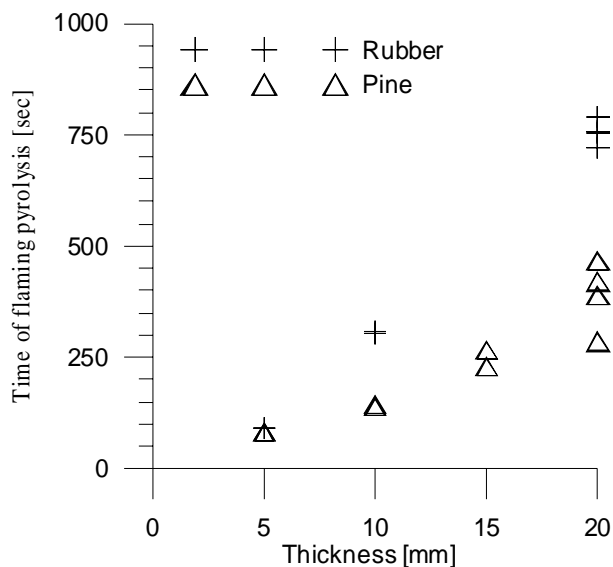


Figure 3 – Results for rubber and pine at 955°C and 9 Vol% O₂

The graph shown in figure 3 shows the time of flaming pyrolysis as a function of initial thickness of the specimen at 955°C and 9 Vol.% O₂ for pine and tread rubber. It is observed that the time of flaming pyrolysis increases linearly with size and that pine volatilises faster than tread rubber. To analyze the obtained results, mathematical models should be developed to elucidate the rate controlling mechanisms.

Conclusion

The current industrial PhD project deals with combustion mechanisms of waste with regard to usage as a fuel in the cement industry. The project is composed of four main elements: Literature study, mathematical modeling, pilot scale/laboratory scale measurements and full scale measurements, which all should contribute to an overall understanding of the combustion mechanisms of waste when used as a fuel in cement production.

Until now, the project has among other subjects dealt particular with combustion mechanisms prevailing on the industrial Hotdisc unit developed by F.L. Smidth. As a starting point, simple experiments are performed in order to analyze the characteristics of flaming pyrolysis of thick particles of tread rubber and pine. The results show that the time of flaming pyrolysis for thick particles of pine and tread rubber is significant and in the order of 100-1000 seconds.

References

1. Smith, I. Co-utilization of coal and other fuels in cement kilns. IEA Clean Coal Centre, August 2003.
2. Chandelle, J.M., Valorisation of waste in cement kilns, World Cement, 75, November 2003.
3. Andersen, P.S., Cementfabrikken (In danish). F.L. Smidth, January 1981.



Thomas Ricco Ølholm Larsen

Address: DPC, Dept. of Chemical Engineering,
Building 423, Technical University of
Denmark
Phone: +45 4525 2974
Fax: +45 4588 2161
e-mail: tol@kt.dtu.dk
www: www.polymer.dk

Supervisor(s): Martin E. Vigild
Tom L. Andersen, Risø

Ph.D. Study
Started: January 2004
To be completed: January 2007

Tribological Properties of Polymer Based Composites when Dry-Sliding Against Metal Counterfaces

Abstract

Polymer based composites are a class of materials which is being used increasingly for purposes where friction and wear are important properties. Beside beneficial properties such as a high strength to density ratio and chemical resistance, polymers generally also have a low coefficient of friction even when dry-sliding against metal counterfaces. This is due to self-lubricating properties which can be utilized in systems where lubricants such as oil or grease should be avoided.

Introduction

Tribology is the science of friction, wear and lubrication of interacting surfaces in relative motion [1]. Polymer based composites (PBC) are a class of materials, which is being increasingly used for purposes where friction and wear are important parameters [2]. Examples of this are gears, seals, rollers, tank track pads, bearings, brakes and artificial joints. PBC are often preferred to other materials because of their easy processability, high strength to density ratio, chemical resistance and generally low coefficient of friction [3-4]. Furthermore, some PBC have self-lubricating properties, which make them an excellent choice for systems where addition of lubricants such as oil or grease is inexpedient [5]. The dry sliding ability of PBC decreases the need for maintenance and the risk of emergency sliding conditions, which are seen in the case of metals, when lubricating systems fail [6].

Despite of the increasing use of PBC, the knowledge on their tribological behaviour are largely empirical and have limited predictive capability. Thus, there is a need for a better understanding of how different designs and compositions of PBC affect their tribological properties [2].

The tribological behaviour of polymeric materials have frequently been optimized by reducing adhesion to

the counterpart and improving the mechanical properties e.g. hardness, toughness and stiffness. This has traditionally been done by adding solid lubricants, e.g. PTFE (polytetrafluoroethylene) or graphite flakes, different strength giving fibers, e.g. carbon, glass and aramid fibers [7], or inorganic microscale particles e.g. CuO, Pb₃O₄ and TiO₂. [4].

Results regarding the ability of inorganic nanoscale particles to optimize tribological properties of PBC have been published recently [8-14]. The mechanism behind this optimization is not entirely understood, however, it seems to be the case that such particles in some cases promote adhesion of a transfer film to the counterface, which reduces wear and often also friction. Furthermore, a unique feature of nanoparticles is their ability to increase toughness and stiffness simultaneously [15], which is a desired property combination according to basic tribological models [16-17].

Objectives

The aim of this study is partly to produce a PBC with excellent tribological properties when performing in a well defined system, and partly to examine new material combinations and thereby contributing with new knowledge in this area. The choice of polymer matrix, solid lubricant and reinforcing fibers is based on

a literature review. Given these components, the focus of this project will be on an examination of how, and why, addition of nanoscale CuO particles influence the mechanical and tribological properties.

Methods

The tribological properties of the produced composites will be tested on a tribotester build on DTU for the purpose. This equipment is of the Pin-On-Disk type which is illustrated in figure 1.

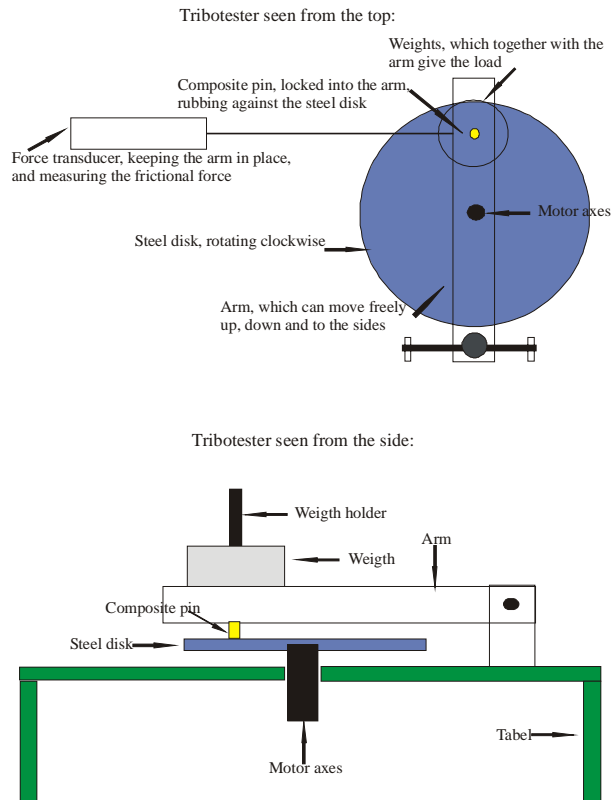


Figure 1. The principle of a Pin-On-Disk tribotester.

The coefficient of friction is obtained by knowing the load, given by the weights, and the forces collected from the force transducer. A wear rate can be obtained by measuring the weight loss of the composite pin as a function of time.

The mechanical properties of the produced composites will be examined mainly by tensile tests. Information about the microstructure of the composites, wear mechanisms and the appearance/morphology of transfer films on the counterface will be examined by different microscopic methods such as optical, SEM and TEM.

References

1. Serope Kalpakjian and Steven R. Schmid, *Manufacturing Engineering and Technology*, Prentice Hall, 2001.

2. Friedrich, K. & Reinicke, P, *Mechanics of Composite Materials* 34, 1998.
3. Harsha, A. P. & Tewari, U. S., *Polymer Testing* 21, p. 697–709, 2001
4. Schwarts, C. & Bahadur, S., *Wear* 251, 1532–1540, 2001.
5. Unal, H. & Mimaroglu, A. , *Materials and Design* 24, p. 182–187, 2003.
6. Häger, A. M. & Friedrich, K. , *Wear* 162, 1993.
7. Zhang, Z., Breidt, C., Chang, L. & Friedrich, K., *Tribology International* 37, p. 271–277, 2004.
8. Li, F., Hu, K. a., Li, J. I. & Zhao, B. y., *Wear* 249, p. 877–882, 2002.
9. Sawyer, G. W., Freudenberg, K. D., Bhimaraj, P. & Schadler, L. S., *Wear* 254, 2003.
10. Shi, G., Zhang, M. Q., Rong, M. Z., Wetzal, B. & Friedrich, K., *Wear* 254, 2003.
11. Christian J. Schwarts and Shyam Bahadur, *Wear* 237, p. 261-273, 2000.
12. Jin Lu, Ming Qui Zhang, Min Zhi Rong, Shu Li Yu, Bernd Wetzal and Klaus Friedrich, *Journal of Materials Science* 39, p. 3817-3820, 2004.
13. Ming Qui Zhang, Ming Zhi Rong, Shu Li Yu, Bernd Wetzal and Klaus Friedrich, *Wear* 253, p. 1086-1093, 2002.
14. Min Zhi Rong, Ming Qiu Zhang, Liu Hong, Hanmin Zeng, Bernd Wetzal and Klaus Friedrich, *Industrial Lubrication and Tribology* 53, p. 72-77, 2001.
15. Bernd Wetzal, Frank Hauptert, Klaus Friedrich, Ming Qiu Zhang, and Min Zhi Rong, *Polymer Engineering and Science* 42, 1988.
16. Klaus Friedrich, in: Klaus Friedrich (Eds.), *Friction and Wear of Polymer Composites - Composite Materials Series volume 1*, Elsevier, New York, 1986, p. 233-285.
17. I. M. Hutchings. *Tribology: Friction and Wear of Engineering Materials*, Edward Arnold, 1992.



Hongwen Li

Address: Dronninggårdsvej 2, 2 TV, 2840 Holte
Phone: +45 4525 2909
Fax: +45 4593 2906
e-mail: lhw@kt.dtu.dk
www: www.CAPEC.dtu.dk

Supervisor(s): Rafiqul Gani
Sten Bay Jørgensen

Ph.D. Study
Started: November 2001
To be completed: Oktober 2004

Input Multiplicity in Distillation

Abstract

The influence of pressure dynamics upon distillation control appears not to be well understood in the open literature, as contradicting statements concerning the importance of pressure control on binary distillation are found. In order to minimize energy consumption it is recommended to run columns at the minimum pressure; however, if the column pressure is controlled, instability may still occur. In this paper input multiplicity is shown to occur in the separation factor for increasing vapor flow rate through theoretical analysis, simulation and an extended series of experiments. This multiplicity is relevant for control structure selection and pressure dynamics, i.e. for where to place sensors in distillation columns for controlling pressure. The input multiplicity can be explained by two opposite effects; the first one comes from the well-understood effect of the changing the slope of the operating lines, while the second is due to the effect of pressure on the equilibrium curve. The results from the experiments verify the existence of the input multiplicity. It is concluded that controlling column pressure at one end of the column may be crucial to column stability when both product purities are controlled in a decentralized control structure.

Introduction

Distillation is by far the most widely used industrial separation technique. In chemical production and refinement plants energy integration provides a significant potential for energy saving. However, the increase in complexity caused by the introduced couplings may change plant characteristics drastically and thereby have significant impact on operability and on control configuration selection for the plant. The study of a heat integrated distillation pilot plant reveals some general characteristics of energy integrated distillation plant. The characteristics of interest are those, which affect the operability of distillation plants. Here two steady states aspects are pertinent for binary distillation:

Output multiplicity: The existence of multiple steady state outputs when the inputs are specified constant.

Input multiplicity: The existence of multiple steady state inputs when the outputs are specified constants. The dynamics consequence of output multiplicity is the occurrence of open loop unstable poles, which must be stabilized through control. This phenomenon has been investigated theoretically by Jacobsen and Skogestad (1). They found that output multiplicity for binary distillation might arise from singular points in the nonlinear conversion between mass or volumetric flow

rates and molar flow rates. This type of output multiplicity was experimentally verified by Kienle et al. (2) and Koggersbøl et al. (3). A possible dynamic consequence of input multiplicity is the occurrence of right half plane zeroes, which in case of multi-loop control may give rise to unstable closed loop behavior. Thus to facilitate selection of control configuration it is most relevant to investigate also this phenomenon for conventional binary distillation.

The purpose of this paper is to investigate the possible occurrence of input multiplicity, which will influence the selection of control structure. First the analysis of the possible input multiplicity is given. Then simulations were carried out in order to reveal the phenomenon behind the multiplicity. Thereafter experimental verification of this multiplicity is undertaken.

Description of the pilot plant

Figure 1 shows a schematic of an energy integrated distillation plant suitable for separating a mixture of methanol and isopropanol with a little impurity water. The plant consist of a distillation column, a thermosiphon reboiler, a total condenser and a reflux drum. The column has 19 sieve trays. In order to reduce energy consumption, the reboiler and condenser are

energy integrated through a heat pump. The heat pump transfers the energy released from the condenser to the reboiler. The experimental facility is located at the Department of Chemical Engineering at the Technical University of Denmark.

On tray 1,5,10, 15 and 19 PT100 temperature sensors are located in the liquid hold-up. In combination with pressure measurements (located in the column bottom, on tray 10 and in the column top) the temperature measurements are used for concentration estimates. All flows in and out of the system and the reflux flow rate are measured on a mass basis. Feed, bottom product, and distillate are sampled manually at each steady state for later gas chromatography analysis.

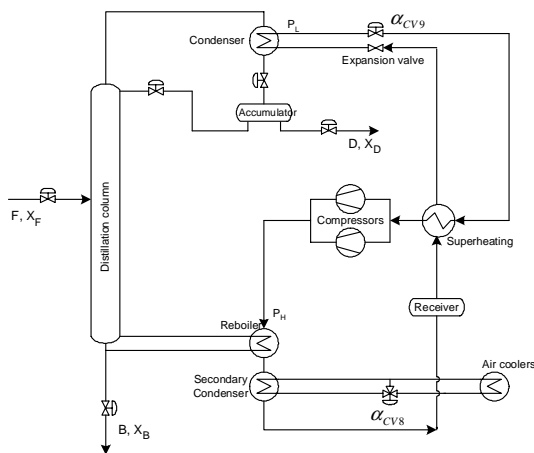


Figure 1: The flow sheet of the heat integrated pilot plant

The heat pump has an expansion valve (Exp. Valve) which throttles high pressure liquid Freon to a lower pressure (P_L) suitable for evaporation in the condenser. After the condenser there is a control valve (CV9) by which the freon vapor flowrate can be manipulated. After superheating the vapor the compressor elevates the pressure to a high pressure (P_H) suitable for condensation in the reboiler. A small part of the condensation takes place in a secondary condenser, which by a cooling water circuit is connected to a set of air fan coolers. The cooling rate can be manipulated by the control valve CV8, thus controlling P_H . Through a storage tank (Rec) and the super heater heat exchanger the Freon circuit is closed at the expansion valve.

The basic control configuration for the plant is as follows: the column pressure and column vapor flow are control by Multivariable Selftuning Control (MIMOSC). The accumulator level is controlled by reflux flow rate L and reboiler level is controlled by bottom product flow rate B . The concentration profile is retained in the column by maintaining the internal profile at tray 15 at $x_{15}=0.75$ by manipulating distillate flow rate D .

Model analysis

The mixture of methanol and isopropanol with a little impurity water has equilibrium property that separation decreases with increasing pressure.

From a model analysis five degrees of freedom are obtained, where two are designed to control the decanter and reboiler levels. Then for determining steady state three degrees of freedom remain. Here distillate flow rate D , high pressure P_H and low pressure P_L on the heat pump section are used for analysis of the control structure selection as actuators. Assume that distillate flow rate D is a manipulated variable for controlling the top composition. There remains two controlled variables, bottom composition and column pressure with the two manipulating actuators, high pressure P_H and low pressure P_L . In this discussion these two loops are assumed decentralized controlled, i.e. the loops are independent. Suppose first that column top pressure is controlled. Now, if suddenly the bottom purity is decreased due to a disturbance, then the controllers would increase P_H and decrease P_L in order to increase the vapor flow rate while keeping the condenser pressure constant. The increased internal flows enhance the separation and this way disturbance should be rejected. But in addition this increase results in larger pressure drop across the trays such that pressure on the lower trays is increased, and this results in reduced separation capability on these trays. If the internal flows are relatively high then the variation of these will have relatively small direct impact upon the separation but large impact on the pressure effect such that the pressure on the lower trays increase hence the relative volatility is reduced and the bottom purity is decreased further. In this case the process may actually still be unstable even though "column pressure" is controlled since a decentralized control structure is used.

Now let us analyze the process in the same situation except that the pressure in the reboiler is controlled instead. If the bottom purity is decreased due to some disturbance then again P_H will be increased and P_L decreased such that the vapor flow rate is increased but now the reboiler pressure is kept constant. As before the increased internal flows enhance the separation, however, if these flows are relatively large the effect may be relatively small. Due to the increased vapor flow rate the pressure drop across each tray is also increased as before, but since it is now the bottom pressure which is fixed, this results in a reduction of the pressure on all trays above the reboiler, hence this reduction results in a higher relative volatility such that the separation capability is further improved. The two effects are no longer opposing and therefore the process remains stable even if the pressure-drop effect dominates the effect of the internal flows.

In conclusion for any real distillation column where the separation increases with decreasing pressure the conflict between internal flows and column pressure potentially exists. The above analysis shows that for such systems operated at higher purities it is necessary to control column pressure and this pressure should

preferably be measured in the reboiler. This analysis was performed on our example of a distillation column with the actuators that are specific for this column. But it is valid for any column for which the boil-up flow rate and column pressure are indirectly manipulated by the heat input into the reboiler and the cooling rate in the condenser, and this is the case for the majority of distillation plants.

Simulation study

From the above model analysis, this conclusion can be obtained that a possible dynamic consequence of input multiplicity exists, which could be the occurrence of right half plane zeroes which in case of multi-loop control may give rise to an unstable closed loop behavior. Thus to facilitate selection of control strategy and configuration it is most relevant to investigate also this phenomenon both for conventional binary distillation and for energy integrated distillation pilot plant.

Køggersbøl (4) showed by simulations that the development of the real part of the right most eigenvalue when varying boil up under two point product composition control for different pressure control schemes. The three pressure control schemes simulated were: No control of column pressure; Pressure control of top tray pressure; Pressure control of bottom tray pressure. The initial operating points of the simulation are listed in Table 1 and results are shown in Figure 2.

Table 1. Initial operating condition for the simulation

| Pressure (kPa) | Feed | Flows | Purity |
|----------------|-------------------------|------------------|-------------|
| $P_L=1070$ | $F_{16}=1.0$ (l/min) | $D=0.39$ (l/min) | $X_C=0.93$ |
| $P_H=501.8$ | $X_{F,MeOH}=0.495$ | $L=9.0$ (l/min) | $X_B=0.025$ |
| $P_B=76.0$ | $X_{F, Iso-PrOH}=0.595$ | $L/D=23.1$ | |
| $P_C=71.3$ | $X_{H_2O}=0.01$ | | |

The simulations showed for increasing boil up rate, that when both product compositions were controlled (after having changed the boil up in open loop), eigenvalues with positive real part eventually occurred in the case of column pressure floating and for top pressure controlled. The real parts of the eigenvalues, in the case of bottom pressure controlled, however remained negative. The experimental plan is to investigate this input multiplicity.

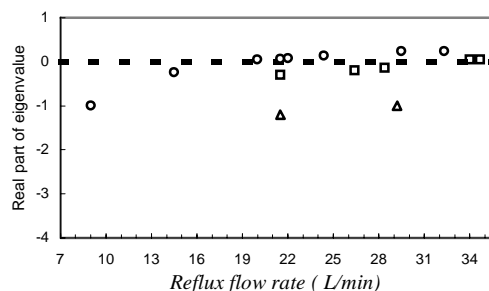


Figure 2: Real part of the eigenvalue of the plant model plotted as a function of the reflux rate. X_D controlled by D ; X_B controlled by P_H (corresponding to Q_B). (Data from Køggersbøl [4]). \circ - No control of column pressure; \square - Pressure on top tray controlled; Δ - Pressure in the reboiler controlled

Experimental plan

Four experiments (5) have been carried out to investigate the presence of an input multiplicity. The four experiments were carried out with measuring feed flow rates given in Table 2. Column top pressure was controlled in all three experiments. Set points for this loop were 100kPa. For the fourth experiment carried out on January 2003, both the top pressure and bottom pressure control were carried out; at the end of top pressure control, the pressure control was changed such that the bottom pressure was controlled. The composition profile was fixed at an interior point within the column. Therefore the estimated methanol mole fraction at tray 15, XPTT15, is controlled by manipulating the distillate flow rate D . The effect of shifting the pressure control point and thus changing the separation should best be seen in the composition of the bottom product, since the concentration profile is "fixed" at tray 15 (set point 0.75).

Table 2: The feed flow rates for the four experiments

| Name | February 2000 | October 2000 | November 2000 | January 2003 |
|------------------------------------|---------------|--------------|---------------|--------------|
| Feed flow rate set point [tons/hr] | 0.066 | 0.070 | 0.110 | 0.12 |

The means and standard deviations of the measured values and the time period were recorded for the individual steady states obtained during these experiments.

Experimental results

The separation, which can be obtained with any particular separation process, is indicated by the separation factor. Since the object of a separation column is to produce products of differing compositions, it is logical to define the separation factor in terms of product composition. The inherent separation factor is:

$$\alpha_{MeOH, iso-PrOH}^S = \frac{x_{MeOH,D} / x_{iso-PrOH,D}}{x_{MeOH,B} / x_{iso-PrOH,B}} \quad (1)$$

The separation factor reflects the differences in equilibrium compositions and transport rates due to the fundamental physical phenomena underlying the separation.

For the top pressure control, the inherent separation factor was four calculated and shown in Figure 3 for all the experiments in the heat integrated distillation pilot plant. From Figure 3 the input multiplicity became more and more clearly as the feed flow increased from 0.066 to 0.12 (ton/hr) shown in Table 1. Both the top and bottom pressure control is shown in Figure 4. The input multiplicity is clearly indicated in Figure 4 for both the top and bottom pressure control.

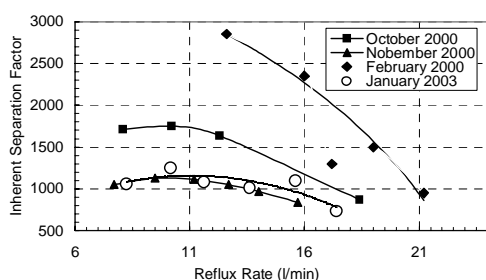


Figure 3: Inherent separation factor vs. reflux flow rate at top pressure control for the four input multiplicity experiments

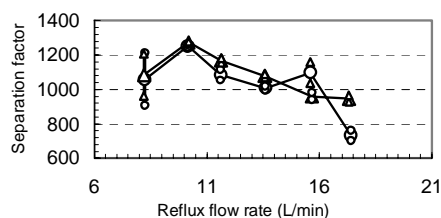


Figure 4: Inherent separation factor vs. reflux flow rate at both top pressure control and bottom pressure control for the input multiplicity experiments on January 2003

Conclusions

The distillation column pressure dynamics is investigated reveal influence upon distillation column control configuration. Phenomenological analysis and simulation results reveal a possibility for input multiplicity in a heat integrated distillation pilot plant. Experiments were carried out with two control structures, i.e. top pressure and bottom pressure control structures. The results from these experiments verify the existence of the proposed input multiplicity at top pressure controlled structure that match the simulation results by Koggersbøl (4). This conclusion can be obtained from the experiments that the bottom pressure control structure is to be desired compare the top pressure control structure because of the high separation factor. The practical relevance of these findings is that suitable control configurations and strategies can be selected to deduce the possibility of performance degradation due to these phenomena. The findings also show that attention from the process design community should be drawn to this field of research, since it is driven by changes in operability and stability resulting in performance reducing behavior, which is brought about by these phenomena. The results with control of pressure in the top of the distillation column indicate the existence of the proposed input multiplicity. The phenomenological analysis suggests for mixtures where the separation improves with decreasing pressure that pressure should be controlled at the bottom of the distillation column. The experimental results with control of bottom pressure indeed showed a higher separation factor, but also indicated presence of the input multiplicity.

References

- Jacobsen, E. W. and Skogestad, S. (1991). Multiple Steady States in Ideal Two-Product Distillation. *AIChE Journal*, 37, 499-511
- Kienle, S. Groebel, M. and Gilles, E. D. (1995). Multiplicities and Instabilities in Binary Distillation – Theoretical and Experimental Results. *Chem. Eng. Sci.*, 50 S2691-S2703
- Koggersbøl, A.; Anderson, T. R.; Bagterp, J. And Jørgensen, S. B. (1996). An Output Multiplicity in Binary Distillation: Experimental Verification. *Comput. Chem. Eng.*, 20, S835-S840
- Koggersbøl, A. (1995). *Distillation Column Dynamics, Operability and Control*. Ph.D thesis, DTU
- Torben R. A. (2002) Optimal Design and Operation of Process Integrated Distillation. Ph.D thesis, DTU



Yi Lin

Address: Building 229 Room 220
Phone: +45 4525 2869
Fax: +45 4588 2258
e-mail: yil@kt.dtu.dk
www: www.ivc-sep.kt.dtu.dk

Supervisor(s): Kaj Thomsen

Ph.D. Study

Started: September 2003
To be completed: September 2006

New Equation of State for Electrolytes

Abstract

The aim of the project is to develop a new equation of state for electrolytes over wide range of temperature and pressure, which is simple to implement. Several successful theories have been studied such as Poisson-Boltzmann equation theory, Integral Equation theories, Perturbation theories and Fluctuation theory from the literature about the electrolyte solution. The development of several equations of state for electrolytes is also studied. Among the equation of state for electrolytes, the equation of state from Mayer, Sandler and Wood has been studied in details and implemented. Based on the performances of Mayer, Sandler and Wood's equation of state, improvement will be made and new term will be introduced to substitute the old terms. The computational results from Mayer, Sandler and Wood have been reproduced to validate the performance of the EoS. Later the equation will be applied to a new test system to further study its performance. An analytical analysis of the difference between the results from the simplified Debye-Hückel theories and the simplified Mean Spherical Approximation has been conducted. The comparison is based on the excess Helmholtz free energy.

Introduction

Oil and Gas production in the North Sea involves transporting complex mixtures of oil, gas and formation water over large distances. Crude oil and natural gas consist mainly of hydrocarbons of varying molecular size, acetic acid and carbon dioxide and various amounts of dissolved minerals such as sodium chloride, calcium, barium, strontium sulfate and carbonate. In order to avoid problems such as clogging of pipes due to the formation of gas hydrates, wax, minerals or other solids, it is necessary to be able to predict the phase behavior of such mixtures. To avoid the formation of gas hydrates, additives like methanol or MEG (Mono Ethylene Glycol) can be added to the gas-oil-water mixture. Salts and acetic acid will however accumulate in the water/MEG phase and with time minerals will precipitate from this phase. Some acetic acid and carbon dioxide will remain in the gas phase where it will cause corrosion in connection with condensation in the top part of the pipe. Today it is possible to perform equilibrium calculations for complex mixtures of hydrocarbons and various production chemicals. It is also possible to separately perform equilibrium calculations with aqueous solutions of minerals and non-electrolytes, usually done by use of an activity

coefficient model. Activity coefficient models however lack the ability to describe the gas phase properties and need to be combined with cubic equations of state in order to describe such properties. In order to describe the phase behavior of complex mixtures of oil, gas, water, and minerals, the activity coefficient model approach can be expanded to encompass a proper description of the gas phase or the cubic equation of state can be expanded to encompass a proper description of the liquid phase. The second approach is chosen and the challenge addressed in this project is to develop an equation of state that also includes components such as minerals and sour gases. Some preliminary results from the literature study about the electrolyte solution theories and models are presented. An analytical analysis of the difference between the results from the simplified Debye-Hückel theories and the simplified Mean Spherical Approximation has been conducted.

Myers, Sandler and Wood Electrolyte EoS

Myers and Sandler's Electrolyte equation of state is intended to be developed for the systems more general than just containing hydrocarbons, water and salt and

over wide ranges of temperature, pressure and composition.

Use the property of a state function; we get the expression for the total change in Helmholtz free energy to form the electrolyte system:

$$A(T, V, \mathbf{n}) - A^{IGM}(T, V, \mathbf{n}) = \Delta A_{dis}^{Born} + \Delta A^{PR} + \Delta A_{chg}^{Born} + \Delta A^{Coul}$$

where \mathbf{n} is the vector of the number of moles of each component of the mixture, and A^{IGM} is the Helmholtz free energy of an ideal mixture.

Peng-Robinson term The Peng-Robinson term is given by

$$\Delta A^{PR}(T, V, \mathbf{n}) = \frac{an}{2\sqrt{2}b} \ln \left(\frac{v+c+(1-\sqrt{2})b}{v+c+(1+\sqrt{2})b} \right) + nRT \ln \left(\frac{v}{v+c-b} \right)$$

In this term, a volume translation parameters c has been introduced here for the Peng-Robinson EoS. This single parameter can improve the volumetric predictions of Peng-Robinson EoS significantly.

The mixing rules used here are the van der Waals one-fluid mixing rules:

$$a = \sum_i \sum_j x_i x_j \sqrt{a_i a_j} (1 - k_{ij}), b = \sum_i x_i b_i \text{ and } c = \sum_i x_i c_i$$

where k_{ij} is the binary interaction parameter. It is the only adjustable parameters in the model.

The parameters for pure compound water and ions are calculated in the following way:

$$a_{H_2O} = 1.269440 - 0.89381Tr + 0.16937Tr^2,$$

$$b_{H_2O} = 15.6345 + 6.14518Tr - 5.2795Tr^2,$$

$$c_{H_2O} = -2.7227 + 11.4201Tr - 6.0157Tr^2,$$

$$Tr = T / T_{c_{water}}$$

$$a_{ion} = a_{ion}^{(1)} + a_{ion}^{(2)} / T,$$

$$b_{ion} = b_{ion}^{(1)}, \quad c_{ion} = 0.0$$

The $a_{ion}^{(1)}$, $a_{ion}^{(2)}$ and $b_{ion}^{(1)}$ are fitted constant which are different for different salt.

Born contribution The free energy required to discharge ions in vacuum is calculated by the equation proposed by Born.

$$\Delta A_{dis}^{Born}(T, V, \mathbf{n}) = -\frac{N_A e^2}{4\pi\epsilon_0} \sum_{ions} \frac{n_i Z_i^2}{\sigma_i}$$

The free energy required to charge an ion in a medium of electric constant ϵ is calculated by the equation proposed by Born.

$$\Delta A_{chg}^{Born}(T, V, \mathbf{n}) = \frac{N_A e^2}{4\pi\epsilon_0 \epsilon} \sum_{ions} \frac{n_i Z_i^2}{\sigma_i}$$

The Born equation provides a means of calculating salvation free energies of ions in water. Born contribution has no effect on the ion activity coefficients but affect the water activity. Note that the Born equation provides good predictions of the free energies of hydration for most systems, it fails at very low solution densities. The reason for this is that the Born equation ignores the compressibility of the solvent.

Coulomb contribution The additional Helmholtz free energy change due to the Coulomb interaction between ions is calculated through the simplified mean spherical approximation (MSA). The simplified common ion-size solution of MSA has been employed by Myers et. al.. It is derived under the assumption that all ions have the same average diameter σ . The average diameter σ can be calculated through various mixing rules and here the conventional linear mixing rule has been adopted. The expression of the Helmholtz free energy is given by:

$$A^{Coul} = -\frac{2\Gamma^3 RTV}{3\pi N_A \epsilon_0 \epsilon} \left\{ 1 + \frac{3}{2} \Gamma \sigma \right\},$$

$$\Gamma = \frac{1}{2\sigma} \left[\sqrt{1 + 2\sigma\kappa} - 1 \right], \quad \text{where } \kappa = \left(\frac{e^2 N_A^2}{\epsilon \epsilon_0 RTV} \sum_{ions} n_i Z_i^2 \right)^{1/2}$$

$$\text{where } \sigma_i = \sigma_i^{(1)} + \sigma_i^{(2)} / T, \quad \sigma = \sum_{ions} n_i \sigma_i / \sum_{ions} n_i$$

Γ is the MSA screening parameters and κ is the Debye screening length ($\Gamma \rightarrow \kappa/2$ at infinite dilution). e is the electronic charge, k is the Boltzmann's constant, ϵ is the relative permittivity of the medium, ϵ_0 is the vacuum permittivity, z_i is the valence and σ_i is the diameter of species i , where $\sigma_i^{(1)}$ and $\sigma_i^{(2)}$ are fitted constant which are different for different salt. T is the absolute temperature, ρ_i is the number density of species i . Here a mixing rule is needed for the average ion diameter σ .

The above simplified MSA equation reduces to the Debye-limiting law as σ approaches zero. However the MSA equation gives more accurate predictions of the thermodynamic properties at high electrolyte concentrations.

The Uematsu and Frank model has been used to calculate the relative permittivity of the medium ϵ for pure water.

$$\epsilon(T, \rho_{water}) = 1 + (7.62571/Tr)\rho_r + (244.003/Tr - 140.569 + 27.7841Tr)\rho_r^2 + (-96.2805/Tr + 41.7909Tr - 10.2099Tr^2)\rho_r^3 + (-45.2095/Tr^2 + 84.6395/Tr - 35.8644)\rho_r^4$$

$$Tr = T / 298.15, \quad \rho_r = \rho_{water} / \rho_0,$$

$$\rho_0 = 1000 \text{ kg/m}^3,$$

Their model gives the dielectric constant as a function of temperature and density over a temperature range of 238-1273 K and pressures up to 1200MPa.

The limitations of Mayer, Sandler and Wood's EoS are mainly the following two. First, the Born equation predicting the free energies of hydration fails at very low solution densities due to ignorance of the compressibility of the solvent. Second the primitive model of electrolyte solution is not valid at high ion concentrations. The EoS should not be used for systems with salt concentrations greater than about 15 M.

The Computation Results

The equation of state was fitted to experimental data for 138 aqueous electrolyte solutions at 25 °C and 1 bar to 300 °C and from 1 to 120 bar. The equation does well in correlating activity coefficients osmotic coefficients, densities over the wide range of conditions. In the following Fig. 1, Fig. 3, Fig. 4, the calculated density, activity coefficient and osmotic coefficient are presented graphically.

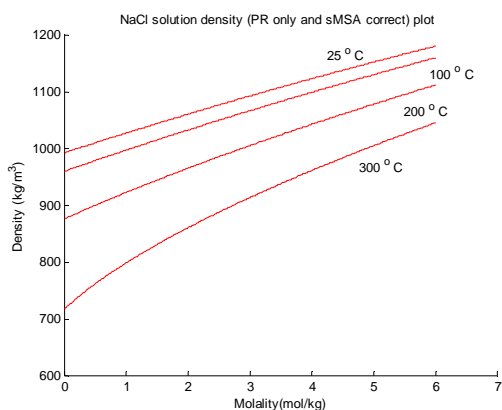


Figure 1 Plot of density of aqueous NaCl verse molality at different temperature and pressure.

In Fig.2, the original computational results and the experimental results are provided for comparison with Fig. 1. It can be seen that the re-produced results agrees with the published results.

A more comprehensive application to mixed-salt systems will be given in the future. The selected test system for future study is H₂O, Na⁺, Ca²⁺, Cl⁻, SO₄²⁻, CO₃²⁻, HCO₃⁻, CO₂ and Glycol.

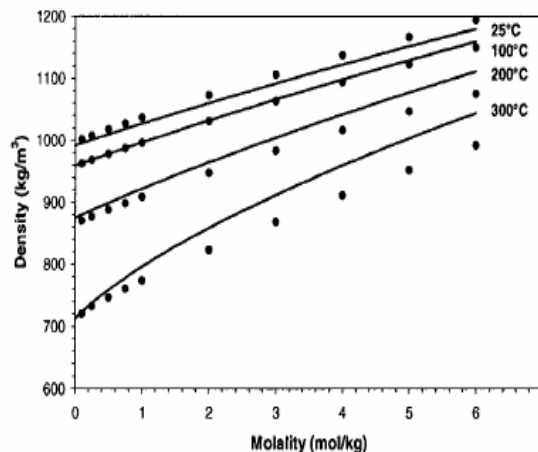


Figure 2 The published plot of density of aqueous NaCl verse molality at different temperature and pressure by Mayer, Sandler and Wood.

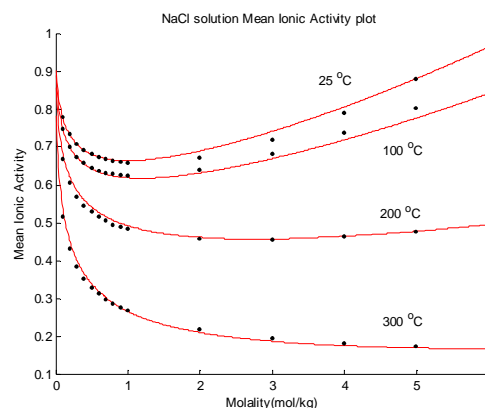


Figure 3 Plot of activity coefficient verse molality of aqueous NaCl at different temperature and pressure. The black dots are experimental data generated.

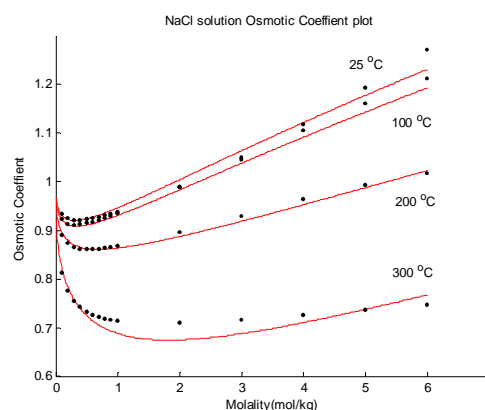


Figure 4 Plot of Osmotic coefficient verse molality of aqueous NaCl at different temperature and pressure. The black dots are experimental data generated.

The Analytical Results: Comparison of Debye-Hückel Helmholtz function with MSA

In this section, the difference between the Debye-Hückel and the simplified MSA solution will be compared analytically in the term of the Helmholtz Free energy. There only a brief overview will be give and from it we can see that the differences between them are very small.

The expression of the excess Helmholtz function from the simplified MSA turns to be the following simplified expression:

$$A^E = -\frac{2\Gamma^3 RTV}{3\pi N_A} \left\{ 1 + \frac{3}{2} \Gamma \sigma \right\}$$

Rearrange A^E and substitute Γ into the expression for A^E , we have

$$\frac{A^E}{RT} = -\frac{V}{3\pi 2^2 \sigma^3 N_A} \left(\left[\sqrt{1+2\sigma\kappa} - 1 \right]^3 + \frac{3}{4} \left[\sqrt{1+2\sigma\kappa} - 1 \right]^4 \right)$$

Knowing that, $\frac{A^E}{RT}$ can be simplified as:

$$\frac{A^E}{RT} = -\frac{V}{3\pi 2^2 \sigma^3 N_A} \left(\frac{3}{4} (1+2\sigma\kappa)^2 - 2(\sqrt{1+2\sigma\kappa})^3 + \frac{3}{2} (1+2\sigma\kappa) - \frac{1}{4} \right)$$

Expand the $(1+2\sigma\kappa)$ term, we have:

$$\frac{A^E}{RT} = -\frac{V}{4\pi \sigma^3 N_A} \left(\sigma^2 \kappa^2 + 2\sigma\kappa + \frac{2}{3} - \frac{2}{3} (1+2\sigma\kappa)^{3/2} \right)$$

Taylor expand the term $(1+2\sigma\kappa)^{3/2}$ in the expression

$$\frac{A^E}{RT}, \text{ we have:}$$

$$\frac{A^E}{RT} = -\frac{V}{4\pi \sigma^3 N_A} \left(\frac{1}{3} (\sigma\kappa)^3 - \frac{1}{4} (\sigma\kappa)^4 + \frac{1}{4} (\sigma\kappa)^5 - \frac{7}{24} (\sigma\kappa)^6 + O((\sigma\kappa)^7) \right), \quad (|\sigma\kappa| < 1/2)$$

From Debye-Hückel equation, we know the excess Helmholtz function derived from Debye-Hückel equation has the following form:

$$\frac{A^E}{RT} = -\frac{V}{4\pi N_A \sum x_i z_i^2} \sum \frac{x_i z_i^2}{a_i^3} \cdot \left(\frac{3}{2} + \ln(1+a_i\kappa) - 2(1+a_i\kappa) + \frac{(1+a_i\kappa)^2}{2} \right)$$

where a_i is the closest approach distance and x_i is the mole fraction of species i . The rest of the parameters are the same as in MSA. If we substitute the closest

approach distance a_i with the average diameters of the ions σ , we obtain the following expression:

$$\frac{A^E}{RT} = -\frac{V}{4\pi N_A \sigma^3} \left(\ln(1+\sigma\kappa) - \sigma\kappa + \frac{(\sigma\kappa)^2}{2} \right)$$

Taylor expand the term $\ln(1+\sigma\kappa)$ in the expression $\frac{A^E}{RT}$,

we have:

$$\frac{A^E}{RT} = -\frac{V}{4\pi N_A \sigma^3} \left(\frac{1}{3} (\sigma\kappa)^3 - \frac{1}{4} (\sigma\kappa)^4 + \frac{1}{5} (\sigma\kappa)^5 - \frac{1}{6} (\sigma\kappa)^6 + O((\sigma\kappa)^7) \right), \quad |\sigma\kappa| < 1$$

Comparing with the results from MSA,

$$\frac{A^E}{RT} = -\frac{V}{4\pi \sigma^3 N_A} \left(\frac{1}{3} (\sigma\kappa)^3 - \frac{1}{4} (\sigma\kappa)^4 + \frac{1}{4} (\sigma\kappa)^5 - \frac{7}{24} (\sigma\kappa)^6 + O((\sigma\kappa)^7) \right), \quad (|\sigma\kappa| < 1/2)$$

we can see that the error between the excess Helmholtz free energy is

$$\left(\frac{A^E}{RT} \right)_{MSA} - \left(\frac{A^E}{RT} \right)_{D-H}$$

$$= -\frac{V}{4\pi \sigma^3 N_A} \left(\frac{1}{20} (\sigma\kappa)^5 - \frac{1}{24} (\sigma\kappa)^6 + O((\sigma\kappa)^7) \right)$$

$$\approx -\frac{V}{4\pi \sigma^3 N_A} \left(\frac{O((\sigma\kappa)^5)}{20} \right), \quad (|\sigma\kappa| < 1/2)$$

The excess Helmholtz free energy from MSA and Debye-Hückel is very small difference if the $\sigma\kappa$ is a small quantity. From this mathematic analysis, it also partly validates the literature report that the numerical results from MSA are very close to that of Debye-Hückel.

Conclusion

The numerical results of Helmholtz Free Energy from the simplified MSA and the Debye-Hückel are very close. It is possible to develop an EoS for multiple electrolytes over wide ranges of temperature and pressure. The results published have been reproduced and computation has been conducted. The density, mean ionic activity coefficient and osmotic coefficient calculation agrees well with the reported values from Mayer, Sandler and Wood. The influence of the interaction parameter k_{ij} to the density is very small. The Volume Translation Parameter c contributes the most.

References

1. Loehe, J.R.; Donohue, M.D. "Recent advances in modeling thermodynamic properties of Aqueous Strong Electrolyte Systems", *AIChE Journal*, 43, (1997), 180-195.
2. Friedman H.L.. "Electrolyte solutions at equilibrium", *Ann. Rev. Phys. Chem.*, 32, (1981), 179-204.
3. McQuarrie D. A. "Statistical Mechanics", HARPER & ROW Publishers, 1976.
4. Kaj Thomsen; "Mixture with Electrolytes", IVC-SEP Ph. D. Summer School August 14, 2003
5. Debye P.; Hückel E. "Zur Theorie der Elektrolyte. I. Gefrierpunktserniedrigung und verwandte Erscheinungen", *Physikalische Zeitschrift*, 24, (1923), 185-206.
6. Zareen Abbas, Magnus Gunnarsson, Elisabet Ahlberg, and Sture Nordholm. "Corrected Debye-Hückel Theory of Salt Solutions: Size Asymmetry and Effective Diameters", *J. Phys. Chem. B* 2002, 106, 1403-1420.
7. Blum L.. "Mean Spherical model for asymmetric electrolytes I. Method of solution", *Molecular Physics*. Vol. 30, No.5, 1529-1535, 1975.
8. Blum, L.; Høye J.S.. "Mean Spherical Model for Asymmetric Electrolytes. 2. Thermodynamic Properties and the pair Correlation Function", *Journal of Physical Chemistry*, 81(13), 1311-1316, 1977.
9. Wei D.; Blum L.. "Internal Energy in the Mean Spherical Approximation As Compared to Debye-Hückel Theory". *Journal of Physical Chemistry*, 91: 4342-4343, 1987.
10. Jin G., Donohue M. D.. "An equation of state for electrolyte solutions. 1. Aqueous systems containing strong electrolytes", *Ind. Eng. Chem. Res.* 27,1073-1084, 1988.
11. Jin G. and Donohue M.D.. "An Equation of State for Electrolyte Solutions. 3. Aqueous Solutions Containing Multiple Salts", *Ind. Eng. Chem. Res.* 30, (1991), 240-248.
12. Wu, J. and Prausnitz, J.M.. "Phase Equilibrium for systems Containing Hydrocarbons, Water and Salt: An Extended Peng-Robinson Equation of State", *Ind. Eng. Chem. Res.* 37, (1998), 1634-1643.
13. Myers, J.A., Sandler, S. I. and Wood R. H.. "An Equation of State for Electrolyte Solutions Covering Wide Range of Temperature, Pressure and Composition", *Ind. Eng. Chem. Res.* 41, (2002), 3282-3297.
14. Dimitrios P. Tassios. Applied Chemical Engineering Thermodynamics, Springer-Verlag; Germany, 1993.
15. Planche H., Renon H.. "Mean Spherical Approximation applied to a simple but non-primitive model of interaction for electrolyte solutions and polar substances", *J. Phys. Chem.*, 5, (1981), 3924-3929.
16. Fürst W., Renon H.. "Representation of Excess Properties of Electrolyte Solutions Using a New Equation of State", *AIChE Journal*, 39, (1993), 335-343.
17. Kaj Thomsen, Ph. D. thesis, "Aqueous electrolytes: model parameters and process simulation", Technical University of Denmark, Denmark, 1997.
18. Breil M. P., Ph D. Thesis. "Thermodynamics, Experimental, and Modelling of Aqueous Electrolyte and Amino Acid Solutions", Technical University of Denmark, Denmark, 2001.
19. Zuo J. Y., Zhang D. and Fürst W.. "Predicting LLE in Mixed-Solvent Electrolyte Systems by an Electrolyte EOS", *AIChE Journal*, 46, (2000), 2318-2328.
20. Prausnitz, J. M.; Lichtenthaler, R. N.; de Azevedo, E. G.; *Molecular Thermodynamics of Fluid-Phase Equilibria (Third Edition)*, Prentice Hall International Series in the Physical and Chemical Engineering Sciences; USA, 1999.



Simone C. van Lith

Address: DTU-building 229
 Phone: +45 4525 2846
 Fax: +45 4588 2258
 e-mail: sl@kt.dtu.dk
 www: www.chec.kt.dtu.dk

Supervisors: Peter Glarborg
 Flemming J. Frandsen
 Peter Arendt Jensen

Ph.D. Study
 Started: January 2002
 To be completed: March 2005

Release of Inorganic Metal Species, Sulfur and Chlorine during Combustion of Woody Biomass on a Grate

Abstract

The objective of this Ph.D. project is to improve the understanding of the release of inorganic metal species, S and Cl during combustion of woody biomass on a grate. This understanding is essential for the development of models for aerosol and fly-ash formation and behavior, aiming to find solutions for the ash-related problems occurring during combustion of woody biomass in power plants. The release of inorganic metal species, S and Cl during combustion of specific woody biomass fuels has been quantified by lab-scale experiments under well-controlled conditions, simulating a grate-fired system. The release of the studied elements is dependent on both the temperature and the inorganic composition of the fuel.

Introduction

The use of wood as a fuel for power and heat production has become increasingly important world wide, because (1) wood constitutes a renewable resource; (2) the net emission of CO₂ is reduced when replacing coal combustion by wood combustion; and (3) wood is a waste product from forestry management and numerous types of wood industry, and is therefore

easily available and relatively cheap on most locations. However, there are also a number of problems related to wood combustion, as illustrated in Figure 1. First of all, environmentally harmful gases (e.g. SO₂ and HCl) are emitted during the combustion of wood. Another important problem is the formation of particulate matter (aerosols and fly-ashes) during wood combustion, causing deposit formation on superheater tubes, which

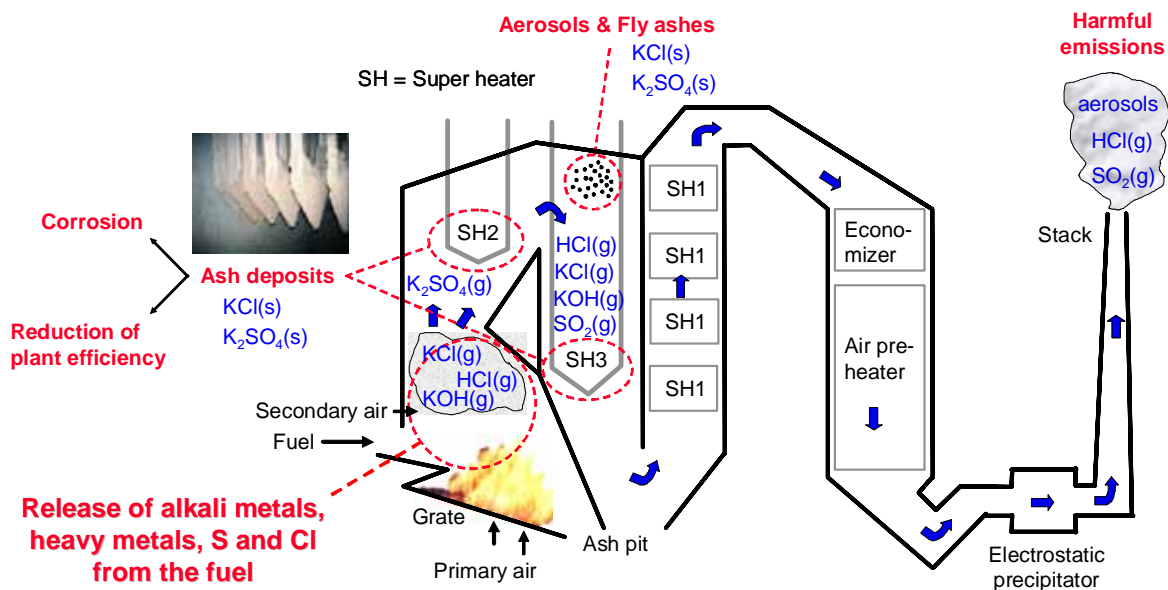


Figure 1: Schematic drawing of a wood-fired boiler, indicating the (main) inorganic species occurring during wood combustion and the problems they may cause within the system.

in turn leads to a reduction of the heat transfer efficiency to the water/steam system and corrosion of the superheater tubes. Furthermore, the smallest fraction of the particulate matter cannot be captured by the filter system, and is emitted to the atmosphere, where it may cause environmental and health problems.

The ash-related problems during wood combustion are due to the presence of inorganic elements in wood fuels. Wood naturally contains a small fraction of inorganic elements (such as Ca, K, S, and Cl), but due to handling and manufacturing inorganic elements may be added to the wood before it is used as a fuel. During combustion, a part of the inorganic elements may be released to form inorganic gases and particulate matter. To be able to tackle ash-related problems occurring during the combustion of woody biomass, it is therefore important to have an understanding of the quantity and mechanism of the release of the inorganic elements from the fuel during combustion.

Specific Objectives and Relevance

The objectives of this Ph.D. study are to quantify the release of inorganic metal species, S and Cl during combustion of woody biomass on a grate and to investigate the mechanisms by which the release takes place.

Quantitative and qualitative release data are essential for the modeling of aerosol formation and behavior, and for the subsequent development of solutions for problems involving aerosol and fly-ash formation and emissions of gaseous pollutants during the combustion of woody biomass. Figure 2 indicates the specific study area of this Ph.D. project in relation to aerosol and fly-ash formation.

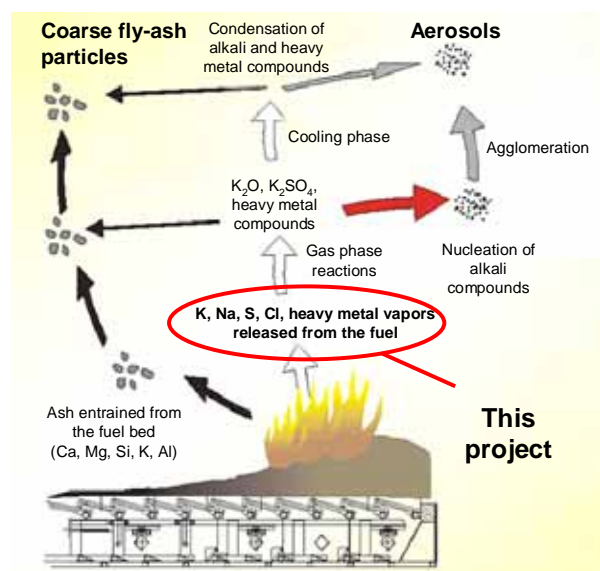


Figure 2: Study area of the Ph.D. project [1].

Literature Investigation

Most wood types contain 0.2 to 1.0 wt% ash, which is very low compared to straw (5-10 wt%) and coal (often > 10 wt%). Furthermore, woody biomass

generally has a low concentration of K, S and Cl compared to straw and coal. However, the amount of calcium and heavy metals (such as Zn, Cu and Pb) are relatively high in most woody biomass fuels. Inorganic matter in biomass can be present in four general forms: (1) easily leachable salts, (2) inorganic elements associated with the organic matter of the biomass, (3) minerals included in the fuel structure, and (4) inorganic material added to the biomass during fuel processing [2]. In the biochemical literature, it was found that the inorganic elements in biomass can be divided into three groups, according to their growth requirement: (1) macronutrients, which have a high growth requirement; (e.g. Ca, K, S, Mg, N, and P), (2) micronutrients, which have a low growth requirement (e.g. Zn, Fe, Mn, Cu, and Cl), and (3) beneficial elements, which stimulate growth, but are not essential (e.g. Na, Si and Al) [3]. The distribution of the inorganic elements in the plant cells and the way in which the elements are bound are related to the function of the elements in the plant [3].

Some information was found on the release of inorganic elements during wood combustion, but very little quantitative data is available in the literature. Misra et al. [4] studied the combustion of various types of woody biomass fuels and found that K began to release at 800-900°C, probably due to the dissociation of potassium carbonates. The release of S began at 1000-1200°C, probably due to the dissociation of sulfates. They observed a release of K of 63-90% and a release of S of 7-55% during combustion at 1300°C, depending on wood fuel type. Dayton and Milne [5] directly sampled the hot gases liberated from the devolatilization and combustion of small samples of various types of biomass fuels (including various types of wood) in a quartz-tube reactor employing a molecular beam mass spectrometer (MBMS) system, and identified the alkali metal species being released during pyrolysis and combustion. Their results indicated that small amount of K is released during the pyrolysis phase, at low temperatures (below 500°C), whereas the major part of the release takes place in the high temperature region (above 500°C) during the char combustion and ash cooking phases. They observed that in the case of woody biomass combustion, K is mainly released as potassium hydroxide (KOH), probably due to the low chlorine content of woody biomass fuels, limiting the release of K in the form of KCl(g). The formation of KOH(g) is probably due to the dissociation of potassium carbonate (K₂CO₃(s)) and the reaction with water vapor, according to Eq. 1.



Experimental Equipment and Procedure

The main part of the experimental work is focused on the quantification of the release of inorganic metal species, sulfur and chlorine during wood combustion. An experimental set-up has been built up (see Figure 3), consisting of an electrically heated oven (max. 1150°C) with an alumina tube inside, in which a fuel sample (max. 45 g) can be inserted and a gas (max. 10 NI/min)

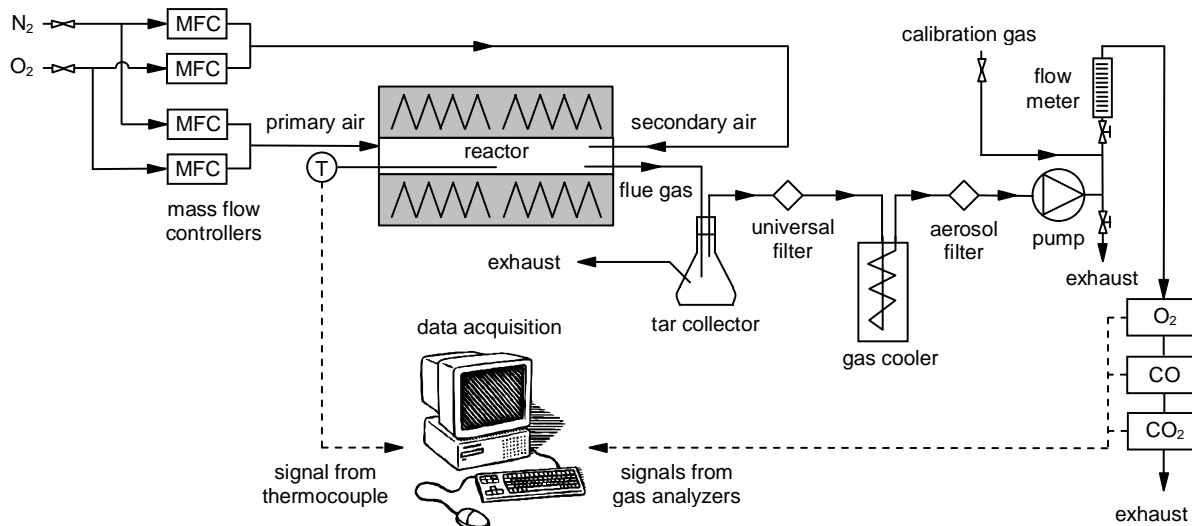


Figure 3: Schematic drawing of the experimental set-up used to study the release of inorganic elements during wood combustion.

can be introduced in order to provide a pyrolysis or combustion atmosphere around the fuel sample. A gas conditioning system and gas analyzers make it possible to measure the contents of O₂, CO and CO₂ in the flue gas in order to monitor the pyrolysis and combustion behavior and to determine if the fuel sample is completely combusted and the remaining ash residue can be assumed to contain inorganic elements only. The release of inorganic elements during combustion was quantified by mass balance calculations based on the weight measurements and chemical analysis of the wood fuels and the residual ash samples. Focus was on the alkali metals K and Na, and the heavy metals Zn and Pb, since they were known to form aerosols during wood combustion. Furthermore, the non-metals S and Cl were studied, since they were expected to influence the volatility of the metal elements. The influence of fuel type and chemical composition of the fuel was investigated by using various types of wood fuels.

Various experimental methods were tested and compared in order to find the most appropriate method for obtaining accurate quantitative release data.

Fuel and Ash Characterization

The woody biomass fuels investigated in this study are wood chips of spruce and beech, bark, and fiberboard. Each fuel type has a characteristic ash content and inorganic composition (see Table 1).

In order to obtain more information about the fuel and ash structure and the association of inorganic elements in the fuels and ashes, Scanning Electron Microscopy in combination with Energy Dispersive X-ray analysis (SEM-EDX) was used. It was observed that spruce, beech, and fiberboard have a well-ordered fuel structure, and contain few small minerals inside and outside the fuel structure, which have as major element Zn, Ti, Fe, Mn, or Si. Bark, on the other hand, has very irregular fuel structure, and contains many minerals inside and outside the fuel structure, such as clay and sand particles, and calcium-rich particles. The change in ash structure and chemical composition was studied by

analyzing ashes obtained at various temperatures by SEM-EDX. This showed that in the case of wood chips, the ash structure resembles structure of wood (even at 1150°C). This structure mainly consists of K, Ca, Mg, and P, but with increasing temperature, less K is present, and the structure becomes more compact. The ash from bark has an irregular structure, which also becomes denser with increasing combustion temperature. The ash structure mainly consists of Ca and K, and the calcium-rich particles were still observed at 1150°C.

Chemical Fractionation (CF) is a technique based on leaching with increasingly acidic solvents, and provides information about the reactivity / association of inorganic elements in the fuel. The results of CF analysis were available for some of the studied fuels and were compared to the SEM-EDX results and the experimental release data.

Table 1: Chemical composition of the woody biomass fuels used in the experimental study.

| Fuel type | Spruce | Beech | Bark | Fiberboard |
|-----------------|--------|-------|------|------------|
| Moisture (wt%) | 6.6 | 4.5 | 10.7 | 6.8 |
| Ash (wt% d.b.) | 0.95 | 0.52 | 4.41 | 1.24 |
| Cl (wt% d.b.) | <0.01 | <0.01 | 0.01 | 0.05 |
| S (mg/g d.b.) | 0.10 | 0.12 | 0.42 | 0.30 |
| K (mg/g d.b.) | 0.85 | 0.92 | 2.4 | 0.64 |
| Na (mg/g d.b.) | 0.02 | 0.01 | 0.07 | 0.18 |
| Ca (mg/g d.b.) | 1.9 | 1.0 | 16 | 1.5 |
| Mg (mg/g d.b.) | 0.20 | 0.21 | 0.76 | 0.21 |
| Si (mg/g d.b.) | 0.43 | 0.03 | 2.2 | 0.55 |
| Al (mg/g d.b.) | 0.08 | 0.01 | 0.45 | 0.35 |
| Ti (mg/g d.b.) | | | | 4.5 |
| Zn (mg/kg d.b.) | 14 | 3.7 | 67 | 27 |
| Pb (mg/kg d.b.) | 0.44 | 0.40 | 1.6 | 16 |

Experimental Results and Discussion

Quantitative release data were obtained for four different woody biomass fuels during combustion at various temperatures in the range of 500-1150°C. The results for the elements K and S are presented in Figures 4 and 5, respectively. The results show that almost all Cl is released from the fuel already at 500°C in the case of all fuels, indicating that Cl is probably mainly released from wood during the devolatilization stage. This has been observed in the case of straw combustion (e.g. [6]), and it was suggested that this is due to the reaction of KCl(s) with chain-bonded carboxylic groups yielding HCl(g) and an alkaline carboxylate that is eventually degraded, or due to the release of Cl from its original bonding sites and the transfer to a liquid tar phase, from where it is released to the gas phase as HCl(g). Since the release of K (see Figure 5) and Na increases with increasing temperature in the range 500-1150°C, the release of alkali metals during combustion does probably not take place by evaporation of chlorides. More likely is the decomposition of alkali carbonates, and the reaction with water vapor resulting in the formation of gaseous alkali hydroxides. Furthermore, the release of K and Na at high temperature may be due to the dissociation of alkali sulfates, which is in agreement with the observed increase in the release of S above 850°C (see Figure 6). A large part of S (~50-70%) is released below 500°C. The release of Zn and Pb increases sharply from around 0% at 500°C to close to 100% above 850°C in the case of all the investigated fuels. Besides the comparison with literature data and the results of the SEM-EDX study and CF analysis, thermodynamic equilibrium calculations were used to facilitate the interpretation of the release data. According to the equilibrium calculations, Zn may be released in the form of elemental Zn(g), and Pb in the form of PbO(g). Differences in the release trends between the different fuels are probably due to the presence of elements such as Si, Al and Ti, which may react with the volatile elements to form compounds that are more stable at higher temperatures.

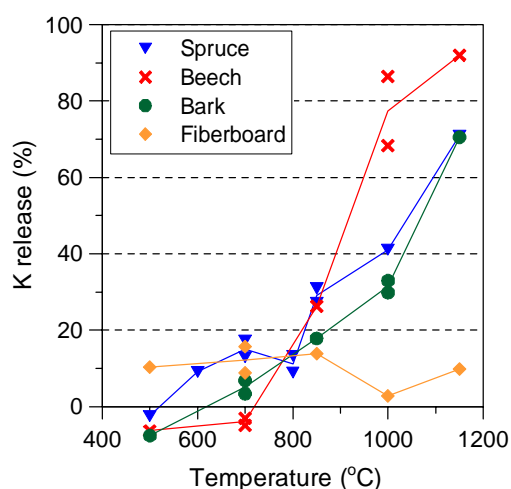


Figure 4: Release of K as function of combustion temperature.

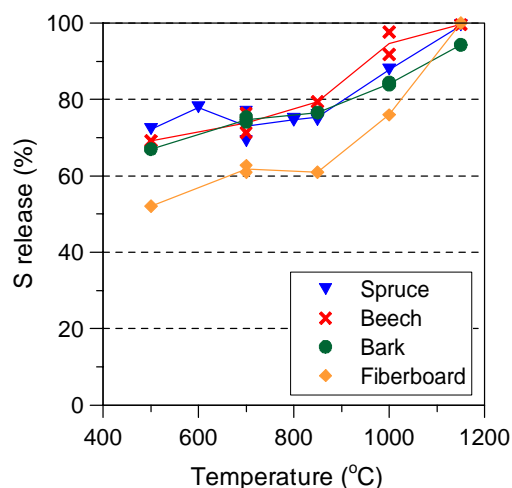


Figure 5: Release of S as function of combustion temperature.

Conclusions

The main objective of this Ph.D. study is to quantify and understand the release of inorganic metal species, S and Cl during combustion of woody biomass on a grate. Quantitative release data were obtained by lab-scale combustion experiments in the range of 500-1150°C. In general, the release of the studied elements is dependent on both the temperature and the fuel composition. The release data were interpreted by use of literature information, (scanning electron) microscopic studies of the fuels and ashes, chemical fractionation analysis, and thermodynamic equilibrium calculations.

Acknowledgements

This Ph.D. project is funded by the Danish Technical Research Council (STVF). The technicians of the CHEC Research Centre and the KT workshop are acknowledged for their help with the build-up of the experimental set-up and technical support. Violeta Alonso Ramírez and Laura Lambea García are acknowledged for their contributions to the experimental work.

References

1. I. Obernberger, T. Brunner and M. Jöller, Characterisation and Formation of Aerosols and Fly-ashes from Biomass Combustion, Report EU Project 'Aerosols from Biomass Combustion', 2001.
2. M. Zevenhoven-Onderwater, Ash-forming Matter in Biomass Fuels, Ph.D. dissertation Åbo Akademi, Finland, 2001, p. 88.
3. H. Marschner, Mineral Nutrition of Higher Plants, Second Edition, Academic Press, London, U.K., 2002, p. 889.
4. M.K. Misra, K.W. Ragland and A.J. Baker, Biomass and Bioenergy 4 (1993) 103-116.
5. D.C. Dayton and T.A. Milne, In: Applications of Advanced Technology to Ash-Related Problems in Boilers, Edited by L. Baxter and R. DeSollar, Plenum press, New York, 1996, p. 161-185.
6. P.A. Jensen, F.J. Frandsen, K.Dam-Johansen and B. Sander, Energy & Fuels 14 (2000) 1280-1285.

**Matías A. Monsalvo**

Address: DTU-Building 229-2800 Lyngby
Phone: +45 4525 2978
Fax: +45 4588 2258
e-mail: mmo@kt.dtu.dk
www: www.ivc-sep.kt.dtu.dk

Supervisor(s): Alexander Shapiro
Kaj Thomsen

Ph.D. Study

Started: November 2002
To be completed: October 2005

Phase Behaviour and Viscosity Modelling of Refrigerant-Lubricant Mixtures

Abstract

The understanding of thermophysical properties and phase behaviour of refrigerant-lubricant oil mixtures is highly important for optimal design of refrigeration and air-conditioning systems. Refrigerant-lubricant mixtures, which are likely to have strong asymmetry, may develop complex type of phase behaviour that must be considered when designing a cooling circuit. Such behaviour may include, open miscibility gaps, closed miscibility gaps, liquid-liquid-vapour equilibrium and even barotropic phenomena showing mass density inversions. This will also have a profound effect in the mixtures transport properties. For that reason, the study (measurements and modelling) of phase behaviour and thermophysical properties of such mixtures is essential. Thus, the main research objective of this project is the accurate numerical modelling of the phase, P - V - T and P - η - T behaviour of refrigerant-lubricant mixtures under wide ranges of temperature and pressure.

Introduction

The ability to model the phase behaviour and thermophysical properties of refrigerant-lubricant mixtures is of considerable industrial and academic interest. From an industrial point of view, the study (measurements and modelling) of the thermophysical properties of such mixtures is necessary for the successful transition into new environmentally alternative refrigerants. Information on solubility, density, and viscosity for this type of systems is extremely important for optimal design of refrigeration machines. Moreover, depending on the oil miscibility within the refrigerant-rich phase, even with an efficient oil separator installed, part of the lubricant oil may migrate from the compressor to other parts of the system such as the evaporator, condenser, expansion device and piping. Therefore, some related problems might also develop, for example, oil accumulation may take place inside the heat exchanger tubes reducing heat transfer capabilities and resulting in an overall decrement of the refrigeration cycle performance. These problems may become more serious in the presence of unforeseen barotropic behaviour that may induce a refrigerant-rich phase denser than the lubricant-rich phase [1]. Furthermore, good description of the thermophysical properties and phase equilibria is invaluable in choosing a proper lubricant for a particular compressor [1]. From an academic perspective, the

ability to predict phase, P - V - T and P - η - T behaviour of asymmetric mixtures (as in the case of refrigerant + lubricant systems) can serve as a rigorous test for the different models.

During the past few years new refrigerants, such as 1,1,1,2-tetrafluoroethane (HFC-134a, $\text{CF}_3\text{CH}_2\text{F}$), have been proposed as alternative refrigerants to chlorofluorocarbons (CFCs). This development has been based on a detail understanding of the refrigeration application and the chemistry of the refrigerants. However, this transition into new environmentally friendly alternative refrigerants requires the choice of suitable compatible lubricants. Polyalkylene glycol dimethyl ethers, polyol esters, and alkylbenzenes have been proposed as suitable lubricants for hydrofluorocarbons.

In spite of their importance, there are only a few studies available in the literature that present the study of thermophysical properties of refrigerant + lubricant mixtures. Thus, in this work the phase, P - V - T and P - η - T behaviour of this kind of mixtures is studied using different models available in the literature.

Objectives

The main objective of this project is the accurate numerical modelling of the phase, P - V - T and P - η - T behaviour of refrigerant + lubricant mixtures

under wide ranges of temperature and pressure. For that reason, different cubic EoS such as the Soave-Redlich-Wong (SRK) [2], the Peng Robinson (PR) [3] and the Stryjek and Vera modification of the Peng-Robison (PRSV) [4] were tested for their ability to predict the phase and *PVT* behaviour.

For the viscosity modelling of refrigerant + lubricant mixtures, based on the concepts of the friction theory (*f-theory*) [5], different viscosity models have been derived. This type of approach has been shown to deliver a high degree of accuracy with the help of simple cubic equations of state (EoS).

Results and Discussion

Phase and *P-V-T* behaviour

The type of phase behaviour that refrigerant-lubricant mixtures may develop, has been studied based on experimental information found in the literature. In addition to larger immiscibility regions, it has been shown [6] that asymmetric mixtures such as refrigerant-lubricant mixtures may develop density inversions, as observed by Hauk and Weiner [1]. For the understanding and study of the type of phase behaviour that can be found in refrigerant + lubricant mixtures, one can take advantage of simple models such as the Peng Robinson EoS. This equation is commonly used in phase equilibria correlations at low and high pressures as well as in the design and simulation of a wide variety of industrial processes. Similarly to all of the van der Waals family EoS, the PR EoS is divided into a repulsive pressure term (p_r) and an attractive pressure term (p_a),

$$p = p_r + p_a \quad (1)$$

where

$$p_r = \frac{R T}{(v-b)} \quad (2)$$

and

$$p_a = \frac{a}{v(v+b) + b(v-b)} \quad (3)$$

For mixtures the PR EoS was employed in combination with the one-parameter van der Waals quadratic mixing rule for a and linear for b , given by:

$$a = \sum_i \sum_j x_i x_j \sqrt{a_i a_j} (1 - k_{ij}) \quad (4)$$

and

$$b = \sum_i x_i b_i \quad (5)$$

where, k_{ij} is a binary interaction parameter.

An example of the phase diagram prediction for the HFC-134a + triethylene glycol (TRIG) mixture

is shown in Figure 1 where it can be observed multiple phase equilibria and the presence of a high-pressure liquid-liquid immiscibility region. In Fig. 3 a relevant feature is shown: barotropic phenomena showing density inversion. Both facts, immiscibility regions and barotropic phenomena, are associated with asymmetric mixtures [6].

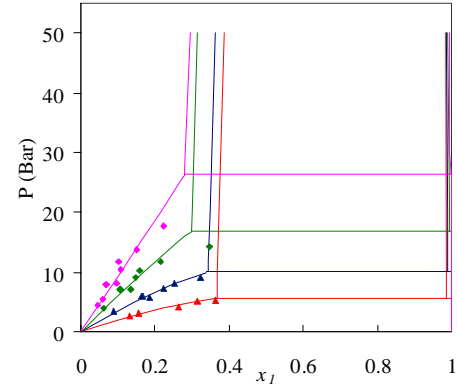


Figure 1. Example of solubility data correlation and VLLE prediction for HFC-134a (1) + TRIG, experimental data [7] at 293.15 K (\blacktriangle), 313.15 K (\blacktriangle), 333.15 K (\blacklozenge), 353.15 K (\blacklozenge). Solid lines denote the calculated data by the PR EoS. Horizontal lines represent the predicted VLLE region.

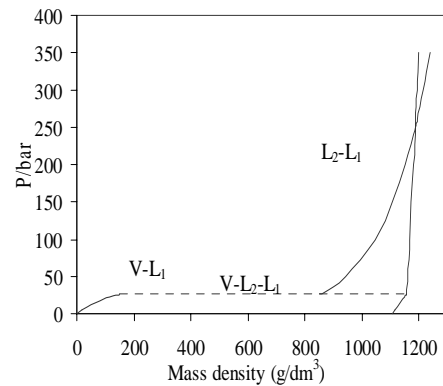


Figure 2. Pressure-density PR phase diagram of HFC-134a + TRIG at 353.15 K.

It is well known that simple cubic EoS can correlate PTx data with sufficient accuracy. However, it is also of relevance to mention that cubic EoS are known for not being too accurate in the prediction of the density of dense phases showing, in optimal circumstances, 2-5% overall absolute average deviations. For some applications a 5% density deviation may be considered quite tolerable. However, in other better-defined process this uncertainty may not be acceptable and alternative more accurate approaches are required. In cases when the process operates at subcritical conditions, within moderate pressure ranges, a widely used method for the improvement of the density accuracy given by cubic EoS is the Péneloux volume translation [8]. This approach consists of a simple translation of the frame of reference so that the

volume (or density) representation may better be overlapped to the experimental data. Alternatively, other type of highly accurate reference EoS can be used, such as the Soave modification of the BWR EoS [9].

The densities values predicted by the PR EoS for a mixture of HFC-134a + triethylene glycol dimethyl ether (TriEGDME) at $x_1 = 0.69$ are presented in Figure 3 where it can be seen that the performance of the PR EoS is not satisfactory.

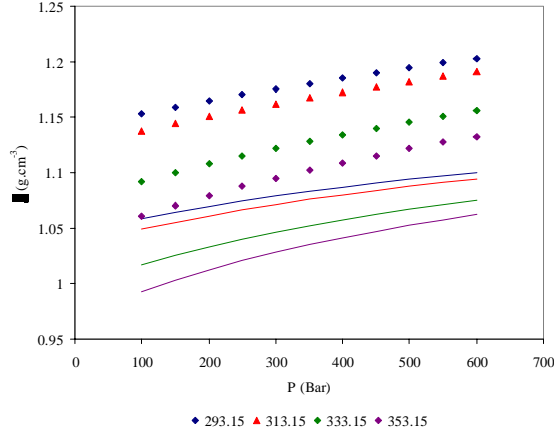


Figure 3. Density for HFC-134a (1) + TriEGDME using the PR EoS compared with experimental values [10] at 293.15 K (▲), 313.15 K (▲), 333.15 K (◆), 353.15 K (◆).

Viscosity behaviour

The friction theory (*f-theory*) [5] has been applied to model the viscosity of refrigerant + lubricant systems. The *f-theory* in combination with simple cubic EoS has shown to deliver accurate viscosity estimation from low to high pressures, regardless of how accurate the density performance may be. This model has been successfully applied to the accurate modelling of several types of fluids including complex systems such as reservoir fluids among others. In the *f-theory* the total viscosity, η , is separated into a dilute gas viscosity term η_0 and a residual friction term η_f ,

$$\eta = \eta_0 + \eta_f \quad (6)$$

The dilute gas term applies at the zero pressure limit of the gas phase, and for many fluids it can be estimated with simple empirical models such as the one proposed by Chung [11]:

$$\eta_0 = 40.785 \frac{\sqrt{M_w T}}{v_c^{2/3} \Omega^*} F_c \quad (7)$$

the residual friction term can be written as follow:

$$\eta_f = \kappa_r p_r + \kappa_a p_a + \kappa_{rr} p_r^2 \quad (8)$$

where the kappas are temperature dependent friction coefficients and p_r and p_a are given by the EoS.

The mixture viscosity has been estimated using the predictive mixing rules proposed in Ref. [5]. That is,

the mixture friction coefficients κ_r , κ_a , and κ_{rr} are obtained by the following mixing rules:

$$\kappa_r = \sum_{i=1}^n z_i \kappa_{r,i} \quad (9)$$

$$\kappa_a = \sum_{i=1}^n z_i \kappa_{a,i}$$

$$\kappa_{rr} = \sum_{i=1}^n z_i \kappa_{rr,i}$$

Here, a mass weighted fraction of the form

$$z_i = \frac{x_i}{MW_i^{0.3} MM} \quad (10)$$

with

$$MM = \sum_{i=1}^n \frac{x_i}{MW_i^{0.3}} \quad (11)$$

is used in order to enhance the accuracy of the results; MW_i is the molecular weight of compound “i”.

Figure 4 shows the *f-theory* PR model results for the mixture HFC-134a + tetraethylene glycol dimethyl ether (TEGDME) for a molar fraction of $x_1 = 0.63$. It can be observed that the *f-theory* shows a good, consistent and stable performance from low to high pressures.

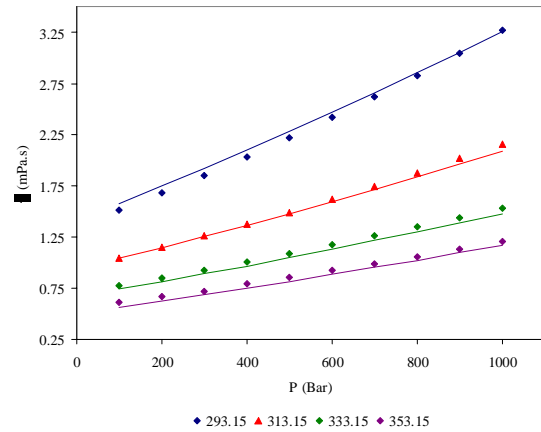


Figure 4. Viscosity for HFC-134a (1) + TEGDME using the *f-theory* PR model compared with experimental values [11] at 293.15 K (▲), 313.15 K (▲), 333.15 K (◆), 353.15 K (◆).

Conclusions and Future Work

In spite of their simplicity, it appears that simple cubic EoS such as the PR EoS with classical mixing rules may be appropriate for a description of the phase behaviour of complex systems such as refrigerant + lubricant systems. Classical cubic EoS represent a powerful tool for the actual design of refrigeration cycles. This modelling approach can be used to prevent technical problems such as barotropic effects, decrease solubility-related compressor oil viscosity, among others. However, it should be pointed out that the

accuracy of the density predictions is still limited by the algebraic structure of the cubic EoS. For that reason, the study of non cubic EoS capable of delivering a good P - V - T performance, such as the Soave modification of the BWR EoS [9], remains to be addressed.

For the viscosity modelling the friction theory has been applied in combination with simple cubic EoS. The viscosity of refrigerant + lubricant mixtures has been predicted with a good degree of accuracy. However, it is of theoretical as well as of industrial interest to explore the extension of the f -theory approach to other kinds of models besides the cubic EoS.

Acknowledgments

The present study is supported by the Danish Research Council (project No. 26-01-0217).

References

1. Hauk and E. Weidner, Thermodynamic and Fluid-Dynamic Properties of Carbon Dioxide with Different Lubricants in Cooling Circuits for Automobile Application, *Industrial and Engineering Chemistry Research*, 39, (2000) 4646.
2. G.S. Soave, Equilibrium Constants from a Modified Redlich-Kwong Equation of State, *Chem. Eng. Sci.*, 27, (1972) 1197-1203.
3. D.-Y. Peng and D.B. Robinson, A New Two-Constant Equation of State, *Ind. Eng. Chem. Fundam.*, 15, (1976) 59-64.
4. R Stryjek, J.H. Vera, *Can. J. Chem. Eng.* 64 (1984) 215-333.
5. S.E. Quiñones-Cisneros, C.K. Zéberg-Mikkelsen and E.H. Stenby, The Friction Theory (f -theory) for Viscosity Modelling, *Fluid Phase Equilib.* 169, (2000) 249-276.
6. S.E. Quiñones-Cisneros, Phase and critical behaviour in type III phase diagrams, *Fluid Phase Equilib.*, 134, (1997) 103.
7. S. I. Tseregounis, M. J. Riley, *AIChE J.* 40 (1994) 726-737.
8. Pénéloux A, Rauzy E, and Fréze R. A Consistent Correction for Redlich-Kwong-Soave Volumes. *Fluid Phase Equilib.* 1982; 8: 7-23.
9. Soave GS. An effective modification of the Benedict-Webb-Rubin equation of state. *Fluid Phase Equilib.* 1999; 164: 157-172.
10. M. J. P. Comuñas, J. Fernández, A. Baylaucq, X. Canet, C. Boned, *Fluid Phase Equilib.* 199 (2002) 185-195.
11. T.-H. Chung, M. Ajlan, L.L. Lee and K.E. Starling. *Ind. Eng. Chem. Res.* 27(1998), 671.
12. M.A. Monsalvo, A. Baylaucq, P. Reghem, S.E. Quiñones-Cisneros, C. Boned, Viscosity measurements and correlations of binary mixtures: HFC-134a + TEGDME, *submitted*.

List of Publications

1. J. García, M. A. Monsalvo, S. E. Quiñones-Cisneros and J. Fernandez, Modelling Phase Equilibria and Viscosity for Refrigerant-Lubricant

Oil Systems, *21st IIR International Congress of Refrigeration*, Washington D. C., 2003.

2. S. E. Quiñones-Cisneros, M. A. Monsalvo, J. García and J. Fernandez, Phase Behaviour of Refrigerant-Lubricant Mixtures, *20th European Symposium on Applied Thermodynamics*, Germany, 2003.
3. S. E. Quiñones-Cisneros, J. Fernandez, J. García and M. A. Monsalvo Phase and Viscosity Behaviour of Refrigerant-Lubricant Mixtures. *Int. J. Ref.; in press*.
4. M.A. Monsalvo, A. Baylaucq, P. Reghem, S.E. Quiñones-Cisneros, C. Boned, Viscosity measurements and correlations of binary mixtures: HFC-134a + TEGDME, *submitted*.



Jens Kromann Nielsen

Address: KT, DPC, Building 423, Room 220
Phone: +45 4525 6809
Fax: +45 4588 2161
e-mail: jkn@kt.dtu.dk
www: www.student.dtu.dk/~s973715/dpc/

Supervisor(s): Ole Hassager
Kristoffer Almdal, Risø
Kell Mortensen, Risø

Ph.D. Study
Started: February 2004
To be completed: January 2007

Rheology, Structural Studies and Synthesis

Abstract

The elongational flow dynamics of polymer melts reveals much about the structural information of the individual behavior chains in the melt. Current well established constitutive models for polymer flows are in good agreement with shear flow experiments, but recent experiments on linear and branched polymers [1-2], performed at DTU, cannot be explained by any of the available models. An essential part of the project is to measure the elongational rheology of polymers with well-known molecular structure and set up corrections to current models to get better agreement between theory and experiments.

Introduction

The project builds on the work done by PhD Anders Bach who constructed a rheometer, which is able to measure the elongational properties of both polymer- melts and -solutions. With the rheometer Bach was the first to experimentally determine the steady elongational viscosity for monodisperse polystyrene melts at high Deborah numbers, i.e. in the flow region where elastic forces dominate over viscous forces [1]. These kinds of measurements have great importance in verifying polymer physical flow models, and other kinds of constitutive fluid mechanical models for polymers.

Project summary

The purpose of this project is to investigate elongational properties of different polystyrene melts and to produce data that could verify models for monodisperse melts, which within the last decades have build on the tube model, introduced by DeGennes [3], Doi and Edwards [4]. The elongational properties of polydisperse melts will also be measured, which will be compared to the commonly used empirical constitutive models.

Elongational measurements on commercial low-density polyethylene, LDPE using the newly build rheometer have shown that the viscosity as function of time, goes through a maximum and stabilizes at a constant value for fast flows [2]. The latter is expected, but the former is an entirely different behavior as compared to linear polystyrenes, where the viscosity is a

monotone function of time. We believe that this property for LDPE can be explained by the branched nature of the polymer. The specific structure of commercial LDPE is not known and the polymer is not suited for model working, because of its polydispersity and structural uncertainty. It's therefore decided to synthesize polystyrene with well-characterized branching using anionic polymerization [5]. If the extensional measurements for these polymers also display a maximum in the viscosity in the time dependent start-up flow, it will be proved that it is due to the branching.

Another part of the project is to study what happens to the steady elongational viscosity as function of elongational rate for linear polymer melts. Recently published theory [6] claims, that polymer melts have different steady elongational behavior if the number of entanglements in the chains, Z , is above or below 15. Polystyrene has an entanglement molecular weight of 13,300 g/mole, and since it is almost impossible to do rheological measurements if $M_w > 400,000$ g/mole for polystyrene, the elongational behavior for $Z > 30$ has to be measured for polymers with lower entanglement molecular weights. One candidate for this could be polyethylene, which has an entanglement molecular weight that is below 1,000 g/mole. Linear polyethylene can be made by anionically polymerizing butadiene and subsequent hydrogenation. This method makes it possible to rheologically examine polymers with $Z > 100$.

References

1. Bach, A.; Almdal, K.; Rasmussen, H. K.; Hassager, O. *Macromolecules* (2003), *36*, 5174.
2. Rasmussen, H. R.; Nielsen, J. K., et. al. Viscosity overshoot in the start-up of uni-axial elongation of LDPE melts. *J. Rheology*, March/April (2005) (in press)
3. de Gennes, P. G. *Scaling Concepts in Polymer Physics*; Cornell University Press: Ithaca, NY, (1979).
4. Doi, M.; Edwards, S. F. *The Theory of Polymer Dynamics*; Clarendon Press: Oxford, (1986).
5. Knauss and Huang. *Macromolecules* (2002), *35*, 2055-2062
6. Marrucci and Ianniruberto, *Macromolecules* (2004), *37*, 3934-3942



Anne Kathrine Kattenhøj Overgaard
Address: DPC, Dept. of Chemical Engineering
Building 423, Office 206
Technical University of Denmark
Phone: +45 4525 6817
Fax: +45 4588 2161
e-mail: ako@polymers.dk
www: www.polymers.dk
Supervisor(s): Søren Hvilsted
Jakob Vange, Coloplast Research
Hanne Everland, Coloplast Research
Ph.D. Study
Started: September 2004
To be completed: August 2007

Coupling of Active Components to Synthetic Polymers

Abstract

Materials for medical devices should provide more than just structure. Some synthetic polymers are ideal materials for healing of chronic wounds because of their high biocompatibility and the possibility of tailoring their properties. Active components can be coupled to the synthetic polymers to obtain wound healing materials that support cell ingrowth. This coupling could take place via the very mild and highly efficient “click” coupling of azides and alkynes.

Introduction

Future materials for medical devices should be more than just materials that provide structure. The materials should be intelligent and take an active part in the process, e.g. by absorbing smell or by initiating cell growth.

In the case of a chronic wound the normal biological wound healing process has been impaired and the application of a scaffold as a kind of artificial skin is necessary to help the healing process.

When a polymer is to be used for therapeutic purposes several issues have to be considered. The ideal material for wound healing should be biocompatible, biodegradable and easy to process [1,2,3]. The material must mimic the extra cellular matrix (ECM), it has to uphold structure, and it should promote cell adhesion and growth and degrade as new tissue forms.

The most important requirement for a wound healing material is the biocompatibility. The material should possess the right surface chemistry to promote cell attachment and at the same time not provoke any unwanted tissue response [4]. Therefore it will in some cases be necessary to introduce an active component into the scaffold material to ensure tissue regeneration [5].

Several different materials may be used in a scaffold for wound healing and among these natural as well as synthetic polymers could be considered. The advantage of utilizing natural polymers is their excellent biocompatibility and their favorable interaction with

cells [6]. The disadvantage of employing natural polymers may, however, be the differing batch compositions and their poor mechanical stability [7]. In comparison, the synthetic polymers have a much higher mechanical strength, a more uniform composition and they can in principle be tailored to give a wider range of properties. It is possible in the synthesis of synthetic polymers to incorporate reactive sites or functionalities. These can later be coupled with active components, that can support cell ingrowth.

The coupling reaction of the active component to the synthetic polymer could be achieved through the well known 1,3-dipolar cycloaddition of an azide with an alkyne group to form a 1,3-triazole. This reaction has been known since the early 1960's where Huisgen and coworkers carried out a monumental work in this area.

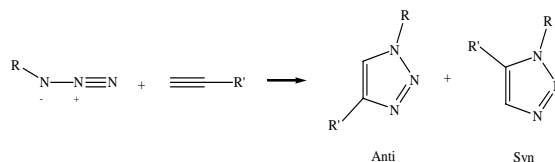


Figure 1 The general Huisgen reaction – 1,3-dipolar cycloaddition

The reaction to form a triazole by the conventional Huisgen 1,3-dipolar cycloaddition at elevated temperature gives rise to two different products: an anti- and a syn-triazole. The formation of two products can

be prevented by running the same reaction in the presence of a Cu(I) catalyst at room temperature. This reaction can take place in water; it gives rise to only one product: the anti product, and the reaction takes place with approximately 100 % conversion. Because of the very mild conditions, the high yield and the stereospecificity this reaction has been termed a “click” reaction by K.B. Sharpless *et al.* [8]. The advantage of this reaction is the formation of a stable bond under mild reaction conditions.

Specific Objectives

The Ph.D. project will primarily be experimental with focus on obtaining the most ideal synthetic polymer for a wound healing material. Several polymers with differing chain lengths and compositions will be synthesized, functionalized and characterized. Functionalization and coupling of active components to the synthetic polymers will be attempted through “click” chemistry and the obtained materials will be investigated as to cell growth and degradation.

Conclusion

The coupling of active components to synthetic polymers to improve cell adhesion and growth will prove an effective method to obtain good wound healing materials, and the utilization of click chemistry in the coupling reaction will ensure mild reaction conditions, stereospecific products and high yields.

Acknowledgements

The Ph.D. project is financed by Coloplast A/S, the Technical University of Denmark and The Graduate School of Polymer Science.

References

1. B.E. Chaignaud, R. Langer, J.P. Vacanti, in: A. Atala, D. Mooney, R. Langer, J.P. Vacanti, (Eds.), *Synthetic Biodegradable Polymer Scaffolds*, Birkhäuser, Boston, 1997, Chapter 1.
2. L.G. Cima, J.P. Vacanti, C. Vacanti, D. Ingber, D. Mooney, R. Langer, *J. Biomech. Eng.* 113 (1991), 143-151
3. C.M. Agrawal, R.B. Ray, *J. Biomed. Mater. Res.* 55 (2001) 141-150
4. S. Yang, K.-F. Leong, Z. Du, C.-K. Chua, *Tissue Engineering* 7 (2001) 679-689
5. J.S. Tjia, B.J. Aneskievich, P.V. Moghe, *Biomaterials* 20 (1999) 2223-2233
6. M.C. Peters, D.J. Mooney, *Materials Science Forum* 250 (1997) 43-52
7. V. Maquet, R. Jerome, *Materials Science Forum* 250 (1997) 15-42
8. H.C. Kolb, M.G. Finn, K.B. Sharpless, *Angew. Chem. Int. Ed.* 40 (2001) 2004-2021

**Irene Papaeconomou**

Address: CAPEC, Dept. of Chemical Engineering
Building 227 Office 226
Technical University of Denmark

Phone: +45 4525 2909
Fax: +45 4593 2906
e-mail: ipa@kt.dtu.dk
www: www.capec.kt.dtu.dk

Supervisor(s): Sten Bay Jørgensen
Rafiqul Gani

Ph.D. Study
Started: June 2000
To be completed: December 2004

Integration of Synthesis, Design and Control of Batch Processes for Product Design

Abstract

This thesis describes a general methodology for the synthesis and design of batch processes. However, for the synthesis to be complete the operational modelling of the individual batch operations, such as reaction and separation, needs to be performed. The general methodology consists of two levels, where in the upper level a synthesis algorithm provides the sequence of reaction and separation tasks needed and in the lower level a set of algorithms supply the batch operational model for each task, in a form of a sequence of sub-tasks performed in order to achieve a specific objective for the reaction or separation tasks. The combined algorithms provide the batch route.

Introduction

The observed increase in the production of high-value-added, low-volume specialty chemicals, fine chemicals, pharmaceuticals and biochemicals has created a growing interest in batch processing technologies. The lasting problem of the synthesis of batch processes can be outlined as follows: Given the identity of the raw materials and the product specifications, identify and sequence the necessary tasks, such as reaction, separation or a combination thereof, that need to be performed in order to produce and separate the desired products. This sequence of operations is called the batch route. In addition to the identity and sequence of the tasks, the conditions of operation for each task need to be determined (operational design) for the generated batch route to be complete.

The majority of batch operations are frequently scaled up from the laboratory to the full size plant without much process optimization to reduce the time to market. Consequently, the batch route employed is the one used in the laboratory to produce the specified product. Moreover, in existing methodologies for planning and scheduling, the batch routes are neither determined nor optimized, but assumed given data.

The objective of this Ph.D. project is to propose a methodology for providing feasible (and near optimal) operations for the synthesis and design of batch processes. Thermodynamic and process insights can be used for that purpose. A two-level methodology has

been developed for the complete synthesis of batch processes. The upper level of the methodology is comprised of the synthesis algorithm where the actual batch route is generated. The sequence of reaction and separation tasks is generated from that algorithm and together with that the intermediate objectives for each task in the sequence are calculated. These objectives are the recovery and purity of the specified product of each task. The lower level comprises of three algorithms which tackle the operational design problem for batch reaction and separation, and batch distillation and crystallization in particular. The exact operation of each reaction and separation task is modelled, in terms of generation of a sequence of sub-tasks giving the heating, temperature or reflux ratio profile. In this thesis, the sub-tasks are defined as operations where the manipulated variables remain constant during the period of the sub-task, let that variable be temperature, heating/cooling rate, reflux ratio, etc.. All the developed algorithms are governed by sets of rules based on process and thermodynamic insights. The two levels of the methodology are illustrated in fig. 1.

In the synthesis algorithm the composition of the outflow of a batch reactor is analyzed and the most feasible subsequent separation technique is identified. Mixture analysis (identification of separation boundaries) is used to determine whether a separation task is needed prior to a reaction task. In the case of more than one set of reactions needed to obtain the final product, the necessity of intermediate separation tasks

and the corresponding separation techniques are determined. The decision related to the extent one task should be allowed to progress in terms of specified product recovery is considered in this stage, taking into account the significance the previous task has on the succeeding ones.

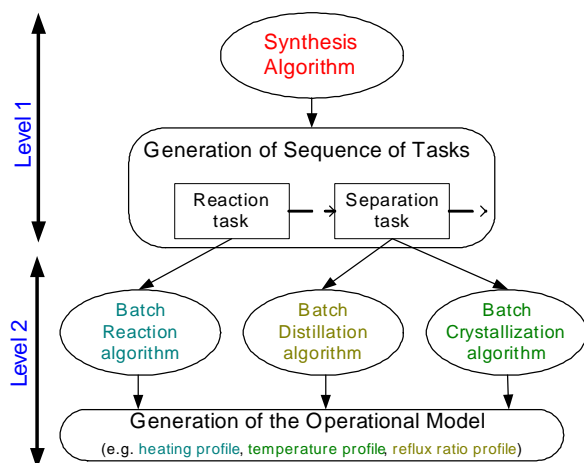


Fig. 1: The two-level methodology for the synthesis and design of batch processes together with the various developed algorithms

The lower level algorithms share the following characteristic, the existence of a number of process and terminal constraints that need to be satisfied and the usage of manipulated variables to ensure feasible operation. The algorithms identify the imminent violation of a constraint, thereby detecting the end of a particular sub-task, and identify the next sub-task that will be able to maintain the operation feasible, until the specified end objectives for the overall task are met. The flexibility of batch processes and the ability of obtaining more than one pure product from a batch separation unit are considered in the developed batch separation algorithms. The suggested batch operations model can serve as a feasible and very good (near optimum) starting point to dynamic optimization of the batch process.

Batch Reaction Algorithm

The developed algorithm deals with the design of the operation of batch reactors, where the reactions take place in the liquid phase and a vapour phase may or may not exist. The considered problem extends to the case where multiple reactions are taking place and operational constraints on temperature (and pressure) are present. The key factor is the existence of desired reactions and of competing reactions, where the latter need to be suppressed. In addition to the operational constraints, there are also end constraints/objectives, namely the molefraction of the limiting reactant in the reaction of interest that should be as low as possible and the progress of the reaction of interest that should be as high as possible. At least one of the end constraints has to be satisfied.

In this algorithm, apart from the operational constraints, a supplementary constraint on selectivity is

used. Selectivity is defined as: “*Selectivity S_{ij} of reaction i over competing reaction j is the ratio of the reaction rate of reaction i to the reaction rate of reaction j* ”. The above description of selectivity covers also the cases when the competing reaction is one that its limiting reactant is other than the limiting reactant for the desired reaction. For example, the competing reaction could be a reaction where the desired product further reacts to form a byproduct. Such a reaction is unwanted and should be suppressed, since it jeopardizes the yield of the desired product.

One of the goals of the algorithm is to keep the selectivity as high as possible or at least above a constraint at all times, until the product objectives are reached. In this way, the reactions are driven in a way that favor the reaction(s) of interest and suppress the competing and unwanted reactions. Keeping the selectivity high ensures that no unnecessary byproducts are formed or that their production is limited. In that way the molefraction of the desired product in the outflow of the reactor is as high as possible. Furthermore, by making sure that the percentage of the reactant that is converted to desired product instead of undesired byproduct is the highest, the yield of the desired products is maximized.

The algorithm identifies the first operation (sub-task) based on the highest selectivity. For the generation of the sequence of the necessary sub-tasks, rules are employed at all points to identify the end of each sub-task because of an imminent constraint violation and also to determine the next feasible sub-task, such as isothermal operation, adiabatic operation, heating, cooling, vapour release, etc. The next sub-task is chosen to reverse the respective imminent constraint violation. The procedure is repeated until at least one of the product (end) objectives is met.

Batch Distillation Algorithm

The operational design of batch distillation columns is supported by another developed algorithm, where the considered problem is the separation of multi-component mixtures where binary azeotropes might be present. The algorithm is applied, in order to obtain an operational route that will either directly obtain the desired products or remove the azeotrope, so that the desired high purity product can later be obtained from the bottom of the vessel. The objective is to achieve the above in minimum time and/or cost.

The algorithm identifies a priori the necessary sequence of sub-tasks, namely providing the reflux ratio and vapour boilup rate profile, in order to achieve desired specified end objectives for the products. These objectives are the product purity and the amount of product (yield) and they both have to be fulfilled. The algorithm employs a repetitive procedure to determine the operating conditions along with a very good approximation of the operating time, for each sub-task. The only given data needed is the amount and composition of the initial charge and the desired product (distillate) specifications. The algorithm uses a set of

simple equations for the distillation column, as described in [1], and adapts well-known methods, such as the driving force approach and the McCabe-Thiele diagram to find quickly a near optimum recipe for the separation task.

The strong feature of this algorithm is the use of the driving force approach to find the minimum reflux ratio and the reflux ratio used for the specific feed. The existence of a driving force is what makes the distillation feasible, and that is why it is not possible to cross a distillation boundary, such as an azeotrope where there is no driving force. As it has been discussed in [2], operating at the largest driving force leads to the near minimum energy expenses. The advantage of using the driving force approach is that it gives you the physical insights to operate in an easy and near optimum energy costs way. Moreover, a large driving force, which corresponds to a low reflux ratio, means a faster separation.

For a specific feed composition, as one can see in fig. 2, the largest driving force corresponds to the minimum reflux ratio, which however can only be supported by an infinite number of plates. Thus, for a specific number of plates a larger reflux ratio has to be used. The objective, however, is to use a reflux ratio that is as close to the minimum as possible. In fig. 2 as the composition of the more volatile component in the still moves to the left (decreases), the reflux ratio used (R_1) approaches the minimum value for the corresponding composition ($R_{\min, 2}$). At that point before the violation takes place, the current sub-task is ended and a new reflux ratio has to be used (R_2). The limiting composition at the end of the sub-task is found using the simple graphical method of McCabe-Thiele. The distillate amount and the amount remaining in the vessel are calculated from simple mass balance equations. The operating time of the sub-task is found from the overall material balance around the top of the column.

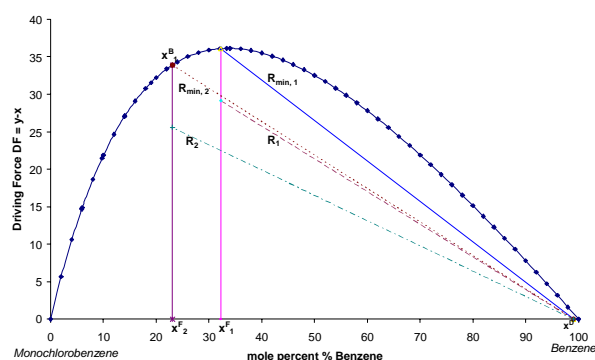


Fig. 2: The driving force approach extended to batch distillation

This is the procedure followed after the first step of the algorithm, where the separation task is identified. This is found as the split between the most volatile and the second most volatile component of the considered mixture and afterwards the driving force diagram is calculated for the given binary pair. The necessity of removing an intermediate cut is also investigated until

all the specified products are obtained. Furthermore, the existence of azeotropes and the impact in the sequence of attainable products is taken into consideration in the first step of the algorithm. The actual operational design for each separation task based on the respective driving force diagram is performed in the next steps of the algorithm.

Batch Crystallization Algorithm

The third algorithm of the lower level algorithms covers the case of the synthesis and operational design of batch crystallization, where the sequence of operational sub-tasks is generated. The considered sub-tasks are evaporation, leaching, dilution, heating or cooling (shift to a higher or lower temperature). Furthermore, the design of each sub-task is also described in the algorithm in terms of the operating conditions, such as temperature or amounts of solvent that need to be removed or added. The objective of the algorithm is to identify in advance the necessary sub-tasks and their sequence, in order to achieve specified objectives for the separation task, namely the recovery of solutes (yield).

The algorithm uses simple principles and methods, such as the conservation of mass and the lever rule [3], and it is solely based on the solid-liquid equilibrium phase diagram. It also uses a set of rules for the identification of the sequence of products whose precipitation is feasible. These rules are based on insights from the understanding of the phase diagrams.

The algorithm consists mainly of a repetitive procedure that identifies the nature of each sub-task and the operating conditions. The initial step is the actual generation of the phase diagram. The phase diagram is derived by drawing the solubility curves for a given temperature range for the operation of the crystallizers. In the repetitive procedure, the feed location is pinpointed to the diagram and the feasibility of the precipitation of the desired solid solution is checked. This is done by relating the feed point with the invariant point connected to the desired solute at each temperature. For the specific feed, the solute to precipitate is identified and the operational task is specified, in terms of choosing the operating temperature, removing or adding solvent, or mixing streams.

The exact amount of solvent to evaporate or add can be found from the lever principle, since the material balances can be represented on the phase diagrams in the form of tie lines. It is significant to avoid regions on the diagram, where two solids precipitate, since this is not effective separation. For that reason evaporation is always less than the maximum and dilution is more than the minimum. Knowing the exact location of the slurry, the product yield can be computed, with the lever principle. The composition of the mother liquor in equilibrium with the precipitated solute can be located on the phase diagram and treated as a new feed. With that in mind, the generated sequence of sub-tasks can be illustrated on the phase diagram, as shown in fig. 3.

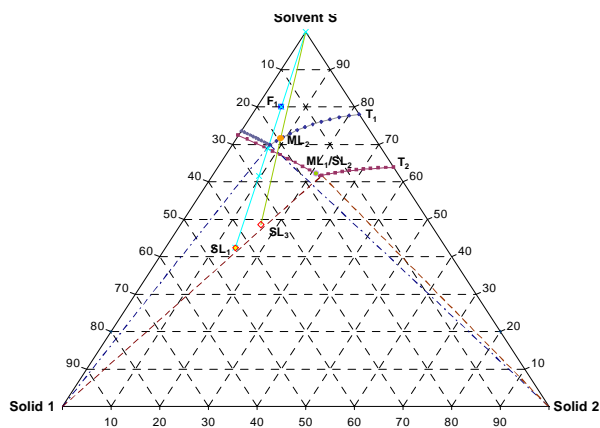


Fig. 3: The sequence of sub-tasks, needed to achieve the desired precipitation of a solute, shown in the solid-liquid equilibrium diagram

The above-described procedure is repeated until the desired or maximum yield for the feed and given temperature range is achieved. The algorithm takes into consideration the fact that the separation of a desired salt from a solution with a specified recovery might not be possible with a single precipitation of the salt at a specific temperature. However, the desired recovery might be able to be achieved with an alternate solids precipitation (between the desired salt and a second salt in the system) at two temperatures T_1 and T_2 (T_{low} and T_{high}). In that case, the number of precipitations for the respective solid necessary to achieve a certain recovery can be found in advance. An important step of the algorithm is the determination of the feasibility of the precipitation of a solute for a given feed based on the comparison on the phase diagram of the coordinates of the feed with the coordinates of the solids and the invariant points. For that purpose, several equations have been produced for the case of ternary systems, while the solubility index is used for the quaternary systems.

Synthesis Algorithm

The methodology presented in [4] for continuous processes has been extended to batch processes and is used as a part of the generation of the batch route, necessary to obtain the final products from a set of raw materials. The identification of the separation technique for each of the separation tasks needed in the batch route is based on the relationship between compound properties and separation techniques, while the order of the separation and reaction tasks is decided according to developed rules, based on thermodynamic and process insights and reaction kinetics analysis. The flexibility of batch processes and the ability of obtaining more than one pure product from a batch separation unit are also considered.

In the Jakslund algorithm [4], the separation technique used for a separation task is the one that is the most feasible and easiest. The feasibility of a separation technique k , for a binary pair i , which is related to property j is decided by comparing the binary property ratio for the pair r_{ij} with certain recommended values for

separation feasibility indices, namely lower limit m_{kj} and upper limit M_{kj} , which are different for each separation task k . For that purpose the “possibility distribution” $\mu(r_{ij})$ is used to determine the extent to which a separation is feasible for a binary separation task, for the case of just feasible separations ($m_{kj} < r_{ij} < M_{kj}$). The “possibility distribution” $\mu(r_{ij})$ is given:

$$\mu(r_{ij}) = (r_{ij} - m_{kj}) / (M_{kj} - m_{kj}) \quad (1)$$

Obviously, from eqn. 1, $\mu(r_{ij})$ is between 0 and unity for just feasible separations. If $\mu(r_{ij})$ was used to compare the extent of feasibility for very feasible separations ($r_{ij} > M_{kj}$), then in those cases it would be greater than unity. For very feasible separations $\mu(r_{ij})$ is set to unity, since the difference of scale of the values of m_{kj} and M_{kj} does not allow the use of $\mu(r_{ij})$ as a reliable measure of comparison.

However, for the property ratios identifying a separation technique as very feasible, their scaled values can be used for comparison as to the extent of the feasibility of these separations. The separation feasibility index M_{kj} is used for this purpose.

$$sr_{ij} = r_{ij}/M_{kj} \quad (2)$$

At a screening phase, some binary pair property ratios may be omitted because the separation techniques suggested might be infeasible due to operating conditions. However, comparing the “possibility distribution” $\mu(r_{ij})$ and the scaled binary property ratios sr_{ij} for the remaining adjacent binary pair property ratios after the screening, then the separation technique that should be used is identified by the largest $\mu(r_{ij})$ or sr_{ij} of all. Once the separation technique is identified, the exact sequence of attainable products is determined from the application of the developed algorithms of this thesis for batch separation.

Furthermore, in the case when more than one set of reactions is needed to obtain the final product then the property ratios for the adjacent binary pairs that the specified product, after a reaction task, is involved can also be used to identify whether a separation task is necessary between the one reaction task succeeds the other. Especially in the case when more than one set of reactions is needed to obtain the final product, the presence of separation boundaries needs to be identified in advance, in particular when the final product is involved and its recovery is endangered.

In general, the presence of either impurities in the raw materials or byproducts in a reactor outlet is investigated regarding their involvement in separation boundaries. In that way, the necessity of a separation task prior to the first reaction task is decided, as well as the necessity of an intermediate separation task between two reaction tasks. Moreover, insights derived from reaction kinetics analysis are used to determine the need of an intermediate separation task.

Once the batch route has been suggested, the intermediate objectives, namely product recovery and

purity are determined. The desired total recovery is actually the product of all the intermediate recoveries r_k for each of the reaction and separation tasks in the sequence.

$$r_T = \prod_{k=1}^N r_k \quad (3)$$

With the initial assumption that all recoveries are equal, the desired intermediate product purities are set according to the feasibility of the separation and the actual recoveries for the last two tasks in the sequence are found solving the system of eqn. 3 and the equation for the final product purity.

For the application of the synthesis algorithm, a number of necessary information needs to be available in advance. That is: a) the identity of the mixture compounds (both reactants and products) and the composition of the feed (raw materials), b) the thermodynamic models, the set of reactions taking place and the respective kinetics, c) The identity of the final product(s) and the end objectives for it, namely the desired purity and recovery, and d) the identity of any separation boundaries present in the respective mixtures considered for separation. The algorithm is described in a stepwise fashion in table 1.

Table 1. The batch process synthesis algorithm in steps

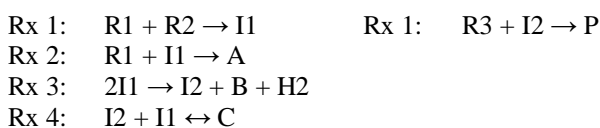
| Steps for the application of the synthesis algorithm | |
|---|--|
| 1. | For each set of reactions, identify a reaction task. Identify the desired & the unwanted reactions |
| 2. | Determine the necessity of a separation task before the first reaction task |
| 3. | Identify the separation technique for the respective separation tasks in the sequence (for all potential separation tasks after a reaction task) |
| 4. | In the case of more than one reaction tasks in the sequence, compare the reactant mixtures at the end of two succeeding reaction tasks. Otherwise, go to step 9 |
| 5. | List the mixture components in decreasing order, for the property that identified the respective separation technique |
| 6. | Calculate the binary property ratios for the adjacent binary pairs, as well as their $\mu(r_{ij})$ or sr_{ij} |
| 7. | From the $\mu(r_{ij})$ or the sr_{ij} of the binary pairs with a specified product, determine the extent of the feasibility of the separation task where the product is obtained |
| 8. | Identify any necessary separation task between two succeeding reaction tasks |
| 9. | Assume, initially, all recoveries r_k equal for the tasks in the sequence |
| 10. | Set the desired product purities for any intermediate separation tasks |
| 11. | Determine whether the last separation task can be avoided |
| 12. | Apply the developed batch reaction and separation algorithms to obtain the operational model for |

each task, given the intermediate end objectives for each task

13. For the last two tasks in the sequence, find the exact recoveries by solving the system of the equation for total recovery and that given by the final product purity
14. If any recovery is found difficult to obtain at step 12 or infeasible (r_k close or greater than unity) at step 13, adjust the initial assumption of step 9 and repeat from there. The adjustment (choosing a higher r_k) should be made for recoveries of very feasible separation tasks and generally for the first recoveries in the sequence

Results and discussion

The problem considered is adapted from [5], but for this case study the final product is reached after two, instead of three, set of reactions and the objective is to obtain high purity (99%) compound P with a recovery of 90% ($r_T=0.9$). The two set of reactions are:



Applying the algorithm for the synthesis of batch processes will provide the batch route (sequence of batch tasks) for attaining product P. In the first step, two reactions tasks are identified for the sequence from the two set of reactions. Initially, the sequence consists of these two reaction tasks and a subsequent separation task. For the second step, since the reactants are pure materials and the solvent does not take part in any competing reactions or form any azeotrope with the final product P, no separation task is necessary prior to the first reaction task.

For the third step, using the CAPSS tool in ICAS, distillation is identified as the separation technique for all potential separation tasks, for the reactant mixtures both after the first and the second reaction task. The corresponding properties that identified distillation are vapour pressure and the normal boiling temperature. The comparison of the reactant mixtures at the end of the respective reaction tasks takes place in the next steps of the algorithm. The intermediate product after the first reaction task is compound I2, while the final product after the second reaction task is compound P. The binary property ratios for the adjacent binary pairs with a specified product, as well as the “possibility distribution” $\mu(r_{ij})$ or the scaled binary property ratios sr_{ij} are compared in table 2.

From the comparison made, it is obvious that the separation of the intermediate product I2 in a distillation column after the first reaction task is much easier than the separation of the final product P. Furthermore, the byproducts that come along from the first reaction task to the second do not form any separation boundaries with the final product P that endanger its recovery or purity. However, the reaction rate of the reaction yielding the final product increases as the volume of the

Table 2. Comparison of the separation tasks after the 1st and 2nd reaction task

| Separation task | Adjacent binary pair | r_{ij} | sr_{ij} or $\mu(r_{ij})$ |
|---|----------------------|-------------|----------------------------|
| Binary property ratio r_{ij} for vapour pressure | | | |
| After 1 st reaction task | I2/R1 | 89.77 > 1.5 | 59.85 |
| After 2 nd reaction task | R1/P | 9.84 > 1.5 | 6.56 |
| | P/I1 | 13.62 > 1.5 | 9.08 |
| Binary property ratio r_{ij} normal boiling point | | | |
| After 1 st reaction task | R1/I2 | 1.39 > 1.02 | 1.36 |
| After 2 nd reaction task | P/I2 | 1.23 > 1.02 | 1.21 |
| | R3/P | 1.03 > 1.02 | 1.01 |

reactant mixture decreases. The application of the algorithm rules indicates that a separation task should take place between the two reaction tasks.

The only way the last separation task could be avoided is if the second reaction task had a recovery equal to 1 (100% conversion), which can not be achieved. Thus, the final batch route consists of the first reaction task, separation in a batch distillation column, the second reaction task and the final separation also with batch distillation, as shown in fig. 4.

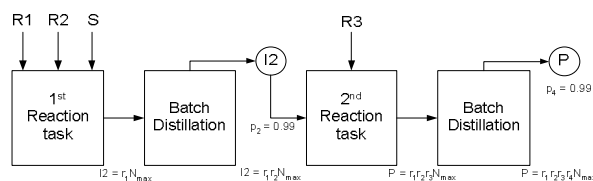


Fig. 4: The suggested batch route for the case study from the synthesis algorithm

The last two recoveries in the sequence are found solving the system of equations:

$$r_1 * r_2 * r_3 * r_4 = 0.9 \quad (4)$$

$$\begin{aligned} P / \{ (I2 + R3) + P \} = \\ (r_1 * r_2 * r_3 * r_4 * N_{max}) / \{ (2r_1 * r_2 * (1-r_3) + r_1 * r_2 * r_3 * r_4) * N_{max} \} = \\ P_4 \\ (r_3 * r_4) / \{ 2(1-r_3) + r_3 * r_4 \} = p_4 = 0.99 \end{aligned} \quad (5)$$

where r_1 and r_2 are already known (from assumption of r_k equality). One can calculate the required recoveries $r_3=0.9952$ and $r_4=0.95$.

The algorithms for batch reaction and distillation have been applied respectively for the tasks in the sequence providing the individual operational models, in terms of heating profile or reflux ratio profile. All operational models were feasible and able to reach the end objectives for each task. The suggested batch route was compared to an alternative route consisting of the two reactions tasks and a separation task in the end and it was found to be at least 76% faster.

Conclusions

A methodology for the synthesis of batch processes has been developed and presented in this paper. A rule-based algorithm for the generation of the batch route has been developed, while other algorithms provide the

operational design of the individual tasks of the batch route, which make it complete. The synthesis algorithm identifies the easiest and most feasible separation technique for each separation task and the position of the separation tasks in the sequence. This is done without the use of rigorous optimization techniques, but rather based on thermodynamic and process insights (reaction and mixture analysis). The exact procedure for the generation of a batch route has been provided in an easy and systematic way. The synthesis algorithm has been applied to a case study and the suggested route has been verified as feasible by dynamic simulation. The suggested route was also compared to an alternative route and found to be much faster. The route can further on be used as a starting point of dynamic optimization and for scheduling and planning purposes.

Acknowledgements

Financial support from the 5th Framework Knowledge – Driven – Batch – Production (BatchPro) project (Contract no. HPRN-CT-2000-0039) is highly appreciated. Additionally, the author would like to express gratitude to Syngenta and Mrs J. Cordiner for providing a case study and further financial support to the project.

References

- U.M. Diwekar, Batch Distillation: Simulation, Optimal Design and Control, Taylor & Francis, USA, 1995, p. 15-30
- R. Gani and E. Bek-Pedersen, AIChE J., 46 (6), (2000), p. 1271-1274
- B. Finch, Ind. Eng. Chem, 62, (1970), p. 6-
- C. Jaklsland, Separation Process Design and Synthesis Based on Thermodynamic Insights. PhD thesis, Tekst og Tryk A/S, Vedbæk, DK, 1996.
- R. Allgor, M. Barrera, P. Barton, and L. Evans, Computers Chem. Engng., 20 (6/7), (1996), p. 885–896.

List of publications

- I. Papaiconomou, R. Gani, S.B. Jørgensen, Proceedings Topical Conference Batch Processing, AIChE Annual Meeting, Reno, USA, 2001, p. 146-155.
- I. Papaiconomou, R. Gani, S.B. Jørgensen, Computer Aided Chemical Engineering, 10, (2002), p. 289-294
- I. Papaiconomou, S. B. Jørgensen, R. Gani and J. Cordiner, Proceedings FOCAPO-2003, Florida, USA, 2003, p. 473-476
- I. Papaiconomou^a, S.B. Jørgensen^a, R. Gani^a and J. Cordiner^b, Computer Aided Chemical Engineering, 14, (2003), p. 245-250
- I. Papaiconomou^a, S. B. Jørgensen^a, R. Gani^a and J. Cordiner^b, Computer Aided Chemical Engineering, 15, (2003), p. 990-995
- I. Papaiconomou, R. Gani, S.B. Jørgensen, BatchPro Proceedings Symposium on Knowledge-Driven-Batch-Production (BatchPro), Poros, Greece, 2004, p. 111-117



Kim Vestergaard Pedersen

Address: CHEC, Dept. Of Chemical Engineering
Building 229, Office 052
Phone: +45 4525 2890
Fax: +45 4588 2258
e-mail: kvp@kt.dtu.dk
www: www.chec.kt.dtu.dk

Supervisor(s): Anker Degn Jensen
Kim Dam-Johansen
Martin Skov Skjøth-Rasmussen

Ph.D. Study
Started: September 2004
To be completed: August 2007

Application of Fly Ash in Concrete

Abstract

Fly ash, a by-product from pulverized coal combustion, is utilized in the concrete manufacture where it serves as partial replacement of Portland cement. The residual carbon in fly ash is known to interfere with the chemicals added to the concrete to enhance air entrainment. The degree of adsorption is not only related with the amount of residual carbon, but also the properties of this carbon. The main objective of this project is to obtain knowledge of how the combustion conditions of pulverized coal is related with the amount and properties of the residual carbon in fly ash with emphasis on its utilization in concrete.

Introduction

About 24 % of the electricity produced worldwide (2002) is generated in coal fired power plants. As a consequence, large amounts of solid materials such as bottom ash and fly ash are produced. The demand for environmentally clean and cost effective power generation has increased the motivation of fly ash recycling.

The pozzolanic property of fly ash i.e. its capability to react with water and calcium hydroxide to form compounds with cementitious properties at ambient temperature, makes it useful in the concrete industry where it serves as partial replacement of cement [1]. Several benefits arise from this including increased strength of the concrete and economic savings in the concrete manufacture due to the lower price of the fly ash compared with cement. For typical durable concrete the amount of fly ash ranges from 15 wt% to 35 wt% [2].

To improve the resistance of concrete toward freezing and thawing conditions, air is entrained into the concrete paste [3]. The amount of air (typically 5-6 vol%) is controlled by special surfactants called air-entraining admixtures (AEAs). These surfactants adsorb strongly to the air-water interface with the result that the air is distributed into small stabilized air bubbles (<0.25mm).

The utilization of fly ash in concrete has been reported to interfere with air entrainment in concrete [4]. Instead of being collected at the air-water interface,

the AEAs are adsorbed by the fly ash and this leads to a decrease in the amount of air entrained. Increasing the dosage of the AEAs may compensate for the adsorption loss, but normal variations in ash properties leads to large and unacceptable variations in the entrained air [5]. The degree of interference of fly ash with air entrainment in concrete is usually determined by the foam index test, which is a simple laboratory titration procedure [6].

Even though modern coal fired power plants have high burnout efficiencies, significant amounts of carbon still exist in the fly ash after combustion. This residual carbon and not the mineral matter of fly ash are responsible for this adsorption of AEAs [5]. A large part of the carbon surface is non-polar compared with the polar surface of the mineral matter. This provides active adsorption sites for the hydrophobic part of the surfactants, thus the carbon competes with the sites at the air/water interface [7].

The problem with air entrainment in fly ash concrete has worldwide lead to regulations for fly ash application in concrete taking the presence of carbon in fly ash into account. These regulation are based on a maximum limit of the amount of carbon in fly ash, e.g. according to the Danish Standard DS/EN 450 the carbon content in fly ash are not allowed to exceed 5 wt%. However, in recent years the carbon content of a fly ash has been found insufficient as a criterion for its application in concrete and problems with air entrainment has been observed with fly ashes having levels of carbon below

the limits [5]. These observations have led to further studies of the interactions between AEA adsorption and carbon in fly ash; factors such as accessible surface area and surface chemistry of the residual carbon are believed to also affect the AEA adsorption [7]. In other words, not only the amount of carbon in fly ash but also the properties of this carbon influence the application of carbon containing fly ash in concrete.

The combustion conditions under which the fly ash has been produced influences the properties of the residual carbon. The worldwide introduction of improved burner technologies in order to reduce NO_x-emissions has led to problems with achieving a correct amount of air entrainment in fly ash concrete [8]. These burner technologies work with hot fuel rich zones in order to combust under reducing conditions and these conditions are believed to create fly ash being poor in quality in terms of concrete utilization.

Specific Objectives

The aim of this project is to obtain further knowledge of how the combustion conditions of pulverized coal influences the fly ash quality for concrete utilization with emphasis on the air entrainment in concrete. Furthermore, since the foam index test is not standardized and has a low reproducibility, steps will be taken towards the development of a standardized test method to replace this test.

References

1. K. Wesche, Fly Ash in Concrete: Properties and Performance, Spoon, London, 1991, p. 5.
2. O.E. Manz, Fuel 78 (1999) 133-136.
3. A.M Paillere, Application of Admixtures in Concrete, Spoon, London, 1995, p. 14.
4. Y-M. Gao, H-S. Shim, R.H. Hurt, E.M. Suuberg, NY.C.Yang, Energy & Fuels 11 (1997) 457-462.
5. E. Freeman, Y-M. Gao, R. Hurt, E. Suuberg, Fuel 76(8) (1997) 761-765.
6. V.H. Dodson, Concrete Admixtures, Van Nostrand Reinhold, New York, 1990, p. 140.
7. L. Hachmann, A. Burnett, Y-M. Gao, R.H. Hurt, E.M. Suuberg, Proceedings of the Combustion Institute 28 (1998) 2965-2971.
8. Y. Gao, I. Külaots, X Chen, E.M. Suuberg, R.H. Hurt, J.M. Veranth, Proceedings of the Combustion Institute 29 (2002) 475-483.



Trine Lütken Petersen

Address: Novozymes Bioprocess Academy
Department of Chemical Engineering
Currently sitting in:
Building 223, Room 211
Technical University of Denmark

Phone: +45 4525 2708
Fax: +45 4588 4148
e-mail: tlp@biocentrum.dtu.dk
www: www.biocentrum.dtu.dk

Supervisor(s): John Villadsen
Timothy Hobley
Jesper Brask, Novozymes

Ph.D. Study
Started: April 2004
To be completed: April 2007

PEGylation of Enzymes: Novel *In-Vitro* Methods for Their Study and Scale-Up

Abstract

The process of attaching polyethylene glycol groups (PEG) to enzymes needs to be controlled in order to obtain PEG conjugates with the desired properties. Magnetic adsorbents with appropriate ligands can be used for binding enzymes in their active site, thus orientating the protein and protecting the catalytic pocket. It is proposed that the immobilised enzyme can then be added to activated PEG and the time of exposure controlled due to manipulation with a magnetic field. The enzyme chosen for study in this project is Savinase and magnetic supports having bacitracin as the ligand have been manufactured and show high affinity for Savinase.

Introduction

Covalent binding of polyethylene glycol groups to enzymes (PEGylation) may lead to improved physico-chemical and biological properties. For example the enzyme may be protected against proteolytic degradation, have improved stability over a wide range of pH values and temperatures or enhanced solubility and activity in organic solvents. Furthermore, PEG covering the surface of an enzyme shields the protein from the immune system leading to reduced immunogenicity and antigenicity. Evasion of the immune system is important for protein based therapeutics but also for applications such as low allergenic washing powder. The attachment of the correct amount of PEG groups in the right positions on an enzyme is fundamental to obtain the desired properties. Conventional batch PEGylation, however, often gives rise to a family of by-products with too few or too many PEG groups, leading to reduced product yield, and also requiring concentration and purification of the desired PEG-conjugate. Therefore a scaleable process with improved control over PEGylation is desirable.

Specific Objectives

The concept behind this project is that it is possible to bind an enzyme via its active site to a *magnetic* support by using an affinity ligand (Figure 1). The non porous nature of the adsorbents leads to rapid binding and adsorption that can be conducted in a pipe reactor with short residence time (eg. seconds).

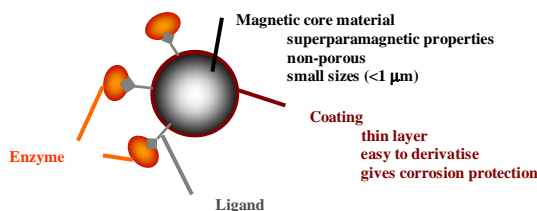


Figure 1: Schematic representation of enzyme binding to affinity ligands on a magnetic adsorbent. The adsorbent core is superparamagnetic (no remnant magnetism when removed from a magnetic field). Thus the supports can be captured or released from a magnetic filter when the field is turned on or off. The small support size increases the surface area to volume ratio giving high capacity. Coupling chemistries and ligands used for chromatography adsorbent manufacture can be employed.

Following binding the active site will be protected from the PEG groups. Also, the enzyme molecules should all be bound in the same orientation with respect to the support surface. When this is combined with a means of controlling the time of exposure of the immobilised enzyme to activated PEG due to manipulation with a magnetic field (i.e. rapid removal from the reactants by pumping at high velocity (10 – 100 m/h) through a magnetic filter), it is expected that the extent and location of attachment of PEG groups should be controllable. Furthermore, the use of an affinity ligand for binding the enzyme permits concentration and purification of the PEGylated product. Figure 2 shows the principle behind the process proposed.

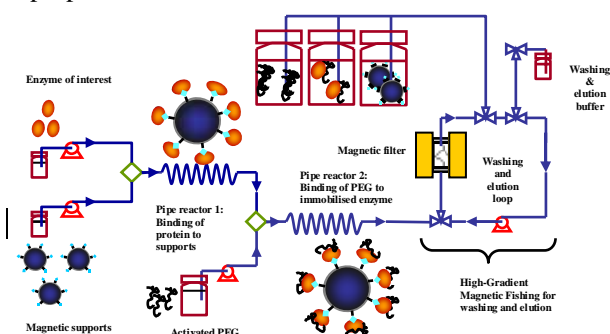


Figure 2: Schematic of the process proposed for magnetic support mediated control of enzyme PEGylation. The enzyme is rapidly bound to the adsorbent in a pipe reactor. Activated PEG is then added which attaches to the enzyme, the mixture is pumped into a magnetic filter leading to rapid capture of the adsorbent-PEGylated-enzyme complex and the reactants pass through. Washing is then conducted and the PEGylated enzyme is eluted from the supports.

The process proposed above is novel and has never been examined before, thus the aim of this project is to examine how magnetic solid phases can be exploited for conducting *in vitro* PEGylation of proteins. Specifically to study: (i) how magnetic supports can be used to control the extent of PEGylation of enzymes, (ii) how the number and position of PEG groups affects enzyme activity as well as pH and temperature stability.

Results and Discussion

Different enzyme-ligand model systems have been identified with the most promising being the binding of the subtilisin Savinase, to the inhibitor bacitracin.

Magnetic supports derivatised with bacitracin have been constructed using divinylsulfone for activation. The binding characteristics of the resulting supports have been tested by determining a static binding isotherm (Figure 3) by adding a defined amount of magnetic particles to different concentrations of savinase, removing the particles (at equilibrium) and measuring the amount of free (C^*) and bound (Q^*) protein.

The Langmuir model (equation 1) fits the data with a maximum capacity, $Q_{max} = 3.6 \times 10^3$ U/g (158 mg/g) and dissociation constant, $K_d = 1.8 \times 10^3$ U/L (0.79 μ M). These parameters show that the particles have high affinity for Savinase and excellent binding capacity.

$$Q^* = Q_{max} \frac{C^*}{C^* + K_d} \quad \text{Eq. 1}$$

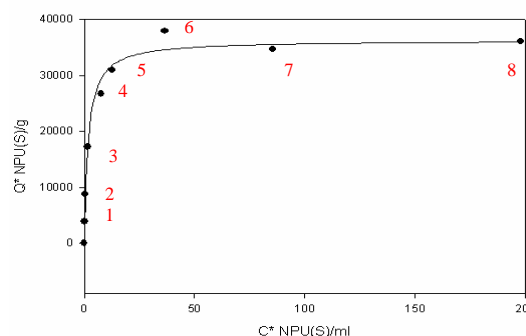


Figure 3: Adsorption isotherm for Savinase. The concentration of savinase left in the supernatant after applying the magnetic particles (C^*) is plotted versus the amount of savinase bound on the magnetic particles (Q^*).

Propylene glycol has been used for eluting savinase from the magnetic supports. Figure 4 shows the recovery of Savinase in three different elution cycles; E1, E2 and E3. The recovery is approximately 60% in all samples.

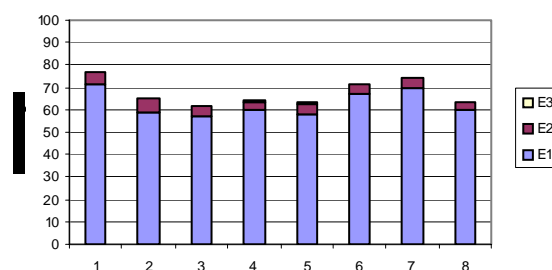


Figure 4: Recovery of Savinase activity following elution with propylene glycol. The numbers of the bars correspond to the sample numbers on the adsorption isotherm in Figure 3

Identification and quantification of the PEG-conjugates of Savinase will be carried out using Electrospray Mass Spectrometry (ES-MS). Determination of the specific sites where the PEG groups are located requires tryptic digestion of the PEG-conjugates followed by analysis of the fragments using ES-MS.

Acknowledgements

Novozymes Bioprocess Academy is acknowledged for funding the project



Christian Lund Rasmussen

Address: Building 229/126
Phone: +45 4525 2923
Fax: +45 4588 2258
e-mail: clr@kt.dtu.dk
www: www.chec.kt.dtu.dk

Supervisor(s): Peter Glarborg

Ph.D. Study

Started: February 2004
To be completed: February 2007

Direct Partial Oxidation of Natural Gas to Liquid Chemicals

Abstract

Conversion of natural gas to methanol by a homogeneous direct partial oxidation at high pressure and low temperature is an attractive industrial process to improve the utilization of the World's natural gas reserves. Optimization of the process relies on a fundamental understanding of the interactions between the reaction conditions and the complex chemistry involved. Detailed chemical kinetic modeling enables such investigations of the governing chemistry on an elemental reaction level.

Introduction

A significant fraction of the World's natural gas reserves is presently unavailable to the markets of utility duo to transport limitations. Large quantities are allocated under the tundra and beneath the sea near the continental shelves. If a fraction of these reserves could be captured and converted to a readily transportable state, it would have a significant effect on the environmental impact of power production as well as the production of chemical feedstock. This can be achieved if the natural gas is converted to a liquid chemical, known as the gas-to-liquid (GTL) process.

The direct partial oxidation of methane to methanol or mixtures of oxygenated hydrocarbons in a homogeneous process is a promising industrial GTL process. Direct conversion is an exothermic process, which is superior in terms of energy efficiency and simplicity to the conventional industrial production of methanol based on synthesis gas (CO/H₂) obtained from steam reforming of natural gas. Economic assessments show that the direct process is competitive with the conventional indirect process if 80% selectivity of methanol can be achieved at 10% methane conversion in a single pass of the reactor [1]. Previous efforts to reach this goal have mainly been unsuccessful, which may to some extent be attributed to theoretical and experimental shortcomings.

Kinetic Approach

The gas phase partial oxidation of methane is operated by a free radical mechanism, which is only partly understood and extremely difficult to control. The very stable methane molecule must be converted to

methanol without promoting further oxidation to undesired carbon oxides. The rate limiting step is the breaking of the very stable C-H in methane. This typically requires high temperature, which has an adverse effect on the selectivity towards the desired product. The selectivity is greatly improved by applying relatively low temperatures and high pressure, which are conditions with a low reaction rate and thus a low yield. However, this difficulty is expected to be overcome by interactions with gas phase initiators or sensitizers, e.g. nitrogen oxides, sulphur oxides and alkali metals.

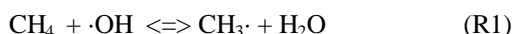
Project Objectives

The main objective of this project is to identify a combination of sensitizers and process conditions that results in a competitive yield and selectivity in the gas phase direct partial oxidation of natural gas to liquid products.

Reaction Mechanism

The primary reaction pathway that controls the oxidation of methane at high pressure and low temperature is shown in Figure 1. The reactions are with few exceptions reversible radical reactions.

Methane is converted to methyl radicals in reaction (R1), where the hydroxyl radical originates from initiating reactions between hydrogen and oxygen.



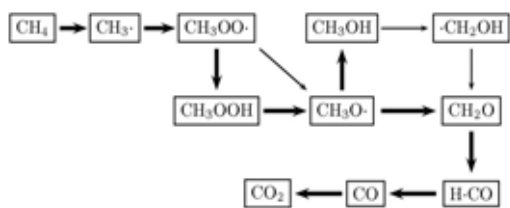
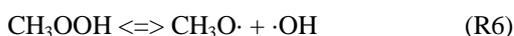
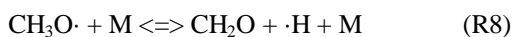


Figure 1: Reaction mechanism for oxidation of methane at high pressure and low temperature. The width of the arrows indicates their relative contribution. Intermediate species are methyl ($\text{CH}_3\cdot$), methylperoxy ($\text{CH}_3\text{OO}\cdot$), methylperoxide (CH_3OOH), methoxy ($\text{CH}_3\text{O}\cdot$), methanol (CH_3OH), methylhydroxyl ($\cdot\text{CH}_2\text{OH}$), formaldehyde (CH_2O), formyl ($\text{H}\cdot\text{CO}$) and carbonmonoxide (CO).

Subsequent reaction with O_2 in (R2) leads to the production of methylperoxy radicals that decompose and form methoxy radicals either directly in reaction (R3) and (R4) or through intermediate formation of semi-stable methylperoxide via reaction (R5) and (R6).



The further conversion of methoxy radicals is an important branching in the reaction network. Reaction with methane in (R7) leads to the desired product, while collision with an arbitrary collision partner (M) in reaction (R8) results in decomposition to formaldehyde.



Formaldehyde is the entry to the full oxidation branch in the reaction network, so the reaction conditions should be optimized to favor (R7).

Important Reaction Conditions

A high CH_4/O_2 ratio favors methanol formation, while the opposite has an adverse effect and increases production of CO and CO_2 . This is a direct result of the ability of methane to act as an H-donor in the conversion of methoxy to methanol via reaction (R7), which thus suppresses alternative reactions with methoxy. Based on experiences from the literature $10 < \text{CH}_4/\text{O}_2 < 30$ is recommended [1,2].

The most promising results reported in the literature are obtained in the temperature range from 300-500°C [1,3]. The free radical chain reaction is initiated at a characteristic *transition* temperature and rapidly continues until full conversion of O_2 is reached. A monotonic increase in the methanol concentration is

observed during this conversion followed by stabilization of the concentration on a constant level. This means that the residence time after full O_2 conversion is without importance.

High pressure increases the collision frequency, and thus improves the reaction rate and stabilizes some important intermediate products. Reported studies of the pressure dependency indicate a significant increase in the methanol concentration when pressure is increased up to 100 bar after which, this dependency declines until no apparent effect is observed after 150 bar [2].

Nitrogenoxides are the most promising gas phase sensitizers. This is attributed to a number of recirculation reactions between NO and NO_2 that either directly catalyses propagation of the reaction chain in Figure 1 or increases the production of important radicals, e.g. $\cdot\text{OH}$, that helps to initiate the chain via (R1).

Kinetic Modeling and Experimental Work

Optimization of the process relies on a fundamental understanding of the interactions between the reaction conditions and the complex chemistry involved. For this purpose, a detailed chemical kinetic model (DCKM) is under development enabling the user to investigate the governing chemistry on an elemental reaction level. The current model describes C_{1-2} chemistry using 85 species and 578 elemental reaction steps that are collected from available knowledge about hydrocarbon oxidation chemistry. Validation of the model is currently achieved from comparison with experimental data obtained from the literature. However, an experimental facility is under construction applying a pressurized laboratory scale flow reactor designed to handle pressures up to 150 bars at 600°C. Figure 2 shows the performance of the model when compared to experimental results obtained from the work of Thomas et al., 1992 [4].

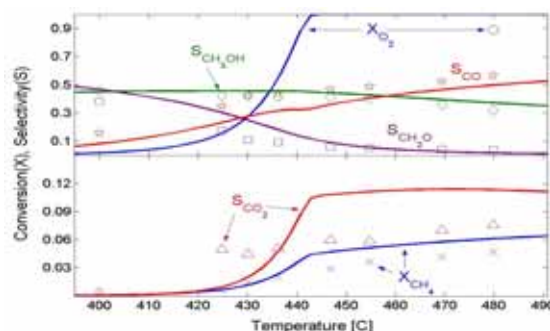


Figure 2: Oxidation of 95% CH_4 with 5% O_2 at 20 bar and 500 NmL/min. Exp. uncertainty is $\pm 5\%$ [4]. Calculations are performed in CHEMKIN using the SENKIN code.

References

1. Q. Zhang, D. He, Q. Zhu, J. Nat. Chem. 12 (2003) 81-89.
2. V.S. Arutyunov, V.Y. Basevich, V.I. Vedeneev, Ind. Eng. Chem. Res. 34 (1995) 4238-4243.
3. H.D. Gesser, N.R. Hunter, C.B. Prakash, Chem. Rev. 85 (4) (1985) 235-244.
4. D.J. Thomas, R. Willi, A. Baiker, Ind. Eng. Chem. Res. 31 (1992) 2272-2278.



Jan Kamyno Rasmussen

Address: CAPEC, Dept. of Chemical Engineering
Building 227, Office 250
Technical University of Denmark

Phone: +45 4525 2801
Fax: +45 4588 2258
e-mail: jkr@kt.dtu.dk
www: www.capec.kt.dtu.dk
Supervisors: Sten Bay Jørgensen
Henrik Madsen, IMM-DTU
Henrik Steen Jørgensen, Novozymes A/S

Ph.D. Study
Started: September 2003
To be completed: August 2006

Datadriven and Mechanistic Model based Control and Optimization of Fed-batch Fermentations

Abstract

Fed-batch processes are widely used in chemical and biochemical industry. Fermentations in biochemical industry are most often carried out as fed-batch processes. Operation of these processes is not possible using standard regulatory control schemes because of their non-linear nature and limitations in the production equipment. In this project a methodology for control and optimization of such processes will be developed based on the use of mathematical models.

Introduction

Fermentation processes are commonly used in biochemical industry for production of a wide variety of products. The true nature of these processes is rarely fully understood which makes the implementation of efficient control schemes very difficult. First principle engineering models are not used because the limited knowledge about the processes would make them very time consuming to develop.

Another promising strategy is to develop datadriven models entirely based on data from actual fermentations. When knowledge about the process is available a hybrid modelling approach to extract pertinent information from data can be applied.

The purpose of modelling these processes is to develop control structures that ensure uniform operation and optimize the productivity of the process.

This project is a part of the Novozymes Bioprocess Academy which is a newly established cooperation between Novozymes A/S, The department of Chemical Engineering and Biocentrum at DTU.

Process studied

The process studied is fermentation of the filamentous fungi *Aspergillus oryzae* for production of the enzyme amylase. The fermentation is initiated by transferring the contents of a seed tank to the main fermentation tank when a certain transfer criterion has been satisfied. The main fermentation tank contains an initial amount of substrate and the main fermentation

process starts immediately after inoculation. The main fermentation is carried out in a batch and fedbatch phase. When the initial substrate has been consumed by the microorganisms the fedbatch phase is initiated. Feed dosing is started at a low level and increased to its final value within a certain time span. The fedbatch phase continues for the rest of the fermentation process.

The fermentors are equipped with sensors for online measurements of different variables but some values are only available as offline measurements which makes closed loop control more difficult and requires a more accurate model for predicting the variable values.

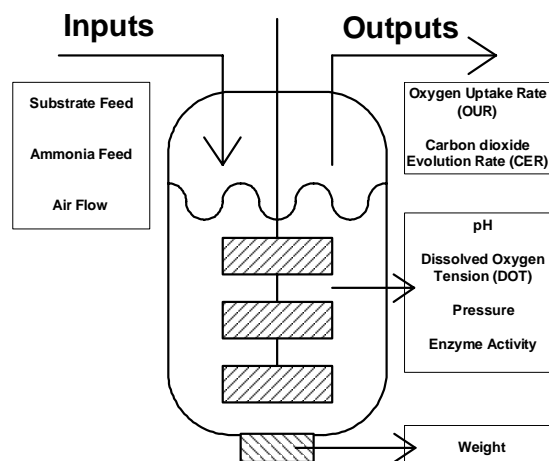


Figure 1. Sketch of fermentor used in the fermentation process

Specific Objectives

The objective of this project is to develop a methodology to identify mathematical models which can predict the behaviour of fed-batch fermentations in biochemical industry. Based on the identified models it is possible to control the fed-batch process. The models may also be developed for optimizing the process performance. The results of the models will be validated against experimental data obtained on the plant and a control structure based on the models will be implemented in a pilot plant for validation purposes.

Two different modelling strategies will be used for this purpose: Black-box modelling and grey-box modelling.

Black-box modelling

Black-box modelling is also referred to as datadriven modelling. The advantage of datadriven modelling is that only limited prior information about the process is required. The disadvantage is that the resulting models do not have any physical interpretation and can not directly provide any information about the biological state of the fermentation process.

A methodology for generation of such models has already been developed in earlier projects [1]. It has been shown that this kind of datadriven models is able to account for disturbances that occur in the process. The methodology divides the duration of the entire batch into time steps, termed grid points. A linear time invariant model is fitted to each grid point and each model describes the behaviour of the process between two grid points. The combination of these linear models results in a model which covers the entire time span of the fermentation and approximates the highly non-linear behaviour of the process. The principle behind this methodology has been sketched in figure 2.

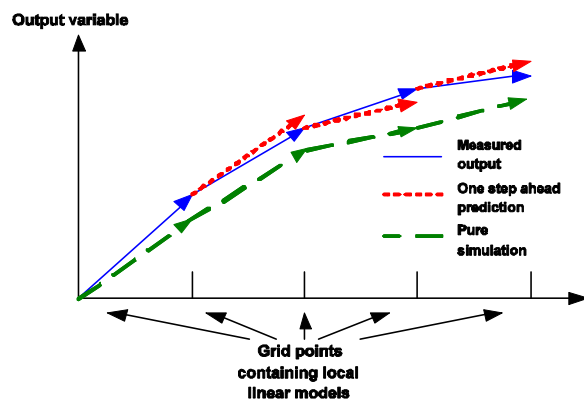


Figure 2. Illustration of the principle behind the GoLM modelling framework

Two types of simulation is shown in figure 2. One step ahead prediction is a prediction for the successive grid point based on the information available at the current grid point Pure simulation is a prediction of the entire batch based only on the information available at the beginning of the batch ($t=0$). The GoLM modelling

framework models deviations from a given reference trajectory. A reference batch therefore needs to be specified before a simulation can be carried out. Based on a given reference batch and a trajectory for the input signal/signals exerted on the system all the output variables included in the model can be simulated.

Successful application of data-driven models shows that the data contains sufficient information to predict the behaviour of future batches.

A GoLM model has been identified based data from 37 historical batches from a production plant. The duration of the entire batch has been divided into 112 grid points. One hour intervals have been used for the first 60 hours and 2.5 hour intervals have been used for the last 130 hours. The finer division in the beginning of the process is due to the dynamic batch phase. Here strongly varying behaviour is observed as opposed to the fed-batch phase where the process is less dynamic.

The model contains 7 outputs and 1 input. These are given in table 1.

Table 1. Output variables and their sampling rates used for the GoLM model identified.

| Output variable | Sampling interval |
|----------------------------------|-------------------|
| Dissolved O ₂ tension | 10 minutes |
| Enzyme concentration | 24 hours |
| Weight | 10 minutes |
| O ₂ uptake rate | 10 minutes |
| CO ₂ evolution rate | 10 minutes |
| Ammonia flow | 10 minutes |
| Air flow | 10 minutes |

Most of the variables are available as online measurements but the enzyme activity, which can be regarded as the quality variable, is only measured once a day.

Simulations based on this GoLM model are presented in the following.

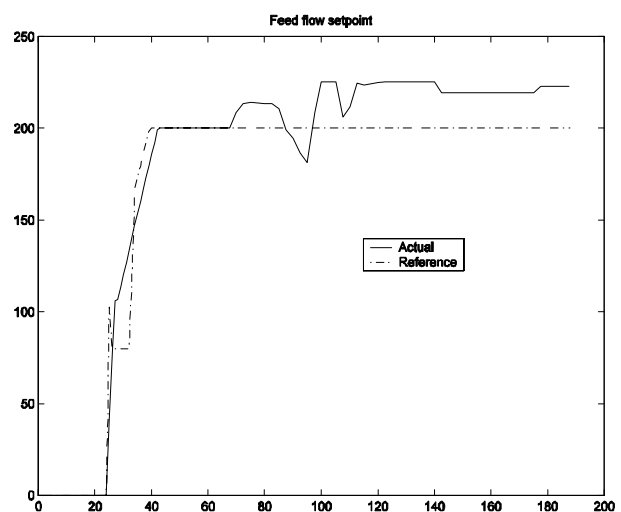


Figure 3. Feed flow setpoint (input variable) used for GoLM model. Actual: simulated trajectory. Reference: Trajectory used in the reference batch.

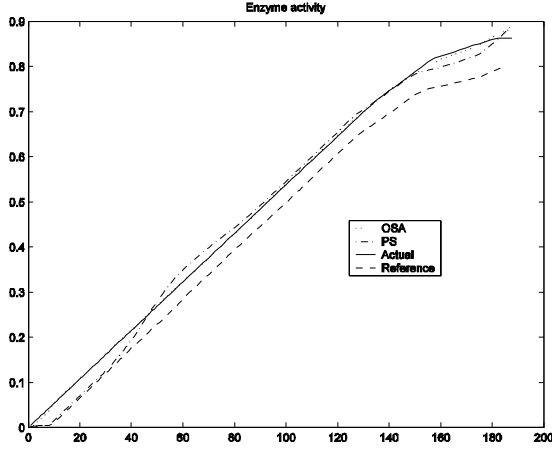


Figure 4. Enzyme activity predicted by GoLM model. OSA: One step ahead prediction. PS: Pure simulation. Actual: Simulated batch. Reference: Reference batch

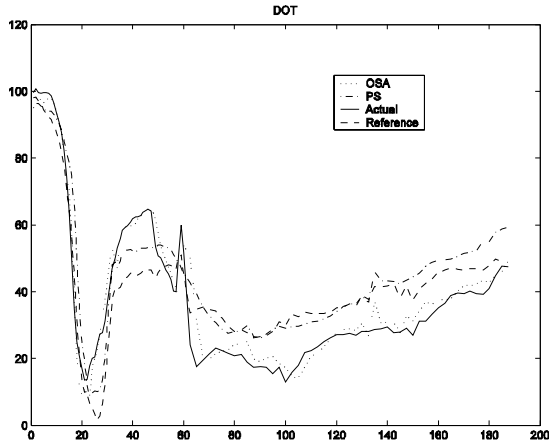


Figure 5. Dissolved oxygen tension predicted by GoLM model. OSA: One step ahead prediction. PS: Pure simulation. Actual: Simulated batch. Reference: Reference batch

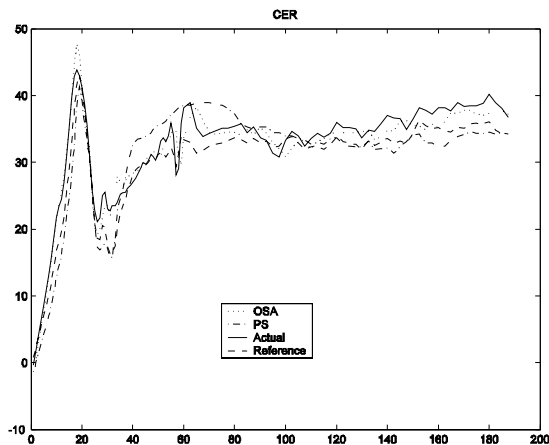


Figure 6. Carbon dioxide evolution rate predicted by GoLM model. OSA: One step ahead prediction. PS: Pure simulation. Actual: Simulated batch. Reference: Reference batch

The model generally provides good predictions of the final enzyme concentration and it is able to catch much of the dynamics occurring in the process.

Grey-box modelling

In the grey-box modelling framework knowledge about the micro-organism and how the process is carried out is combined with operational data in order to develop knowledge based models. A methodology for development of such knowledge based grey-box models has already been developed [2]. It is based on the use of stochastic differential equations which are well suited for combining first principle engineering models with data because they account for random uncertainty and noise.

The first principles engineering model to be studied here is proposed by Agger et al. [3]. The model is based on the assumption that the total filamentous biomass can be divided into three distinct regions:

- Active region (x_a): Responsible for uptake of substrate and growth of the hyphal element. α -Amylase synthesis occurs in this region.
- Extension zone (x_e): Building of new cell wall.
- Hyphal region (x_h): Contains the degenerated part of the hyphal elements and can be considered as an inactive region.

The original model contains 5 states, (The 3 morphological states, substrate concentration (s) and product concentration (p)). During the development of the model it has been assumed that no oxygen limitation is present. In order to be able to model the behaviour at low dissolved oxygen values and relate the morphological states to off-gas measurements the model has been extended [4]. The oxygen concentration has been introduced as an extra state and as the volume is changing this also constitutes an additional state of the system.

The formation rate of the three regions is given in equation (1)-(3).

$$\frac{dx_e}{dt} = q_1 - Dx_e \quad (1)$$

$$\frac{dx_a}{dt} = q_3 - q_1 - q_2 - Dx_a \quad (2)$$

$$\frac{dx_h}{dt} = q_2 - Dx_h \quad (3)$$

If the concentration of active biomass is below a certain threshold value no production of extensive region occurs, this phenomenon is included in the expression for q_1 . The three kinetic expressions are given in equation (4) to (6).

$$q_1 = \begin{cases} 0; & \frac{x_a}{c_n} < \left(\frac{x_a}{c_n} \right)_0 \\ \frac{k_1 s}{a(s + K_{s1})}; & \frac{x_a}{c_n} \geq \left(\frac{x_a}{c_n} \right)_0 \end{cases} \quad (4)$$

$$q_2 = k_2 x_a \quad (5)$$

$$q_3 = \frac{k_3 s}{s + K_{s3}} \frac{x_a / c_n}{x_a / c_n + K_3} a x_a \frac{C_{O_2}}{k_{O_2} + C_{O_2}} \quad (6)$$

In order to account for the decrease of growth rate for the active region under oxygen limiting conditions the last Monod term in equation (6) has been introduced.

For more information on the details of the model please refer to [3]. Simulations based on one industrial batch are given in the figures below.

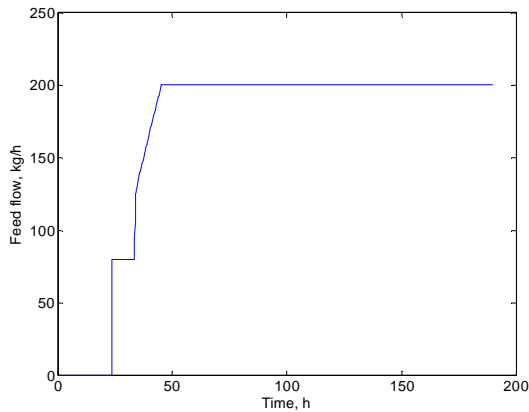


Figure 7. Feed flow set point (input variable) used in the simulation of the Agger model

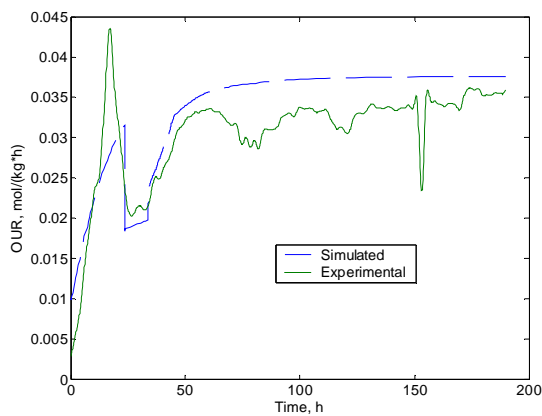


Figure 8. Oxygen Uptake Rate (OUR) predicted by the Agger model. Simulated values (dashed line). Experimental values (Continuous line)

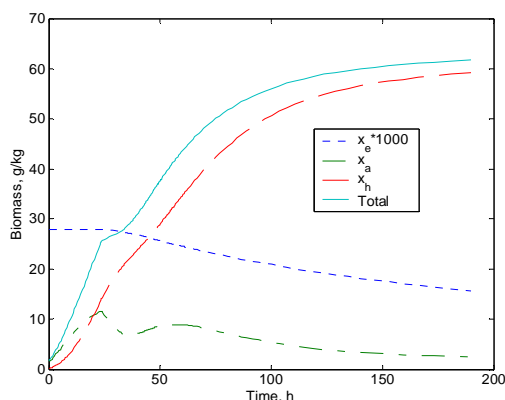


Figure 9. Extension zone*1000 (dotted line). Active region (dash dotted line). Hyphal region (dashed line). Total biomass (continuous line)

The morphologically structured model presented is able to predict a large part of the behaviour of the industrial fermentation. The model has been developed in laboratory scale equipment where no oxygen limitation has occurred in the experiments. In order to be able to simulate an industrial scale fermentor some of the model parameters need to be re-estimated and new functional relationships have to be introduced. Parameter (re-) estimation and investigation of new functional relationships in the model based on experimental data are carried out in the software program CTSM (Continuous Time Stochastic Modelling) (Kristensen et al., 2004).

Conclusions

The limited knowledge about the nature of the fermentation processes used in industry makes it time consuming to develop first principle engineering models. An alternative is datadriven modelling based on process data. If some information about the process is available knowledge based grey-box models can be developed and efficiently used to uncover unknown functional relationships.

The control structures used today are most often decentralized and lack the ability to account for limitations in the process equipment and micro-organisms. Furthermore industrial operation often relies on the operators experience and can not be guaranteed to be uniformly reproducible

In this project both types of modelling are being explored and the results will be validated against actual plant data.

References

1. D. Bonn , S. B. J rgensen, Datadriven Modelling of Nonlinear and Time-Varying Processes, IFAC SYSID 2003, 2003.
2. N. R. Kristensen, H. Madsen and S. B. J rgensen, 2004, A Method for Systematic Improvement of Stochastic Grey-Box Models, Comp. & Chem. Eng., 28/8, 1431-1449
3. T. Agger, A. B. Spohr, M. Carlsen and J. Nielsen, 1998, Growth and Product Formation of *Aspergillus oryzae* during Submerged Cultivations: Verification of a Morphologically Structured Model Using Fluorescent Probes, Biotechnol. Bioeng., 57, 321-329.
4. T. C.Zangirolami, 1998 Modeling of Growth and Products Formation in Submerged Cultures of Filamentous Fungi, Ph.D. thesis, Technical University of Denmark, Denmark.

**Alfonso Mauricio Sales-Cruz**

Address: CAPEC, Building 227, Office 266
Phone: +45 4525 2911
Fax: +45 4593 2906
e-mail: msc@kt.dtu.dk
www: www.capec.kt.dtu.dk/People/phds

Supervisor(s): Rafiqul Gani

Ph.D. Study

Started: December 2002.

To be completed: November 2005.

Development of a Computer Aided Modeling System for Bio and Chemical Process and Product Design

Abstract

This project deals with the development of an advance computer aided modeling system (CAMS) that aids to model developer in model generation, model analysis, model identification and model solution in a fast, reliable and efficient manner. The advantages of using CAMS are highlighted through case studies in terms of reduction of modeling time and effort. Case studies are related to the steady state, dynamic simulation, optimization and control of bio- and chemical processes. In particular, in this contribution, the process modeling and a systematic strategy of solution for a short-path evaporator to obtain the desired product specification is presented. Up to now the results show that this contribution proposes an integrated modeling framework that allows understanding main characteristics of chemical processes.

Introduction

In general, modeling is one of the fundamental activities related to research and development of processes and/or products. There is an increasing trend to use computer- aided modeling systems (CAMS) and tools for integrated process analysis. CAMS provide the opportunity to reduce the time to market and investment costs through integrated product and process design with fast, reliable and efficient modeling steps. CAMS must ensure the integration of existing tools and models into a software environment to support model construction, analysis, solution, and validation.

The aim of this project is to highlight the use of a generic modeling framework for CAMS called ICAS-MoT [1], which is applicable to a wide range of modeling and associated problems. Several cases have been implemented using the current CAMS. Table 1 shows a brief description of the process models that have been solved. In this contribution, the process modeling and a systematic strategy of solution for a short-path evaporator to obtain the desired product specification is presented. The model describes the influence of the evaporator design and the operational conditions for obtaining an efficient separation and improving yield of the desired chemical product. The model performance is illustrated with the purification of a pharmaceutical product, using ICAS-MoT for the model analysis and solution.

Modeling Framework

The process of mathematical model building is a trial and error procedure. The iterative feedback/feedforward nature of this process is shown in Figure 1. The model developer usually repeats the steps more than once. He gets closer reaching the model objectives with each cycle while, at the same time, refining the definition of the modeling purpose. The modeling approach can be subdivided into the following steps [10]: problem definition, system characteristics, problem data evaluation, model construction, model solution, model verification, and model validation. Usually all of these steps consume a lot of human resources and time. However, if the work is divided between human and computer, so that the computer assists to the model developer where it is efficient and leaving to the human the parts that require important decisions, then time and cost for model development can be significantly reduced.

The modeling framework used in this work is ICAS-MoT, which is an integrated modeling environment to build, analyze, manipulate, solve and visualize mathematical models. ICAS-MoT provides an intuitive and flexible way of integrating several aspects of the modeling needs at different stages of the process lifecycle, including the following modeling steps:

(a) Model Construction (Translation): The model developer does not need to write any programming

Table 1. Case studies solved in ICAS-MoT

| Process | Description | Type | Equations | Variables | Ref. |
|--|--|-----------|------------------------------------|--|------|
| Anaerobic bioprocess (two CSTR in series) | Parameter Identification, dynamic simulation and system optimization. | DAE | 5 explicit 5 ODE | 10 known 18 design | [2] |
| Short path Evaporator | Separation technique for thermally unstable materials | PDAE, DAE | 142 explicit 17 ODE | 1 Unknown 177 known 7 parameters | [3] |
| Membrane distillation | Dynamic simulation. | DAE | 75 explicit 5 ODE | 3 Unknown 17 known | [4] |
| Mass polymerization reactor MMA | Steady state and dynamic simulation. | DAE | 14 explicit 6 ODE | 0 Unknown 28 known 2 parameters | [5] |
| Emulsion copolymerization reactor (MMA/S) | Dynamic simulation for different open-loop configurations. | DAE | 70 explicit 4 ODE | 2 Unknown 36 known | [6] |
| Solution copolymerization reactor (MMA/VA) | Open-loop steady state analysis (multiplicity and stability) and dynamic behavior. | DAE | 77 explicit 18 ODE | 18 dependent 54 parameters 59 explicit | [7] |
| Tennessee Eastman Challenge problem | Large scale problem. Dynamic simulation. Control structure. | DAE | 175 explicit 30 ODE | 2 Unknown 168 known | [8] |
| Thermal cracker | Profit maximization. The variables to be optimized are the feed amounts. | NCMP* | 7 explicit 1 objective function | 7 design (parameters) | [9] |
| Isothermal batch reactor | Calculate the optimal residence time to yield a maximum value of intermediate product. | NCMP* | 4 AE | 1 explicit 3 unknown 2 parameters | [9] |

* Nonlinear Constrained Minimization Problem

codes to enter the model equations. Models are entered (imported) as text-files or XML-files, which are then internally translated.

(b) Model Analysis: First, the (non-explicit) variables and equations are classified by the user. Afterwards, several tools and algorithms are included to ensure that the problem is not ill-posed before going to the solution step, such as generation and analysis of the incidence matrix, inspection for singularity, verification of the degrees of freedom, and decomposition, partitioning and ordering of the model equations.

(c) Model Solution: After an interactive model analysis step, the appropriate solver for the model equations is selected together with a solution strategy. As solver options, ICAS-MoT provides several solvers for AEs (algebraic equations), ODEs (ordinary differential equations), DAEs (differential algebraic equations) and numerical optimization methods.

(d) Model Validation: ICAS-MoT permits to simulate very easily and quickly different models and/or process configurations in the same environment, since a core model can be built and gradually expanded during the process lifecycle generating and passing the results from one stage to another.

(e) Model Transfer: A COM-object of the solved model can be generated to transfer it to the ICAS library and to use in external software (like Excel). A model transfer is recommended for a repetitive model use, for example, for different sets of parameters, compound properties, reaction kinetics and equipment sizing data.

For our case study we will follow this modeling framework, which should serve as a robust basis to get an appropriate process description

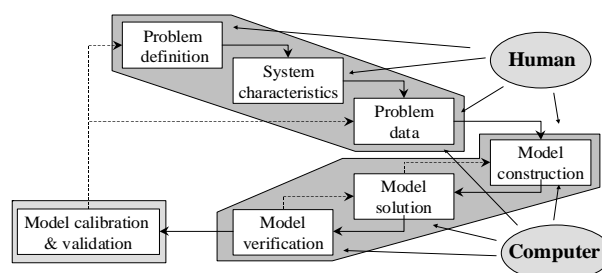


Figure 1. Modeling framework.

Short-Path Evaporator

Conventional distillation is one of the oldest methods to separate liquid or molten substances. However it is not recommended for substances that can be degraded under distillation temperatures, such as vitamins, insecticides, drugs and flavors/fragrances. The short-path distillation is a separation technique used as an alternative in various processes of the chemical, pharmaceutical, fragrance and food industry. It is a safe method suitable for separation and purification of thermally unstable materials, through a small distance between the evaporator and the condenser, and characterized by low temperatures, short residence times of the distilled liquid on the thermally exposed surface and sufficiently low pressure in the distillation gap (space between evaporator and condenser). Therefore, the modeling, design and analysis of short-path evaporation (or molecular distillation) are important elements in many chemical product engineering problems.

Information about the film surface temperature on the condensation surface is important to determine yield and purity of the distilled product, as well as to define the evaporator design (i.e., the feed position and the evaporator geometry). However, direct measurement on the temperature profiles in the film of the condensate is extremely difficult, so that a key issue is the building of an appropriate model that can describe the separation process as a function of the (concentration, temperature and velocity) film profiles, and which can be useful for operation analysis and process design.

Thus, the aim of this section is to present a systematic strategy for process modeling with particular emphasis in analysis and design of a short path evaporator, to establish the operational conditions for obtaining an efficient separation, improving yield and purity of the desired chemical product.

Process description

The short-path separator consists of a cylindrical body surrounded by a cylinder, one of them acts as evaporation surface and the other as condensation surface (see Figure 2). The liquid material to be distilled is fed in the evaporation wall. The evaporation and condensation surfaces are kept at constant temperatures T_{w1} and T_{w2} , respectively. Due to the low pressure inside the separator, a falling film (without boiling) is formed and the concentration and temperature profiles (see Figure 3) of the most volatile compounds decrease in the axial and radial directions.

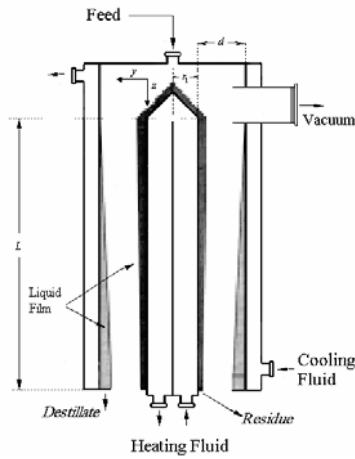


Figure 2. The short-path evaporator

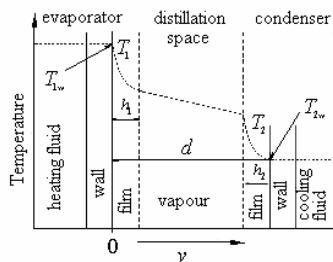


Figure 3. Temperature profile.

Mathematical Model

Let consider the liquid films on the evaporation and condensation walls are much thinner than the corresponding cylinder diameters then rectangular coordinates can be used. The mathematical model for the short-path evaporator under steady state comes from momentum, energy and mass balances for both evaporation and condensation films as follows [3].

Momentum balance

In most cases of short-path evaporation, the evaporating liquid is highly viscous and hence the Reynolds numbers are small. The Navier-Stokes equation (at steady state) for laminar regimen describes the velocity profile (v) of falling film

$$v(z) \frac{\partial^2 v(y, z)}{\partial y^2} = -g \quad (1)$$

This has the following boundary conditions

$$v(0, z) = 0, \quad v(h, z) = v_{\max} \quad (2)$$

Where v is the velocity, g is the gravity constant, and y and z are the radial and axial coordinates respectively.

Energy balance

The temperature (T) profile in the falling film is given by the equation

$$v(y, z) \frac{\partial T(y, z)}{\partial z} = \frac{\lambda}{\rho C_p} \left[\frac{\partial^2 T(y, z)}{\partial y^2} + \frac{\partial^2 T(y, z)}{\partial z^2} \right] \quad (3)$$

With boundary conditions

$$T(y, 0) = T_F \quad (4a)$$

$$T(0, z) = T_{w1} \quad (4b)$$

$$\lambda \frac{\partial T(y, z)}{\partial y} \Big|_{y=h_1} = \Delta H^{vap} \cdot k \quad (4c)$$

Where λ , ρ , C_p , ΔH^{vap} are the thermal conductivity, density, thermal capacity and heat of evaporation of the multicomponent mixture respectively.

Mass balances

The composition (C_i) profiles for each component are calculated from the diffusion equation

$$v(y, z) \frac{\partial C_i(y, z)}{\partial z} = D_i \left[\frac{\partial^2 C_i(y, z)}{\partial y^2} + \frac{\partial^2 C_i(y, z)}{\partial z^2} \right], \quad i = 1, \dots, N \quad (5)$$

Where D_i is the diffusion coefficient for the i -th component. The boundary conditions for Eq. (5) are

$$C_i(y, 0) = C_{i,0} \quad (6a)$$

$$\frac{\partial C_i(0, z)}{\partial y} = 0 \quad (6b)$$

$$D_i \left. \frac{\partial C_i(y, z)}{\partial y} \right|_{y=h_i} = I_i(z) \quad (6c)$$

Rate of evaporation

The flow rate I_i for each component is describe by the continuity equation

$$\frac{\partial I_i(z)}{\partial z} = -2\pi \cdot R \cdot k_i, \quad i = 1, \dots, N \quad (7)$$

Where the effective rate of evaporation (k_i) is calculated through a modified Langmuir-Knudsen equation [11]

$$k_i = \frac{P_i^{vap} T_s(z)}{\sqrt{2\pi R_g M_i T_s(z)}} \left(\frac{P}{P_{ref}} \right) \left\{ 1 - (1-F) \left[1 - e^{-h/(\kappa\beta)} \right]^n \right\}, \quad i = 1, \dots, N \quad (8)$$

It contains a factor (P/P_{ref}) for correcting the vacuum pressure of operation, as well as a correction that takes into account the anisotropic properties of the vapor, where β is the mean path of vapor molecule, h is the distance between evaporator and condenser, n is the number of intermolecular collision before the vapor reaches the isotropic state, F is the surface ratio and κ is the anisotropy of the vapor phase given by

$$F = \frac{A_k}{A_k + A_v}, \quad \log \kappa = 0.2F + 1.38(f + 0.1)^4 \quad (9)$$

A_k and A_v are the condensation and evaporation areas, respectively. The effective rate of evaporation [Eq. (7)] also depends on some mixture properties (the vapor pressure p_i^{vap} and molecular weight M_i of each compound) as well as on design parameters (the radius of the evaporator inside cylinder R and the surface temperature T_s).

Thickness film

Finally, an important variable of interest is the thickness film (h_i) along the evaporator height that is calculated as follows [11]

$$h_i(z) = \sqrt[3]{\frac{3v}{2\pi \cdot R \cdot g \cdot c}} I_i(z) \quad (10a)$$

Where

$$I(z) = \sum_{i=1}^N I_i(z) \quad (10b)$$

$$c = \sum_{i=1}^N C_i(z) \quad (10c)$$

Strategy of Solution

In order to solve the evaporator model that involves PDAEs [Eqs. (1)-(10)], Method of lines using centered finite difference is applied considering an M -point discretization scheme for the radial coordinate “ y ” as shown in Figure 4 [12]. Good performances can be achieved with a minimum value of $M = 10$. Afterwards, the resulting DAE system is solved through ICAS-MoT using the Backward Difference Formula method. One particular advantage of the integrated ICAS is that all physicochemical properties are called from modules that can be easily integrated to the short-path evaporator model. Therefore a large number of chemical products can be studied very fast and with minimum effort.

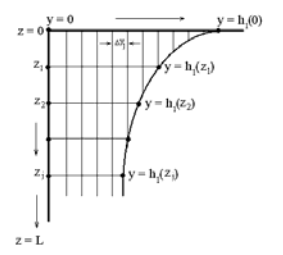


Figure 4. Discretization scheme.

Model evaluation

Case study: a pharmaceutical mixture

Consider the process production of a drug where after the reaction stage, the active molecule of the active pharmaceutical ingredient (API) is formed. Then the resulting liquid mixture composed of six heat sensitive compounds (that are called A, B, C, D, E and F for confidentially reasons) needs to be purified. A is the lightest and more volatile compound and F is the one with the highest boiling point. The role of the short-path evaporator is to separate the active molecule (form mainly by C, D and E) together with the inert component F from the feed multi-component mixture coming from the reactor.

Model analysis

The classification of variables and model equations was done through ICAS-MoT as follows: (a) there are 128 equations sorted as 17 ODEs, 1 implicit and 110 explicit AEs, and (b) 306 variables sorted as 17 Dependent, 1 Unknown, 4 known, 174 Parameters, and 110 Explicit. Afterwards, the incidence matrix, degrees of freedom and non-singularity were verified to ensure that the problem was not ill-posed before going to the solution step.

Simulation results

The feed flows as well as experimental and calculated flows of the distillate and residual are reported in Table 2, where it can be seen that the model is able to predict quite satisfactory the exit flow rates.

Table 2. Experimental and calculated flow rates of distillate and residual.

| Compound | Experimental flows (kmol/h) | | Calculated flows (kmol/h) | |
|----------|--------------------------------|-----------------------|------------------------------|-----------------------|
| | Residual | Distillate | Residual | Distillate |
| | I_R | I_D | I_R | I_D |
| A | 0.0 | 6.11×10^{-5} | 0.0 | 6.11×10^{-5} |
| B | 0.0 | 1.22×10^{-5} | 0.0 | 1.22×10^{-5} |
| C | 4.46×10^{-2} | 2.61×10^{-3} | 4.46×10^{-2} | 2.61×10^{-3} |
| D | 1.88×10^{-4} | 2.09×10^{-6} | 1.87×10^{-4} | 3.07×10^{-6} |
| E | 2.16×10^{-3} | 6.79×10^{-6} | 2.14×10^{-3} | 2.46×10^{-5} |
| F | 6.66×10^{-4} | 0.0 | 6.66×10^{-4} | 0.0 |

As the chemical product (C, D, E and F) is obtained as the residual in the short-path evaporator, then the surface velocity, temperature, thickness and some flow rates are shown for the evaporating film in Figures 5 and 6. The rise in temperature (Figure 5) is related to the evaporation of compounds A and B as can be seen in Figure 6. In fact, A and B are the main compounds that are evaporated from the mixture and are obtained as distillate product. The surface velocity (Figure 5) has a rapid increase at the first part of the evaporator axial position achieving a maximum point, and then decreasing slightly due to the decrease of the total evaporation rate. Figure 6 also shows the dependence of the film thickness throughout evaporator cylinder axis. Film thickness decreases with the increasing surface temperature due to evaporation. Both film surface temperature and film thickness turn asymptotic as soon as a constant film thickness has formed.

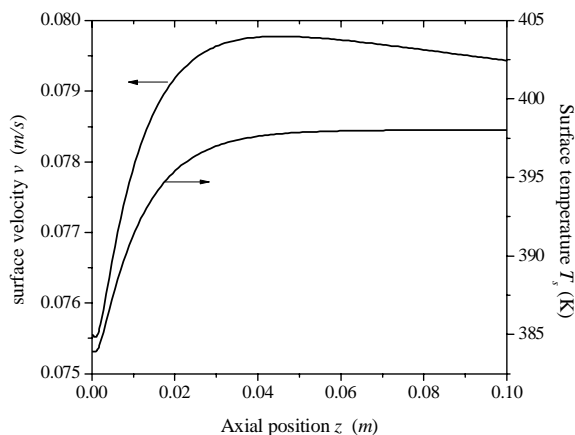


Figure 5. Surface velocity and temperature.

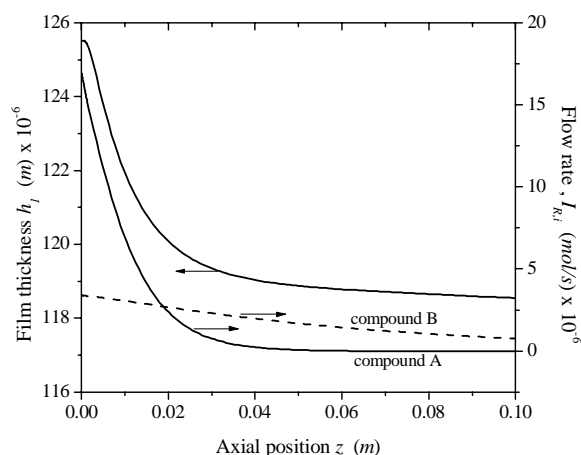


Figure 6 Film thickness and flow rate for compound A.

Conclusions

A short-path evaporator model has been presented for the purification of multi-component mixtures. The modeling methodology presented illustrates how the design and analysis aspects of a short-path evaporator are related to the purity and stability of the chemical product and the corresponding conditions of operation. The process flexibility allows designing the separator in such way that the mixture to be separated can be fed either in the cylindrical body or in the outside cylinder wall, depending on whether the chemical product need to be recovered as a distilled product or concentrated as the heavy residue. On the other hand, the results also highlight the importance of a general-purpose and easy to use modeling toolbox for computer-aided design and analysis of complex process operations.

References

1. M. Sales-Cruz, R. Gani, in: S.P. Asprey, S. Macchietto (Eds.), Computer-Aided Chemical Engineering, vol. 16: Dynamic Model Development, Elsevier, Amsterdam, 2003, 209-249.
2. I.V. Skiadas, H.N. Gavala, G. Lyberatos, Water Res., 34 (2000) 3725-3736.
3. J. Lutišan, J. Cvengroš and M. Micov, Chem. Eng. J., 85 (2002) 225-234.
4. K.W. Lawson, D.R. Lloyd, J. Membrane Sci., 120 (1996) 111-121.
5. A. Silva-Beard, A. Flores-Tlacuahuac, Ind. Eng. Chem. Res., 38 (1999) 4790-4804.
6. J. Dimitratos, C. Georgakis, S. El-Aasser, A. Klein, Comp. Chem. Eng., 13 (1989) 21-33.
7. J.P. Congalidis, J.R. Richards, W. H. Ray, AIChE J., 35 (1989) 891-907.
8. J. J. Downs, E.F. Vogel, Comp. Chem. Eng., 17 (1993) 245-255.
9. T.F. Edgar, D.M. Himmelblau, Optimization of Chemical Processes, McGraw Hill, New York, 1998.

10. K. Hangos, I. Cameron, Process Modeling and Model Analysis. Academic Press, San Diego, CA, 2001.
11. Z. Kawala, K. Stephan, Chem. Eng. Techn., 12 (1989) 406-413.
12. J. Cvenegroš, J. Lutišan, M. Micova, Chem. Eng. J., 78 (2000) 61–67.

List of publications of M. Sales-Cruz

13. M. Sales-Cruz, R. Gani, in: S.P. Asprey, S. Macchietto (Eds.), Computer-Aided Chemical Engineering, vol. 16: Dynamic Model Development, Elsevier, Amsterdam 2003, 209-249.
14. M. Sales-Cruz, I. Skiadas, I., R. Gani, Proceedings ECCE-4 (4th European Congress in Chemical Engineering), EFCE-ANCHE Ed., Spain (2003), Vol. 9.
15. M. Sales-Cruz, R. Gani, I. Skiadas, Proceedings AIChE annual meeting, San Francisco, CA, USA , 2003.
16. M. Sales-Cruz, R. Gani, Proceedings ESCAPE-14, Lisbon, Portugal, 2004.
17. M. Sales-Cruz, R. Gani, Proceedings AMIDIQ, Jalisco, Mexico, 2004.
18. M. Sales-Cruz, R. Gani, Proceedings FOCAPD'2004, Princeton, NJ, USA, 2004.
19. M. Sales-Cruz, R. Gani, Proceedings AIChE annual meeting 2004, Austin, Texas, USA , 2004.
20. M. Sales-Cruz, T. Lopez-Arenas, R. Gani, Proceedings AIChE annual meeting 2004, Austin, Texas, USA, 2004.
21. M. Sales-Cruz, R. Gani, Proceedings CHISA'04, Prague, Czech Republic, 2004.
22. M. Sales-Cruz, R. Gani, Proceedings Product Technology, Product design and Engineering, Groningen, The Netherlands, 2004.
23. M. Sales-Cruz, R. Gani, Proceedings, accepted in ESCAPE-15, to be held in Barcelona, Spain, 2005.
24. T. Lopez-Arenas, M. Sales-Cruz, R. Gani, accepted in ESCAPE-15, to be held in Barcelona, Spain, 2005.
25. T. Lopez-Arenas, M. Sales-Cruz, R. Gani, accepted in 5th World Congress in Chemical Engineering, to be held in Glasgow, UK, 2005.
26. T. Lopez-Arenas, M. Sales-Cruz, R. Gani, submitted to Chem. Eng. Sci., 2004.



Jakob Sloth

Address: CHEC, Dept. of Chemical Engineering
Building 229, Office 126
Technical University of Denmark
Phone: +45 4525 2923
Fax: +45 4588 2258
e-mail: jsl@kt.dtu.dk
www: www.chec.dtu.dk

Supervisor(s): Søren Kiil
Anker Degn Jensen
Poul Bach, Novozymes A/S

Ph.D. Study
Started: September 2004
To be completed: August 2007

Formation of Enzyme Granules by Spray Drying

Abstract

The droplet drying process which takes place inside a spray dryer is investigated using both a modelling based and an experimental approach. The modelling is carried out to quantify the phenomena controlling the drying kinetics and to achieve a fundamental understanding of morphology formation. Experiments are conducted to support the theoretical approach and validate developed models. The knowledge obtained by the investigations is used to meet product requirements such as mechanically stable particles and a narrow particle size distribution when spray drying enzyme containing slurries.

Introduction

Spray drying is of one several methods used in industry for conversion of a solution or slurry into a dried powder product. Spray drying is a flexible process which allows production of powders with many different properties such as a special particle size, particle morphology and residual solvent content. Enzymes for detergents are subject to spray drying because product handling is easier and enzyme stability is better than in liquid formulations.

In production of enzyme granules it is crucial that the formed particles have a low porosity to provide mechanical stability. Further, the particles must have a narrow size distribution to prevent segregation in the final detergent product. These particle properties must be obtained while avoiding thermal enzyme deactivation due to the high temperatures which exist in the spray dryer.

Though spray drying is used in numerous industrial applications fundamental understanding of drying kinetics and morphology formation remains limited.

Spray Drying and Single Droplet Drying

In spray drying a slurry or solution is fed to the drying chamber where it is atomized (figure 1). The formed droplets are mixed with a hot gas and the contact between the droplets and the gas causes the solvent of the droplets to evaporate, leaving dried particles. These particles may subsequently be separated

from the gas stream, using a cyclone or a particle filter [1].

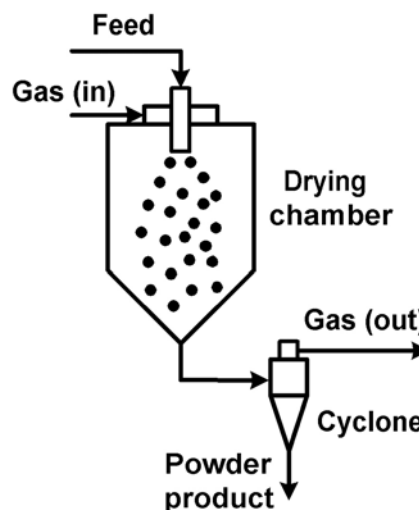


Figure 1: Spray dryer

Droplets drying in a spray dryer undergo different periods with different rates of evaporation and droplet temperatures. Changes in droplet mass and temperature during the course of drying is shown on figure 2.

After atomization the droplet experiences initial heating followed by a period where the evaporation is fast because the solvent is readily available at the droplet surface. As drying progresses the droplet shrinks

and the concentration of solute at the droplet surface increases. The concentration is a significant resistance to evaporation and the rate of mass change decreases. This gives rise to considerable droplet heating [2].

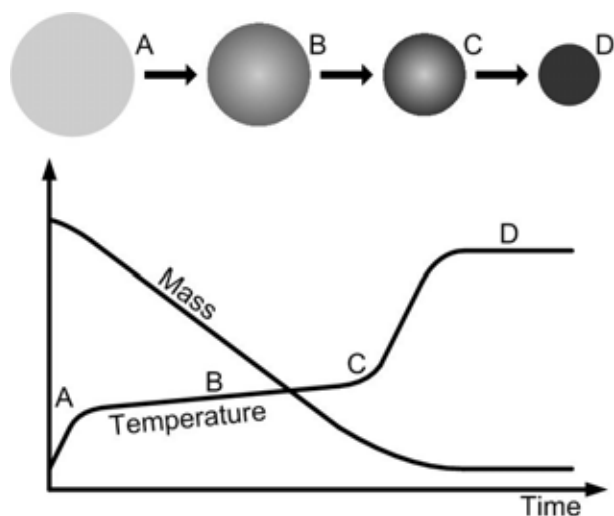


Figure 2: Mass and temperature change during the course of drying for a droplet in a spray dryer. The formation of a solid dense particle is shown – darker color indicates higher concentration.

The droplet drying process is complex and several different morphologies may form depending on drying conditions and the nature of the droplet (figure 3).

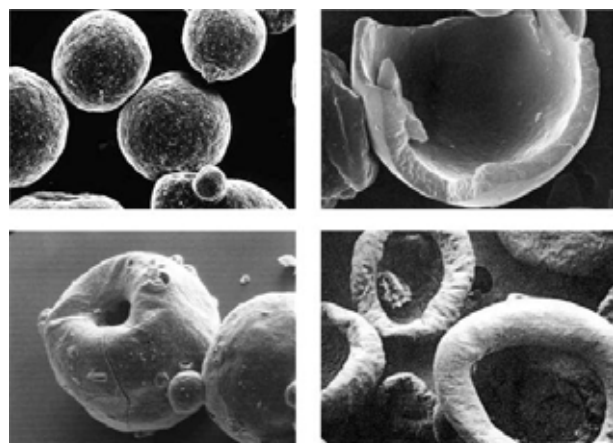


Figure 3: Examples of different morphologies of spray dried particles [3].

Specific Objectives

In this PhD project the effect of formulation on the drying kinetics and morphology formation of enzyme-containing granules during spray drying is investigated and modelled. This knowledge is subsequently used in the design of improved granules (*i.e.* stable particles with uniform size distribution). Also, methods to avoid enzyme deactivation are suggested.

Experimental Work

A novel apparatus has been built in a previous PhD study (Kåre Jørgensen), which allows well-controlled spray drying experiments to be performed. In the initial investigations simplified enzyme granule formulations (*i.e.* granules containing the main compounds needed for establishing a representative drying behaviour) are used. The various effects of the individual compounds and their potential interactions are mapped. Subsequently, full commercial formulations are used to analyse the consequences on the particle formation process. Further, the influence of drying conditions and formulation on enzyme activity is investigated.

Modelling

The experimental investigations from the laboratory are supplemented by theoretical modelling studies. The various phenomena controlling the drying process are quantified and the most important ones identified. Coupling the thermodynamic properties of the formulation mixture is important in order to achieve a fundamental understanding of drying kinetics and morphology formation. Based on model simulations, possible solutions for formulation changes are proposed.

Acknowledgements

The Novozymes BioProcess Academy is acknowledged for financial support.

References

1. K. Masters, *Spray Drying Handbook*, 5th ed., Longman Scientific and Technical, 1991.
2. S. Nestic & J. Vodnik, *Kinetics of Droplet Evaporation*, *Chem. Eng. Sci.*, 46, 1991, pp. 527-537.
3. D. E. Walton and C. J. Mumford, *Spray Dried Products - Characterization of Particle Morphology*, *Trans IChemE*, 77, 1999, pp. 21-38.



Vipasha Soni

Address: CAPEC, Dept. of Chemical Engineering
Building 227, Office 264
Phone: +45 4525 2910
Fax: +45 4588 2258
e-mail: vso@kt.dtu.dk
www: www.capec.kt.dtu
Supervisor(s): Rafiqul Gani
Gunnar Jonsson
Jens Abildskov

Ph.D. Study
Started: November 2004
To be completed: October 2007

Modeling and Design of Chemically Formulated Products

Abstract

The project in general is about the development of a computer aided method for identification, design and modeling of “intelligent” multifunctional chemically formulated products. The products in this case are the polymeric membranes that could be used for the membrane based separation processes. The modeling issues will deal with the integration of property models to the more general process operation models as well as the product application models.

Project Description

The project revolves around the design of polymeric membranes and the design/analysis of various separation processes where they are typically used. A homogeneous, non porous polymeric membrane is a semi-permeable barrier, which separates two phases, and filters various components of different sizes selectively. While a porous membrane is just a filter that separates components by a sieving mechanism or diffusion kinetics determined by the component size, the pore size, and overall porosity.

It is proposed to develop separation models for different membrane based separation processes. A part of project includes designing of the polymers for a given separation in terms of the properties of these polymers, which would need the development of models for the estimation of needed properties of the polymer membrane. The focus is on developing a systematic approach to deal with membrane separation processes in product – process development. This could be achieved if a systematic framework for design and analysis of membrane based process is developed that is able to propose the candidate polymer for the membrane that could be used for a desired separation with proper justification and validation.

Initially, two types of problems are proposed to be handled. The first type deals with designing only the functional part of the separation process. Polymer used for the system is essentially fixed. A model would be developed for a membrane based separation system that gives the degree of separation for a given fixed (selected) polymer and a given mixture to be separated. This would also need some experimental data to

validate the models developed. The separation process that would be studied first in this kind of problem is Membrane distillation.

Another type of problem, which is more complete in itself, would include both the designing of the separation system and the design of the membrane that needs to be used. Here the polymer that could be used is a variable and would be chosen based on the mixture to be separated. The strategy would be to check for the best polymer candidates among all the possible polymers for a given mixture based on both the degree of separation and the obtained fluxes. Once the appropriate polymer is identified then the problem essentially reduces to designing of the separation process. Models would also be developed to validate if the polymer so found actually can perform the separation to a desired degree. The separation processes that would be included for this analysis are membrane based gas separations and pervaporation. For both these membrane processes the property of the polymer that must be calculated in order to design it is the permeability for which the models would be developed.

The first type of problem could be used for already existing industries and it could help the operator in deciding upon the value and effect of certain variable parameters like temperatures, pressures, flowrates etc. for a better performance. The solution could also be used to find/analyze alternatives to current conventional separation techniques (such as distillation).

The other problem is proposed to have its applications where a new process is planned to be established. Here also, better and sustainable alternatives to currently used separation techniques are being sought.

The later stage of the project would deal with the formulations of the basic polymeric membranes that would enhance the performance and would lead to improved results. Formulations could be both of the system that needs to be separated or a copolymer (which is a blend of two polymers) or a structural polymer (a polymer where the repeat units are arranged in a particular manner to improve the performance).

The schematic overview of the project is given below in Figure 1 and the various polymer based membranes and their applications in separation processes is given in the Table 1.

References

1. Osada Y., Membrane Science and Technology, 1992, New York, Marcel Dekker
2. Baker R., Membrane Technology 138 (2001) 5-10

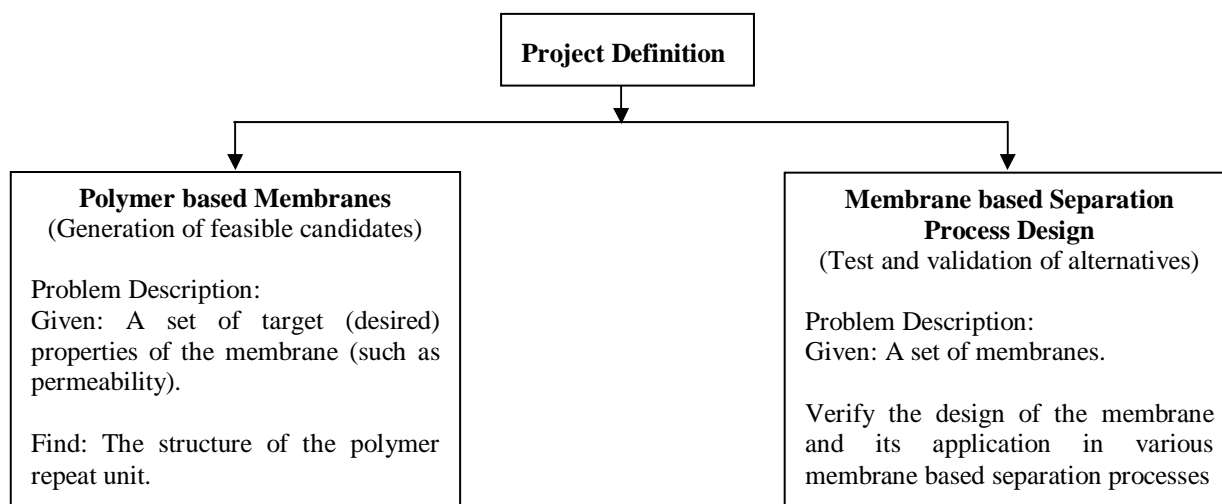


Figure 1: Schematic Overview of the project

| | Types of polymer based membranes | Separation processes where applicable |
|----|---|--|
| 1. | Cellulose acetate, Polysulfone, Silicon rubber, Polyimide, Polysulfone amide, Polyphenylene oxide, Polyacrylate, Alkylsulfonylethylated polyvinyl - alcohol. | Membrane based gas separations |
| 2. | Sulfonated polyethylene membranes, Polyacrylic acid, Poly vinylpyrrolidone, Polyvinyl alcohol, Poly dimethylsiloxane, Poly substituted acetylene, Poly tetraflouroethylene-poly vinylpyrrolidone. | Pervaporation |
| 3. | Cellulose nitrate or acetate, polyvinylidene difluoride, polyamides, Polysulfones, Polycarbonate, Polypropylene, Poly tetraflouroethylene, Teflon, Polyethylene. | Microfiltration |
| 4. | Polysulfones, Poly ethersulfone, Polyimide, Cellulose acetate, Poly acrylnitrile, Poly vinylalcohol, Poly phenylene sulfide, Poly propylene, nylon – 6, Poly tetraflouroethylene, Poly vinyl chloride | Ultrafiltration |
| 5. | Polysulfones, Polyamides, Polyureas | Reverse Osmosis |
| 6. | Poly tetraflouroethylene, Poly ethylene, Poly propylene, polyvinylidenedifluoride, Cellulose nitrate. | Membrane Distillation |

Table 1: Polymer based membranes and their applications



Nùria Muro Suñé

Address: Søltofts Plads, Build. 227
Phone: +45 4525 2805
Fax: +45 4593 2906
e-mail: nms@kt.dtu.dk
www: www.capec.kt.dtu.dk

Supervisor(s): Rafiqul Gani

Ph.D. Study

Started: August 2002
To be completed: August 2005

Prediction of the Solubility and Diffusion Properties of Pesticides in Polymers

Abstract

A model capable of predicting the release of an Active Ingredient (AI) from a specific device would be very useful in the field of pesticide controlled release technology for design purposes. For the release of an AI from a microcapsule a mathematical model is briefly presented, as an introduction to the principal objective of this work, which is the prediction of the model parameters (diffusion and partition coefficients). We focus here on the estimation of the partition coefficient of the AI in the polymer through activity coefficients that are estimated with a group-contribution model for polymers (GC-Flory EoS). This model is extended to suit the needs of the complex pesticide molecules. The extension of the GC-Flory EoS model, together with a case study dealing with the release of a pesticide from a microcapsule is presented.

Introduction

Controlled release technology was initially developed by the pharmaceutical industry with the aim of producing oral drug forms that could keep an effective drug level in the body avoiding, at the same time, the side effects caused by the administration of high doses of these drugs. Later on this technology was taken up in the pesticide industry for the controlled release of pesticides. The improvement in this field consists of an extension of the crop protection with respect to the conventional methods (for example, spraying the pesticide solution over the crop), together with a reduction of the amount of pesticide used and the number of applications needed (optimization of the dose). Another advantage is the fact that the encapsulation of the pesticide diminishes the environmental hazards and the human toxicity.

A great effort has been made up until now in developing mathematical models to describe a wide variety of existing controlled release devices. These systems consist generally of a pesticide encapsulated or incorporated within a polymer membrane, therefore the most critical properties of these models are the ones that relate to the pesticide and the polymer, that is, the solubility of the pesticide in the polymer and its diffusivity through the membrane.

The objective of this work is to convert the available controlled release models to their predictive forms in order to aid and simplify the product design process. The first step is the development of a property

model for the prediction of the solubility of the pesticide in the polymer that together with a microcapsule model [1] can describe the release behavior of the pesticide from a fabricated device for different pesticide-polymer combinations.

Modeling of controlled release

There is a wide variety of controlled release devices for pesticide delivery to the environment. Here, only the microcapsule type is considered as this is the device of interest in this study. A microcapsule consists of an active ingredient that is enclosed within a polymer membrane, as shown in Figure 1. There are several commercial examples of these reservoir systems containing encapsulated pesticides for different application purposes [2].

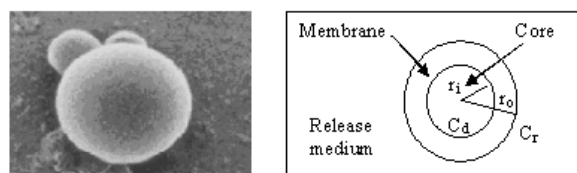


Figure 1. Microcapsule picture (left) and schematic representation (right).

In an earlier work a mathematical model was developed [1] to describe the delivery of an Active Ingredient (AI) from a microcapsule. This model considered a normal distribution of the size of the

microcapsules (Eq. 1), to account for the different microcapsule radii (r), with a mean value of the radius μ and a specified standard deviation σ . The controlled release was modeled using the equations for non-constant activity source (Eqs. 2 and 3, [3]), derived from Fick's law of diffusion, that provided the concentration dependence with time. More details of the model are given in [1], where the model has been solved and validated with experimental data.

$$f(r; \mu; \sigma) = \int_{-\infty}^r \frac{1}{\sqrt{2\pi}\sigma} \exp\left(-\frac{(r-\mu)^2}{2\sigma^2}\right) \quad (1)$$

$$\frac{dC_d}{dt} = \frac{DA}{V_b h} K_{m/d} \left[1 - \left(\frac{K_{m/r}}{K_{m/d}} + \frac{V_b}{V_d} \right) C_{d,initial} \times \exp\left(-\frac{DA}{h} \left(\frac{V_d K_{m/r} + V_b K_{m/d}}{V_b V_d} \right) t \right) \right] \quad (2)$$

$$\frac{dC_r}{dt} = \frac{DA}{V_b h} K_{m/d} C_{d,initial} \exp\left(-\frac{DA K_{m/d}}{V_b h} \left(\frac{K_{m/r}}{K_{m/d}} + \frac{V_b}{V_d} \right) t \right) \quad (3)$$

Through a careful study of the model equations it has been observed that there are two parameters that are critical for the applicability of the model to a wide range of products (different microcapsules and pesticides). These two parameters are the diffusion coefficient and the partition coefficient. In this paper, a predictive model for pesticide partition coefficients is presented.

Partition coefficient

The partition coefficients ($K_{m/d}$ and $K_{m/r}$), are defined according to Eq. 4. In a general manner, these partition coefficients can be represented by $K_{p/solv}$, where the membrane (m) is a polymer (p), and the donor (d) and release medium (r) are solvents (solv).

It can be seen from Eq. 4 that values of infinite dilution activity coefficients of the AI (1), $\Omega_{1,solv}^\infty$ and $\Omega_{1,p}^\infty$ are needed. These can be obtained from a suitable predictive model for activity coefficients.

$$K_{p/solv} = \frac{\Omega_{solv}^\infty}{\Omega_p^\infty} \quad (4)$$

The solubility of AI's in solvents has been widely studied (being an essential part of formulation design), thus the activity coefficient of the AI in the solvent can generally be calculated from experimental data. In the case of AI solubility in polymers there is still a lack of experimental data. Therefore, our interest is focused on the estimation of the activity coefficients of AI's in polymers. For this purpose a group-contribution model (GC-Flory EoS, [4]) has been chosen, with an existing parameter table that provides accurate and predictive results, which can be further extended in order to

include the complex pesticide molecules. A test of the applicability of the GC-Flory EoS model to complex drug molecules (comparable to pesticide structures) has been reported elsewhere [1].

GC-Flory EoS model

The GC-Flory EoS ([5], [4]) is a group-contribution method based on a modified form of the Flory equation of state for polymer systems [6]. In this paper the revised model form of the GC-Flory EoS [4] is used. The equations of this model can be found in [4] and therefore, not given here.

The GC-Flory EoS model has certain advantages over other similar polymer models, such as the Entropic-FV [7] or the UNIFAC-FV [8] that need precise data of the density of both solvent and polymer at the studied temperature. The GC-Flory EoS, on the other hand, does not need pure component or mixture properties for the calculation of the activity coefficients apart from the molecular structure of the AI and the polymer repeat unit.

At the same time as being simple, it provides good qualitative predictions for all kinds of compounds, as it has been shown previously [9], [10].

For the extension of the GC-Flory EoS in order to include the pesticide (AI) molecules, some new groups have been introduced. The group definition is based on the UNIFAC group description, and the group-parameter estimation is done following the procedure suggested by [4], where experimental data for thermal expansivities and enthalpies of vaporization are used for estimation of the pure component parameters (C_i and ϵ_{mn}), while VLE data of low molecular weight compounds is used to estimate the group interaction parameters (ϵ_{mn}).

GC-Flory EoS model: Extension of the parameter table

In this section the new groups and the estimated parameters (C , ϵ_{mn} and ϵ_{mn}) are presented in Tables 1 and 2. The new group parameters have been estimated through experimental data involving low molecular weight compounds, not polymers ([11], [12], [13] and [14]). The particular set of compounds and their corresponding groups are considered because these groups are needed for the pesticides of interest, in this case the Pyrethroids (which are relevant for controlled release formulations).

Table 1. Group R_n , Q_n and C values of the GC Flory EoS for the new groups

| Main group | Subgroup | R_n | Q_n | $C_{T0,n}$ | $C_{T,n}$ | C_n^0 |
|------------|----------|--------|-------|------------|-----------|---------|
| aC-O | aC-O | 0.6091 | 0.360 | -0.2303 | -201.8 | -0.9068 |
| aC-OH | aC-OH | 0.8952 | 0.680 | -0.2628 | -133.5 | 0.1161 |
| Cl-(C=C) | Cl-(C=C) | 0.7910 | 0.724 | -0.1804 | -5.7 | 0 |

Table 2. Group-Interaction Parameters ϵ_{mm} and ϵ_{mn} , Calories/q-unit

| | aC-O | aCOH | Cl-(C=C) |
|--------------------|--------|--------|----------|
| CH ₂ | 928.8 | 306.9 | 6.881 |
| aCH | 970.7 | 282.9 | -4.643 |
| CH ₂ CO | 732.8 | -356.9 | -41.85 |
| COO | -2638. | -390.5 | 5.956 |
| COOH | 239.9 | -173.1 | 86.13 |
| CH ₂ O | na | na | -112.8 |
| C=C | 1153. | 232.8 | -55.14 |
| CCl | 293.2 | 246.8 | 156.2 |
| CCl ₂ | na | na | na |
| CCl ₃ | na | na | na |
| CCl ₄ | na | 214.3 | -4.140 |
| ACCl | 456.8 | -395.1 | na |
| CH ₃ OH | 662.9 | -227.3 | 89.48 |
| OH | -1038. | na | 231.0 |
| H ₂ O | na | 566.0 | na |
| aC-O | -611.8 | 1261. | 4.36 |
| aCOH | | -1336. | na |
| Cl-(C=C) | | | -631.9 |

In order to test the new estimated parameters several activity coefficient calculations have been performed with solvent-polymer systems containing the new groups. In these systems the solvent represents the AI compound, given that no data of AI-polymer systems is currently available. The systems included in these calculations contain aromatic ether, phenolic and chlorinated hydrocarbon solvents, together with different acrylic, vinyl polymers, and polyethers. The results have been compared with experimental data ([15], [16] and [10]) in terms of plots of the logarithm of experimental values (Ω_{exp}) and the logarithm of the predicted values (Ω_{calc}), see Figure 2. In Table 3 the results in terms of absolute average percent deviations from experimental data (AAD%, Eq. 5) are presented for each of the new groups.

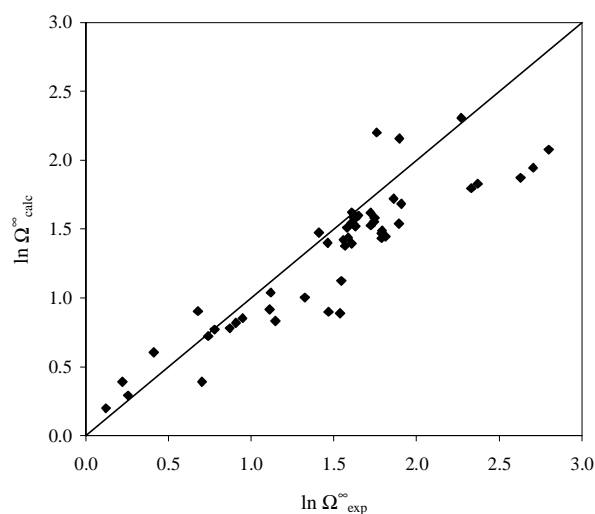


Figure 2. Comparison of experimental and predicted values for polymer systems

Table 3. Summary of the comparison of prediction and experimental results of infinite dilution activity coefficients for polymer-solvent systems

| | aCO | aCOH | Cl-(C=C) | Total |
|----------------|-------|-------|----------|-------|
| nr data points | 27 | 8 | 24 | 59 |
| % AAD | 19.97 | 25.09 | 31.41 | 25.32 |

$$\text{where: } AAD\% = \frac{1}{N} \sum_i^N \frac{|\Omega_{1,i,pred}^{\infty} - \Omega_{1,i,exp}^{\infty}|}{\Omega_{1,i,exp}^{\infty}} * 100 \quad (5)$$

From Figure 2 it can be observed that the model slightly under predicts the value of the infinite dilution activity coefficient (points below the diagonal). There are a few values that are over predicted (points above the diagonal). The results can be considered acceptable for the purposes of this work, due to the qualitatively good accuracy of the predictions (majority of points near the diagonal, not important scatter).

It is important to note that all the data used in the previous comparisons is at infinite dilution due to the lack of experimental finite concentration activity coefficient data for the groups of interest. The estimation of activity coefficients is usually better in the non-dilute region, thus the results presented are considered acceptable.

Note that none of the mixtures used for the test with polymers were included in the parameter estimation.

GC-Flory EoS model: Improvements in the aromatic ether group

The new estimated parameters have also been evaluated for aromatic ethers. Using the new group aC-O significant improvement could be achieved, see Figure 3 and Table 4, where the calculated results with (new groups) and without (old groups) the use of the new aC-O group is highlighted. The experimental data [10] contains different molecular weight Polystyrene at several temperatures.

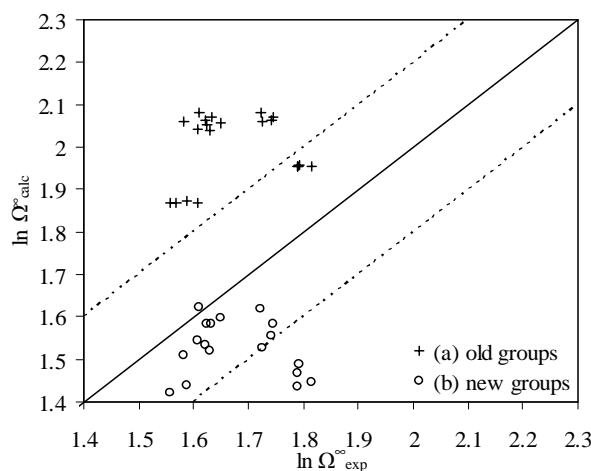


Figure 3. Comparison of estimation of solvent-polymer activity coefficients with the two different sets of parameters. Range of confidence (.....).

Table 4. Group description and error comparison with the two different sets of parameters

| | error in Ω^∞ | | Group description |
|---------|--------------------------|------|-----------------------------------|
| | AAD(%) | Abs. | |
| (a) Old | 40.13 | 2.10 | 1 CH ₃ O, 1 AC, 5 ACH |
| (b) New | 14.76 | 0.78 | 1 CH ₃ , 5 ACH, 1 aC-O |

$$\text{where: } Abs = \frac{1}{N} \sum_i^N |\Omega_{1,i,pred}^\infty - \Omega_{1,i,exp}^\infty| \quad (6)$$

Case study: Permethrin microcapsule

The case study involves a microcapsule device containing a pyrethroid insecticide (Permethrin [52645-53-1], see Table 5 and Figure Figure 4). Some of the advantages to be considered in having this insecticide encapsulated include the reduction of fish toxicity [19] and a longer biological effectivity. The insectically effective amount of Permethrin is 0.02-0.25 lbs/acre, whereas the maximum concentration of Permethrin (related to toxicity) is 18.5 mg of active ingredient/litre.

A microcapsule produced by interfacial condensation, with a polyester wall of 1 to 3 μm thickness that contains a core liquid insecticide solution, will be modeled as an example. The average size of the microcapsules is between 10 and 45 μm and they are delivered into the crop as an aqueous solution (1-50 % weight of microcapsules in water).

In this example we will use the GC-Flory model to estimate the infinite dilution activity coefficient of the Permethrin in a chosen sample polyester, poly(n-butyl methacrylate) (PBMA). A UNIFAC model (or available experimental data, as is the case, [20] is used to calculate the other infinite dilution activity coefficients (not related to polymers). These will then be used to calculate the partition coefficients needed in the microcapsule release model. Since no data is available for the diffusion coefficient of this insecticide in the polymer studied, a value will be assumed for this parameter in order to model the release of Permethrin from this microcapsule device.

With the partition coefficients now obtained from prediction (through the GC-Flory EoS model) and the rest of the variables (Table 6) from experimental data (except the diffusion coefficient, as mentioned above), the controlled release of Permethrin has been successfully modeled and presented in Figure 5. The results indicate that 99.99% of the Permethrin is released in 96 hours (i.e. 4 days), which is considered a long enough period of time for controlled release devices.

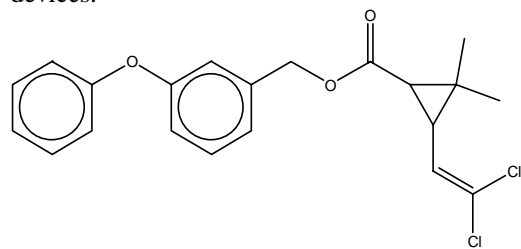


Figure 4. Molecular structure of Permethrin

Table 5. Group representation of Permethrin

| Times | Subgroup | Main Group |
|-------|-----------------|-----------------|
| 2 | CH ₃ | CH ₂ |
| 1 | CH ₂ | CH ₂ |
| 1 | CH=C | C=C |
| 9 | aCH | aCH |
| 2 | aC | aCH |
| 1 | COO | COO |
| 1 | aC-O | aC-O |
| 2 | (C=C)-Cl | (C=C)-Cl |
| 2 | CH | CH ₂ |
| 1 | C | CH ₂ |

Table 6. Inputs for the microcapsule controlled release model

| Variable | Value |
|----------------------------|----------------------|
| Radius (m) | 5e-6 – 2.25e-5 |
| Wall thickness (m) | 2e-6 |
| K _{wall/core} | 2.083 |
| K _{core/receiver} | 1.73·10 ⁸ |
| D (m ² /s) | 1.0e-16 |

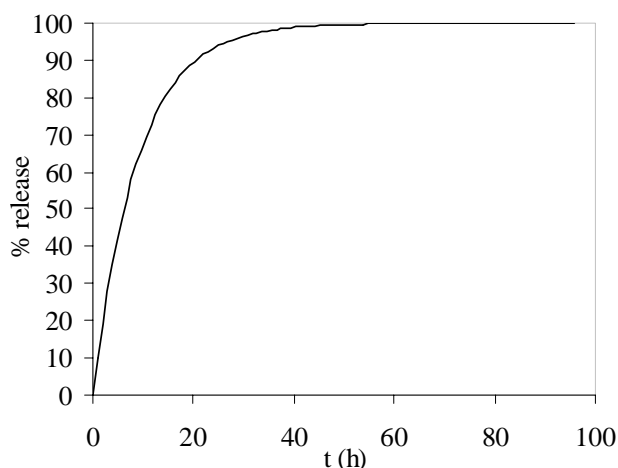


Figure 5. Results of release using the microcapsule model

Conclusions

A model for the release of an AI from a microcapsule device has been developed and validated. In order to make the model predictive the critical parameters have been identified. In this paper a procedure has been proposed to estimate the partition coefficient of the AI in the polymer through activity coefficients.

A group-contribution model (GC-Flory EoS) has been extended to include a wider range of molecules. The new parameters have been tested with all the experimental data available at the moment and the results are considered acceptable for the purposes of this work.

At the same time, some improvement has been observed in the applicability of the GC-Flory EoS, where the aromatic ethers are now better represented.

Finally, the microcapsule model has been successfully used to perform a simulation of the pesticide release involving the prediction of one of the model parameters.

Acknowledgements

The author would like to thank Syngenta for the funding provided for this work, as well as the advice and the interest received.

References

1. N. Muro-Suñe; R. Gani; G. Bell; I. Shirley, *Computer Aided Chemical Engineering* 18, A. Barbosa-Póvoa and H. Matos, 301-306, 2004.
2. H.B. Scher; M. Rodson; L. Kuo-Shin, *Pesti. Sci.* 54 (1998) 394-400.
3. J. Comyn, *Polymer permeability*, Elsevier, NY, 1985.
4. G. Bogdanic; Aa. Fredenslund, *Ind.Chem.Eng.Res.*, 33 (1994) 1331.
5. F. Chen; Aa. Fredenslund; P. Rasmussen, *Ind.Chem.Eng.Res.*, 29 (1990) 875.
6. P.J. Flory; R.A. Oriji; A. Vrij, *J.Am.Chem.Soc.*, 86 (1964) 3507.
7. G.M. Kontogeorgis; Aa. Fredenslund; D.P. Tassios, *Ind.Chem.Eng.Res.*, 32 (1993) 362.
8. T. Oishi; J.M. Prausnitz, *Ind.Chem.Res.Dev.*, 17 (1978) 333.
9. B. Lee; R.P. Danner, *Fluid Phase Equilibria*, 128 (1997) 97.
10. R.P. Danner; M.S. High, *Handbook of Polymer Solution thermodynamics*, Design Institute for Physical Property Data, AIChE, New York, NY, 1993.
11. G.M. Foco; S.B. Bottini; E.A. Brignole, *J.Chem.Eng.Data*, 37 (1992) 1.
12. J.Gmehling; U. Onken; W. Arlt; P. Grenzhauer; U. Weidlich; B. Kolbe; J. Rarey, *Vapor-Liquid Equilibrium Data Collection*, vol. I, Part 2d, DECHEMA. Chemistry data series, 1982.
13. D. Tiegs; J.Gmehling; A. Medina; M. Soares; J. Bastos; P. Alessi; I. Kikic., *Activity coefficients at infinite dilution*, vol. IX, Parts 1 and 2, DECHEMA. Chemistry data series, 1986.
14. M.A. Yañez; S.B. Bottini; E.A. Brignole, *Fluid Phase Equilibria*, 71 (1992) 85-98.
15. W. Hao; H.S. Elbro; P. Alessi, *Polymer solution data collection*. Part 2+3 (vol. 14), DECHEMA Chemistry data series, 1992.
16. Z.Y. Al-Saigh; P. Munk, *Macromolecules*, 17 (1984) 803-809.
17. J. Gross; G. Sadowski, *Ind.Chem.Eng.Res.* 40 (2001) 1244-1260.
18. J. Gross; G. Sadowski, *Ind.Chem.Eng.Res.* 41 (2002) 1084-1093.
19. G. Dahl; J. Simkin, *USpat* 4,670,246. Microencapsulated Pyrethroids, 1987.
20. Tomlin, C.D.S., *The pesticide manual*. 13th edition, British Crop Protection Council, Farnham, 2003.

List of Publications

1. Muro-Suñe, N., Gani, R., Bell, G., Cordiner, J., *Computer Aided Modeling of Pesticide Uptake in Plants for Pesticide Formulation and Design*, AIChE Annual Meeting, Indianapolis, 3-8 November 2002.
2. Muro-Suñe, N., Gani, R., *Extending property estimation methods to beyond their application range: property estimation for pesticide design*, ESAT-2003, 9-12 October 2003.
3. Muro-Suñe, N., Gani, R., Bell, G., Shirley, I., *Computer-aided and predictive models for design of controlled release of pesticides*, *Computer Aided Chemical Engineering* 18, A. Barbosa-Póvoa and H. Matos, 301-306, 2004.
4. Muro-Suñe, N., Gani, R., Bell, G., Shirley, I., *Predictive property models for use in design of controlled release of pesticides*, *Fluid Phase Equilibria* (accepted)
5. Muro-Suñe, N., Munir, A., Gani, R., Bell, G., Shirley, I., *A framework for product analysis: Modelling and design of release and uptake of pesticides*, ESCAPE-15 (submitted).
6. Muro-Suñe, N., Gani, R., Bell, G., Shirley, I., *Computer-aided and predictive models for design of controlled release of pesticides*, in DK2 conference, 2004.

**Mads Thaysen**

Address: Hallas Alle BM 3.12, 4400 Kalundborg
Phone: +45 3077 0256
Fax:
e-mail: madt@novozymes.com
www: www.capec.kt.dtu.dk

Supervisor(s): Sten Bay Jørgensen
Jørgen Petersen, Novo Nordisk A/S
Erik Steffensen, Novo Nordisk A/S

Ph.D. Study
Started: May 2001
To be completed: May 2004

Software Sensors for Monitoring Industrial Cultivation Processes

Abstract

A number of simple software sensors have been constructed for offline analysis and online monitoring of important cultivation variables. Using cultivation data from an industrial production site, 2 first principles engineering models and a data driven model were constructed for monitoring of the biomass and product concentration. More detailed first principles engineering models were constructed from cultivation data from pilot plant supporting online analysis and monitoring of cultivation process.

Introduction

For almost 2 decades Novo Nordisk A/S has used genetically modified organisms (GMO) in the industrial production of insulin. At Novo Nordisk A/S a continuous improvement of existing production processes as well as investigation and development of new processes for new products are carried out. The cultivation of the microorganism is only one of the many steps in the production line and what makes the cultivation step special and difficult to develop is the involvement of microorganisms, in this case a genetically engineered strain of *Sacchromyces cerevisiae*.

There is still a long way from successful genetically modifying a microorganism in the laboratory to obtaining optimal productivity and effectiveness in large scale industrial cultivations of that microorganism. Although many biological variables are being measured during a typical cultivation at Novo Nordisk A/S most of these variables are measured offline at a frequency that does not allow for detailed analysis of the state of the metabolism, and definitely not online, since the time delay between sampling and analysis are more likely days than hours. The cultivations are mostly evaluated on the productivity of the product and the biomass with only few attempts to provide a physiological explanation for variations in the cultivation data and offline measurements.

The industrial Ph.D. project was established on the desire to use more of the information available in the cultivation process data in order to monitor the state of the process and detect disturbances and upsets. Different types of models were to be tested in order to evaluate

the information content of the cultivation data and which type of model that best captured the important information.

Specific Objectives

The project was divided into two parts. The first part considered cultivation data from the production site and investigated what type of models that could be developed from the available cultivation information. It was found that the quality of the process data was not sufficient to support detailed modeling of the cultivation process, since the sampling frequency and the precision of measurement devices was not accurate enough. Therefore the second part of the project considered cultivation data from pilot plant cultivations carried out with the purpose constructing process models that could be applied at the production site.

Two types of models have been investigated in this study: first principle engineering (FPE) models and data driven (DD) models. The two modeling types are different in the way knowledge of the process is applied in the model identification. FPE models are largely constructed based on intrinsic process knowledge, using process data for parameter identification, while DD models are primarily constructed from the information in process data, where process knowledge is used to select the process variables used in the modeling.

Results from Modeling Production Data

A simple FPE model for online monitoring of the biomass concentration in an industrial bioreactor during fed-batch and continuous operation was constructed based on knowledge of process dynamics and the

physiology of the microorganism. Linking the ammonia flow rate used to maintain a constant pH in the bioreactor to the production rate of biomass yielded a simple equation to evaluate the biomass concentration. Examples of resulting estimates of the biomass concentration are illustrated in figure 1, where also offline measurements of the biomass concentration are shown.

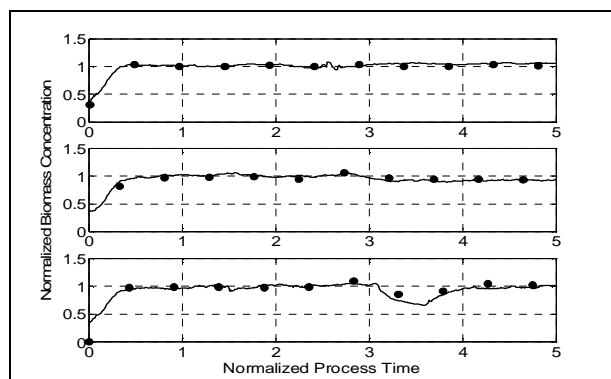


Figure 1: Normalized online estimate of biomass concentration (line) compared to offline measurements of cell dry mass measurements (●).

The FPE model for monitoring of the biomass concentration was extended in order to be used for estimating the concentration of the product, an insulin precursor. The extension was based on knowledge of the strategy behind the genetic engineering for transcription and expression of the recombinant product. Examples of the resulting estimate of the product concentrations are shown in figure 2, where also offline measurements of the biomass concentration are shown.

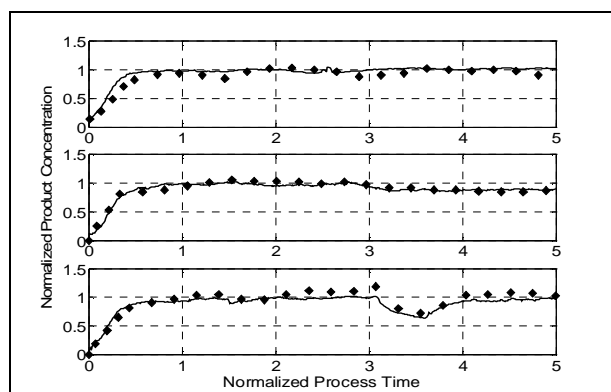


Figure 2: Normalized online estimate of product concentration (line) compared to offline measurements of product concentration (◆).

A data driven approach for modeling the product concentration in an industrial cultivation has also been tested. Using Multi-way Partial Least Squares Regression (MPLS-R) it was possible to construct a DD model for estimating the product concentration and furthermore provide an end point prediction of the production concentration. The MPLS-R was restricted to a fixed time period, comprising of the fed-batch

operation and the beginning of continuous operation until a time point where the process from experience was known to have settled into a stationary operation. Reasonable results were obtained that could be used both for analysis and monitoring of the production process. Examples of the results obtained using the MPLS-R approach is shown in figure 3.

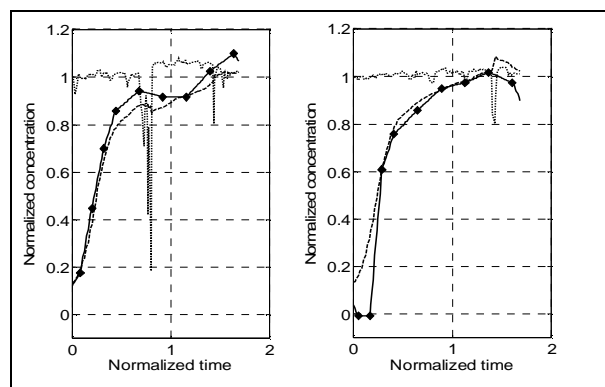


Figure 3: Estimations of product concentration profiles (dashed line), prediction of end point product concentration (dotted line) and linear interpolated offline measurements of product concentration (◆, full line).

Results from Modeling Pilot Plant Data

As mentioned in the objectives, it was found that the quality of cultivation data at the production site was not sufficient to support detailed modeling of the cultivation process. To provide data of higher quality a number of cultivations were conducted at the company's pilot plant facility, and a different production strain of *S. cerevisiae* was chosen to support the development of a new production process. The cultivations indeed provided a higher quality of data, but also revealed a rather surprising behavior in one of the operating regions. Using FPE modeling it was possible to construct a model, which was able to explain the surprising behavior as large conversions of acetate, at levels not normally seen in *S. cerevisiae*, as well as provide estimates of both acetate and biomass concentrations. This is shown in figure 4.

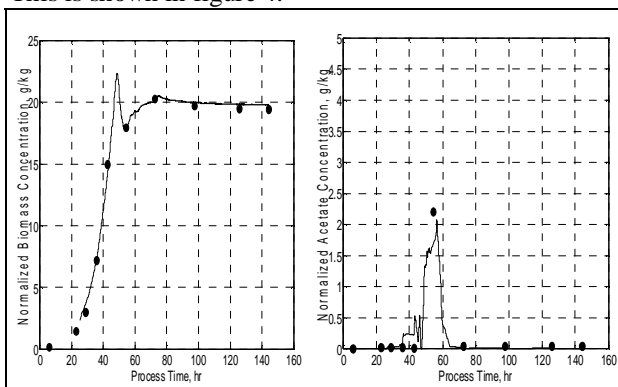


Figure 4: Normalized online estimate of biomass concentration (full line, left hand plot) and acetate concentration (full line, right hand plot) compared to offline measurements of concentrations (●).

With an online estimate of the biomass concentration at hand it is possible to evaluate the influence of variations in process data from the microorganism's point of view. Constructing a simple model of a network of metabolic flux pathways, it was possible to monitor the metabolic flux distribution online. This tool can be used by the process operator to evaluate the state of the microorganisms and subsequently provide information for control of the cultivation process. Figure 5 illustrates how the metabolic flux model indicates a severe change in the metabolic flux distribution during a process disturbance.

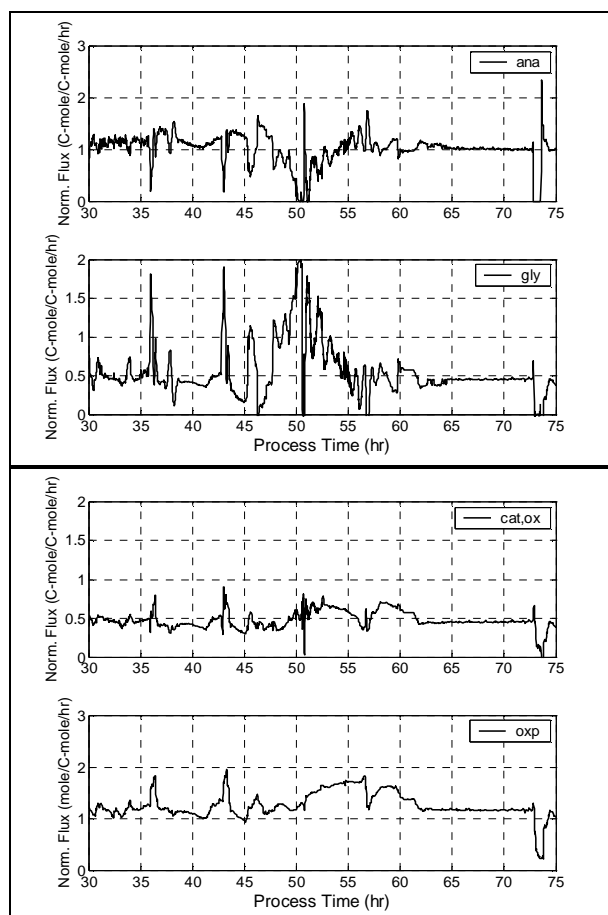


Figure 5: Examples of estimated intrinsic metabolic fluxes. Fluxes through anabolic (ana), glycolytic (gly), oxidative catabolism (cat,ox) and oxidative phosphorylation (oxp) pathways.

Finally an empirical model for the production of the product, which in this case is another insulin precursor, was constructed. The model provided reasonable online estimates of the product trajectory. The model furthermore highlighted how the specific productivity did not reach its stationary level until far into the continuous operation regime, which is a little surprising considering the strategy applied for the genetic engineering of the strain, where a constitutive promoter has been used for the expression of the product gene. An example of estimated product concentration trajectories are shown in figure 6.

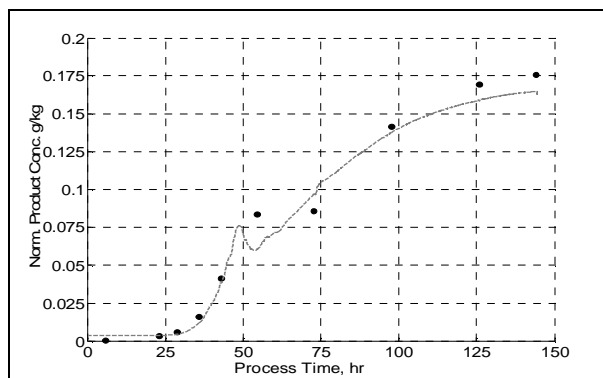


Figure 6: Normalized online estimate of the product concentration profile (line) compared to the offline measurements of the product concentration (●).

Conclusion

The results illustrate how simple process models can provide important detailed information of cultivation processes. At a production facility such information is vital for optimization. The process models can be used for: analysis of process performance, monitoring of current process operation and provide online information to be used in process scheduling for streamlining of the production line from cultivation to down stream processing thereby getting closer to achieving optimal productivity.

Although the purpose of constructing the process models is to provide information on the process state and performance, another important application of such simple process models is to highlight what can not be explained and what is not known/modeled. Recognition of lack of knowledge can help focusing on areas where research and development is most needed.

Acknowledgements

Mads Thaysen has been financially supported by the Academy of Technical Sciences, Denmark and BioProcess Laboratories, Novo Nordisk A/S.



Sylvain Verdier

Address: DTU - Building 229 – 2800 Lyngby
Phone: +45 4525 2877
Fax: +45 4588 2258
e-mail: syv@kt.dtu.dk
www: www.ivc-sep.kt.dtu.dk

Supervisor(s): Simon I. Andersen
Erling H. Stenby

Ph.D. Study
Started: May 2003
To be completed: May 2006

Experimental Study and Modelling of Asphaltene Precipitation Caused by Gas Injection

Abstract

CO₂ injection is a major part of the Enhanced Oil Recovery process (EOR). In miscible CO₂-EOR, the gas aims at decreasing the viscosity and, hence, at recovering more oil (around 10-15% of the original oil in place). As for the immiscible CO₂-EOR, the gas is only used to re-pressurize the reservoir and to push the oil towards the well. However, this injection seriously modifies the pressure and the composition of the oil and it can induce asphaltene precipitation. In this work, it was aimed at determining useful parameters such as the solubility parameter of the oil and the asphaltenes and to study the stability of oil after CO₂ injection over a wide pressure and temperature range.

Introduction

Gas injection is part of the tertiary recovery and it helps stimulating oil and gas flow to produce remaining fluids that were not extracted during primary or secondary recovery phases (figure 1).

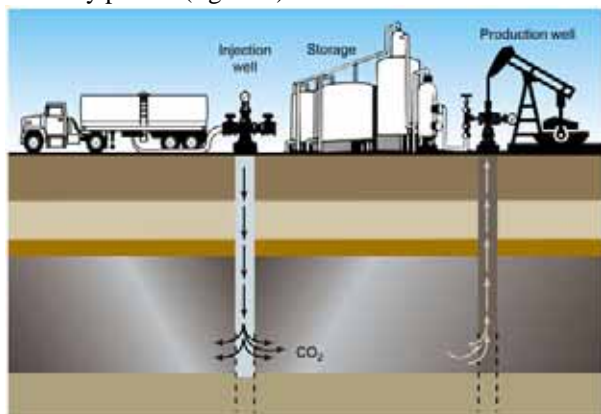


Figure 1: Schematic representation of the gas injection during the EOR

However, these modifications of the composition, the temperature and pressure conditions can induce asphaltene precipitation. This precipitation can cause a momentous loss of money since a well-bore can get plugged, especially (and it could seem contradictory at first sight) when the asphaltene concentration is low

(Ula field in North Sea, with 0.57 wt% asphaltenes and Hassi Messaoud in Algeria, with 0.062% asphaltenes).

Several issues rise when asphaltenes are investigated:

- the asphaltene behaviour is complex due to the self-association of the molecules (it makes difficult simple measurements such as molecular weight determination). Aggregation is likely to take place even at very low concentrations.
- they are defined as a solubility class (soluble in toluene and insoluble in heptane) and, hence, they do not have a general and common structure (they are known to be heavy and polar molecules). Thus a huge amount of work has to be done about the structure, the exact role of the interactions (especially hydrogen bonding, Pi-Pi stacking), etc...
- Aggregation, precipitation and deposition are the three consecutive steps that lead to plugging. However, no model or theory can explain properly these phenomena for asphaltenes.

This work was, first, focused on the determination of the properties of the solvent (i.e. the oil) and, then, on the determination of the onset of precipitation as a function of pressure and temperature after CO₂ injection.

Specific Objectives

1. The first point we decided to investigate was the solubility parameter δ and its measurement, especially as a function of pressure. Indeed, the solubility parameter has a key role in the regular solution theory and its accurate determination remains problematic. The solubility parameter can be linked to the internal pressure with the following relationship [1]:

$$\delta^2 = \pi + \delta_v^2 \quad (1)$$

where δ is the global solubility parameter, π is the internal pressure (it takes into account dispersion and polar forces) and δ_v is the “chemical” solubility parameter, taking into account other forces such as hydrogen bonding.

Internal pressure can also be linked to thermal properties such as thermal expansivity α (determined by calorimetry) and isothermal compressibility κ_T (determined by density measurements):

$$\pi = T \frac{\alpha}{\kappa_T} - P \quad (2)$$

2. The second point was the determination of the onset of flocculation after CO₂ injection. This part has been done at the University of Pau (France) at the “Laboratoire des Fluides Complexes”. A novel high-pressure equipment was recently developed [2] (figure 2).

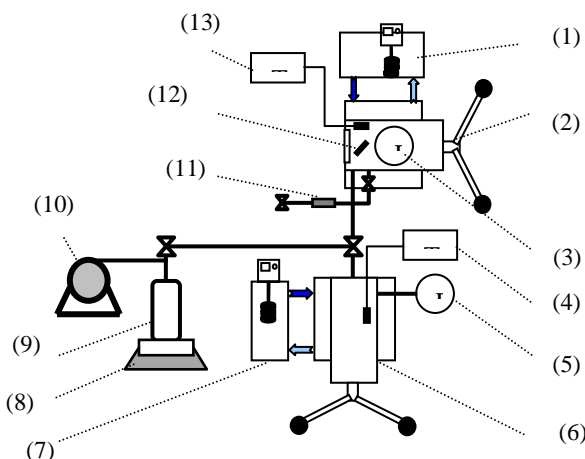


Figure 2. Experimental device: (1) thermostat, (2) high pressure cell, (3) pressure gauge, (4) thermometer, (5) pressure gauge, (6) injection pump (liquid or gas), (7) thermostat, (8) high precision balance, (9) sample, (10) vacuum pump, (11) filter, (12) magnetic stirrer, (13) thermometer

The idea is to check the effect of pressure and temperature of the quality of the solvent (i.e. its ability to keep the asphaltenes in solution) and, then, to model it since contrary effects are seen in literature [3]. Various crude oils will be investigated over a wide

temperature and pressure range (the cell can stand up to 700 bar and 200°C).

3. A third objective was the determination of the solubility parameter of asphaltenes: it is often used as a fitting parameter though it can be experimentally determined. In this work, the solubility parameter of a n-heptane asphaltene was determined by means of density measurements at 303.15 K and 1 bar. Low concentrations of asphaltenes are dissolved in two solvents at least and the density is measured as a function of concentration. Afterwards, using an equation based on the regular solution theory, the solubility parameter can be determined, providing that the internal pressures and the solubility parameters of the pure solvents are known at this temperature.

Liron and Cohen [4] used the regular solution theory and density measurements to determine the solubility parameter of cholesterol. The equation was modified to be in agreement with the original articles by Hildebrand et al. and is:

$$\frac{\overline{V}_{s2} - V_{s2}^0}{V_{s2}} = \frac{(\delta_1 - \delta_2)^2}{\pi_1} \quad (3)$$

where \overline{V}_{s2} is the partial specific volume of the solute, V_{s2}^0 is the specific volume of the solute, δ is the solubility parameter and π is the internal pressure. The subscript 1 refers to the solvent and 2 to the solute (the asphaltenes).

Note that this equation is a combination of empirical and theoretical relationships. In addition, it assumes that there are no excess volumes and it considers asphaltenes as a pseudo-component

Results and Discussion

1. After studying pure compounds and comparing it to literature data [5] (with a deviation within 1 MPa^{1/2} from 1 to 300 bar at 303.15 K), dead oils were investigated as well as a recombined one [6], [7], as seen in figure 3.

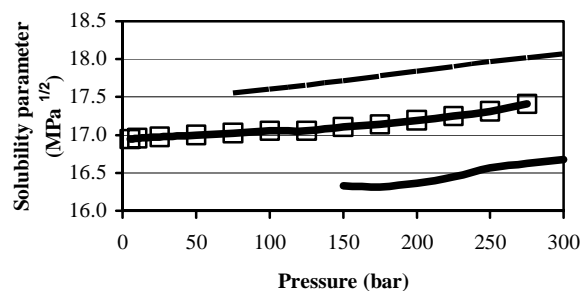


Figure 3. Physical solubility parameter crude oils at 303.15 K
 —●—, live oil 1; —■—, dead oil 1; —▲—, dead oil 2.

Let us notice that calorimetry also enabled the determination of the bubble point (figure 4).

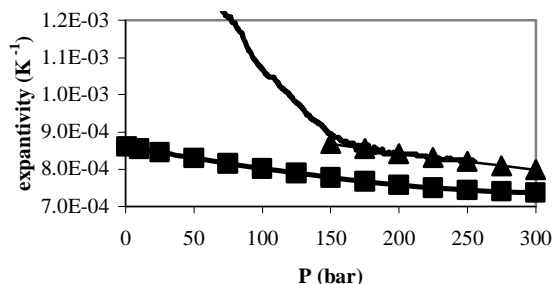


Figure 4. Thermal expansivity of oil 1 at 303.15 K

—, live oil 1, fast decompression;

▲, live oil 1, slow decompression; ■, dead oil 1.

Two cubic equations of state (SRK and PR) were combined to a characterization method to estimate this parameter but, although the density was given as an input, the deviation with experimental data was greater than $5 \text{ MPa}^{1/2}$, which is by far too much. Thus, other characterization methods should be used. Furthermore, since this method is indirect, uncertainties add up and it eventually leads to strange results, such as a decreasing slope with pressure. Other techniques are currently investigated to improve the accuracy.

2. As for the onset determination, one Venezuelan crude was tested so far and the onset was determined at several temperatures. Let us remind here one important point: the asphaltene precipitation occurs above the bubble point pressure. Thus, attention has to be paid on the number of phases for every experimental condition. Since this work is still going on, the results will be presented later.

This equipment also enables a filtration under pressure (element 11 on figure 2) and the filtrate is further analyzed with a simple technique: 20 solutions (going from 5% n-heptane/95% toluene to 100% n-heptane) are prepared and one drop of the filtrate is mixed in each of them (the onset of flocculation is almost independent of the dilution [8]). After 24 hours, a spot test is made in order to check in which sample precipitation occurred. This simple test evaluates the influence of temperature and pressure on the quality of the solvent, i.e. if the solvent can keep asphaltenes in solution or not. However, since one single crude had been tested, results will be presented later on as well.

Microscopy was used to counter-check the viability of the spot tests. Figures 5 and 6 show the influence of the solutions toluene-heptane on the precipitation. Precipitation occurs on figure 6 although the concentrations only vary within 5%. Aggregates are quite visible.

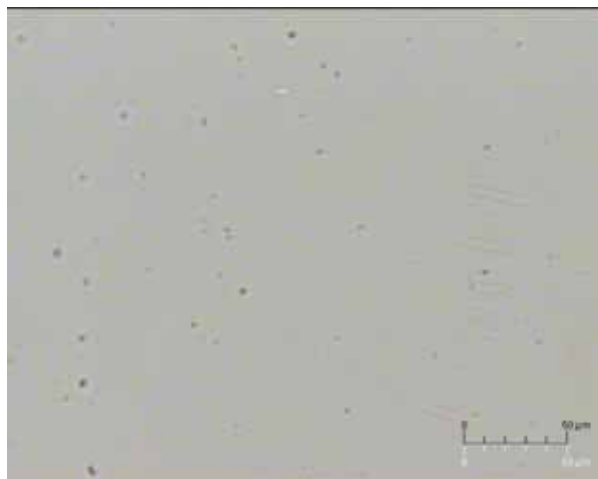


Figure 5: One drop of oil 1 in 2 mL of 40% n-heptane/60% toluene – no precipitation

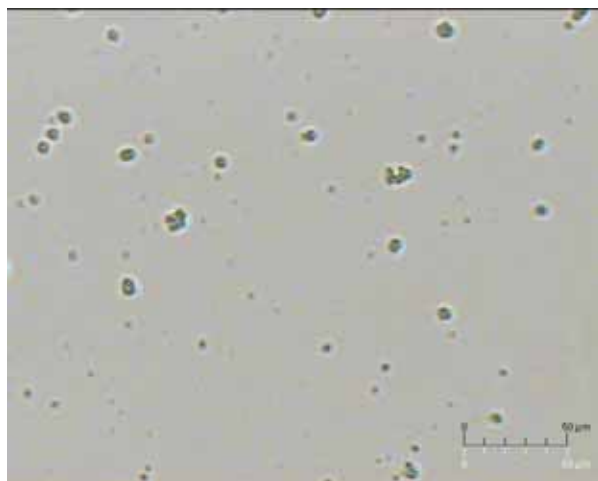


Figure 6: One drop of oil 1 in 2 mL of 45% n-heptane/55% toluene - precipitation

3. The solubility parameter of several asphaltenes were determined. Three solvents were tested: toluene, m-xylene and carbon disulfide. The values for their respective internal pressures and solubility parameters have a huge impact on the results.

Table 1 presents the results for the three combinations for one kind of asphaltenes. The pair toluene/m-xylene gives results out of the usual range ($19 - 22 \text{ MPa}^{1/2}$, [9]).

Table 1: Solubility parameter and densities of the asphaltenes OLEO D at 303.15 K

| Solvents | Solubility parameter ($\text{MPa}^{1/2}$) | Density (kg/m^3) |
|-------------------------|---|-----------------------------|
| Toluene/m-xylene | 28.22 | 1533 |
| Toluene/ CS_2 | 21.49 | 1092 |
| CS_2 /m-xylene | 20.82 | 1088 |

As for the density, Rogel and Carbognani [10] measured the densities of 13 different asphaltenes at 298.15 K and they vary between 1.17 and 1.52 g/cm³. Thus, the value of 1.09 g/cm³ found in this work seems relevant.

This method is still being tested but, this simple technique only requires a little quantity of asphaltenes, is quite fast and seems to give relevant results.

Conclusions

Simple tests and experiments were carried on asphaltenes and crude oils (both dead and recombined ones) in order to test their stabilities. The experimental techniques are ready and will be extensively used the coming months. The modelling part is the next step and also under investigation.

Acknowledgements

The author would like to thank Diep Duong for her great work as well as the teams of the University of Pau and Total for the warm welcome and the constructive atmosphere.

References

1. E.B. Bagley, T.P. Nelson, J.M. Scigliano, J. Paint Technol. 43 (1971), 35
2. H. Carrier, V. Lazzeri, H. Zhou, J.L. Daridon, An experimental approach to study pressure and temperature effect on asphaltene stability, presented at the Heavy Organics Deposition International Conference, November 14-19 2004, Los Cabos Baja California Sur, Mexico
3. Andersen S.I., Fuel Science and Technology International (1994), 12, 51 – 74
4. X. Liron, S. Cohen, J. Pharm. Sci. (1983), 72, 499
5. S. Verdier, S.I. Andersen, Fluid Phase Equilibr. (2004), accepted for publication
6. D. Duong, Determination of solubility parameters for crude oils, Kemiteknik, DTU, M.Sc. thesis, September 2004
7. S. Verdier, D. Duong, S.I. Andersen, Experimental determination of solubility parameters of oils as a function of pressure, presented at the 5th International Conference on Petroleum Phase Behaviour and Fouling: June 13 - 17, 2004, Banff, Alberta, Canada
8. G. Porte, H. Zhou, V. Lazzeri, Langmuir (2003), 19, 40 – 47
9. S.I. Andersen, Energ. Fuel. (1999), 13, 315 – 322
10. E. Rogel, L. Carbognani, Energ. Fuel. (2003), 17, 378 - 386

List of Publications

1. S. Verdier, S.I. Andersen, Fluid Phase Equilibr. (2004), accepted for publication
2. S. Verdier, D. Duong, S.I. Andersen, Experimental determination of solubility parameters of oils as a function of pressure, presented at the 5th International Conference on Petroleum Phase

Behaviour and Fouling, June 13 - 17, 2004, Banff, Alberta, Canada



Ada Villafáfila García

Address: IVC-SEP, Dept. of Chemical Engineering
Building 229, Office 212
Technical University of Denmark
Phone: +45 4525 2864
Fax: +45 4525 2258
e-mail: aga@kt.dtu.dk
www: www.ivc-sep.kt.dtu.dk/staff/AGA/AGA.htm

Supervisor(s): Kaj Thomsen
Erling Stenby

Ph.D. Study
Started: October 2002
To be completed: October 2005

Prediction of Mineral Scale Formation in Geothermal and Oilfield Operations using the Extended UNIQUAC model

Abstract

Pressure parameters are added to the Extended UNIQUAC model presented by Thomsen and Rasmussen [1]. The improved model has been used for correlation and prediction of vapor-liquid-solid equilibrium of scaling minerals (CaSO_4 , $\text{CaSO}_4 \cdot 2\text{H}_2\text{O}$, BaSO_4 , SrSO_4 , CaCO_3 , MgCO_3 , BaCO_3 , SrCO_3) at temperatures up to 300°C and pressures up to 1000 bar. The solubility of NaCl and CO_2 in pure water, and the solubility of CO_2 in solutions of different salts (NaCl and Na_2SO_4) have also been correlated. The results show that the Extended UNIQUAC model, with the proposed pressure parameters, is able to represent binary, ternary and quaternary solubility data within the experimental accuracy.

An experimental setup has been developed in order to complete literature data on solubility of scaling minerals in NaCl solutions at high temperature (up to 300°C) and pressure (up to 650 bar).

Introduction

Scale formation is a common problem in many industrial processes, such as the production of oil and the production of geothermal energy. It can be defined as hard adherent mineral deposits that precipitate from brine solution. The amount and location of scale depends on different factors, such as the degree of supersaturation, kinetics, solution pH and composition, CO_2 content, temperature and pressure.

In the reservoir, the natural water is in equilibrium with its surroundings at ambient temperature and pressure. As the brine flows up through the well, both temperature and pressure decrease considerably and the equilibrium is disturbed. This will generally lead to solid-phase deposition. The formation of carbonate scale is mainly associated with the pressure and pH changes of the production fluid, while the occurrence of sulphate scale is mainly due to the mixing of incompatible brines. When sulphate-rich injection water (often seawater) is mixed with the Ba^{2+} , Ca^{2+} and Sr^{2+} -rich formation water, it is very likely that barite (BaSO_4), celestite (SrSO_4), and/or anhydrite (CaSO_4) precipitation takes place.

Mineral scale deposition causes serious damage in utilization systems and reduces the flow area. Therefore, the production rate (and the re-injection capacity) drops down, with the consequent economical loss. The cross section decrease caused by solid deposition onto the inner wall of a pipe is shown in Figure 1. Scaling can also cause safety problems due to blockage and failure of valves.



Figure 1. CaCO_3 deposition in tubing [2]

In the geothermal field, mineral deposition limits the economical development and competitiveness of this type of power plants.

The first step towards scale prevention is its prediction. In that context, a reliable thermodynamic model able to predict mineral solubility in natural waters, under conditions of varying brine composition, temperature and pressure is required. The quantity and quality of experimental data is low, especially at high temperatures and pressures. Thus, the use of a simple but accurate model is a clear advantage. In the present work, the aqueous phase activity coefficients will be determined by the Extended UNIQUAC thermodynamic model, as it was presented by Thomsen and Rasmussen [1]. The vapor phase fugacities will be determined by the Soave-Redlich-Kwong (SRK) cubic equation of state, using classical mixing rules.

The Extended UNIQUAC model is capable of accurately representing multicomponent systems with common ions, covering a range of temperature and ionic strength large enough to represent the conditions found in geothermal and oil production wells. Two additional parameters have been added to the model in order to account for the pressure dependency. The results obtained through this modification are very satisfactory in the pressure range investigated (1 to 1000 bar).

Project Objectives

This project consists of a theoretical and an experimental part. In the experimental part, a setup to measure the solubility of sparingly soluble salts at high temperature and pressure has been designed and built.

In the theoretical part of the project a model for calculating solid-liquid-vapor equilibrium and crystallization processes for electrolyte solutions has been developed on the basis of the experimental data found in literature. The model will also be applied to the experimental data obtained in this project. The Extended UNIQUAC model [1] is used to represent speciation, solid-liquid equilibrium (SLE) and vapor-liquid equilibrium (VLE). Gas fugacities are calculated from the SRK equation of state.

Thermodynamics of Solubility

The condition for chemical equilibrium for a species B at a given temperature T and pressure P in the phases α and β is that the chemical potential of B is equal in the two phases:

$$\mu_B^\alpha(T, P, \mathbf{n}^\alpha) = \mu_B^\beta(T, P, \mathbf{n}^\beta) \quad (1)$$

where \mathbf{n} represents the concentrations of the different components in the system and μ_B the chemical potential of B . If more than two phases are present, Eq. 1 is extended to all of them.

Calculation of solid-liquid equilibrium

For a mineral $MX \cdot nH_2O$ the SLE can be expressed as



The condition for equilibrium, corresponding to Eq. 1 is:

$$\mu_{M^+(aq)} + \mu_{X^-(aq)} + n\mu_w = \mu_{MX \cdot nH_2O(c)} \quad (3)$$

The chemical potential of water can be defined as $\mu_w = \mu_w^0 + RT \ln a_w = \mu_w^0 + RT \ln(\gamma_w x_w)$ (4)

where a_w is the water activity, μ_w^0 is the molar Gibbs energy of pure liquid water at the system temperature and pressure and γ_w is the symmetric water activity coefficient, where $\gamma_w \rightarrow 1$ as $x_w \rightarrow 1$. The asymmetric convention is adopted for ions. Under this convention, the chemical potential of ion i is $\mu_i = \mu_i^* + RT \ln(\gamma_i^* x_i)$ (5)

where μ_i^* is the standard state chemical potential of ion i on mole fraction basis at the system temperature and pressure and γ_i^* is the rational asymmetric activity coefficient for ion i , where $\gamma_i^* \rightarrow 1$ as $\sum x_i \rightarrow 1$.

Calculation of vapor-liquid equilibrium

For a volatile component as H_2O , the VLE is represented as



and Eq. 1 becomes

$$\mu_{w,l} = \mu_{w,g} \quad (7)$$

where the subscripts l and g refer to liquid and vapor phases, respectively.

The chemical potential in the vapor phase can be calculated as

$$\mu_{i,g} = \mu_i^{IG} + RT \ln \hat{f}_{i,g} \quad (8)$$

where μ_i^{IG} is the chemical potential of component i at the standard state, which is the pure ideal gas at 1 bar and the temperature of the system, and $\hat{f}_{i,g}$ is the fugacity of component i in the gas phase at the temperature and pressure of the system, which can be written as

$$\hat{f}_{i,g} = y_i \hat{\phi}_{i,g} P \quad (9)$$

where y_i refers to the mole fraction of component i in the gas phase, P is the total pressure, and $\hat{\phi}_{i,g}$ is the fugacity coefficient for component i in the gas phase.

For reactions involving an aqueous phase at temperatures above the boiling point of water, the standard state pressure is the saturation pressure of the solution.

By combining Eq. 4, 7, 8 and 9, the condition (1) for equilibrium between vapor and liquid can be written:

$$\mu_{w,l}^0 + RT \ln x_w \gamma_w = \mu_{w,g}^{IG} + RT \ln(y_w \hat{\phi}_{w,g} P) \quad (10)$$

and the vapor-liquid equilibrium equation for water can be expressed as:

$$\ln \frac{y_w \hat{\phi}_{w,g} P}{x_w \gamma_w} = \frac{\mu_{w,l}^0 - \mu_{w,g}^{IG}}{RT} \quad (11)$$

Experimental Setup

The solubility of BaSO₄ and SrSO₄ in 0.1 to 6 m NaCl solutions will be determined experimentally in the temperature range 25-300°C and the pressure range 1-650 atm. Fig. 2 shows the experimental setup developed for the measurements. An oven is used for heating and keeping a constant temperature during the run. An ISCO pump will be used to pressurize the system, containing two HP tubular reactors with piston made in Hastelloy C and with Kalrez o-rings to stand temperatures up to 300°C. The 0.5 μm filter and the rest of connections, tubing, instrumentation and valves are made in 316 SS.

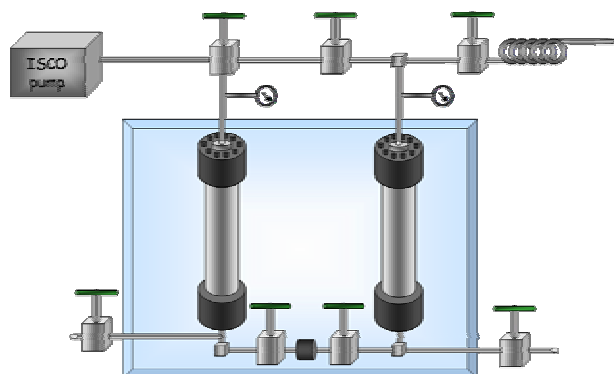


Figure 2. Experimental Setup

An excess of commercial BaSO₄ or SrSO₄ crystalline powders will be dissolved in NaCl brine and the suspension will be placed in the first HP vessel. The second HP vessel will be filled with NaCl solution of the same ionic strength as the test brine. The vessels are then closed and connected through a filter, heated to the desired temperature and pressurized to the desired pressure. After equilibrium is reached, the saturated solution contained in the first HP vessel is filtered and transferred to the second HP vessel by applying a small pressure drop in the system by means of a capillary tube open to the atmosphere. The dilution of the solution after filtration was performed in order to prevent the salt from precipitating during the period of decreasing temperature and pressure to ambient conditions required for the analytical determination. The Ba²⁺ or Sr²⁺ concentration will be determined by inductively coupled plasma mass spectrometry (ICP-MS) after dilution of the sample to a total dissolved solids (TDS) concentration below 2% (upper limit of TDS allowed by ICP-MS).

Results and Discussion

The Extended UNIQUAC thermodynamic model improved by the addition of two pressure parameters is able to give a very good representation of the solid-liquid and vapor-liquid phase equilibrium in the binary, ternary and quaternary systems, in the whole temperature, pressure and concentration range investigated. The high accuracy of the model can be observed in Fig. 3 to Fig. 8, where the appearance and disappearance of the different solids and the solubility

dependency with temperature and pressure is very nicely correlated by the model. In most of the cases, the absolute deviation between Extended UNIQUAC calculations and the experimental data is within experimental accuracy.

The different binary, ternary and quaternary data studied in this project are shown in Table 1. The range of temperature and pressure covered by the different sources found in literature is also reported in Table 1, together with the number of data given and used (in brackets) for parameter estimation. All data were analyzed previously to their use. Those found to be inconsistent were not used for parameter estimation. The data out of the temperature (-20-300°C) or pressure (1-1000 bar) range of interest in the present project were not used for parameter estimation, but were correlated in many cases by our model (Fig.6 and Fig. 8).

Table 1. Experimental binary, ternary and quaternary data sets used for parameter estimation.

| System | T(°C) | P (bar) | Number of data |
|---|-----------|----------|----------------|
| BaSO ₄ -H ₂ O | 25-600 | 1-2100 | 93 (67) |
| BaCl ₂ -H ₂ O | -7.6-100 | 1 | 80 (80) |
| BaSO ₄ -Na ₂ SO ₄ -H ₂ O | 0-80 | 1 | 60 (60) |
| BaCl ₂ -NaCl-H ₂ O | -6.4-50 | 1 | 40 (40) |
| BaSO ₄ -NaCl-H ₂ O | 0-340 | 1-560 | 330 (298) |
| BaCl ₂ -SrCl ₂ -Na ₂ SO ₄ -H ₂ O | 20-60 | 1 | 112 (112) |
| BaCO ₃ -H ₂ O | 18-40 | 1 | 6 (4) |
| BaCO ₃ -CO ₂ -H ₂ O | -2-225 | 1-107 | 177 (162) |
| SrSO ₄ -H ₂ O | 0-426 | 1-1013 | 195 (120) |
| SrCl ₂ -H ₂ O | -6-114 | 1 | 30 (30) |
| SrSO ₄ -Na ₂ SO ₄ -H ₂ O | 0-25 | 1 | 9 (9) |
| SrCl ₂ -NaCl-H ₂ O | 18-114 | 1 | 27 (27) |
| SrSO ₄ -NaCl-H ₂ O | 0-305 | 1-600 | 680 (658) |
| SrCO ₃ -H ₂ O | 5-40 | 1 | 9 (3) |
| SrCO ₃ -CO ₂ -H ₂ O | 2-200 | 1-50 | 134 (60) |
| CaSO ₄ -H ₂ O | 0-408 | 1-1410 | 337 (236) |
| CaSO ₄ -Na ₂ SO ₄ -H ₂ O | 0-110 | 1 | 264 (126) |
| CaSO ₄ -CaCl ₂ -H ₂ O | 0-110 | 1 | 90 (90) |
| CaSO ₄ -NaCl-H ₂ O | -21.2-302 | 1-1063 | 581 (581) |
| CaCO ₃ -H ₂ O | 1-350 | 1-1000 | 50 (0) |
| CaCO ₃ -CO ₂ -H ₂ O | 0-302 | 1-1000 | 859 (735) |
| NaCl-H ₂ O | 0-646.2 | 1-1911 | 82 (53) |
| CO ₂ -H ₂ O | 0-350 | 0.1-3500 | 1247 (877) |
| CO ₂ -NaCl-H ₂ O | 0-500 | 1-2500 | 672 (328) |
| CO ₂ -Na ₂ SO ₄ -H ₂ O | 0-160 | 0.3-200 | 194 (144) |
| MgCO ₃ -H ₂ O | 0-290 | 0.06-200 | 27 (10) |
| MgCO ₃ -CO ₂ -H ₂ O | 0-158 | 1-64 | 343 (56) |
| MgCO ₃ -CaCO ₃ -CO ₂ -H ₂ O | 0-340 | 1-200 | 293 |

The experimental and calculated phase diagrams for different systems from Table 1 are shown in Fig. 3 to Fig. 8.

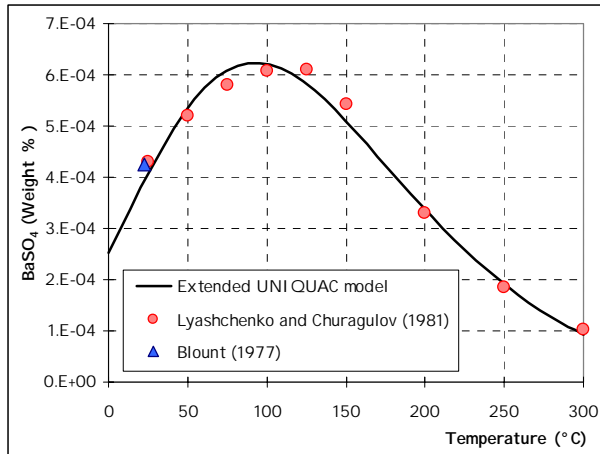


Figure 3. Experimental and calculated solid-liquid phase diagram for the $\text{BaSO}_4\text{-H}_2\text{O}$ system at 500 bar.

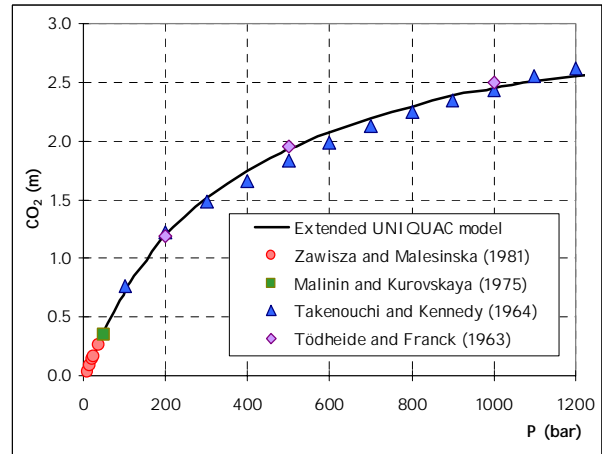


Figure 6. Experimental and calculated vapor-liquid phase diagram for the $\text{CO}_2\text{-H}_2\text{O}$ system at 150°C .

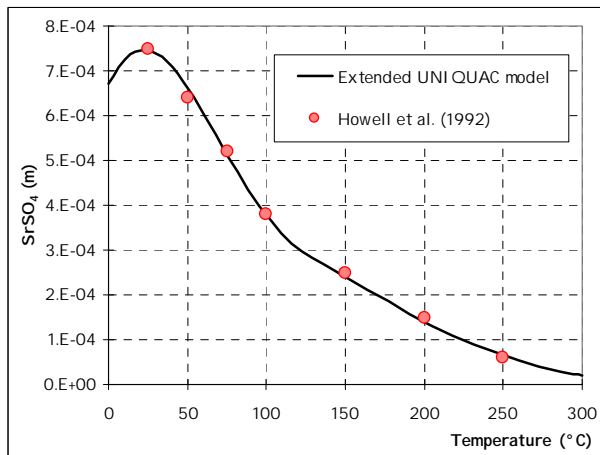


Figure 4. Experimental and calculated solid-liquid phase diagram for the $\text{SrSO}_4\text{-H}_2\text{O}$ system at 200 bar.

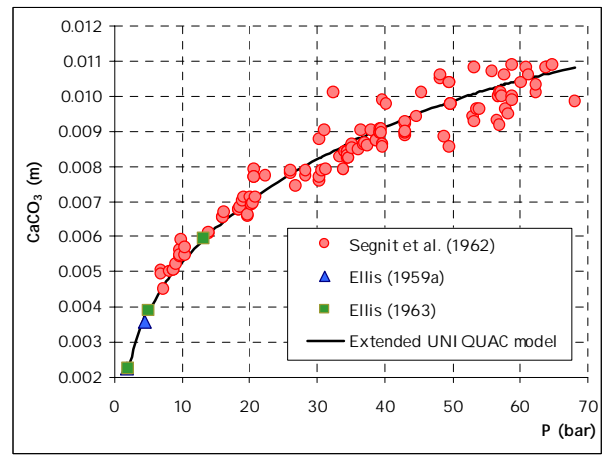


Figure 7. Experimental and calculated solid-liquid phase diagram for the $\text{CaCO}_3\text{-CO}_2\text{-H}_2\text{O}$ system at 100°C . Gas phase formed by CO_2 (g) and H_2O (g).

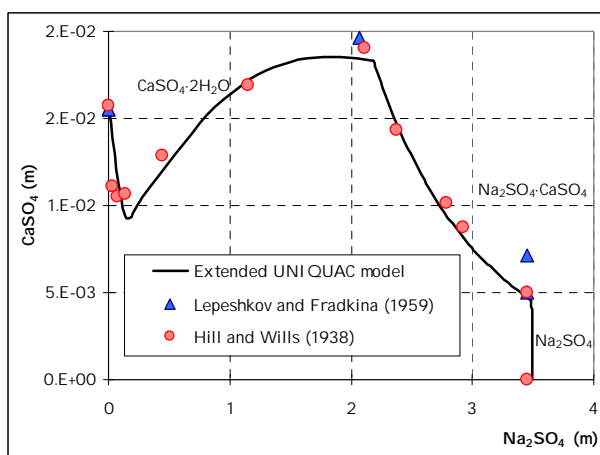


Figure 5. Experimental and calculated solid-liquid phase diagram for the $\text{CaSO}_4\text{-Na}_2\text{SO}_4\text{-H}_2\text{O}$ system at 35°C and 1 bar.

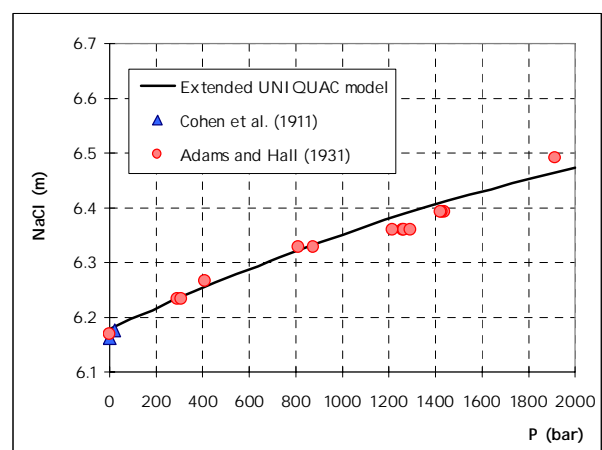


Figure 8. Experimental and calculated solid-liquid phase diagram for the $\text{NaCl-H}_2\text{O}$ system at 30°C .

Conclusions

The Extended UNIQUAC model presented by Thomsen and Rasmussen [1] has been used to calculate VLE and SLE in systems found to be problematic in geothermal and oilfield operations, due to their tendency to form scale. Some of the most problematic scaling minerals (BaSO_4 , SrSO_4 , CaSO_4 , CaCO_3) and their mixtures with NaCl have been studied. Two additional parameters have been included in the model in order to account for the pressure dependency of the solubility, obtaining a good performance for pressures up to 1000 bar.

More than 7000 SLE measurements have been collected and analyzed, covering a wide range of temperature (up to 300°C), pressure (up to 1000 bar) and concentrations up to saturation. Only reliable data were used for parameter estimation. The figures presented show that the Extended UNIQUAC model is capable of giving accurate results even at very high temperatures and pressures. Most of the data used for the parameter estimation could be reproduced by the model within the experimental accuracy.

The simplicity of the model (only two parameters per species, two parameters per species pair and two pressure parameters per salt are required), together with the good performance obtained for all the systems investigated, make the Extended UNIQUAC model an appropriate choice as a tool to study scale formation. As the model only contains binary interaction parameters it can be applied to any multicomponent system for which the binary parameters are known.

References

1. Thomsen, K., Rasmussen, P. *Chemical Engineering Science* 54 (1999) 1787-1802.
2. Kaasa, B. *Prediction of pH, Mineral Precipitation and Multiphase Equilibria during Oil Recovery*, PhD thesis, Institutt for Uorganisk Kjemi, Norges Teknisk Naturvitenskapelige Universitet, Trondheim, Norway, 1998, p.24.

List of Publications/Conferences

1. Villafáfila García, A., Thomsen, K., Stenby, E.H. *Scale Formation in Geothermal Plants*, Report No. SEP 0207, IVC-SEP, 2002.
2. Villafáfila García, A., Thomsen, K., Stenby, E.H. *Modeling of scale formation in geothermal plants*. Oral presentation at the IAPWS symposium, Vejle, Denmark, 27th August 2003.
3. Villafáfila García, A., Thomsen, K., Stenby, E.H. *Solid-Liquid-Vapor equilibrium for sparingly soluble salts found in natural waters*. IUPAC poster prize for our presentation at the 11th International Symposium on Solubility Phenomena, Aveiro, Portugal, 26th-29th July 2004. I
4. Villafáfila García, A., Thomsen, K., Stenby, E.H. *Prediction of Mineral Scale Formation in Geothermal and Oilfield Operations using the Extended UNIQUAC Model. Part I: Sulphate*

Scaling Minerals. Geothermics (accepted for publication).

5. Villafáfila García, A., Thomsen, K., Stenby, E.H. *Prediction of Mineral Scale Formation in Geothermal and Oilfield Operations using the Extended UNIQUAC Model. Part II: Carbonate Scaling Minerals. Geothermics* (submitted for publication).



Diego Meseguer Yebra
Address: Department of Chemical Engineering
Technical University of Denmark, B229
2800 Kgs. Lyngby (Denmark)
Phone: +45 4525 2837
Fax: +45 4588 2258
e-mail: dmy@kt.dtu.dk
Supervisor(s): Søren Kiil
Kim Dam-Johansen
Claus Erik Weinell, Hempel A/S

Ph.D. Study
Started: May 2002
To be completed: April 2005

Efficient and Environmentally Friendly Antifouling Paints

Abstract

Antifouling paints are highly specialized coatings designed to combat the natural process of marine biofouling on immersed artificial structures. This project deals with the identification, characterization and quantification of the main processes responsible for the antifouling activity of an environmentally friendly tin-free system. In this paper, the main results attained are presented together with the current research directions. A successful mathematical description of the paint activity is expected to speed up the paint design, testing and optimization greatly.

Introduction

Marine biofouling is a natural and spontaneous process which involves significant economical losses on ocean-going ships. The most widespread preventive solution is to coat the underwater part of the vessel's hull with an antifouling (A/F) paint. In addition to the tight durability requirements inherent to paints exposed to such a harsh environment as seawater is, these products must be capable of releasing active compounds in a controlled manner during long periods of time (e.g. up to 5 years). Consequently, the design, optimization and testing of new products is a time-consuming and very complex tuning task.

As a result of the prohibition of the very efficient tin-containing coatings, paint companies were urged to develop tin-free alternatives with similar performance to that of the toxic tin-based products. While the first granted patents related to some of today's commercially available products date back to the mid 80's [1], the moderate results of these technologies forced the marine paint companies to commercialize tin-containing products until the suggested date for the entry into force of the ban.

With the advent of new progressively stricter environmental regulations, there is a need for faster procedures for effective screening and development of promising environmentally benign alternatives. Kiil et al. [2] showed how the mathematical quantification of some key processes in the A/F paint activity can result in reliable estimations of paint performance. Although originally based on a tin-based technology, the ideas underlying the model are directly applicable to any system based on a controlled reaction with seawater.

The latter involves that the outputs of this research can be applied to a number of promising non-toxic A/F alternatives subjected to investigation elsewhere.

Project Objectives

The main goals of this research project are:

- o To characterize the main processes determining the activity of a tin-free A/F paint
- o To quantify and implement them into an advanced mathematical model
- o To analyze the influence of A/F paint components on the paint activity: (e.g. different (in)soluble pigments, (un)reactive binder components)
- o To develop fast testing methods based on model simulations and short rotary experiments
- o To adapt the model from artificial to natural seawaters in the extent possible.

The fulfillment of these objectives requires extensive rotary testing of different paint compositions, together with chemical reaction studies and mathematical modeling.

Working Mechanisms of Biocidal A/F Paints

All the currently marketed chemically-active tin-free alternatives are based on similar working principles (Figure 1).

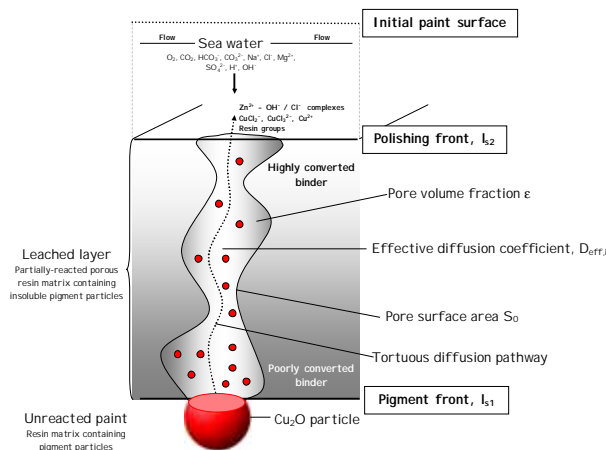


Figure 1: Schematic illustration of the working mechanisms of a chemically active A/F paint

Seawater and seawater ions diffuse to the paint surface where they rapidly react with the soluble pigments (typically Cu_2O):



The copper complexes formed diffuse out into the bulk seawater thereby forming a pore network in the paint (the so-called leached layer). At the paint surface and at the pore walls, seawater also reacts with the paint's binder system. In the case of the rosin-based system of interest in this study, the following reactions have been hypothesized to take place [3]:

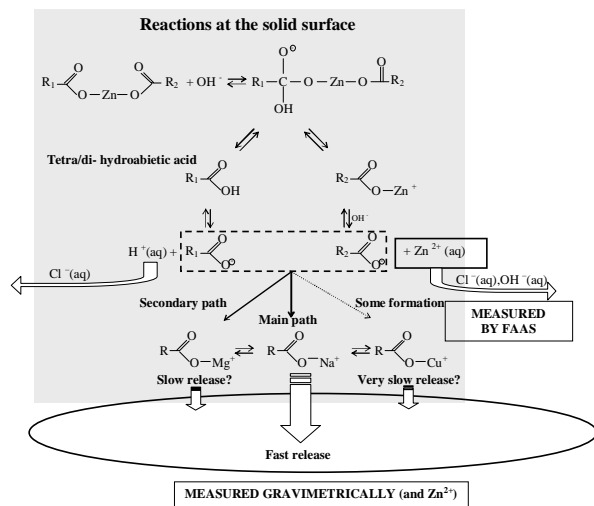


Figure 2: Alkaline hydrolysis reaction of the Zn carboxylate of abietic-acid with seawater. This mechanism has been characterized in this project by means of Fourier Transform IR Spectroscopy Scanning Electron Microscopy coupled with Electron Dispersive X-Ray detectors (SEM-EDX)

This reaction results in the formation of very soluble soaps which diffuse out into the bulk seawater. If a biocidal compound is embedded in the binder, it will

thus be exposed and released. Consequently, both the reaction with the pigments and the reaction with the binder lead to the release of active compounds which give rise to the A/F activity.

At a certain point in time, the binder at the pore walls of the leached layer shows different degrees of reaction. The more converted binder will be that at the paint surface (longer exposure to seawater). The latter can be analyzed by means of (SEM-EDX) (Figure 3).

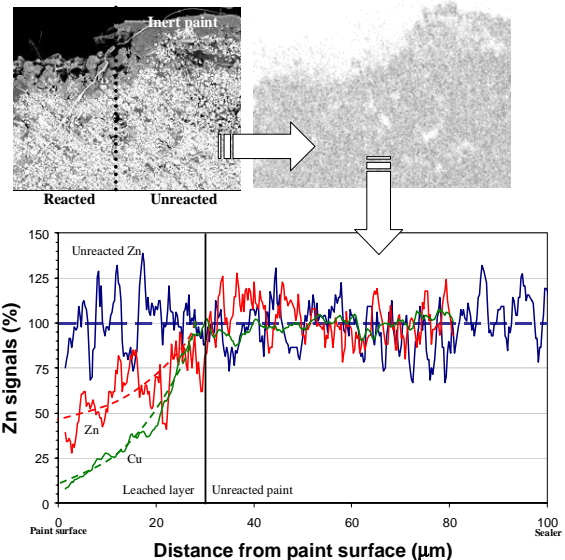


Figure 3: SEM picture and its corresponding EDX analysis showing the Zn atom signals (up). The intensity of the signal is processed by means of ImagePro, showing a distinct gradient from the unreacted paint to the paint surface (bottom).

The model assumes that a very thin paint layer is released (polishing process) when the reaction at the paint surface has reached a certain conversion (X_{max}), thus exposing a less reacted binder surface. This parameter constitutes an innovative concept in A/F paint modeling and it is thought to depend strongly on the insoluble paint components, i.e. insoluble pigments and retardants.

The system must be designed in such a way that the release rate of the biocides are sufficient to prevent fouling throughout the paint's lifetime (typically 5 years). If it is intended to use a model-based approach to assist the design process, it is customary to determine the rate at which the reaction schematized in Figure 2 takes place. This is presented in the next section.

Dissolution Rate Measurements

In this investigation, the zinc carboxylate of a refined and prereacted rosin compound is used. Natural rosin is distilled in order to eliminate impurities and subsequently hydrogenated. The resulting mixture consists mainly of tetrahydroabietic and dihydroabietic acids. Zinc resinate (ZnR) was prepared after reaction of the hydrogenated rosin dissolved in xylene 1:1 wt with excess ZnO for two hours in a high speed disperser. The

excess ZnO particles was removed by centrifugation (20 min, 3000 r.p.m.). The supernatant liquid was extracted from the very upper part of the avoid contamination by ZnO particles and further filtered (0.45 μm). A Fourier Transform IR Spectroscopy analysis of the resulting mixture shows virtually 100% conversion to the dimeric carboxylate. Flame Atomic Absorption Spectroscopy (FAAS) is used to trace the release of Zn²⁺ into the sea water.

To expose the samples, very thin glass panels of dimensions 2.4x6 cm were used. The panels were cleaned with xylene to remove potential surface contaminants. A surface area of 9.6 cm² was coated with ZnR by means of a Bird applicator. High wet film thicknesses were avoided in order to minimize crack failure due to poor cohesive strength of the binder. Overall, around 0.2 g of binder was applied to a ~0.53 g glass panel. The binder should be applied on a perfectly horizontal surface to avoid heterogeneous distribution. The latter was possible due to low viscosities and the absence of any flow or thixotropic additives which could impart a rheologic structure to the binder.

The dissolution rates at different seawater pH values and temperatures are shown in Figure 4 [3]. No influence of the seawater NaCl content was observed (results not shown).

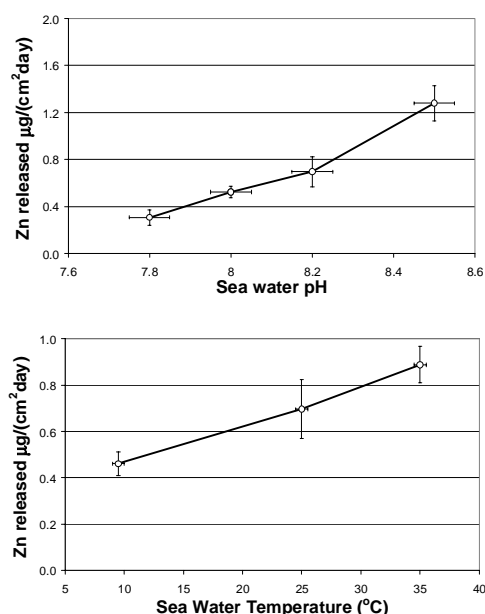


Figure 4: Zn²⁺ release rates obtained at different sea water pH values with the AAS-based method (top). The influence of the sea water temperature on the Zn²⁺ release rate is also shown (bottom).

The kinetic expression with reproduces the seawater reaction rate of ZnR within the range of experimental conditions tested is:

$$(-r_{ZnR}) = k_1 \cdot C_{OH^-}^a - k_{-1} \cdot C_{R^-}^b \cdot C_{Zn^{2+}}^c \cdot \frac{\mu g \text{ Zn}^{2+}}{(\text{cm}^2 \text{ film}) \cdot \text{day}}$$

$$k_1 = A \cdot e^{\left(\frac{E_a}{R \cdot T}\right)} \cdot \frac{\mu g \text{ Zn}^{2+}}{(\text{cm}^2 \text{ film}) \cdot \text{day}} \cdot \left(\frac{1}{\text{mol}}\right)^a$$

$$k_{-1} = \frac{k_1 \cdot C_{OH^-}^a}{L_{ZnR} \cdot 2^{b-2} \cdot (C_{Zn^{2+}}^{eq})^{b+c-3}} \cdot \frac{\mu g \text{ Zn}^{2+}}{(\text{cm}^2 \text{ film}) \cdot \text{day}} \cdot \left(\frac{1}{\text{mol}}\right)^{b+c}$$

where ln(A) is 18±2.5, the activation energy is 18.5±6.0 kJ/mol and the reaction order with respect to the hydroxide ion concentration, a, is 0.86±0.42. The reverse reaction was found to be negligible for the reaction within the pores of an antifouling paint.

The Mathematical Model

As it comes from the discussion above, the basic phenomena modeled are (see Figure 5):

- o Cu₂O and binder kinetics
- o Seawater chemical speciation
- o Transport phenomena
- o A condition for paint polishing (X_{max})

Overall, the model describes the profiles inside the paint film for CuCl₂/CuCl₃²⁻, Cu²⁺, Na⁺, H⁺/OH⁻, Cl⁻, O₂, HCO₃⁻/CO₃²⁻, Zn²⁺/ZnCl⁺/ZnCl₂/ZnCl₃⁻/ZnCl₄²⁻ and Na resinate. The oxidation of Cu⁺ complexes to Cu²⁺ in the leached layer has been included for the first time according to the kinetics measured by Millero (2000) [4]. The incorporation of that process allows the study of the potential formation of insoluble Cu²⁺ salts, traditionally associated with rosin-based systems. An advanced numerical solution technique [5] is used to immobilize the moving boundaries (i.e. paint surface and pigment front) and allow the use of orthogonal collocation to solve the system of differential equations [6].

Regarding the seawater chemistry, the activity coefficients for the individual ionic species present within the leached layer and in the diffusive boundary layer are estimated by means of Extended UNIQUAC. This model is based on the addition of a Debye-Hückel term to the UNIQUAC expression of the molar excess Gibbs energy to account for the long-range interactions between the ionic species (electrostatic forces) as presented by Thomsen et al. [7]. The Random Pore Model [8] is used to describe the changes in the morphology of the porous leached layer as a result of the binder degradation.

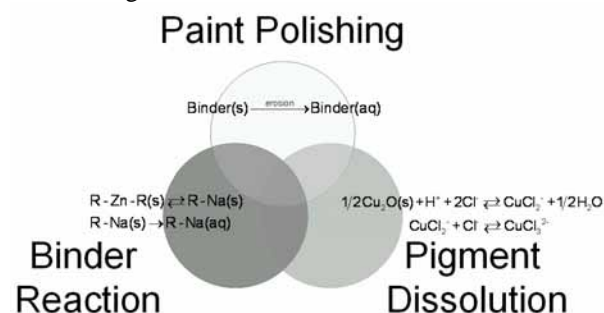


Figure 5: Scheme of the tin-free rosin-based (TFR) mathematical model. The main processes involved in the activity of the paint and their interactions are combined with chemical speciation calculations and transport phenomena.

Controlled-Shear Stress Rotary Experiments

The model outlined above has to be capable of reproducing the activity of model A/F paints. Such activity can be characterized by means of two experimental parameters (see Figure 6):

- o The degree of polishing
- o The thickness of the leached layer

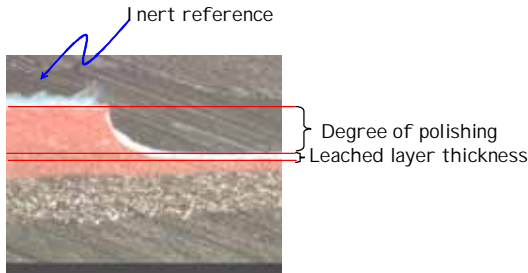


Figure 6: Measurement of the degree of polishing and leached layer thickness through optical microscopic analysis of the cross-section of exposed paints

To measure such parameters, a rotary set up (Figure 7) is available simulating the conditions experienced by the paint on a sailing ship's hull. By providing a Couette flow in the water around the paint samples, the shear stress could be adjusted to reach realistic values.

The controlled-shear stress capabilities of the rotary paint simulator used by Hempel A/S and KT for A/F paint research were demonstrated by Weinell et al. [9]. In Figure 8, the estimated and experimental torque values resulting from the rotation of the cylinder in seawater are shown at different rotational speeds (Figure 8). In spite of the latter, computational fluid dynamics (CFD) calculations on the rotary rig showed the presence of a non-ideal flow in the narrow seawater channel next to the cylinder surface where the paints were attached (Figure 9). The latter could involve that different shear stress would be applied to the paints depending on the vertical location on the rotor surface.

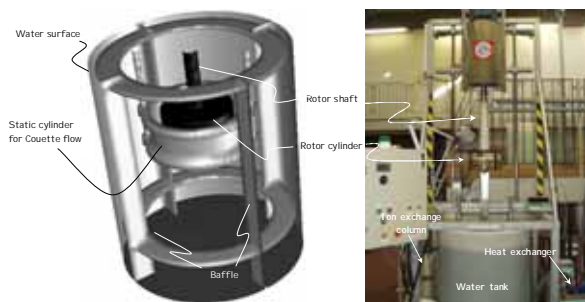


Figure 7: Rotary set-up (up). Inner cylinder and Couette flow regime (down)

Nevertheless, CFD generated shear stress calculations on the rotor surface showed no significant profiles at the rotating cylinder surface in the direction parallel to the axis of rotation. Also the results of testing a standard

commercial paint at different positions in the rotor showed no significant differences (Figure 10).

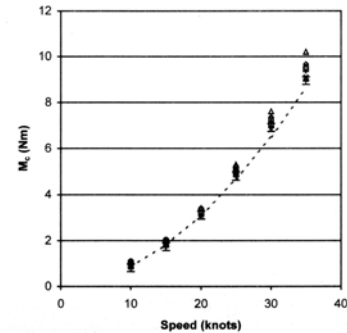


Figure 8: Theoretical torque values in a smooth rotating cylinder (dashed line) versus the measured values obtained by means of PVC discs (experimental points with error bars). From [9]

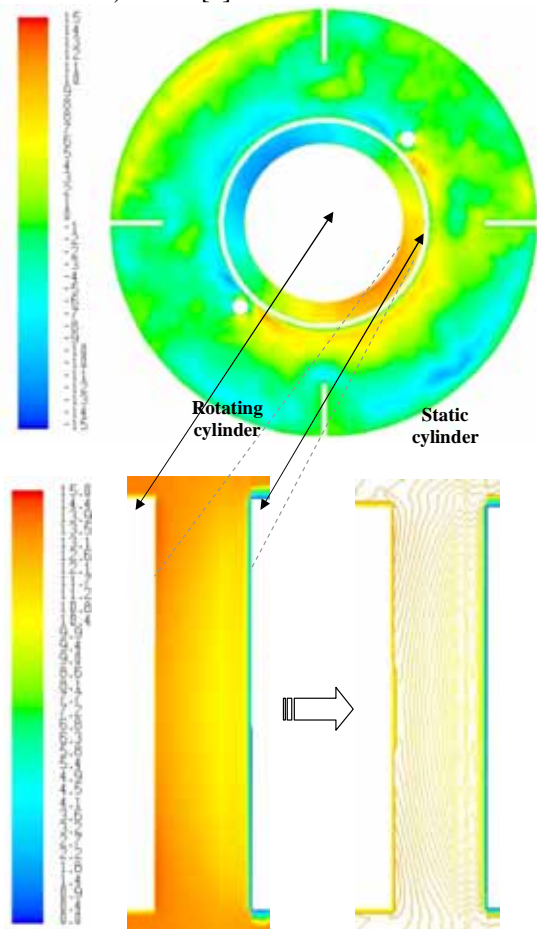


Figure 9: CFD simulation results showing the tangent velocity (m/s) profiles along a cross section of the tank at the level of the rotating cylinder (top) and the radial gradients in the tangent velocity (m/s) in the channel between the rotating and the static cylinders (bottom).

We can conclude that this rotary set-up can successfully simulate different shear stress scenarios, actually better than the currently used standard rotary biocide release procedures (ASTM D6442-99 and ISO/DIS 15181-1,2; [10]). These kind of set-ups are a

very important development for the testing of A/F paints and, indirectly, for environmental biocide loading estimates used to predict their fate and effects on the environment.

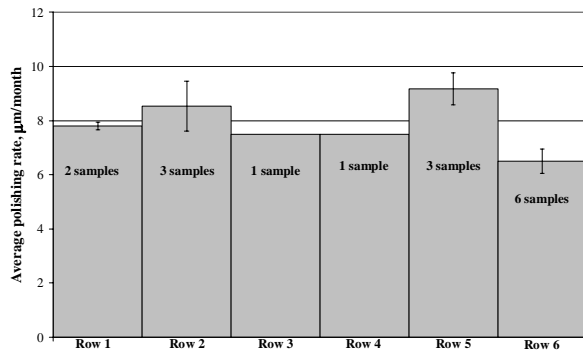


Figure 10: Polishing results after exposing a commercial fast polishing reference paint at different positions in the rotor.

A/F Performance Results

Up to now, an important amount of rotary data is available studying the influence of different model paint compositions (e.g. Figure 11). It is presumed that the polishing process can be tailor-made through an identification of the individual roles of:

- o Insoluble pigments
- o Insoluble resins (retardants)
- o Pigment PSD
- o Pigments of controlled dissolution rate

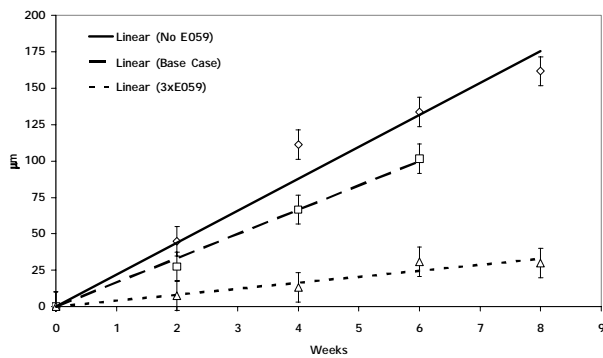


Figure 11: Influence of the amount of retardant on the paint polishing rate (paints containing Cu_2O only)

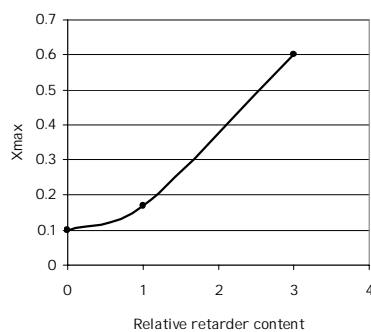


Figure 12: Influence of the amount of retardant on the X_{max} value

The use of the model provides interesting information which would have been not been available from empirical paint testing:

- o Very fast pigment dissolution rate is observed, which suggest a higher binder hydrophobicity compared to TBT-SPC coatings.
- o Very low tortuosity coefficients are found to characterize the leached layer.
- o The influence of the amount of retardant resin on the X_{max} parameter is shown in Figure 12.

As a further improvement, the A/F paint model is now capable of reproducing the performance of paints containing insoluble pigments (Figure 13). Once the X_{max} value is measured by SEM-EDX, only the tortuosity value had to be adjusted. It is expected that once a sufficient number of paints have been modeled, a relationship between pigment loading and tortuosity factor will be available (all the model parameters could be then known beforehand or measured after short rotary experiments).

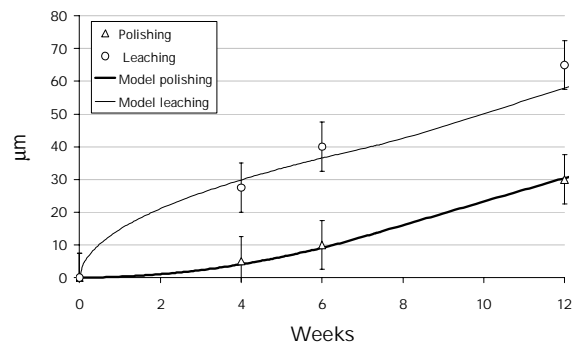


Figure 13: Experimental results and model simulations of a paint containing 20% Cu_2O and 20% TiO_2 .

Accelerated Paint Testing

Relatively simple experimental procedures can be designed to provide a fast estimation of the required input parameters for the model. Subsequent simulations can be used to select the most promising formulations which should be subjected to more thorough testing. Future work will address the development of procedures for:

- o Fast estimation of binder and pigment kinetics.
- o Fast determination of X_{max} (SEM/EDX)

The dissolution kinetics of ZnO and low leaching Cu_2O pigments are currently being determined and verified by the use of the model and rotary experiments.

Other results

The A/F paint model has also been used to assess the role of marine microbial biofilms on the release rate of A/F biocides. A biofilm growth model was first implemented in order to describe the extra diffusion pathway for the biocides released from the A/F paint.

The main conclusion attained is that the decrease in the biocide release rate reported in the literature for Cu^{2+} and TBT^+ is mainly due to chemical adsorption at the negatively charged sites of the extracellular polymeric matrix (EPS) secreted by the microorganisms to adhere to the surface. Very little effect on the paint performance is predicted.

The A/F paint model is also expected to model the sea water behavior of full paints (i.e. containing additives) of slightly simplified composition which are currently exposed in the rotor. The latter would constitute a very important step forward for this research project.

Conclusions

The use of A/F paints as a means of preventing the undesired settlement of marine organisms on the hulls of ocean going ships entails important economical benefits. Moreover, it involves reduced fuel consumption and, thereby, lower emissions of harmful compounds into the atmosphere. The prohibition of the very effective but environmentally harmful tributyltin-based coatings was the first of a series of expected restrictions which will regulate the A/F compounds that can be used on a bottom coating. The transition from the tin-based to the tin-free coatings has demonstrated the drawbacks of design and optimization processes based on trial and error tests after long-term rotary experiments. New approaches must thus be developed in order to adapt the current A/F products to the more environmentally friendly active compounds in an efficient manner.

A mathematical model of the performance of a rosin-based tin-free alternative is being validated against the rotary data. The tin-free binder's reaction mechanisms and kinetics have been determined. Also, an experimental procedure to measure the seawater reaction of soluble pigments is being developed. The last set of rotary data, which is currently being generated, will test the ability of the model to describe the performance of model paints of varying binder composition and pigment loadings. The information extracted from these experiments will not be limited to polishing and leaching rates but also mass transfer resistance in the leached layer, paint erodability, binder hydrophobicity, etc.

With such information, a fast estimation of the paint performance without the need of too long rotary experiments can be attained. Fast experimental procedures can be identified to provide the necessary input parameters for the model. Ideally, the latter should only be performed with a few selected systems which have shown promising characteristics from the model analysis. In addition, information about the paint behavior under different seawater conditions could also be simulated, which is only feasible today at the expense of increasing testing costs.

The generic nature of the model, would make it extensible to innovative alternatives as long as they rely on the release of active compounds. In this way, the

development of non-biocidal chemically active alternatives would be eased.

Acknowledgements

The work presented in this article was carried out in the CHEC Research Centre in collaboration with Hempel A/S. Financial support from The Danish Technical Research Council is gratefully acknowledged.

I would like to thank Neel Winther-Hinge (Hempel A/S) for her invaluable help with the SEM-EDX analysis and Eva Thale (KI,DTU) for facilitating the access to the AAS. This work is also strongly indebted to Kaj Thomsen who provided the Extended UNIQUAC routines. Martin Skov Skjøth-Rasmussen is partly responsible for the success of the CFD calculations. The B.Sc. and M.Sc. students Rikke Lykke Pedersen, Morten Rasmussen, Kenneth Olsen, Rubén Martín Sacristán and Beatriz Coronas Heras have also contributed to this research.

References

- [1] Yebra, D.M., Kiil, S., Dam-Johansen, K. Progress in Organic Coatings. 50 (2) (2004),75-104
- [2] Kiil, S., Weinell, C.E., Pedersen, M.S., Dam-Johansen, K. Ind. Eng. Chem. Res. 40 (18) (2001) 3906-3920.
- [3] Yebra, D.M., Kiil, S., Dam-Johansen, K. Weinell, C.E. Progress in Organic Coatings. Submitted for publication (2004)
- [4] Millero, F.J. The Physical Chemistry of Natural Waters, Wiley-Interscience, NY, U.S.A, 2001.
- [5] Kiil, S., Bathia, S.K., Dam-Johansen, K. Chemical Engineering Science 50 (17) (1995) 2793
- [6] Villadsen, J., Michelsen, M.L. Solution of Differential Equations Models by Polynomial Interpolation, Prentice Hall, Englewood Cliffs, U.S.A, 1978.
- [7] Thomsen, K., Rasmussen, P. Chemical Engineering Science, 54, (1999), 1787-1802
- [8] Bhatia, S.K., Perlmutter, D.D. A Random Pore Model for Fluid-Solid Reactions: I. Isothermal, Kinetic Control, AIChE Journal, 26(3) (1980), 379-386
- [9] Weinell, C.E., Olsen, K.N., Christoffersen, M.W., Kiil, S. (2003). Biofouling, Vol. 19 (Supplement) pp. 45-51
- [10] Valkirs, A.O., Seligman, P.F., Haslbeck, E., Caso, J.S. Marine Pollution Bulletin, 46 (6) (2003), pp. 763-779.



Jacob Zeuthen

Address: DTU, building 227, room 122
Phone: +45 4525 2964
Fax: +45 4588 2258
e-mail: jz@kt.dtu.dk
www: www.aerosol.kt.dtu.dk

Supervisor(s): Hans Livbjerg

Ph.D. Study

Started: August 2003
To be completed: July 2006

Laboratory Investigation of Formation of Aerosols and Chemical Reactions in Flue Gas from Biomass- and Waste-Combustion

Abstract

The aim with this project is to investigate the formation of aerosol particles and deposits during combustion of the so-called CO₂-neutral fuels, biomass and waste. The kinetics of the chemical reactions leading to the formation of these particles and deposits, and the phase transitions involved, will be studied. In general, combustion aerosols should be avoided due to their harmful behavior in the environment. Particles from combustion of bio-fuels are particularly harmful due to their sticky and corrosive behavior in the process equipment.

This project involves experiments performed in a tubular furnace and also CFD (computational fluid dynamics) simulations using Fluent. The focus will be on developing a quantitative model based on experiments and simulations. The quantitative model can be used for design and control of Danish power plants using biomass and waste combustion in the future.

Introduction

Straw, some sorts of wood, and various kinds of waste contain considerable amounts of volatile inorganic salts, in particular the chlorides of sodium, potassium and zinc, which evaporate during combustion. When the flue gas cools down after combustion the inorganic vapors condense and form aerosol particles and deposits on walls and super heater tubes. This phenomenon is much more pronounced for bio-fuels than for other fuels. Dealing with the problems caused by deposition of salts in the process equipment increases the cost of 'CO₂-neutral' combustion considerable. The aerosol particles and the deposits have previously been studied intensively by field-studies and the chemical compositions of these have been found. However, the proposed qualitative models for the chemical reactions involved are not clear and are contradictory. Also, no quantitative models have been developed. Field-data are influenced by a highly varying chemistry of the fuel and by complicated distributions of residence times, temperatures and flow-patterns. Therefore it is not possible to develop quantitative models based on these data.

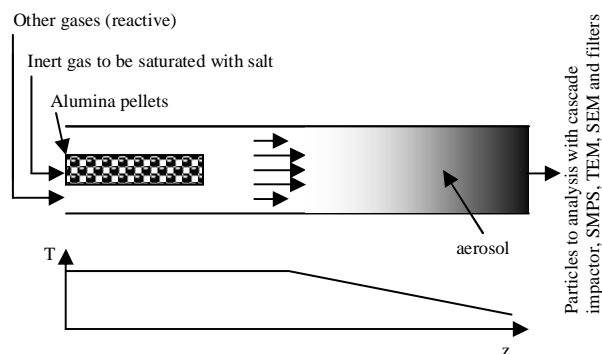


Figure 1: Schematic drawing of the tubular furnace. Gas enters the reactor in one end. The inert gas is led through a packing of pellets to be saturated with a volatile salt. The salt concentration of the gas is adjusted by changing the temperature of this part of the reactor. A temperature profile is applied on the reactor and particles are formed in the cooling zone by nucleation. The aerosol leaving the reactor can be studied by using a cascade impactor, SMPS (Scanning Mobility Particle Sizer), SEM (Scanning Electron Microscopy), TEM (Transmission Electron Microscopy) and other methods.

In order to set up a quantitative model the important reactions involving the key chemical components must be studied separately. In this project a bench-scale tubular furnace with well-defined flue gas flow, temperature and gas-composition is used to establish a qualitative as well as a quantitative model for the formation of particles and deposits.



Figure 2: Experimental setup. To the left the SMPS system is placed and to the right the tubular furnace is seen.

Experimental work

For the experimental work a 173 cm long tubular furnace ($\varnothing=25$ mm) with laminar flow is used (see figure 1 and 2). It is possible to control the temperature up to ~ 1200 °C in nine separate axial sections along the flue gas flow direction. In the first part of the reactor an inner tube is placed. In this inner tube a flow of inert

nitrogen passes pellets of inert alumina impregnated with the salt to be volatilized (e.g. NaCl or KCl). The nitrogen gets saturated and by changing the temperature of the pellets it is possible to adjust the salt-concentration in the gas (see figure 3). Other reactive gases (SO_2 , H_2O , NO and O_2/air) enter the reactor on the outside of the salt-containing alumina pipe. The temperature is kept constant in the first part of the reactor and is then decreased in the flow direction after a given length. Using this technique, it is possible to study effects of different temperature gradients, flow velocities and chemical compositions on the formation of particles and deposits. It is also possible to introduce particle seeds with the inlet gas to study the effect of foreign seeds in the flue gas. These will serve as nucleation sites for further growth of inorganic materials and may serve to suppress homogeneous nucleation. Homogeneous nucleation leads to sub-micron particles ($D_p < 1\mu\text{m}$), which are the most harmful particles for the environment, spreading over larger distances and with harmful impact on the human lungs. These particles are also more difficult to separate from the flue gas.

Homogeneous nucleation

Particles can be formed directly from a gas phase if this gets super-saturated by either cooling or chemically. In homogeneous nucleation, particles are formed in very high concentrations. The concentration depends on the properties of the nucleating compound and on the temperature at which it nucleates. When nucleation takes place at higher temperatures the diffusion coefficient will be higher and the resulting particle concentration will be lower. However, the particles

Nucleation of KCl particles with different saturation temperatures

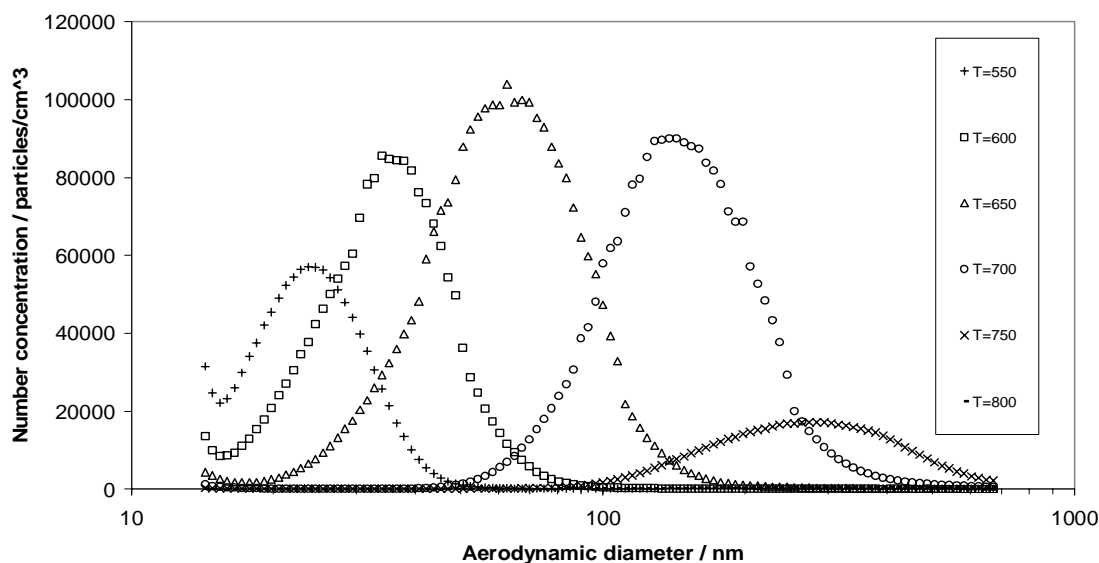
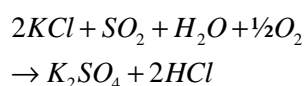


Figure 3: Size distribution of pure KCl-particles from experiments with homogeneous nucleation in a tubular furnace. The temperature of the saturation zone with alumina pellets impregnated with the salt is varied to obtain different concentrations of $\text{KCl}_{(g)}$. With increasing temperature the concentration of $\text{KCl}_{(g)}$ is increased and the average particle diameter increases, because the temperature where nucleation takes place is higher. However, while the mass of particles formed will keep increasing with higher temperature the number of particles formed is highest at some given temperature. Above this temperature coagulation of the small particles with the larger ones will dominate.

formed will be larger, since they are growing faster due to the higher diffusion coefficient. This is investigated in the tubular furnace. Different temperature profiles and nucleation of different salts are investigated. By introducing seeds to the experiments, it is also found that suppression of homogeneous nucleation occurs by the presence of a particle concentration of only 10^5 $1/\text{Nm}^3$. If sulfation of the potassium chloride is applied, the suppression is not possible. The sulfation is given by the reaction:



This could indicate that potassium sulfate (and not potassium chloride) is the nucleating compound in the system.

Field measurements

A measuring campaign at a full scale power plant firing straw has been carried out at Avedøre Power Plant (AVV2) in November-December 2004. In the 2½ weeks measuring campaign, experiments with different additives were performed and the effects on temperature, deposits, emissions, particles loads, and aerosols were done. The Aerosol Laboratory performed aerosol measurements and total dust samplings in the flue gas upstream from the bag house filter. The Aerosol measurements were carried out using a gas ejector for diluting and cooling the flue gas. When the flue gas is diluted, coagulation is minimized and furthermore, by changing the dilution rate, the concentration can be optimized for the sampling method used. The flue gas leaving the gas ejector is conditioned in a gas conditioner to remove moisture. By measuring the CO_2 concentration in the diluted flue gas and in a non-diluted, filtered flue gas, the dilution rate is found, and saved by data-logging. The temperature and the concentration of NO are also logged, since these also may influence the formation of submicron particles. The aerosol is characterized by cascade impactor and SEM/EDX. The total dust samplings are made on a filter from Haldor Topsøe which samples the flue gas iso-kinetically. These filter measurements are used to find total dust load and chemical composition of the solid fraction of the flue gas. The measuring campaign was carried out by E2, RISØ, Vattenfall, Force and The Department of Chemical Engineering, DTU.

Mechanism for aerosol formation

Before developing a model for aerosol formation during biomass combustion the mechanism of the initial nucleation leading to particle formation has been investigated. To determine how particles are nucleated two approaches are used. In the first approach the aerosol is filtered from the gas phase at high temperature ($>800^\circ\text{C}$). This prevents the volatile compounds from nucleating. The hot filtration showed

potassium sulfate condensation at temperatures where potassium chloride was only in gas phase (see figure 4).

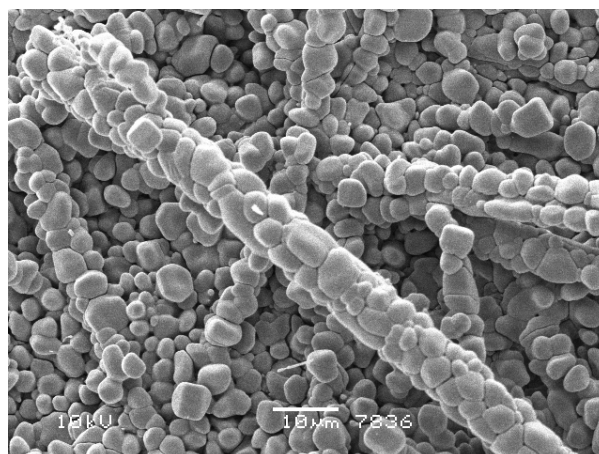


Figure 4: SEM micrograph of potassium sulfate 'filtered' from the gas phase in the tubular furnace. The mean diameter of the particles on the filter is very large compared to the typical size range of aerosol particles from similar experiments.

However, the deposits on the filter showed particles with diameters larger than $5 \mu\text{m}$. Since these are larger than the aerosol particles, a growth on the filter must take place. This can happen by either sintering of small particles or by heterogeneous condensation. To find out if small particles hit the surface and then sinter with the existing deposits a slide to be used for quench cooling of the filter has been made.

By quench cooling the filters, small particles on top of the deposits has been observed (see figure 5). These could indicate that potassium sulfate is the nucleating species.

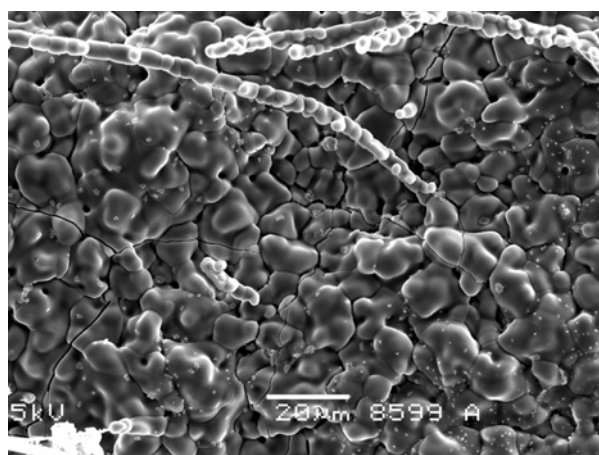


Figure 5: SEM micrograph of quench-cooled potassium sulfate substrate 'filtered' from the gas phase in an experiment with sulfation of KCl . Small particles are observed on top of the big filter cake.

Another technique developed is a 'hot impactor'. In this probe gas hits a plate with high velocity causing

particles (if any) to be caught by impaction. Thus, if deposits at the impaction plate are observed, the existence of particles at high temperatures can be proved. The first experiments with this device are just being done at the time of writing and no results are available yet.

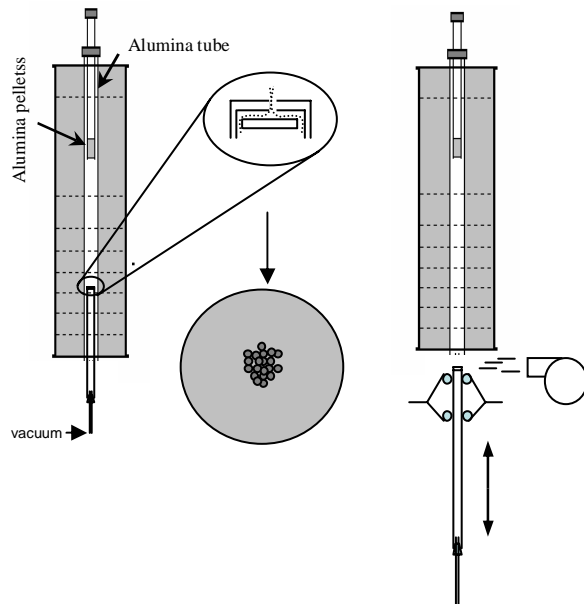


Figure 6: Experiments for investigating the aerosol formation mechanism. To the left is shown the 'hot impactor' inserted into a tubular furnace. If particles are present in the gas phase (at high temperatures) they will impact on the impaction plate. To the right is shown the hot filter with a slide that allows fast extraction of the filter and subsequently quench-cooling of the sample.

Modeling

Mathematical models will be used to describe the experiments performed. The models should account for the kinetics of chemical reactions involving the volatilized ash species, homogeneous nucleation, coagulation, particle growth by condensation, and particle transport by thermophoresis and diffusion. By applying the models the experimental results will be analyzed and alternative mechanisms will be compared and fitted to the experimental data. The modeling will be made by Computational Fluid-particle Dynamics using the programme package Fluent.

